BioMed Research International

Recent Developments of Carbonic Anhydrase Inhibitors as Potential Drugs

Guest Editors: Jamshed Iqbal, Mariya Al-Rashida, Serdar Durdagi, Vincenzo Alterio, and Anna Di Fiore

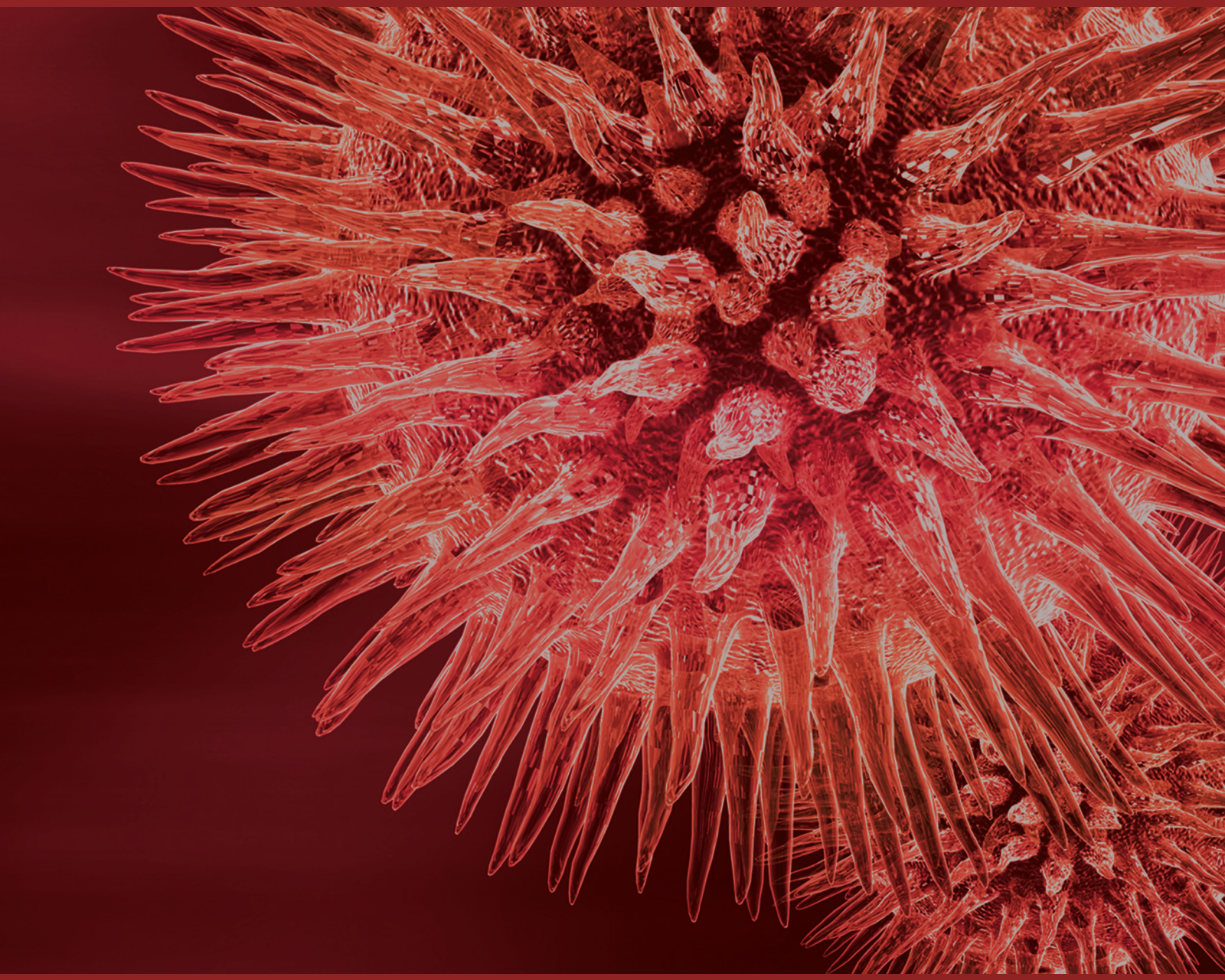

Recent Developments of Carbonic Anhydrase Inhibitors as Potential Drugs

BioMed Research International

Recent Developments of Carbonic Anhydrase Inhibitors as Potential Drugs

Guest Editors: Jamshed Iqbal, Mariya Al-Rashida, Serdar Durdagi, Vincenzo Alterio, and Anna Di Fiore

Contents

Hindawi Publishing Corporation
BioMed Research International
Volume 2015, Article ID 174178, 2 pages
http://dx.doi.org/10.1155/2015/174178

Editorial

Recent Developments of Carbonic Anhydrase Inhibitors as Potential Drugs

Jamshed Iqbal,[1] Mariya Al-Rashida,[2] Serdar Durdagi,[3] Vincenzo Alterio,[4] and Anna Di Fiore[4]

[1]*Department of Pharmaceutical Sciences and Centre for Advanced Drug Research, COMSATS Institute of Information Technology, Abbottabad, Pakistan*
[2]*Department of Chemistry, Forman Christian College (A Chartered University), Ferozepur Road, Lahore 54600, Pakistan*
[3]*Division of Biophysics, Department of Basic Medical Sciences, School of Medicine, Bahçeşehir University, Turkey*
[4]*Institute of Biostructure and Bioimaging (IBB), The Italian National Research Council, Via Mezzocannone 16, 80134 Naples, Italy*

Correspondence should be addressed to Jamshed Iqbal; drjamshed@ciit.net.pk

Received 10 December 2014; Accepted 10 December 2014

Carbonic anhydrases (CAs, EC 4.2.1.1) are metalloenzymes which are ubiquitous in nature and are found in a variety of organisms. In mammals at least 16 different isozymes of CAs have been found. CAs catalyze the reversible hydration of carbon dioxide to bicarbonate with the release of protons. Abnormal levels and/or activities of these enzymes have been associated with many disorders such as glaucoma, obesity, gastric ulcers, acid-base imbalances, cancer, and epilepsy. Carbonic anhydrases, therefore, have emerged as a valuable drug target for treatment or prevention of these disorders. Many clinically established drugs are CA inhibitors, and it is highly anticipated that many more will eventually find their way into the market. Much development has been made in this field; however, in order to find isozyme selective inhibitors with increased CA inhibition activity, it is necessary for new classes of compounds to be screened. This special issue has been dedicated to showcasing recent developments made in the field of CA inhibitors.

In "Carborane-Based Carbonic Anhydrase Inhibitors: Insight into CA II/CA IX Specificity from a High-Resolution Crystal Structure, Modeling, and Quantum Chemical in Calculations," P. Mader et al. report crystal structure of CA II in complex with 1-methylenesulfamide-1,2-dicarba-closo-dodecaborane at 1.0 Å resolution. Using computational chemistry techniques, they then modelled the same carborane-based inhibitor inside the active site of cancer related isozyme CA IX. This virtual model may provide helpful insights into the structure based design of other (more efficient and possibly selective) carborane-based CA IX inhibitors.

In "Sulfa Drugs as Inhibitors of Carbonic Anhydrase: New Targets for the Old in Drugs," M. al-Rashida et al. have identified N-substituted sulfonamide containing drugs, the sulfa drugs, and their chlorotriazine derivatives as inhibitors of CA II. The trichlorotriazine derivatives of sulfa drugs are invariably more active inhibitors than their parent drugs. This study provides a rationale for investigating other derivatives of sulfa drugs able to act as selective inhibitors against various CA isozymes.

In "Saccharin Sulfonamides as Inhibitors of Carbonic Anhydrases I, II, VII, XII, and in XIII," V. Morkūnaitė et al. have designed and synthesized a series of sulfonamide containing saccharin derivatives and investigated their CA inhibition activity against CA I, CA II, CA VII, CA XII, and CA XIII. Saccharin itself contains a secondary sulfonamide group and weakly binds to CAs. Introduction of another free sulfonamide group greatly increases the CA inhibition activity of saccharin derivatives. Many isozyme selective inhibitors were identified with binding affinities in nanomolar range.

In "Hydrophobic Substituents of the Phenylmethylsulfamide Moiety Can Be Used for the Development of New Selective Carbonic Anhydrase in Inhibitors," G. De Simone et al. have reported the synthesis of a family of structurally related compounds containing a sulfamide moiety together with an inhibition study of these compounds for the CA isoforms I, II, IX, and XII. The X-ray structure of the cytosolic dominant isoform hCA II in complex with the best inhibitor of the series is also reported, providing insights into sulfamide binding mechanism to CAs. These results confirm that such zinc-binding group, if opportunely derivatized, can be usefully exploited for obtaining new potent and selective CA inhibitors.

In "Natural Product Polyamines That Inhibit Human Carbonic in Anhydrases," R. A. Davis et al. have identified a series of naturally occurring polyamines, based on either a spermine or spermidine core, as inhibitors of CAs. Some of these compounds were found to be submicromolar inhibitors of cancer related isozyme CA IX. Interestingly, these naturally occurring compounds do not contain the typical zinc bind functional groups, which make up a large majority of CA inhibitors known. This paves way for exciting new opportunities to design and investigate CA inhibitors with alternate mechanism of inhibition that may or may not involve zinc binding.

In "Synthesis and In Vitro Inhibition Effect of New Pyrido[2,3-d]pyrimidine Derivatives on Erythrocyte Carbonic Anhydrase I and in II," H. Kuday et al. have synthesized a series of indolylchalcones and pyrido[2,3-d]pyrimidine derivatives containing indole ring. All compounds were found to be able to inhibit CA I and CA II. These compounds represent an interesting class of nonsulfonamide containing CA inhibitors that need to be explored further to elucidate their mechanism of inhibition and to exploit structural features for the development of more effective and possibly selective CA inhibitors.

In "Binding of Carbonic Anhydrase IX to 45S rDNA Genes Is Prevented by Exportin-1 in Hypoxic in Cells," E. Sasso et al. have provided evidence for regulated binding of CA IX to nucleolar 45S rDNA genes in human cells. In their efforts to reveal novel mechanisms in cell and cancer biology, the authors have described for the first time a function for CA IX and XPO1 (one of its major interactors) in nucleoli, highlighting a XPO1-based decoy mechanism. In particular, in hypoxic conditions the occurrence of CA IX/XPO1 complexes was related to decreased transcription of 45S rDNA genes. Such findings are helpful to unravel the complex hypoxic cancer cell biology and its inevitable link with CA IX.

In "Probing the Surface of Human Carbonic Anhydrase for Clues towards the Design of Isoform Specific in Inhibitors," M. A. Pinard et al. have adopted a clever approach in their quest for design of isozyme selective CA inhibitors. In most of the alpha-CA isozymes the active site residues are highly conserved, presenting a particular challenge for the design of isozyme selective CA inhibitors. However, some variation in amino acid residues occurs towards the exit of the active site. A comparison of conserved and nonconserved regions of CA catalytic site of various CA isozymes provides a template by virtue of which these subtle differences can be exploited for the design of isozyme selective CA inhibitors.

Jamshed Iqbal
Mariya Al-Rashida
Serdar Durdagi
Vincenzo Alterio
Anna Di Fiore

Hindawi Publishing Corporation
BioMed Research International
Volume 2015, Article ID 453543, 15 pages
http://dx.doi.org/10.1155/2015/453543

Review Article

Probing the Surface of Human Carbonic Anhydrase for Clues towards the Design of Isoform Specific Inhibitors

Melissa A. Pinard, Brian Mahon, and Robert McKenna

Department of Biochemistry and Molecular Biology, College of Medicine, University of Florida, P.O. Box 100245, Gainesville, FL 32610, USA

Correspondence should be addressed to Robert McKenna; rmckenna@ufl.edu

Received 28 February 2014; Accepted 1 September 2014

Academic Editor: Anna Di Fiore

The alpha carbonic anhydrases (α-CAs) are a group of structurally related zinc metalloenzymes that catalyze the reversible hydration of CO_2 to HCO_3^-. Humans have 15 different α-CAs with numerous physiological roles and expression patterns. Of these, 12 are catalytically active, and abnormal expression and activities are linked with various diseases, including glaucoma and cancer. Hence there is a need for CA isoform specific inhibitors to avoid off-target CA inhibition, but due to the high amino acid conservation of the active site and surrounding regions between each enzyme, this has proven difficult. However, residues towards the exit of the active site are variable and can be exploited to design isoform selective inhibitors. Here we discuss and characterize this region of "selective drug targetability" and how these observations can be utilized to develop isoform selective CA inhibitors.

1. Introduction

Carbonic anhydrases (CAs, EC 4.2.1.1) are a family of ubiquitous, mostly zinc metalloenzymes that catalyze the reversible hydration of carbon dioxide to bicarbonate and a proton [1, 2]. These enzymes are expressed in most living organisms and are encoded by five evolutionary distinct gene families: α-, β-, γ-, δ-, and ζ-CAs [3–5]. The α-CAs are expressed predominantly in vertebrates and are the only class observed in humans. β-CAs are found in prokaryotes, algae, and plants [6]; the γ-CAs are present in archaebacteria [7], while the δ- and ζ-CAs are found in diatoms [8]. The α-CAs have been extensively studied due to their role in human physiology and disease pathology [9]. Humans express 15 different isoforms, 12 of which are catalytically active and differ in their enzymatic efficiency. These isoforms also differ in cellular distribution and physiological function (Table 1). Specifically, there are eight cytosolic (CA I, II, III, VII, VIII, X, XI, and XIII), two mitochondrial (CA VA, and VB), one secreted (CA VI), three transmembrane (CA IX, XII and XIV), and one GPI-anchored (CA IV) isoforms of CA [10]. CA VIII, X and XI are noncatalytic due to the absence of one or more of the coordinating histidine residues and are termed CA related proteins (CA-RPs) [11].

The α-CA active site is located at the base of a large conical cavity spanning from the protein's surface to its center. This cavity is approximately 15 Å wide at its opening and 15 Å deep [4, 12, 13] based on observations in human CA II. At the core of the active site is a Zn(II) ion in a distorted tetrahedral coordination with His94, 96, and 119 (CA II numbering; used throughout) and a water/hydroxide molecule [14] (Figure 1). The active site of CA exhibits an amphiphilic nature and contains both a hydrophobic (Val121, Val143, Leu198, Val207, and Trp209 in purple, Figure 1(b)) and hydrophilic side (Tyr7, Asn62, His64, Asn67, Thr199, and Thr200 in green, Figure 1(b)) [15]. A high degree of residue conservation between the CA isoforms exists in each region.

The first step of catalysis by CA is the nucleophilic attack of a Zn-bound OH^- (active basic form) on a CO_2 molecule, (Figure 2, I-II) to produce HCO_3^- (III). The HCO_3^- remains weakly bound to the Zn(II) ion (III) until it is displaced by a water molecule (III-IV) (inactive acidic form) and released into solution [16]. In the second step of CA catalysis (IV-I) the Zn-bound water regenerates to OH^-through a proton transfer event mediated by a highly conserved (in most isoforms). Histidine residue in combination with a network of ordered water molecules that are stabilized by the adjacent hydrophilic region of the enzyme's active site [1, 2, 15]

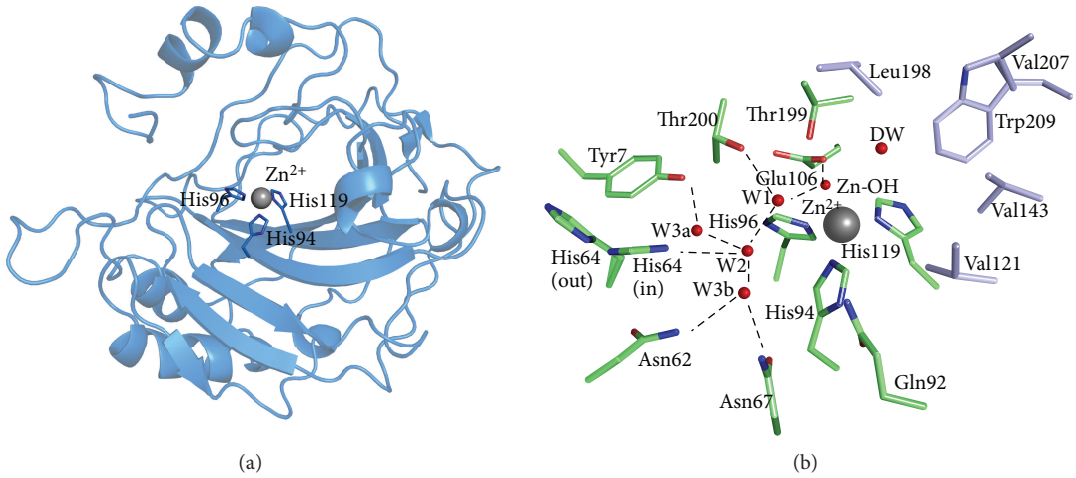

Figure 1: Structure of CA II. PDB ID: 3KS3. (a) Ribbon diagram depicting the overall structural fold. The active site zinc ion and coordinated histidines shown. (b) Active site and ordered waters (red spheres). Also shown are the hydrophilic (green) residues as well as the hydrophobic (purple) residues lining the active site.

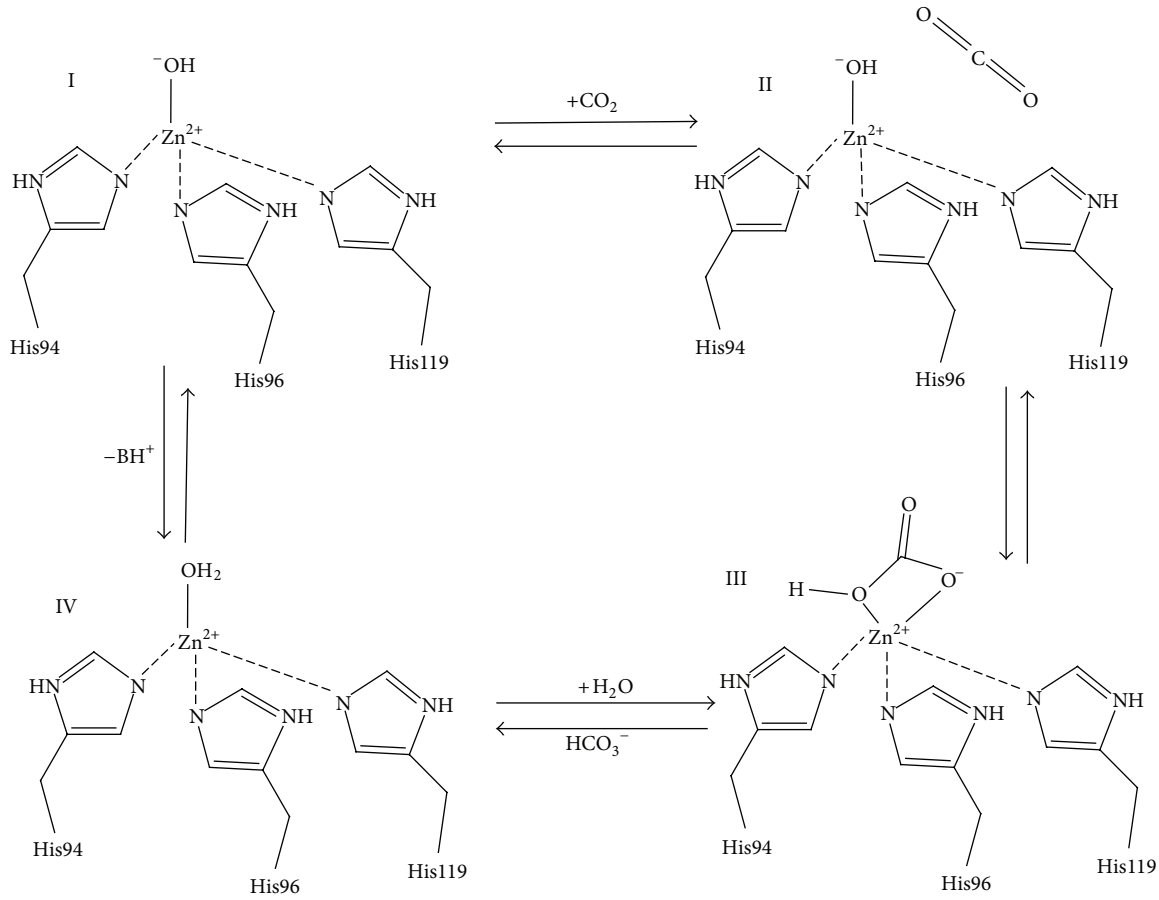

Figure 2: Schematic representation of CA catalytic mechanism.

Table 1: Distribution, associated diseases, catalytic efficiency, and structural characterization of CAs.

Isoform	Localization: Organ/tissue	Localization: Subcellular / Associated disease	K_{cat} (s^{-1})	K_{cat}/K_M (M^{-1} s^{-1})	pI	Oligomeric state	Number of PDB entries	References
I	RBCs, GI tract, and eye	Cytosol Hemolytic anemia	2.0×10^5	5.0×10^7	6.6	Monomer	19	[2, 3, 9, 88, 89]
II	RBCs, kidney, osteoclasts, eye, GI tract, lung, brain, and testis	Cytosol Glaucoma, epilepsy, edema, altitude sickness	1.4×10^6	1.5×10^8	6.9	Monomer	454	[2, 3, 3, 9, 88–90]
III	Adipocytes, skeletal muscle	Cytosol Oxidative stress	1.0×10^4	3.0×10^5	7.0	Monomer	6	[2, 3, 9, 88, 89]
IV	Lung, kidney, brain, eye, RBCs, and colon	Membrane-bound Retinitis pigmentosa, stroke, glaucoma	1.1×10^6	5.1×10^7	6.4	Monomer	4	[3, 9]
VA	Liver	Mitochondria Obesity, insulin resistance	2.9×10^6	2.9×10^7	7.2	Monomer	1*	[4, 91]
VB	Kidney, GI tract, spinal cord, heart and skeletal muscle, and pancreas	Mitochondria Obesity, insulin resistance	9.5×10^5	9.8×10^7	7.7	Monomer	N/A	[4, 91]
VI	Salivary and mammary glands	Secreted Dental caries	3.4×10^5	4.9×10^7	6.5	Dimer	1	[5, 9, 92, 93]
VII	Liver, colon, skeletal muscle, and brain	Cytosol Epilepsy	9.5×10^5	8.3×10^7	6.9	Monomer	2	[6, 9, 94]
IX	GI mucosa, tumors	Transmembrane Cancer	3.8×10^5	5.5×10^7	5.5	Dimer	2	[3, 7, 9, 88, 89, 95]
XII	Eye, tumors, reproductive epithelia, intestines, and kidney	Transmembrane Cancer, glaucoma	4.2×10^5	3.5×10^7	5.8	Dimer	5	[3, 8, 96]
XIII	Kidney, thymus, submandibular glands, small intestine, and reproductive organs	Cytosol sterility	1.5×10^5	1.1×10^7	6.5	Monomer	6	[5, 44]
XIV	Eye, brain, kidney, liver, bladder, and spinal cord	Transmembrane Retinopathy, epilepsy	3.1×10^5	3.9×10^7	5.5	Monomer	1	[9, 97]

*murine.

(Figure 1(b)). In crystal structures of CA II, His64 has been observed to occupy two distinct positions: inward (pointing towards the active site) and outward (pointing away from the active site) conformations (Figure 1(b)). The general consensus is that the inward conformation of His64 is poised to accept the proton that has been transferred from the catalytic zinc to the water network, while the outward conformation is in an orientation that favors proton shuttling to the bulk solvent [16–18].

CAs are among the most efficient catalysts known, however there is variation in catalytic efficiency between isoforms such that the members of the α-CAs with the exception of the CA-RPs can be divided into three generalized categories. As such, CA II, IV, VB, and VII are among the fastest of the human CAs with CA II exhibiting a k_{cat} of 1.4×10^6 sec^{-1}. CA VA, VI, IX, and XII exhibit relatively intermediate catalytic activity, and CA III, XIII and XIV are considered the least efficient CAs [3, 9] (Table 1). The efficiency of these enzymes depends on the speed of proton shuttling during the two-step catalytic mechanism [3, 18]. In most of the CAs, this proton shuttling residue is the aforementioned histidine at position 64 [19–21]. In CA III, which is considered the slowest among the CA isoforms (<1% of CA II activity), a lysine is at position 64 [16].

The human CAs are involved in various physiological functions, ranging from bone resorption to pH regulation, with abnormal levels or activities of these enzymes being commonly associated with various diseases (Table 1). Two main classes of CA inhibitors (CAIs) exist: the metal chelating anions and sulfonamide-based inhibitors. Both classes of CAIs are often referred to as "classical" inhibitors of CA and bind directly to the Zn(II) ion in the active site, displacing

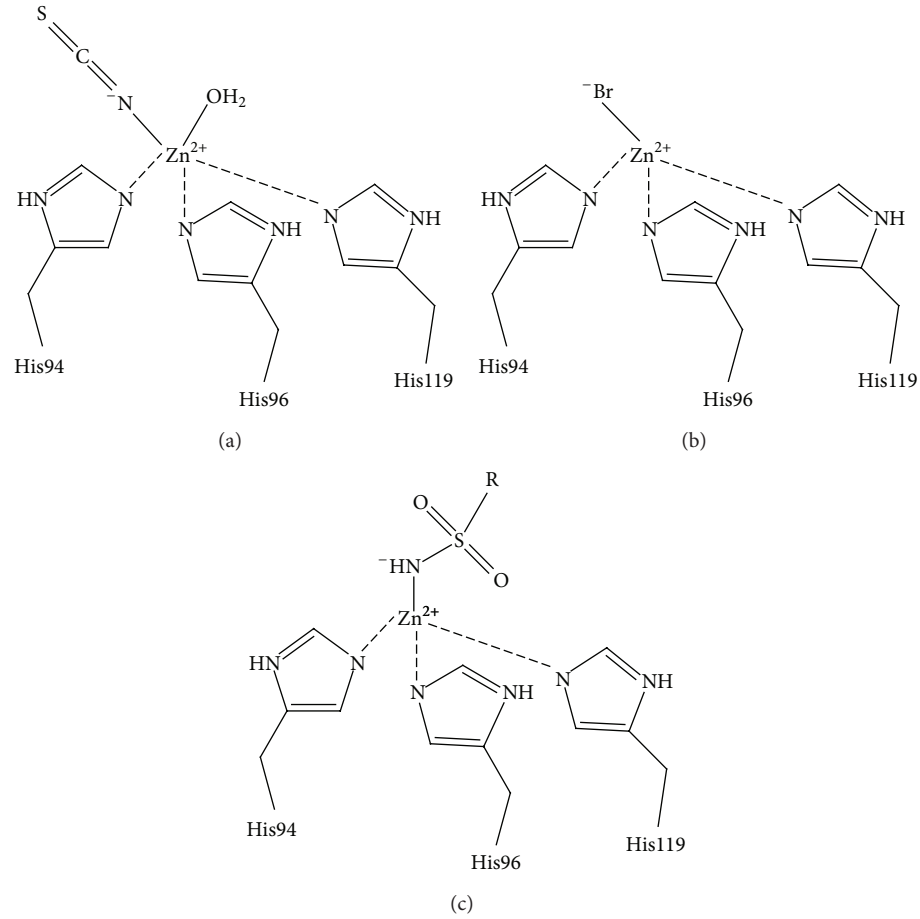

Figure 3: CA inhibition mechanism. (a) Anions such as thiocyanate form trigonal-bipyramidal adducts (b) Anions such as Br^- form distorted tetrahedral adducts (c) sulfonamides as well as some anions form regular tetrahedral adducts.

the Zn-bound solvent molecule. Metal chelating anions bind as either a trigonal-bipyramidal, distorted tetrahedral, or regular tetrahedral adduct [22] (Figures 3(a)–3(c)). Alternatively, sulfonamides generate a tetrahedral geometry upon binding to the catalytic zinc [9] (Figure 3(c)). This "classical" mode of binding of sulfonamide-based and anion CAI will be presented in more detail in later sections of this study.

As mentioned previously, the α-CAs display a remarkable diversity in regards to tissue distribution and overall physiological function. As such, a brief overview of each of these characteristics is presented and is summarized in Table 1.

Cytosolic CAs I and II are both expressed in red blood cells and are necessary for maintaining physiological pH of the blood through production of HCO_3^- [23]. Abnormal levels of CA I in the blood are used as a marker for hemolytic anemia. CA II is ubiquitously expressed in other tissues including the kidney [24], bone, and also in ocular tissues [25]. Interestingly, CA II has also been shown to be associated with several transporters including the Cl^-/HCO_3^- exchanger, AEI [26], the Na^+/HCO_3^- cotransporter, NCB1 [27], and the Na^+/H^+ exchanger, NHE1 [28]. This suggests that CA II acts as a mediator of certain metabolic pathways by further providing the substrates for these various transporters [29]. As a result, CA II is often associated with several diseases such as glaucoma, renal tubular acidosis, and osteoporosis [3, 30]. In addition, CA II has also shown to be essential for the proper functioning of the water-transport channel, aquaporin-1 (AQP1) [31, 32]. Specifically, the relationship between CA II and AQP1 has been shown to be essential for maintaining proper CO_2 transport in oocytes, regulation of AQP1 function, and also maintenance of a stable intracellular pH [31].

CA III expression is limited to skeletal muscle and adipose (both white and brown) tissue [33–35]. Unlike CA I and II, CA III displays (as mentioned previously) a remarkable 200-fold decrease in catalytic activity compared to CA II [36]. Furthermore, CA III contains two surface cysteine residues that can be glutathionylated thus acting as a vessel for reactive oxygen species (ROS) sequestration providing cell protection against oxidative damage [37]. These two attributes have caused speculation that CA III might serve a different physiological role unrelated to its primary catalytic function, although this notion is still unclear. It has been observed that CA III expression is directly correlated to adipogenesis and could potentially act as a regulator of peroxisome proliferator-activated receptor-γ2 (PPARγ2) expression [38]. As a result CA III has not currently been linked to any particular disease. CA VII is primarily expressed in colon,

liver, skeletal muscle, and in the brain [39]. CA VII exists as two forms; one form displaying the complete amino acid sequence and the other containing a 56 residue N-terminal truncation [39]. Like CA III, CA VII has two surface cysteines that can be glutathionylated suggesting that it too can act in preventing cellular oxidative damage [40]. Though the physiological role of CA VII remains unclear, evidence suggests that this enzyme plays a role in neuronal excitement through HCO_3^- production [41]. HCO_3^- can mediate electric current through channels that are coupled to gamma-aminobutyric acid ($GABA_A$) receptors, and upon inhibition of CA VII interruption of the current-gated channel is induced causing a suppression of neural excitement [42]. As a result CA VII has been a proposed target for treatment of seizures and neuropathic pain [43].

CA XIII is another active cytosolic CA. CA XIII expression has been shown to be localized to the thymus, kidney, submandibular gland, small intestine, and predominantly in both male and female reproductive organs [44]. It has been postulated that CA XIII plays a significant role in pH regulation of reproductive processes including sperm mobility [45]. To date, no significant physiological function regarding CA XIII has been observed. However, it should be noted that downregulation of CA XIII has been seen in cases of colorectal cancer; however the significance of this observation has not yet been concluded [45].

The CA-RPs: CA isoforms VIII, X, and XI are also located in the cytosol. It has been observed that the CA-RPs are expressed predominantly in the brain and as mentioned previously show no catalytic activity. To date, no known physiological roles, or relation to particular disease have been established [11]. As a result, we will not focus on these isoforms.

CA VA and VB are the only isoforms expressed in the mitochondrial matrix of hepatocytes and adipocytes, respectively [46]. CA VA has been shown to be directly associated with ureagenesis such that it provides HCO_3^- to be utilized by carbamoyl phosphate synthetase I [47, 48]. Carbamoyl phosphate synthetase is responsible for synthesis of carbamoyl phosphate which is the rate-determining step of ureagenesis [47]. Furthermore, it has been shown that other necessary carboxylase reactions, including that of pyruvate carboxylase for gluconeogenesis, could be mediated by CA VA activity [48]. This indicates that CA VA can act as a key mediator in several metabolic pathways of the liver. In addition the same effect is seen in the mitochondria of adipocytes where CA VB facilitates carboxylase activity and thus causes induction of lipogenesis [49]. The relationship of CA VA and VB with certain metabolic pathways suggests that both enzymes could be considered as drug targets for modulating both gluconeogenesis and lipogenesis in cases of obesity and insulin resistance [50].

CA VI is the only CA that is secreted and has been found in tears, respiratory airways, epithelial lining of the alimentary canal, enamel organs, and most significantly in human saliva [51–55]. The physiological role of CA VI has not been established although it has been suggested that it is required for pH homeostasis of the mouth [56]. Maintenance of proper pH levels in saliva are necessary to protect against enamel erosions and acid neutralization in dental biofilms caused by bacteria [57, 58]. As a result it is suggested that CA VI plays a key role in these pathways. Interestingly, CA VI has also shown to be associated with taste and inhibition of CA VI has been shown to cause irregularities in taste perception or sometimes loss of taste completely [59]. This effect however is restored with exposure to high levels of zinc [60].

The membrane-associated CAs include the transmembrane isoforms: CA IX, XII, and XIV, and GPI-anchored isoform CA IV. CA IV is expressed both in the kidneys and lungs [61] and similarly to CA II, CA IV can interact with the same aforementioned transporters that span the renal cell surface [62]. It has therefore been established that the presence of CA IV in the kidney is necessary for bicarbonate resorption and normal kidney function [30]. Interestingly, mutant forms of CA IV have been shown to be associated with an autosomal dominant form of retinitis pigmentosa despite intrinsic levels of wild-type CA IV not being observed in ocular tissue [63].

Both CA IX and XII are often regarded as the tumor-associated CAs [64]. CA IX however has garnered the majority of the attention due to its intrinsically low level of expression in normal tissues [65], in combination with being a key modulator of tumor growth and survival. Specifically, CA IX acts as a mediator of tumorigenesis, pH control, tumor cell proliferation and migration, and cell adhesion [66–70]. CA IX has been shown to be regulated by tumor hypoxia and has not only been established as prognostic indicator for a variety of cancers but also as a generic anticancer target [71–73]. Similarly, CA XII expression has been observed to be upregulated in multiple tumor tissues but it has not been established as a prognostic marker [74–77]. Unlike CA IX, CA XII also shows a wider range of expression in normal tissue including the kidney, lung, prostate, ovaries, uterine endometrium, breast, and basolateral membrane of gut epithelium [64, 78–80]. Furthermore, it has been postulated that CA XII is important for normal kidney function [81].

CA XIV displays high sequence similarity with CA XII and has been shown to be expressed in most parts of the brain, colon, small intestine, urinary bladder, kidney, and retina [82, 83]. Interestingly, immunohistochemical analysis indicates that there is a strong correlation between CA XIV and CA IV expression suggesting there is functional overlap between the enzymes [84]. CA XIV has been shown to directly interact with membrane-transporters and has been observed to be important for pH balance in muscle and erythrocytes in response to chronic hypoxia. Furthermore, CA XIV activity is shown to be important in terms of hyperactivity of the heart and pH regulation in the retina [85–87].

2. Methods

A multiple sequence alignment of all the human α-CAs was performed in ClustalW2 [98, 99] and used to generate a cladogram that illustrated the evolutionary relationship between the isoforms. The primary sequence identity (%) and number of conserved residues (among the catalytically active isoforms) were calculated in ClustalW2 [98, 99] using

Table 2: Primary sequence identity (%) (lower left) and number of conserved residues (upper right) among catalytic CAs.

	I	II	III	IV	VA	VB	VI	VII	IX	XII	XIII	XIV
I	—	158	141	78	126	128	82	132	83	91	154	85
II	60.5	—	152	88	133	138	90	147	85	89	157	96
III	54.2	58.5	—	82	120	117	87	130	80	86	151	90
IV	30.0	33.5	31.2	—	89	93	97	90	84	91	84	62
VA	48.1	50.8	45.4	23.6	—	184	93	131	83	84	124	88
VB	46.9	51.9	43.5	23.1	58.7	—	82	134	89	79	131	88
VI	31.9	33.5	32.3	27.0	27.9	24.4	—	93	107	104	90	106
VII	50.8	56.2	49.6	31.8	48.5	49.2	34.9	—	95	103	139	97
IX	33.1	34.2	31.1	27.2	31.9	32.7	38.9	37.0	—	101	90	113
XII	35.8	34.2	32.3	28.1	31.6	29.7	38.0	38.0	38.9	—	91	123
XIII	59.2	59.6	57.7	28.2	46.2	47.7	33.2	52.7	35.0	34.7	—	98
XIV	34.2	35.8	34.2	29.0	31.9	29.0	35.8	36.0	44.4	46.0	37.4	—

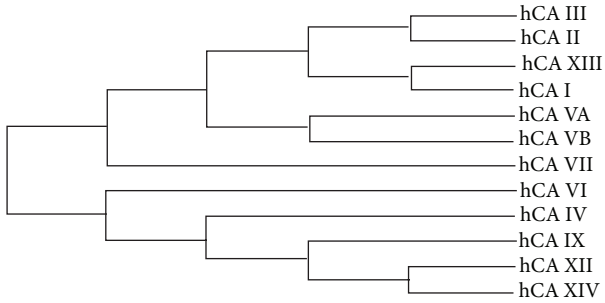

Figure 4: Cladogram of the human α-CAs.

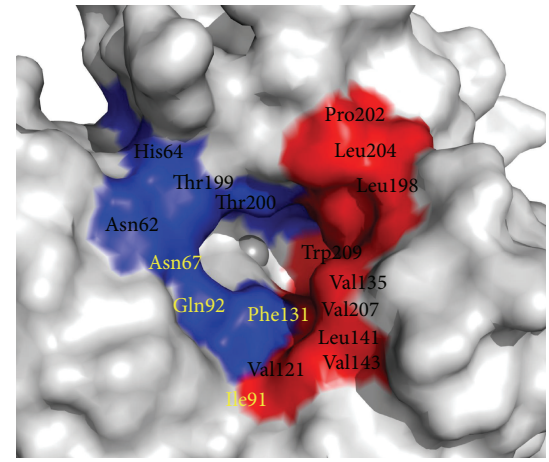

Figure 5: Solvent accessible residues in and around CA II active site. Hydrophilic cleft (blue) and hydrophobic cleft (red). Residues in yellow indicate residues of the "selective pocket."

the same sequence alignment information. The coordinate files for different CA II inhibitor-complexes were obtained from the Protein Data Bank (PDB) (http://www.wwpdb.org/) to compare the region in which these inhibitors bind in CA II's active site. One file was selected as a reference for the alignment to the other coordinate files in the molecular graphics program *Coot* [100]. A surface rendition of CA II in complex with each of the inhibitors was generated in *Pymol* [101]. The hydrophobicity scores for the residues constituting the hydrophobic cleft were calculated based on the Kyte-Doolittle hydropathy plot [102]. All figures were generated in *Pymol* [101].

3. Results and Discussion

3.1. Enzyme Inhibition. The α-CAs are very closely related (Figure 4) as per a >30% primary sequence identity amongst them (Table 2). It is this similarity that leads to complications when designing CAIs that are isoform selective as a majority of the sequence identity translates to residues located in the CA active site. Table 3 shows the number of conserved residues among the different isoforms for residues in the active site and surrounding areas. For example, the 60.5% primary sequence identity that exists between CA I and II (Table 2), in combination with both enzymes being expressed in RBCs, makes CA I a potential off-target isoform when targeting CA II for inhibition [103, 104]. Likewise, when designing selective inhibitors against CA IX, unwanted targeting of CA I and II (with 33.1 and 34.2% identity, resp.) can occur leading to an induced susceptibility to side-effects [9, 105]. The same is true when considering CA VI inhibition where CA II acts as an off-target isoform (33.5% identical) [9].

Therefore, to design highly selective CAIs requires the exploitation of subtle active site differences; predominantly residues found in the hydrophilic and hydrophobic pockets [22] (Figure 4). Comparative analysis of structures of ligand bound CA molecules shows that exploitable residues that contribute to ligand stabilization include residues N67, I91 and F131 (Figure 5), which are also highly variable between isoforms (Table 4). In addition, Q92, though conserved, has also shown to be important in inhibitor binding. Furthermore, structural interpretation of ligands bound to CA II show that inhibitors can extend out of the active site and form extensive and unique contacts with residues of either the hydrophilic or hydrophobic pocket.

3.2. Classical Inhibitors. Both the catalytic and inhibition mechanism of the α-CAs have been studied for several

Table 3: Active site residues of catalytic CAs (*CA II numbering*).

Residues	Isozyme										
	I	III	IV	VA	VB	VI	VII	IX	XII	XIII	XIV
Y7	Y	Y	Y	W	Y	Y	Y	Y	Y	Y	Y
N62	N	N	N	N	N	N	N	N	N	N	N
N67*	H	R	M	Q	L	Q	Q	Q	K	N	Q
I91*	F	R	K	K	K	Q	K	L	T	R	A
Q92	Q	Q	Q	Q	Q	Q	Q	Q	Q	Q	Q
H94	H	H	H	H	H	H	H	H	H	H	H
H96	H	H	H	H	H	H	H	H	H	H	H
H119	H	H	H	H	H	H	H	H	H	H	H
V121	A	V	V	V	V	V	V	V	V	V	V
F131*	L	F	V	Y	F	Y	F	V	A	F	L
V135	A	L	Q	V	A	Q	A	L	S	A	A
V143	V	V	V	V	V	V	V	V	V	V	V
L198	L	F	L	L	L	L	L	L	L	L	L
T199	T	T	T	T	T	T	T	T	T	T	T
T200	T	T	T	T	T	T	T	T	T	V	T
P202	P	T	P	P	P	P	P	P	P	P	P
W209	W	W	W	W	W	W	W	W	W	W	W

* residues making up the selective pocket.

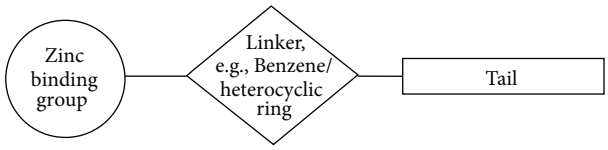

Figure 6: Schematic of the components of a classical CA inhibitor.

decades and have aided in designing potent isoform specific inhibitors that are important in a wide range of clinical applications (Table 1). This includes CAIs used such as antiglaucoma, antiepileptic, and antiobesity agents, as well as diagnostic tools [41]. A schematic of the basic components of a typical CAI is illustrated in Figure 6. It consists of a zinc-binding group (ZBG), a linker region (heterocyclic or benzene ring) and a variable "tail" region.

As discussed previously CAIs that bind directly to the Zn(II) ion can be divided into two groups based on how they coordinate to the metal center. Those that form trigonal-bipyramidal adducts through way of binding directly to the zinc-bound hydroxyl/water (e.g., cyanates and formates) [9, 16, 22], and those that form tetrahedral adducts and interact directly to the catalytic zinc (e.g., sulfonamides and bisulfites) (Figure 3) [9, 16, 22].

The classical CAIs: the metal-chelating anions and the sulfonamides and their isoesters (sulfamides/sulfamates) are the most studied of the CAIs [22]. However, "nonclassical" CAIs that do not bind directly to the Zn(II) ion also exist. This includes compounds such as coumarins and nitrates [106].

3.3. Metal-Chelating Anions. The inorganic anions (e.g., Br^-) are weaker inhibitors than the sulfonamides and have inhibition constants (K_i's) in the millimolar to submillimolar range [9]. However, for certain isoforms some anions show binding affinities in the low micromolar range (e.g., azide, cyanate, and trithiocarbonate) [88, 107–109]. Unlike the sulfonamides the anions may bind to the metal ion in three different coordination geometries: trigonal-bipyramidal geometry, tetrahedral geometry, or in a distorted tetrahedral geometry. The ability to bind in multigeometries is due primarily to the ligand's structural features. For example, hydrogen sulfide's (HS^-) ability to act as an H-bond donor to Thr199 allows it to displace the hydroxyl bound zinc and maintain a tetrahedral coordination [9]. On the other hand, unprotonated ligands such as azide (N_3^-) and bromide (Br^-) adopt either the trigonal bipyramidal geometry or distorted tetrahedral geometry [9, 16, 22]. These inhibitors lack the ability to form H-bonds with the Oγ of Thr199 and so the geometry about the zinc sphere is distorted from the regular tetrahedral geometry [110, 111]. Formate and thiocyanate anions bind as a bipyramidal adduct shifting the zinc bound solvent [12, 112]. Other anions like the nitrates are not coordinated to the metal ion and instead are located in close proximity to it [9, 106].

3.4. Sulfonamide-Based CAIs. The sulfonamide-based compounds and their isoesters (sulfamides/sulfamates) are by far the most widely represented and clinically used CAIs. This class consists of several compounds, many of which have adapted long-term clinical applications [22]. Brinzolamide, dorzolamide, acetazolamide, methazolamide, and zonisamide have been used as antiglaucoma agents, diuretics, and antiepileptics [9]. Sulfonamides and their bioesters are potent inhibitors with K_i's in the nanomolar range and bind in deprotonated forms to the Zn(II) ion displacing the zinc-bound hydroxyl/water while maintaining a tetrahedral coordination about the active site (Figure 3(c)) [113]. X-ray crystallographic structures of CA I, CA II, and CA IV in complex with these sulfonamide inhibitors are available in the PDB and in all complexes the deprotonated sulfonamide group is coordinated to the Zn(II) ion, while the Oγ atom of Thr199 makes a hydrogen bond with the sulfonamide's NH moiety. Thr199 also forms a second hydrogen bond to the carboxylate group of Glu106 [16]. Depending on the nature of the R-group, additional interactions with hydrophobic and/or hydrophilic residues in the region of the active site also influence inhibitor binding. However, it is the combination of the negative charge of the monoprotonated sulfonamide group with the positively charged zinc coupled with the ability of Thr199 to form two strong H-bonds that lends the sulfonamides their unique potency for CA inhibition [9].

3.5. Nonclassical CAIs. Aside from the classical metal chelating anion and sulfonamide-based inhibitors, which currently represent the majority of CAIs, other potent inhibitors exist. These include thiocarbonates, phenols [114, 115], coumarins [116, 117], polyamines [118], carbohydrate-based sulfonamide derivatives [119–121], and steroid sulfatases [122]. In addition peptidomimetic and monoclonal antibody CAIs have also been utilized [123–125].

The thiocarbamates are anion based chemotypes that exhibit monodentate coordination by way of one sulfur

Table 4: Hydrophobicity of CA active sites (*CA II numbering*).

Residues	Isozyme										
	I[1]	II[2]	III[3]	IV[4]	V[5*]	VI[6]	VII[7]	IX[8]	XII[9]	XIII[10]	XIV[11]
I91	F	I	R	K	K	Q	K	L	T	R	A
V121	A	V	V	V	V	V	V	V	V	V	V
V135	A	V	L	Q	S	Q	A	L	S	A	A
V141	L	L	L	I	L	L	L	L	L	L	L
V143	V	V	V	V	V	V	V	V	V	V	V
L198	L	L	F	L	L	L	L	L	L	L	L
P202	P	P	T	P	P	P	P	P	P	P	P
L204	Y	L	E	D	A	T	S	A	N	L	Y
W209	W	W	W	W	W	W	W	W	W	W	W
Total hydrophobicity	**14**	**26**	**8**	**4**	**11**	**7**	**11**	**23**	**9**	**15**	**16**

[1]2FOY; [2]3KS3; [3]3UYN; [4]1ZNC; [5]1DMX *murine; [6]3FE4; [7]3MDZ; [8]3IAI; [9]1JC2; [10]3DAZ; [11]4LU3.

atom binding to the Zn(II) ion in the CA active site. This interaction is coupled with a hydrogen bond observed between an adjacent sulfur molecule reacting with Thr199 [126]. Several compounds currently exist of this chemotype that display nanomolar affinity for CA II and other isoforms. Structural data show that these compounds make unique contacts with several amino acids in the enzymes hydrophilic and hydrophobic binding pockets that can be exploited for design of isoform specific CAIs [127]. Other interesting "nonclassical" CAIs, the phenols, show an alternative mode of binding that is different from both classical sulfonamides and most anions (Figure 8(d)). These compounds anchor directly to the zinc-bound water molecule/hydroxyl rather than the Zn(II) ion itself [114]. However these compounds exhibit a reduction in potency typically in the millimolar range, but there is still a large interest to develop these compounds into potent isoform selective CAIs as they are derived from natural products [128].

Other forms of nonclassical CAIs are the coumarins, which have been both engineered synthetically and isolated as natural products. These compounds vary in regards to isoform inhibition and selectivity [116, 117]. Coumarins, unlike classical CAIs, exhibit "prodrug" characteristics where, prior to binding to the active site, they are hydrolyzed by the esterase activity exhibited by CA that further induces binding at the entrance of the enzymes active site (Figure 8(c)) [116, 117]. This mechanism-based binding event of coumarins suggests that these compounds have potential use in CA isoform selectivity [129–134]. Based off of these observations, sulfur-based derivatives of this chemotype have been formulated and labeled as the "sulfocoumarins" [135]. These compounds also exhibit the same mechanism-based mode of CA binding but show increased affinity via the added sulfur moiety, which forms direct interactions with the catalytic zinc [135].

Polyamines, which belong to an alkaloid structural class, have also shown utility as CAIs [115, 118]. Several polyamine derivatives that have been isolated display high levels of CA isoform selectivity with potencies ranging from millimolar to low nanomolar levels [118]. Unlike the aforementioned CAIs, polyamines exhibit a mode of binding reliant on hydrogen bond formation throughout the active site cavity. Specifically, they anchor to the zinc-bound water/hydroxide (similar to phenols) with the terminal amine interacting with residues in positions 200 and 201 [118]. Most likely this attribute contributes to isoform selectivity of various polyamine CAIs and can thus be further developed to engineer more specific and potent CAIs of this class.

Several glycosyl primary sulfonamides and glycoconjugate sulfamates have been recognized as CAIs [120, 121]. These compounds are typically modifications of classical sulfonamide CAIs that usually have an aromatic-ring branched to the primary sulfonamide group (Figure 6). Instead these compounds replace the aromatic attachments of primary sulfonamides with mono- or disaccharide moieties [119–121]. Interestingly, the addition of a specific sugar moiety induces variable isoform selectivity ranging from micromolar to low nanomolar levels between CAs. More notably, these compounds have found use in inhibiting tumor associated isoforms IX and XII [119–121]. Not only do these compounds exhibit high affinity for CA IX/XII but the bulky sugar moieties cause a reduction in membrane permeability allowing for selective targeting of the extracellular facing catalytic domain of both tumor associated isoforms thus acting as location specific CAIs [119–121].

Similar to adding bulky-carbohydrate moieties to sulfonamides, steroid sulfatase inhibitors, which have been designed based on previously seen antimitotic inhibitors [136, 137] are able to take advantage of the variable residues in the hydrophobic pocket of specific CAs via van Der Waals contacts of the steroidal backbone [136–138]. The same trend was seen in energy calculations from molecular docking studies of such compounds with CA IX [137]. These particular compounds are also useful in locating specific targeting of extracellular CAs due to their reduced membrane permeability [136, 137].

In addition to the development of small-molecule inhibitors of CAs, there are several biologics used for CA inhibition. Utilization of monoclonal antibodies, such as M75 and G250, to recognize the proteoglycan-like (PG) domain (the N-terminal extension unique to this isoform) of CA IX have shown effectiveness in disrupting the ability of the enzymes function in regulating tumor cell adhesion and

motility [139, 140]. More recently, the monoclonal antibody 6A10 has been developed to mediate CA XII activity also acting as a potential anticancer therapeutic [124, 125]. This becomes promising as such monoclonal antibodies exhibit high affinity to their target and can thus be used to distinguish between isoforms [124, 125]. More recently, peptide based inhibitors for CA IX have also been discovered utilizing a phage-display library [123]. However the benefits of these types of ligands are still unclear. Although there is postulation that the specific binding region of such peptides can be further exploited for the development of a biologic drug that is isoform selective [123].

3.6. Preferential Binding. As we have seen the major hurdle in developing isoform selective CAIs is to design inhibitors that can distinguish between the similarities of the α-CA active site architecture. This would require the CAI to have limited interactions with conserved regions of the active site such as the three histidine residues coordinating the Zn(II) ion seen in all 12 catalytically active isoforms, residues that have shown to contribute to inhibitor binding such as Thr199 and Glu106 in CA II, and most of the residues that constitute both the hydrophobic and hydrophilic cleft as they are conserved (Figure 7).

Human CA II is the most well studied and characterized of the CA isoforms [141]. Over 400 X-ray crystallographic structures of CA II (both wild-type and variants) exist in the PDB with over 150 submissions containing CA II inhibitors [106]. Using the CA II active site as a reference it can be observed that the majority of inhibitors are buried deep in the enzymes active site (Figure 8(a)) and are restricted to the highly conserved region, which can be termed the "*conserved pocket*" (green shaded region, Figure 8(a)). Most of these inhibitors are sulfonamides (with short organic scaffolds) and so maintain the tetrahedral coordination about the zinc sphere while the variable "tails" of these inhibitors interact mainly with residues making up the hydrophobic and hydrophilic clefts. Furthermore, these variable "tail" regions are observed to be stabilized by H-bonds and hydrophobic interactions with Thr199, Thr200, Val121, Val143, and Leu198.

Despite the structural similarities observed between the CA isoforms, amino acid differences exist in specific regions of the active site. This region is defined as the "*selective pocket*" [106] (yellow shaded region, Figure 8(b)) and lies towards the edge of the active site relative to the catalytic zinc. Those inhibitors that are restricted to the *conserved pocket* are unable to form interactions with residues residing in the *selective pocket* due to the compact nature of their chemical scaffolds. Simply, the tails of these inhibitors are too short to interact with the residues that constitute the *selective pocket* and therefore cannot establish extensive contacts that can contribute to isoform selective inhibition. Residue positions 67, 91, and 131 establish this region termed the *selective pocket* (Table 3). Gln92, though conserved in all the isoforms, is also instrumental in contributing to inhibitor binding along with these select residues.

In addition to exploiting residues in the *selective pocket* between isoforms, selective CAIs can be designed based on overall hydrophobicity of the active site cleft. For example, CA II and CA IX display the most hydrophobic (hydrophobicity sores of ~26 and ~23, resp.) active site implying that designing CAIs with long flexible tails of a more hydrophobic nature may be beneficial to induce desired selective binding (Table 4). Notably, this attribute of the CA IX active-site coupled with its extracellular location provides an avenue to (1) design more hydrophobic CAIs that favor CA IX binding over other extracellular CAs and (2) engineer more bulky CAIs such that membrane permeability becomes poor thus eliminating the potential for CA II inhibition.

In order to design new isoform specific inhibitors that circumvent off-target CA inhibition, the structural dissimilarities that exist between the isoforms, particularly in the *selective pocket*, can be exploited. In addition, taking advantage of the global hydrophobic nature of the CA II or CA IX active site cleft provides a method to selective CAI design. It is already known that the sulfonamides are the most potent CAIs and this knowledge has been used to develop what is known as the "tail approach" to aid in the development of new inhibitors [142, 143]. This approach involves the appending of variable "tails" to the scaffolds of aromatic/heterocyclic sulfonamides to elongate the molecule. This allows the inhibitor to interact with amino acids from the middle to the edge of the active site relative to the catalytic zinc, which ultimately vary between different isoforms [106]. Small molecules such as phenols (Figure 8(c)) and coumarin (Figure 8(d)) also exhibit this same property by directly interacting with residues of the *selective pocket*.

4. Conclusions

A comparison of the conserved and nonconserved regions in the CA catalytic-site between isoforms revealed areas that can be exploited for rational design of selective CAIs. Specifically, highly variable areas amongst active site residues occur outwardly relative to the catalytic zinc in what has been defined as the *selective pocket*. Sequence alignments show that residues in positions 67, 91, and 131 vary between isoforms and structural analysis of CA II in complex with various inhibitors, show that "tails" of inhibitors make extensive contacts with these residues (Figures 5 and 8). Residues at position 91 seem to have the highest variability, in terms of specific residues type and between amino acid properties (i.e., hydrophilicity/hydrophobicity) between isoforms (Table 3). Interestingly, it is observed that CA II and IX exhibit the most hydrophobic catalytic domain and are the only isoforms (with exception to CA I and XIV) that contain hydrophobic residues at this position as well (Leu91 in CA IX). Position 91 can be termed a "hot-spot" for the design of isoform specific inhibitors, such that it contains both high variations between physical properties of amino acid, but (in the case of CA II and IX) there is also observable variation specific side-chain associated with the residues in this position. This attributes position 91 as being a key area that can be exploited by specific chemotypes and thus provides an alternative path for the design of selective CAIs. Overall, it is observed in Figure 8(b) that the residues farthest from the catalytic

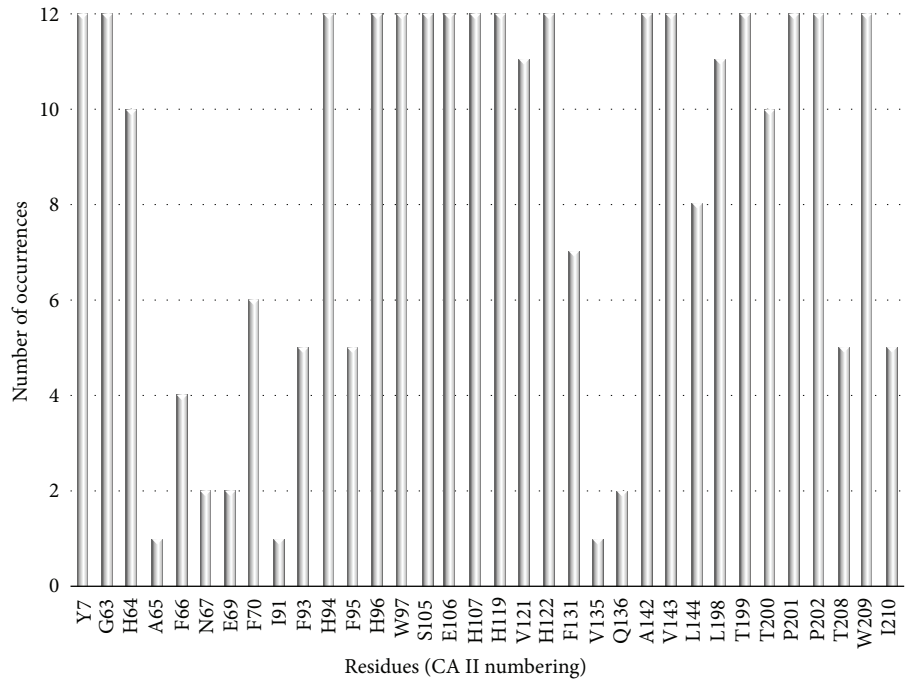

Figure 7: Bar graph of active site residues in the catalytic CA isozymes (CA II numbering).

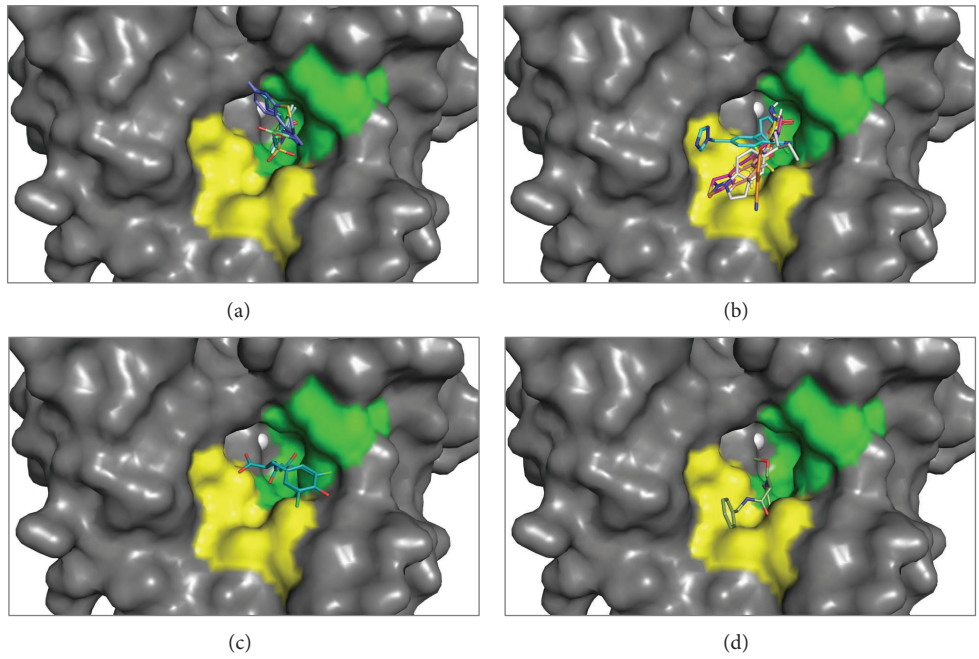

Figure 8: CA inhibitor: (a) several inhibitors binding in the conserved region (green) of CA II's active site. These inhibitors are buried in the active site and are stabilized predominantly by hydrophobic residues (b). Several inhibitors occupying the "selective pocket" (yellow) of CA II. The tails of these inhibitors are extending out of the active site. (c) Coumarin binding on the perimeter of the active site. (d) Phenol binding in the proximity of the active site.

domain (relative to the zinc) remain the least conserved. This provides an exceptional advantage to the rational design of isoform specific inhibitors in that these variable regions can also be exploited by specific chemotypes. This notion is analogous to the idea of utilizing sulfonamide inhibitors with variable "tail" regions for isoform selective inhibitor development however in this study we have presented a more guided approach to this method of CAI design [106].

In summary our observations provide a template to exploit the variable regions of the catalytic domains of

different CA isoforms. These guidelines can be utilized for the development of classical and nonclassical CAIs to overcome the potential of off-target CA inhibition and further lead to the development of more selective CAIs that can be employed in the clinic.

Conflict of Interests

The authors declare that there is no conflict of interests regarding the publication of this paper.

Authors' Contribution

Melissa A. Pinard and Brian Mahon have contributed equally to this study.

Acknowledgments

The authors would like to acknowledge all the contributions of the carbonic anhydrase field that allowed for this study, especially Dr. David Silverman and Dr. Claudiu Supuran. This study was funded in part by the National Institutes of Health Grant GM25154.

References

[1] J. F. Domsic, B. S. Avvaru, U. K. Chae et al., "Entrapment of carbon dioxide in the active site of carbonic anhydrase II," *Journal of Biological Chemistry*, vol. 283, no. 45, pp. 30766–30771, 2008.

[2] B. S. Avvaru, C. U. Kim, K. H. Sippel et al., "A short, strong hydrogen bond in the active site of human carbonic anhydrase II," *Biochemistry*, vol. 49, no. 2, pp. 249–251, 2010.

[3] M. Aggarwal, C. D. Boone, B. Kondeti, and R. McKenna, "Structural annotation of human carbonic anhydrases," *Journal of Enzyme Inhibition and Medicinal Chemistry*, vol. 28, no. 2, pp. 267–277, 2013.

[4] V. M. Krishnamurthy, G. K. Kaufman, A. R. Urbach et al., "Carbonic anhydrase as a model for biophysical and physical-organic studies of proteins and protein-ligand binding," *Chemical Reviews*, vol. 108, no. 3, pp. 946–1051, 2008.

[5] J. Květoň, W. R. Chegwidden, N. D. Carter, and Y. H. Edwards, Eds., *The Carbonic Anhydrases: New Horizons*, vol. 39, Photosynthetica, 2001.

[6] R. S. Rowlett, "Structure and catalytic mechanism of the β-carbonic anhydrases," *Biochimica et Biophysica Acta—Proteins and Proteomics*, vol. 1804, no. 2, pp. 362–373, 2010.

[7] K. S. Smith and J. G. Ferry, "Prokaryotic carbonic anhydrases," *FEMS Microbiology Reviews*, vol. 24, no. 4, pp. 335–366, 2000.

[8] S. del Prete, D. Vullo, V. de Luca, C. T. Supuran, and C. Capasso, "Biochemical characterization of the δ-carbonic anhydrase from the marine diatom Thalassiosira weissflogii, TweCA," *Journal of Enzyme Inhibition and Medicinal Chemistry*, 2014.

[9] V. Alterio, A. Di Fiore, K. D'Ambrosio, C. T. Supuran, and G. de Simone, "Multiple binding modes of inhibitors to carbonic anhydrases: how to design specific drugs targeting 15 different isoforms?" *Chemical Reviews*, vol. 112, no. 8, pp. 4421–4468, 2012.

[10] S. C. Frost, "Physiological functions of the alpha class of carbonic anhydrases," *Sub-Cellular Biochemistry*, vol. 75, pp. 9–30, 2014.

[11] A. Aspatwar, M. E. E. Tolvanen, C. Ortutay, and S. Parkkila, "Carbonic anhydrase related protein VIII and its role in neurodegeneration and cancer," *Current Pharmaceutical Design*, vol. 16, no. 29, pp. 3264–3276, 2010.

[12] A. E. Eriksson, T. A. Jones, and A. Liljas, "Refined structure of human carbonic anhydrase II at 2.0 Å resolution," *Proteins: Structure, Function and Genetics*, vol. 4, no. 4, pp. 274–282, 1988.

[13] Y. Pocker and S. Sarkanen, "Carbonic anhydrase: structure catalytic versatility, and inhibition," *Advances in Enzymology and Related Areas of Molecular Biology*, vol. 47, pp. 149–274, 1978.

[14] S. Z. Fisher, C. M. Maupin, M. Budayova-Spano et al., "Atomic crystal and molecular dynamics simulation structures of human carbonic anhydrase II: insights into the proton transfer mechanism," *Biochemistry*, vol. 46, no. 11, pp. 2930–2937, 2007.

[15] C. D. Boone, M. Pinard, R. McKenna, and D. Silverman, "Catalytic mechanism of α-class carbonic anhydrases: CO_2 hydration and proton transfer," *Sub-cellular biochemistry*, vol. 75, pp. 31–52, 2014.

[16] C. T. Supuran, A. Scozzafava, and A. Casini, "Carbonic anhydrase inhibitors," *Medicinal Research Reviews*, vol. 23, no. 2, pp. 146–189, 2003.

[17] C. Tu, D. N. Silverman, C. Forsman, B.-H. Jonsson, and S. Lindskog, "Role of histidine 64 in the catalytic mechanism of human carbonic anhydrase II studied with a site-specific mutant," *Biochemistry*, vol. 28, no. 19, pp. 7913–7918, 1989.

[18] R. Mikulski, D. West, K. H. Sippel et al., "Water networks in fast proton transfer during catalysis by human carbonic anhydrase II," *Biochemistry*, vol. 52, no. 1, pp. 125–131, 2013.

[19] C. Tu, G. Sanyal, G. C. Wynns, and D. N. Silverman, "The pH dependence of the hydration of CO_2 catalyzed by carbonic anhydrase III from skeletal muscle of the cat. Steady state and equilibrium studies," *The Journal of Biological Chemistry*, vol. 258, no. 14, pp. 8867–8871, 1983.

[20] H. An, C. Tu, D. Duda et al., "Chemical rescue in catalysis by human carbonic anhydrases II and III," *Biochemistry*, vol. 41, no. 9, pp. 3235–3242, 2002.

[21] D. N. Silverman, C. K. Tu, and G. C. Wynns, "Role of buffer in catalysis of the hydration of CO_2 by carbonic anhydrase," in *Biophysics and Physiology of Carbon Dioxide*, P. D. C. Bauer, P. D. G. Gros, and P. D. H. Bartels, Eds., pp. 254–61, Springer, Berlin, Germany, 1980.

[22] R. McKenna and C. T. Supuran, "Carbonic anhydrase inhibitors drug design," *Sub-Cellular Biochemistry*, vol. 75, pp. 291–323, 2014.

[23] T. H. Maren and E. R. Swenson, "A comparative study of the kinetics of the Bohr effect in vertebrates," *Journal of Physiology*, vol. 303, pp. 535–547, 1980.

[24] D. Brown, T. Kumpulainen, J. Roth, and L. Orci, "Immunohistochemical localization of carbonic anhydrase in postnatal and adult rat kidney," *The American Journal of Physiology*, vol. 245, no. 1, pp. F110–F118, 1983.

[25] K. M. Gilmour, "Perspectives on carbonic anhydrase," *Comparative Biochemistry and Physiology: A Molecular and Integrative Physiology*, vol. 157, no. 3, pp. 193–197, 2010.

[26] J. W. Vince and R. A. Reithmeier, "Carbonic anhydrase II binds to the carboxyl terminus of human band 3, the erythrocyte Cl-/HCO3- exchanger," *The Journal of Biological Chemistry*, vol. 273, no. 43, pp. 28430–28437, 1998.

[27] A. Pushkin, N. Abuladze, E. Gross et al., "Molecular mechanism of kNBC1—carbonic anhydrase II interaction in proximal tubule cells," *The Journal of Physiology*, vol. 559, no. 1, pp. 55–65, 2004.

[28] X. Li, B. Alvarez, J. R. Casey, R. A. F. Reithmeier, and L. Fliegel, "Carbonic anhydrase II binds to and enhances activity of the Na^+/H^+ exchanger," *The Journal of Biological Chemistry*, vol. 277, no. 39, pp. 36085–36091, 2002.

[29] H. L. McMurtrie, H. J. Cleary, B. V. Alvarez et al., "The bicarbonate transport metabolon," *Journal of Enzyme Inhibition and Medicinal Chemistry*, vol. 19, no. 3, pp. 231–236, 2004.

[30] W. S. Sly, D. Hewett-Emmett, M. P. Whyte, Y. S. Yu, and R. E. Tashian, "Carbonic anhydrase II deficiency identified as the primary defect in the autosomal recessive syndrome of osteopetrosis with renal tubular acidosis and cerebral calcification," *Proceedings of the National Academy of Sciences of the United States of America*, vol. 80, no. 9, pp. 2752–2756, 1983.

[31] R. P. Henry and E. R. Swenson, "The distribution and physiological significance of carbonic anhydrase in vertebrate gas exchange organs," *Respiration Physiology*, vol. 121, no. 1, pp. 1–12, 2000.

[32] G. J. Cooper and W. F. Boron, "Effect of PCMBS on CO_2 permeability of xenopus oocytes expressing aquaporin 1 or its C189S mutant," *The American Journal of Physiology*, vol. 275, no. 6, pp. C1481–C1486, 1998.

[33] N. D. Carter, "Hormonal and neuronal control of carbonic anhydrase III gene expression in skeletal muscle," in *The Carbonic Anhydrases: Cellular Physiology and Molecular Genetics*, S. J. Dodgson, R. E. Tashian, G. Gross, and N. D. Carter, Eds., pp. 247–256, Plenum Press, New York, NY, USA, 1991.

[34] L. W. Stanton, P. A. Ponte, R. T. Coleman, and M. A. Snyder, "Expression of CA III in rodent models of obesity," *Molecular Endocrinology*, vol. 5, no. 6, pp. 860–866, 1991.

[35] G. E. Lyons, M. E. Buckingham, S. Tweedie, and Y. H. Edwards, "Carbonic anhydrase III, an early mesodermal marker, is expressed in embryonic mouse skeletal muscle and notochord," *Development*, vol. 111, no. 1, pp. 233–244, 1991.

[36] C. T. Supuran, "Carbonic anhydrases—an overview," *Current Pharmaceutical Design*, vol. 14, no. 7, pp. 603–614, 2008.

[37] Y.-C. Chai, C.-H. Jung, C.-K. Lii et al., "Identification of an abundant S-thiolated rat liver protein as carbonic anhydrase III; characterization of S-thiolation and dethiolation reactions," *Archives of Biochemistry and Biophysics*, vol. 284, no. 2, pp. 270–278, 1991.

[38] M. C. Mitterberger, G. Kim, U. Rostek, R. L. Levine, and W. Zwerschke, "Carbonic anhydrase III regulates peroxisome proliferator-activated receptor-γ2," *Experimental Cell Research*, vol. 318, no. 8, pp. 877–886, 2012.

[39] F. Bootorabi, J. Jänis, E. Smith et al., "Analysis of a shortened form of human carbonic anhydrase VII expressed in vitro compared to the full-length enzyme," *Biochimie*, vol. 92, no. 8, pp. 1072–1080, 2010.

[40] E. Truppo, C. T. Supuran, A. Sandomenico et al., "Carbonic anhydrase VII is S-glutathionylated without loss of catalytic activity and affinity for sulfonamide inhibitors," *Bioorganic and Medicinal Chemistry Letters*, vol. 22, no. 4, pp. 1560–1564, 2012.

[41] A. Thiry, J.-M. Dogné, C. T. Supuran, and B. Masereel, "Carbonic anhydrase inhibitors as anticonvulsant agents," *Current Topics in Medicinal Chemistry*, vol. 7, no. 9, pp. 855–864, 2007.

[42] E. Ruusuvuori, H. Li, K. Huttu et al., "Carbonic anhydrase isoform VII acts as a molecular switch in the development of synchronous gamma-frequency firing of hippocampal CA1 pyramidal cells," *The Journal of Neuroscience*, vol. 24, no. 11, pp. 2699–2707, 2004.

[43] M. Asiedu, M. H. Ossipov, K. Kaila, and T. J. Price, "Acetazolamide and midazolam act synergistically to inhibit neuropathic pain," *Pain*, vol. 148, no. 2, pp. 302–308, 2010.

[44] J. Lehtonen, B. Shen, M. Vihinen et al., "Characterization of CA XIII, a novel member of the carbonic anhydrase isozyme family," *Journal of Biological Chemistry*, vol. 279, no. 4, pp. 2719–2727, 2004.

[45] L. Kummola, J. M. Hämäläinen, J. Kivelä et al., "Expression of a novel carbonic anhydrase, CA XIII, in normal and neoplastic colorectal mucosa," *BMC Cancer*, vol. 5, article 41, 2005.

[46] G. N. Shah, D. Hewett-Emmett, J. H. Grubb et al., "Mitochondrial carbonic anhydrase CA VB: differences in tissue distribution and pattern of evolution from chose of CA VA suggest distinct physiological roles," *Proceedings of the National Academy of Sciences of the United States of America*, vol. 97, no. 4, pp. 1677–1682, 2000.

[47] C. J. Lusty, "Carbamyl phosphate synthetase. Bicarbonate-dependent hydrolysis of ATP and potassium activation," *The Journal of Biological Chemistry*, vol. 253, no. 12, pp. 4270–4278, 1978.

[48] S. J. Dodgson and R. E. Forster II, "Inhibition of CA V decreases glucose synthesis from pyruvate," *Archives of Biochemistry and Biophysics*, vol. 251, no. 1, pp. 198–204, 1986.

[49] C. J. Lynch, H. Fox, S. A. Hazen, B. A. Stanley, S. Dodgson, and K. F. Lanoue, "Role of hepatic carbonic anhydrase in de novo lipogenesis," *Biochemical Journal*, vol. 310, part 1, pp. 197–202, 1995.

[50] K. J. Oommen and S. Mathews, "Zonisamide: a new antiepileptic drug," *Clinical Neuropharmacology*, vol. 22, no. 4, pp. 192–200, 1999.

[51] Y. Ogawa, K. Matsumoto, T. Maeda et al., "Characterization of lacrimal gland carbonic anhydrase VI," *Journal of Histochemistry and Cytochemistry*, vol. 50, no. 6, pp. 821–827, 2002.

[52] J. S. Leinonen, K. A. Saari, J. M. Seppänen, H. M. Myllylä, and H. J. Rajaniemi, "Immunohistochemical demonstration of carbonic anhydrase isoenzyme VI (CA VI) expression in rat lower airways and lung," *Journal of Histochemistry and Cytochemistry*, vol. 52, no. 8, pp. 1107–1112, 2004.

[53] M. Kaseda, N. Ichihara, T. Nishita, H. Amasaki, and M. Asari, "Immunohistochemistry of the bovine secretory carbonic anhydrase isozyme (CA-VI) in bovine alimentary canal and major salivary glands," *Journal of Veterinary Medical Science*, vol. 68, no. 2, pp. 131–135, 2006.

[54] C. E. Smith, A. Nanci, and P. Moffatt, "Evidence by signal peptide trap technology for the expression of carbonic anhydrase 6 in rat incisor enamel organs," *European Journal of Oral Sciences*, vol. 114, supplement 1, pp. 147–153, 2006.

[55] J. Breiner Feldstein and D. N. Silverman, "Purification and characterization of carbonic anhydrase from the saliva of the rat," *Journal of Biological Chemistry*, vol. 259, no. 9, pp. 5447–5453, 1984.

[56] J. A. Ship, "Diabetes and oral health: an overview," *Journal of the American Dental Association (1939)*, vol. 134, Spec No:4S–10S, 2003.

[57] F. J. Dowd, "Saliva and dental caries," *Dental clinics of North America*, vol. 43, no. 4, pp. 579–597, 1999.

[58] M. Kimoto, M. Kishino, Y. Yura, and Y. Ogawa, "A role of salivary carbonic anhydrase VI in dental plaque," *Archives of Oral Biology*, vol. 51, no. 2, pp. 117–122, 2006.

[59] Ortho-McNeil-Janssen Pharmaceuticals I, Topomax: drug summary, physicians' desk reference, 2013.

[60] A. R. Shatzman and R. I. Henkin, "Gustin concentration changes relative to salivary zinc and taste in humans," *Proceedings of the National Academy of Sciences of the United States of America*, vol. 78, no. 6 I, pp. 3867–3871, 1981.

[61] X. L. Zhu and W. S. Sly, "Carbonic anhydrase IV from human lung. Purification, characterization, and comparison with membrane carbonic anhydrase from human kidney," *Journal of Biological Chemistry*, vol. 265, no. 15, pp. 8795–8801, 1990.

[62] Z. Yang, B. V. Alvarez, C. Chakarova et al., "Mutant carbonic anhydrase 4 impairs pH regulation and causes retinal photoreceptor degeneration," *Human Molecular Genetics*, vol. 14, no. 2, pp. 255–265, 2005.

[63] G. Rebello, R. Ramesar, A. Vorster et al., "Apoptosis-inducing signal sequence mutation in carbonic anhydrase IV identified in patients with the RP17 form of retinitis pigmentosa," *Proceedings of the National Academy of Sciences of the United States of America*, vol. 101, no. 17, pp. 6617–6622, 2004.

[64] S. Ivanov, S.-Y. Liao, A. Ivanova et al., "Expression of hypoxia-inducible cell-surface transmembrane carbonic anhydrases in human cancer," *American Journal of Pathology*, vol. 158, no. 3, pp. 905–919, 2001.

[65] S. Pastoreková, S. Parkkila, A.-K. Parkkila et al., "Carbonic anhydrase IX, MN/CA IX: analysis of stomach complementary DNA sequence and expression in human and rat alimentary tracts," *Gastroenterology*, vol. 112, no. 2, pp. 398–408, 1997.

[66] Y. Lou, P. C. McDonald, A. Oloumi et al., "Targeting tumor hypoxia: suppression of breast tumor growth and metastasis by novel carbonic anhydrase IX inhibitors," *Cancer Research*, vol. 71, pp. 3364–3376, 2011.

[67] P. Swietach, A. Hulikova, R. D. Vaughan-Jones, and A. L. Harris, "New insights into the physiological role of carbonic anhydrase IX in tumour pH regulation," *Oncogene*, vol. 29, no. 50, pp. 6509–6521, 2010.

[68] S. Parkkila, H. Rajaniemi, A.-K. Parkkila et al., "Carbonic anhydrase inhibitor suppresses invasion of renal cancer cells *in vitro*," *Proceedings of the National Academy of Sciences of the United States of America*, vol. 97, no. 5, pp. 2220–2224, 2000.

[69] N. Robertson, C. Potter, and A. L. Harris, "Role of carbonic anhydrase IX in human tumor cell growth, survival, and invasion," *Cancer Research*, vol. 64, no. 17, pp. 6160–6165, 2004.

[70] E. Švastová, N. Žilka, M. Zaťovičová et al., "Carbonic anhydrase IX reduces E-cadherin-mediated adhesion of MDCK cells via interaction with β-catenin," *Experimental Cell Research*, vol. 290, no. 2, pp. 332–345, 2003.

[71] C. C. Wykoff, N. J. P. Beasley, P. H. Watson et al., "Hypoxia-inducible expression of tumor-associated carbonic anhydrases," *Cancer Research*, vol. 60, no. 24, pp. 7075–7083, 2000.

[72] S. K. Chia, C. C. Wykoff, P. H. Watson et al., "Prognostic significance of a novel hypoxia-regulated marker, carbonic anhydrase IX, in invasive breast carcinoma," *The American Society of Clinical Oncology: Journal of Clinical Oncology*, vol. 19, no. 16, pp. 3660–3668, 2001.

[73] D. Generali, S. B. Fox, A. Berruti et al., "Role of carbonic anhydrase IX expression in prediction of the efficacy and outcome of primary epirubicin/tamoxifen therapy for breast cancer," *Endocrine-Related Cancer*, vol. 13, no. 3, pp. 921–930, 2006.

[74] C. J. Creighton, K. E. Cordero, J. M. Larios et al., "Genes regulated by estrogen in breast tumor cells in vitro are similarly regulated in vivo in tumor xenografts and human breast tumors," *Genome Biology*, vol. 7, no. 4, article R28, 2006.

[75] K. Nordfors, J. Haapasalo, M. Korja et al., "The tumour-associated carbonic anhydrases CA II, CA IX and CA XII in a group of medulloblastomas and supratentorial primitive neuroectodermal tumours: an association of CA IX with poor prognosis," *BMC Cancer*, vol. 10, article 148, 2010.

[76] M. I. Ilie, V. Hofman, C. Ortholan et al., "Overexpression of carbonic anhydrase XII in tissues from resectable non-small cell lung cancers is a biomarker of good prognosis," *International Journal of Cancer*, vol. 128, no. 7, pp. 1614–1623, 2011.

[77] M.-H. Chien, T.-H. Ying, Y.-H. Hsieh et al., "Tumor-associated carbonic anhydrase XII is linked to the growth of primary oral squamous cell carcinoma and its poor prognosis," *Oral Oncology*, vol. 48, no. 5, pp. 417–423, 2012.

[78] S. Parkkila, H. Rajaniemi, A.-K. Parkkila et al., "Carbonic anhydrase inhibitor suppresses invasion of renal cancer cells in vitro," *Proceedings of the National Academy of Sciences of the United States of America*, vol. 97, no. 5, pp. 2220–2224, 2000.

[79] P. Hynninen, S. Parkkila, H. Huhtala et al., "Carbonic anhydrase isozymes II, IX, and XII in uterine tumors," *APMIS*, vol. 120, no. 2, pp. 117–129, 2012.

[80] A. Kivela, S. Parkkila, J. Saarnio et al., "Expression of a novel transmembrane carbonic anhydrase isozyme XII in normal human gut and colorectal tumors," *The American Journal of Pathology*, vol. 156, no. 2, pp. 577–584, 2000.

[81] E. Muhammad, N. Leventhal, G. Parvari et al., "Autosomal recessive hyponatremia due to isolated salt wasting in sweat associated with a mutation in the active site of *Carbonic Anhydrase* 12," *Human Genetics*, vol. 129, no. 4, pp. 397–405, 2011.

[82] K. Fujikawa-Adachi, I. Nishimori, T. Taguchi, and S. Onishi, "Human carbonic anhydrase XIV (*CA14*): cDNA cloning, mRNA expression, and mapping to chromosome 1," *Genomics*, vol. 61, no. 1, pp. 74–81, 1999.

[83] J. D. Ochrietor, M. F. Clamp, T. P. Moroz et al., "Carbonic anhydrase XIV identified as the membrane CA in mouse retina: strong expression in Müller cells and the RPE," *Experimental Eye Research*, vol. 81, no. 4, pp. 492–500, 2005.

[84] K. Kaunisto, S. Parkkila, H. Rajaniemi, A. Waheed, J. Grubb, and W. S. Sly, "Carbonic anhydrase XIV: luminal expression suggests key role in renal acidification," *Kidney International*, vol. 61, no. 6, pp. 2111–2118, 2002.

[85] C. Juel, C. Lundby, M. Sander, J. A. L. Calbet, and G. van Hall, "Human skeletal muscle and erythrocyte proteins involved in acid-base homeostasis: adaptations to chronic hypoxia," *Journal of Physiology*, vol. 548, no. 2, pp. 639–648, 2003.

[86] L. A. Vargas and B. V. Alvarez, "Carbonic anhydrase XIV in the normal and hypertrophic myocardium," *Journal of Molecular and Cellular Cardiology*, vol. 52, no. 3, pp. 741–752, 2012.

[87] P. Linser and A. A. Moscona, "Variable CA II compartmentalization in vertebrate retina," *Annals of the New York Academy of Sciences*, vol. 429, pp. 430–446, 1984.

[88] C. T. Supuran, "Carbonic anhydrases: novel therapeutic applications for inhibitors and activators," *Nature Reviews Drug Discovery*, vol. 7, no. 2, pp. 168–181, 2008.

[89] C. T. Supuran, "Carbonic anhydrase inhibitors: an editorial," *Expert Opinion on Therapeutic Patents*, vol. 23, no. 6, pp. 677–679, 2013.

[90] M. Eichhorn, "Mode of action, clinical profile and relevance of carbonic anhydrase inhibitors in glaucoma therapy," *Klinische*

Monatsblatter fur Augenheilkunde, vol. 230, no. 2, pp. 146–149, 2013.

[91] I. Nishimori, D. Vullo, A. Innocenti, A. Scozzafava, A. Mastrolorenzo, and C. T. Supuran, "Carbonic anhydrase inhibitors. The mitochondrial isozyme VB as a new target for sulfonamide and sulfamate inhibitors," *Journal of Medicinal Chemistry*, vol. 48, no. 24, pp. 7860–7866, 2005.

[92] I. Nishimori, T. Minakuchi, S. Onishi, D. Vullo, A. Scozzafava, and C. T. Supuran, "Carbonic anhydrase inhibitors. DNA cloning, characterization, and inhibition studies of the human secretory isoform VI, a new target for sulfonamide and sulfamate inhibitors," *Journal of Medicinal Chemistry*, vol. 50, no. 2, pp. 381–388, 2007.

[93] E. S. Pilka, G. Kochan, U. Oppermann, and W. W. Yue, "Crystal structure of the secretory isozyme of mammalian carbonic anhydrases CA VI: implications for biological assembly and inhibitor development," *Biochemical and Biophysical Research Communications*, vol. 419, no. 3, pp. 485–489, 2012.

[94] D. Vullo, J. Voipio, A. Innocenti et al., "Carbonic anhydrase inhibitors. Inhibition of the human cytosolic isozyme VII with aromatic and heterocyclic sulfonamides," *Bioorganic & Medicinal Chemistry Letters*, vol. 15, no. 4, pp. 971–976, 2005.

[95] R. Gao, S. Liao, C. Zhang et al., "Optimization of heterocyclic substituted benzenesulfonamides as novel carbonic anhydrase IX inhibitors and their structure activity relationship," *European Journal of Medicinal Chemistry*, vol. 62, pp. 597–604, 2013.

[96] D. A. Whittington, A. Waheed, B. Ulmasov et al., "Crystal structure of the dimeric extracellular domain of human carbonic anhydrase XII, a bitopic membrane protein overexpressed in certain cancer tumor cells," *Proceedings of the National Academy of Sciences of the United States of America*, vol. 98, no. 17, pp. 9545–9550, 2001.

[97] D. A. Whittington, J. H. Grubb, A. Waheed, G. N. Shah, W. S. Sly, and D. W. Christianson, "Expression, assay, and structure of the extracellular domain of murine carbonic anhydrase XIV: implications for selective inhibition of membrane-associated isozymes," *The Journal of Biological Chemistry*, vol. 279, no. 8, pp. 7223–7228, 2004.

[98] J. D. Thompson, D. G. Higgins, and T. J. Gibson, "CLUSTAL W: improving the sensitivity of progressive multiple sequence alignment through sequence weighting, position-specific gap penalties and weight matrix choice," *Nucleic Acids Research*, vol. 22, no. 22, pp. 4673–4680, 1994.

[99] M. A. Larkin, G. Blackshields, N. P. Brown et al., "Clustal W and Clustal X version 2.0," *Bioinformatics*, vol. 23, no. 21, pp. 2947–2948, 2007.

[100] P. Emsley and K. Cowtan, "Coot: model-building tools for molecular graphics," *Acta Crystallographica Section D: Biological Crystallography*, vol. 60, no. 1, pp. 2126–2132, 2004.

[101] The PyMOL Molecular Graphics System, Version 1.5.0.4 Schrödinger, LLC.n.d.

[102] J. Kyte and R. F. Doolittle, "A simple method for displaying the hydropathic character of a protein," *Journal of Molecular Biology*, vol. 157, no. 1, pp. 105–132, 1982.

[103] A. J. Esbaugh and B. L. Tufts, "The structure and function of carbonic anhydrase isozymes in the respiratory system of vertebrates," *Respiratory Physiology and Neurobiology*, vol. 154, no. 1-2, pp. 185–198, 2006.

[104] E. R. Swenson, "Respiratory and renal roles of carbonic anhydrase in gas exchange and acid-base regulation," *EXS*, no. 90, pp. 281–341, 2000.

[105] M. A. Pinard, C. D. Boone, B. D. Rife, C. T. Supuran, and R. McKenna, "Structural study of interaction between brinzolamide and dorzolamide inhibition of human carbonic anhydrases," *Bioorganic and Medicinal Chemistry*, vol. 21, no. 22, pp. 7210–7215, 2013.

[106] M. Aggarwal, B. Kondeti, and R. McKenna, "Insights towards sulfonamide drug specificity in α-carbonic anhydrases," *Bioorganic and Medicinal Chemistry*, vol. 21, no. 6, pp. 1526–1533, 2013.

[107] S. Lindskog, "Structure and mechanism of Carbonic Anhydrase," *Pharmacology and Therapeutics*, vol. 74, no. 1, pp. 1–20, 1997.

[108] C. T. Supuran and J.-Y. Winum, *Drug Design of Zinc-Enzyme Inhibitors: Functional, Structural, and Disease Applications*, John Wiley & Sons, 2009.

[109] C. Temperini, A. Scozzafava, and C. T. Supuran, "Carbonic anhydrase inhibitors. X-ray crystal studies of the carbonic anhydrase II-trithiocarbonate adduct—an inhibitor mimicking the sulfonamide and urea binding to the enzyme," *Bioorganic and Medicinal Chemistry Letters*, vol. 20, no. 2, pp. 474–478, 2010.

[110] B. M. Jönsson, K. Håkansson, and A. Liljas, "The structure of human carbonic anhydrase II in complex with bromide and azide," *FEBS Letters*, vol. 322, no. 2, pp. 186–190, 1993.

[111] S. Mangani and K. Håkansson, "Crystallographic studies of the binding of protonated and unprotonated inhibitors to carbonic anhydrase using hydrogen sulphide and nitrate anions," *European Journal of Biochemistry*, vol. 210, no. 3, pp. 867–871, 1992.

[112] K. Hakansson, M. Carlsson, L. A. Svensson, and A. Liljas, "Structure of native and apo carbonic anhydrase II and structure of some of its anion-ligand complexes," *Journal of Molecular Biology*, vol. 227, no. 4, pp. 1192–1204, 1992.

[113] C. T. Supuran and A. Scozzafava, "Carbonic-anhydrase inhibitors and their therapeutic potential," *Expert Opinion on Therapeutic Patents*, vol. 10, no. 5, pp. 575–600, 2000.

[114] S. K. Nair, P. A. Ludwig, and D. W. Christianson, "Two-site binding of phenol in the active site of human carbonic anhydrase II: structural implications for substrate association," *Journal of the American Chemical Society*, vol. 116, no. 8, pp. 3659–3660, 1994.

[115] *Dictionary of Natural Products (DVD)*, vol. version 21.1., CRC & Taylor & Francis, 2012.

[116] A. Maresca, C. Temperini, H. Vu et al., "Non-zinc mediated inhibition of carbonic anhydrases: coumarins are a new class of suicide inhibitors," *Journal of the American Chemical Society*, vol. 131, no. 8, pp. 3057–3062, 2009.

[117] A. Maresca, C. Temperini, L. Pochet, B. Masereel, A. Scozzafava, and C. T. Supuran, "Deciphering the mechanism of carbonic anhydrase inhibition with coumarins and thiocoumarins," *Journal of Medicinal Chemistry*, vol. 53, no. 1, pp. 335–344, 2010.

[118] F. Carta, C. Temperini, A. Innocenti, A. Scozzafava, K. Kaila, and C. T. Supuran, "Polyamines inhibit carbonic anhydrases by anchoring to the zinc-coordinated water molecule," *Journal of Medicinal Chemistry*, vol. 53, no. 15, pp. 5511–5522, 2010.

[119] M. Lopez, B. Paul, A. Hofmann et al., "S-glycosyl primary sulfonamides—a new structural class for selective inhibition of cancer-associated carbonic anhydrases," *Journal of Medicinal Chemistry*, vol. 52, no. 20, pp. 6421–6432, 2009.

[120] O. M. Rodríguez, A. Maresca, C. A. Témpera, R. D. Bravo, P. A. Colinas, and C. T. Supuran, "N-β-glycosyl sulfamides are selective inhibitors of the cancer associated carbonic anhydrase

isoforms IX and XII," *Bioorganic and Medicinal Chemistry Letters*, vol. 21, no. 15, pp. 4447–4450, 2011.

[121] M. Lopez, J. Trajkovic, L. F. Bornaghi et al., "Design, synthesis, and biological evaluation of novel carbohydrate-based sulfamates as carbonic anhydrase inhibitors," *Journal of Medicinal Chemistry*, vol. 54, no. 5, pp. 1481–1489, 2011.

[122] L. L. Woo, A. Purohit, B. Malini, M. J. Reed, and B. V. Potter, "Potent active site-directed inhibition of steroid sulphatase by tricyclic coumarin-based sulphamates," *Chemistry & Biology*, vol. 7, no. 10, pp. 773–791, 2000.

[123] V. Askoxylakis, R. Garcia-Boy, S. Rana et al., "A new peptide ligand for targeting human carbonic anhydrase IX, identified through the phage display technology," *PLoS ONE*, vol. 5, no. 12, Article ID e15962, 2010.

[124] Y. Li, H. Wang, E. Oosterwijk et al., "Antibody-specific detection of CAIX in breast and prostate cancers," *Biochemical and Biophysical Research Communications*, vol. 386, no. 3, pp. 488–492, 2009.

[125] D. Dekaminaviciute, V. Kairys, M. Zilnyte et al., "Monoclonal antibodies raised against 167-180 aa sequence of human carbonic anhydrase XII inhibit its enzymatic activity," *Journal of Enzyme Inhibition and Medicinal Chemistry*, 2014.

[126] F. Carta, M. Aggarwal, A. Maresca, A. Scozzafava, R. McKenna, and C. T. Supuran, "Dithiocarbamates: a new class of carbonic anhydrase inhibitors. Crystallographic and kinetic investigations," *Chemical Communications*, vol. 48, no. 13, pp. 1868–1870, 2012.

[127] F. Carta, M. Aggarwal, A. Maresca et al., "Dithiocarbamates strongly inhibit carbonic anhydrases and show antiglaucoma action in vivo," *Journal of Medicinal Chemistry*, vol. 55, no. 4, pp. 1721–1730, 2012.

[128] E. Bayram, M. Senturk, O. Irfan Kufrevioglu, and C. T. Supuran, "In vitro inhibition of salicylic acid derivatives on human cytosolic carbonic anhydrase isozymes I and II," *Bioorganic and Medicinal Chemistry*, vol. 16, no. 20, pp. 9101–9105, 2008.

[129] F. Carta, A. Maresca, A. Scozzafava, and C. T. Supuran, "Novel coumarins and 2-thioxo-coumarins as inhibitors of the tumor-associated carbonic anhydrases IX and XII," *Bioorganic and Medicinal Chemistry*, vol. 20, no. 7, pp. 2266–2273, 2012.

[130] F. Carta, D. Vullo, A. Maresca, A. Scozzafava, and C. T. Supuran, "New chemotypes acting as isozyme-selective carbonic anhydrase inhibitors with low affinity for the offtarget cytosolic isoform II," *Bioorganic and Medicinal Chemistry Letters*, vol. 22, no. 6, pp. 2182–2185, 2012.

[131] A. Maresca and C. T. Supuran, "Coumarins incorporating hydroxy- and chloro-moieties selectively inhibit the transmembrane, tumor-associated carbonic anhydrase isoforms IX and XII over the cytosolic ones i and II," *Bioorganic & Medicinal Chemistry Letters*, vol. 20, no. 15, pp. 4511–4514, 2010.

[132] A. Maresca, A. Scozzafava, and C. T. Supuran, "7,8-Disubstituted- but not 6,7-disubstituted coumarins selectively inhibit the transmembrane, tumor-associated carbonic anhydrase isoforms IX and XII over the cytosolic ones i and II in the low nanomolar/subnanomolar range," *Bioorganic and Medicinal Chemistry Letters*, vol. 20, no. 24, pp. 7255–7258, 2010.

[133] R. A. Davis, D. Vullo, A. Maresca, C. T. Supuran, and S.-A. Poulsen, "Natural product coumarins that inhibit human carbonic anhydrases," *Bioorganic and Medicinal Chemistry*, vol. 21, no. 6, pp. 1539–1543, 2013.

[134] F. Carta, A. Maresca, A. Scozzafava, and C. T. Supuran, "5- and 6-Membered (thio)lactones are prodrug type carbonic anhydrase inhibitors," *Bioorganic and Medicinal Chemistry Letters*, vol. 22, no. 1, pp. 267–270, 2012.

[135] K. Tars, D. Vullo, A. Kazaks et al., "Sulfocoumarins (1,2-benzoxathiine-2,2-dioxides): a class of potent and isoform-selective inhibitors of tumor-associated carbonic anhydrases," *Journal of Medicinal Chemistry*, vol. 56, no. 1, pp. 293–300, 2013.

[136] K. H. Sippel, A. Stander, C. Tu et al., "Characterization of carbonic anhydrase isozyme specific inhibition by sulfamated 2-ethylestra compounds," *Letters in Drug Design and Discovery*, vol. 8, no. 8, pp. 678–684, 2011.

[137] B. A. Stander, F. Joubert, C. Tu, K. H. Sippel, R. McKenna, and A. M. Joubert, "In vitro evaluation of ESE-15-ol, an estradiol analogue with nanomolar antimitotic and carbonic anhydrase inhibitory activity," *PLoS ONE*, vol. 7, no. 12, Article ID e52205, 2012.

[138] G. de Simone and C. T. Supuran, "Carbonic anhydrase IX: biochemical and crystallographic characterization of a novel antitumor target," *Biochimica et Biophysica Acta*, vol. 1804, no. 2, pp. 404–409, 2010.

[139] J. Závada, Z. Závadová, J. Pastorek, Z. Biesovä, J. Ježek, and J. Velek, "Human tumour-associated cell adhesion protein MN/CA IX: identification of M75 epitope and of the region mediating cell adhesion," *British Journal of Cancer*, vol. 82, no. 11, pp. 1808–1813, 2000.

[140] P. Buanne, G. Renzone, F. Monteleone et al., "Characterization of carbonic anhydrase IX interactome reveals proteins assisting its nuclear localization in hypoxic cells," *Journal of Proteome Research*, vol. 12, no. 1, pp. 282–292, 2013.

[141] D. M. Duda, C. Tu, S. Z. Fisher et al., "Human carbonic anhydrase III: structural and kinetic study of catalysis and proton transfer," *Biochemistry*, vol. 44, no. 30, pp. 10046–10053, 2005.

[142] A. Casini, A. Scozzafava, F. Mincione, L. Menabuoni, M. A. Ilies, and C. T. Supuran, "Carbonic anhydrase inhibitors: Water-soluble 4-sulfamoylphenylthioureas as topical intraocular pressure-lowering agents with long-lasting effects," *Journal of Medicinal Chemistry*, vol. 43, no. 25, pp. 4884–4892, 2000.

[143] A. Scozzafava, L. Menabuoni, F. Mincione, and C. T. Supuran, "Carbonic anhydrase inhibitors. A general approach for the preparation of water-soluble sulfonamides incorporating polyamino-polycarboxylate tails and of their metal complexes possessing long-lasting, topical intraocular pressure-lowering properties," *Journal of Medicinal Chemistry*, vol. 45, no. 7, pp. 1466–1476, 2002.

Hindawi Publishing Corporation
BioMed Research International
Volume 2015, Article ID 674920, 10 pages
http://dx.doi.org/10.1155/2015/674920

Research Article

Binding of Carbonic Anhydrase IX to 45S rDNA Genes Is Prevented by Exportin-1 in Hypoxic Cells

Emanuele Sasso,[1,2,3] Monica Vitale,[1,2] Francesca Monteleone,[2,3] Francesca Ludovica Boffo,[1,2] Margherita Santoriello,[1] Daniela Sarnataro,[1,2] Corrado Garbi,[1] Mariangela Sabatella,[1,2] Bianca Crifò,[1,2] Luca Alfredo Paolella,[1,2] Giuseppina Minopoli,[1,2] Jean-Yves Winum,[4] and Nicola Zambrano[1,2,3]

[1] *Dipartimento di Medicina Molecolare e Biotecnologie Mediche, Università di Napoli Federico II, 80131 Napoli, Italy*
[2] *CEINGE Biotecnologie Avanzate, Via Gaetano Salvatore 486, 80145 Napoli, Italy*
[3] *Associazione Culturale DiSciMuS RFC, 80026 Casoria, Italy*
[4] *Institut des Biomolécules Max Mousseron, UMR 5247 CNRS, Université Montpellier I & II, ENSCM, 34296 Montpellier, France*

Correspondence should be addressed to Nicola Zambrano; zambrano@unina.it

Received 27 June 2014; Accepted 9 September 2014

Academic Editor: Vincenzo Alterio

Carbonic anhydrase IX (CA IX) is a surrogate marker of hypoxia, involved in survival and pH regulation in hypoxic cells. We have recently characterized its interactome, describing a set of proteins interacting with CA IX, mainly in hypoxic cells, including several members of the nucleocytoplasmic shuttling apparatuses. Accordingly, we described complex subcellular localization for this enzyme in human cells, as well as the redistribution of a carbonic anhydrase IX pool to nucleoli during hypoxia. Starting from this evidence, we analyzed the possible contribution of carbonic anhydrase IX to transcription of the 45S rDNA genes, a process occurring in nucleoli. We highlighted the binding of carbonic anhydrase IX to nucleolar chromatin, which is regulated by oxygen levels. In fact, CA IX was found on 45S rDNA gene promoters in normoxic cells and less represented on these sites, in hypoxic cells and in cells subjected to acetazolamide-induced acidosis. Both conditions were associated with increased representation of carbonic anhydrase IX/exportin-1 complexes in nucleoli. 45S rRNA transcript levels were accordingly downrepresented. Inhibition of nuclear export by leptomycin B suggests a model in which exportin-1 acts as a decoy, in hypoxic cells, preventing carbonic anhydrase IX association with 45S rDNA gene promoters.

1. Introduction

Reprogrammed energy metabolism was considered among the emerging hallmarks in cancer [1]. Cancer cells developing inside a hypoxic environment, but also cancer cells exposed to normal oxygen levels, switch energetic metabolism towards glycolysis. Thus, gene expression programmes mediated by HIF1α transcription factor allow cells to increase the efficiency of glycolysis via enhanced ability to uptake glucose, via stimulation of glycolytic enzymes, and via increased ability to buffer the acidic, pyruvate- and lactate-enriched intracellular environment. The carbonic anhydrases (CAs), a large family of metalloenzymes with wide subcellular distributions, are central to the adaptation of the cancer cells to the glycolytic switch. Namely, CA IX, a membrane carbonic anhydrase possessing an extracellular catalytic domain, is actively involved in the acidification of extracellular space, as a consequence of the need for buffering the intracellular compartments [2, 3]. Cancer cells may also take advantage from the acidic features of their extracellular space, since it may enhance invasiveness potential [4].

CA IX structure was recently defined [5]; these authors proposed a dimeric assembly for the enzyme, exposing a highly glycosylated proteoglycan-like domain and the catalytic domain towards the extracellular compartment, and a short C-terminal tail exposed to the intracellular environment. These regions are separated by a single transmembrane helical region. An intact intracellular domain is required for

extracellular acidification by CA IX [6], implying that its interactions with intracellular proteins are fundamental for biological properties. Due to its ability to participate in the adaptation of the cancer cells to the metabolic stresses, CA IX is actively involved in cancer cell survival [7]. This renders CA IX a cancer biomarker for prognosis and resistance to treatments [8] and an attractive target of therapy. Several classes of inhibitors are currently available to target CAs: among these, sulfonamides and derivatives, acting as metal ion binders; compounds, such as phenols, polyamines, esters, carboxylates, and sulfocoumarins, possessing the ability to anchor to the zinc-coordinated water molecule/hydroxide ion; coumarin and related compounds which bind at the entrance of CA active site [9, 10]. Current efforts in the design and exploitation of selective CA inhibitors deal with the structure-based rational search [11–13] and with their potential as agents sensitizing to combined treatments in cancer [14].

The characterization of protein interactomes is a potent tool to discover and annotate protein functions in cellular physiology and in disease [15], as well as for the design of tumour-targeting peptides and mimetics [16]. We have recently annotated the CA IX interactome [17], highlighting the hypoxia-regulated interaction of CA IX with a list of components of the nuclear import and export machineries. These proteins also shared HEAT/ARM repeat protein domains. Additional intracellular proteins were also able to bind CA IX, such as CAND1, in an interaction occurring also in normoxic cells. The C-terminal region of CA IX was also shown to be necessary and sufficient for these interactions. In agreement with these results, immunofluorescence analysis in permeabilized cells showed a complex subcellular distribution for CA IX, which appeared to be widely distributed in normoxic and hypoxic mammalian cells of different origin. Interestingly, a pool of CA IX and of one of its main interactors, exportin-1 (XPO1), was clearly redistributed to perinuclear regions and nucleoli as a consequence of hypoxia. Finally, occurrence of CA IX in nuclear and/or perinuclear compartments was also highlighted in cases of clear-cell kidney carcinomas [7, 17], confirming previous evidences, describing nuclear CA IX in tumours characterized by poor prognosis [18, 19]. Taken together, these evidences can extend the classical view of CA IX as a cell surface protein, towards a concept of intracellular signalling component and multifunctional effector in cellular physiology and cancer biology. Accordingly, experimental evidences support a constitutive shedding of CA IX ectodomain, which may regulate surface availability of the protein, but also signalling properties of the released N- and C-terminal protein domains both in the extracellular and in the intracellular compartments, respectively [20]. CA IX is also actively internalized in the endocytic pathways, the latter being a route for CA IX redistribution in intracellular compartments, including perinuclear regions and nuclei.

Nucleolus is the organelle for ribosomal 45S rRNA precursor synthesis and processing, as well as for ribosome biogenesis (see [21] for a recent review). 45S rDNA genes are present in 300–400 copies in mammalian genomes. They are typically arranged in tandemly repeated arrays at few chromosome *loci*. 45S rDNA genes can also show different chromatin states, which well correlate with the expression state, thus justifying the occurrence of epigenetic mechanisms underlying transcriptional activity. However, nucleoli are also the sites for regulated sequestration and release of important signalling proteins, such as those modulating p53 activity, such as MDM2 [22]. Thus, nucleoli are currently believed to be multifunctional organelles and modulators of cellular responses to stresses. Cells also cope with nucleolar stress, so that overcoming nucleolar stress can be viewed as an emerging hallmark in cancer [23].

In this paper, we report on a novel, putative nucleolar function for CA IX, since we demonstrate binding of the protein to the 45S rDNA genes in normoxic cells. We also show that hypoxic stimulation releases CA IX from occupancy of the nucleolar chromatin, releasing the protein, which becomes part of complexes with XPO1. Concurrently, 45S rRNA transcript levels are decreased, supporting a functional role, for CA IX, as a regulator of transcription for rDNA genes.

2. Materials and Methods

2.1. Cell Cultures and Manipulations, DNA Constructs. The HEK293 and SHSY-5Y cell lines were purchased from ATCC. Cells were cultured in standard conditions using DMEM complemented with 1% penicillin/streptomycin, 2 mM glutamine, and 10% fetal bovine serum (Euroclone), at 37°C, in 5% CO_2 humidified atmosphere.

Putative and canonical NLS and NES sequences were frame-fused at the C-terminus of EGFP in the vector of expression pEGFP_C1. The corresponding primers were the oligonucleotides 1 and 2 for the construct pEGFP_NLS-SV40 (TAg) and the oligonucleotides 3 and 4 for pEGFP_NES-PKIA. The construct pEGFP_CA IX putative NLS, encompassing sequence from amino acids 434 to 459 of the full length protein, was generated by PCR from cDNA of full length CA IX using the oligonucleotides 5 and 6. The construct pEGFP_CA IX putative NES, including CA IX sequence from amino acid positions 412 to 429, was produced by annealing of the synthetic oligonucleotides 7 and 8.

Oligo 1, NLS_SV40(TAg)_US: 5′-GATCTCCAAAAAAGAAGAGAAAGGTAG-3′;

Oligo 2, NLS_SV40 (TAg)_LS: 5′-TCGACTACCTTTCTCTTCTTTTTTGGA-3′;

Oligo 3, NES_PKIA_US: 5′-GATCTTTAGCCTTGAAATTAGCAGGTCTTGATATCG-3′;

Oligo 4, NES_PKIA_LS: 5′-TCGACGATATCAAGACCTGCTAATTTCAAGGCTAAA -3′;

Oligo 5, CA9_Cterm_For: 5′-ATAAGATCTCAGATGAGAAGGCAGCACAGA-3′;

Oligo 6, CA9_Cterm_Rev: 5′-ACTGTAGTCGACGGCTCCAGTCTCGGCTACCT-3′;

Oligo 7, CA9_NES_FWD: 5′-GATCTGCTGGTGACATCCTAGCCCTGGTTTTTGGCCTCCTTTTTGCTGTCACCAGCG-3′;

Oligo 8, CA9_NES_RV: 5′-TCGACGCTGGTGACA-GCAAAAAGGAGGCCAAAAACCAGGGCTAGG-ATGTCACCAGCA-3′.

All the primers were synthesized at CEINGE Biotecnologie Avanzate. The analysis of putative and canonical NES and NLS sequences was performed in HEK293 and SHSY-5Y cells after transfection of the previously described constructs with the calcium phosphate method [24]. Leptomycin B (Sigma Aldrich) was dissolved in 70% methanol (v/v); treatments with solvent or leptomycin B (20 ng/mL) were performed for 4 hours. Hypoxic treatments were performed for six hours, in an incubator (STEMCELL Technologies), with atmosphere containing 95% N_2 and 5% CO_2. CA inhibitor acetazolamide was dissolved in DMSO and challenged to cell cultures for 16 hours at 1 mM concentration. Vehicle DMSO was used as a carrier control at 0.1% v/v.

2.2. Antibodies, Fluorescence Microscopy, and Immunological Methods. The antibodies used in this study were M75 and VII-20 anti-CA IX mouse monoclonals [25]; anti-XPO1 goat polyclonal (CRM1 C-20, Santa Cruz Biotechnology); anti-UBF mouse monoclonal (F-9, Santa Cruz Biotechnology); anti-HIF1α mouse monoclonal (BD Transduction Laboratories); and anti-β-actin mouse monoclonal (AC-15, Santa Cruz Biotechnology). Western blot analysis was carried out on cellular lysates obtained as described [26]; the latter were resolved on 10% SDS-PAGE gels and transferred to PVDF membranes (Millipore). Filters were probed with the anti-HIF1α antibody or with the M75 antibody for CA IX and the AC-15 antibody for β-actin, followed by anti-mouse secondary antibody.

For fluorescence analysis of the EGFP fusion constructs, cells were fixed with 3% (w/v) paraformaldehyde and 1% (w/v) sucrose in PBS for 20 minutes at room temperature (RT). Immunofluorescence analysis was carried out, as described [17], with VII-20 anti-CA IX mouse monoclonal [25] and with anti-XPO1 goat polyclonal (CRM1 C-20, Santa Cruz Biotechnology). Samples were observed on a Zeiss LM510 confocal microscope.

About 1×10^7 cells from triplicate cultures were used for each chromatin immunoprecipitation assay, which were fixed with 1% formaldehyde for 10 minutes at RT. Glycine 125 mM was added to inactivate the excess of formaldehyde. Chromatin was sonicated in a way to enrich the DNA fragments in the 200–1,000 bp size. Soluble fraction of chromatin was extracted by centrifugation and it was immunoprecipitated using CA IX VII-20, UBF1 (F-9, Santa Cruz) antibodies, and mouse IgGs as control.

2.3. Quantitative PCR Analysis. Triplicate sets of samples were used for quantitative PCR analyses (ChIP and qRT-PCR). Statistical analyses were carried out according to Student's t-test. Real-time PCR was used to detect enrichments of immunoprecipitated DNA in relation to total input chromatin. Supernatant obtained without antibody was used as input control. All the primers were used to a final concentration of 0,5 μM in a 20 μL real-time reaction containing 10 μL of SYBR Green (Applied Biosystem) and 2 μL DNA. The results were expressed as percent of total chromatin according to the following formula: $2\Delta Ct \times 10$, where Ct represents the cycle threshold and ΔCt = Ct (input) − Ct (immunoprecipitation).

Oligonucleotide sequences used to amplify the 45S rDNA region of interest were the following: 5′-GGTATATCTTTCGCTCCGAG-3′ and 5′-AGCGACAGG-TCGCCAGAGGA-3′. The region of amplification was located between the promoter region and the start site of rDNA [27]. To analyze the relative abundance of cellular RNAs, quantitative RT-PCR was performed as described [28] on individual biological triplicates for each sample. Cells were lysed by Trizol (Euroclone), and the total RNA was extracted with phenol/chloroform. DNase-treated total RNA was reverse-transcribed (Im-Prom II, Promega), and then it was amplified in a 7500 Real-Time PCR System (Applied Biosystem) using SYBR Green PCR MASTERMIX (Applied Biosystem). All primers were used to a final concentration of 0,2 μM. The oligonucleotide primers were designed using the bioinformatic tool Primer-BLAST (NCBI/ Primer-BLAST). Their sequences were the following: For_CAIX: 5′-CGGAAGAAAACAGTGCCTATGA-3′; Rev_CAIX: 5′-CTTCCTCAGCGATTTCTTCCA-3′; For_rRNA45S: 5′-CTCCGTTATGGTAGCGCTGC-3′; Rev_rRNA45S; 5′-GCGGAACCCTCGCTTCTC-3′; hLDHA_FOR: 5′-TGGCCTGTGCCATCAGTATC-3′; hLDHA_REV: 5′-CGATGACATCAACAAGAGCAAGT-3′; BActin_FOR: 5′-CGTGCTGCTGACCGAGG-3′; BActin_REV: 5′-GAAGGTCTCAAACATGATCTGGGT-3′. The relative abundance of each RNA was evaluated in relation to ACTB (β-actin) transcripts by $\Delta\Delta$Ct method [29, 30].

3. Results and Discussion

3.1. Putative NLS and NES Sequences in CA IX Direct the Nuclear Trafficking of EGFP in Human Cell Lines. In a previous study we described the interaction of CA IX with the cellular machinery of nuclear import and export [17]. CA IX was indeed found in native complexes with the importin, TNPO1, and the exportin, XPO1; accordingly, CA IX appeared to be widely distributed in the cellular compartments, including nuclei, of several human cell lines. Putative NLS and NES sequences in the CA IX sequence interacting with these proteins were predicted by bioinformatic tools. Thus, we evaluated the function of the putative NES and NLS signals, exploring their ability to direct the subcellular localization of EGFP, used as a reporter. In particular, the function of the putative NLS and NES sequences in CA IX was analyzed comparing the subcellular distribution in HEK293 cells of the isolated EGFP protein and of EGFP fusions bearing either canonical NES and NLS sequences or the putative NES and NLS sequences of CA IX. Figure 1(a) shows the subcellular distributions of isolated EGFP (left panel), of EGFP fused to the reference NLS of the SV40 T antigen (middle) and of EGFP fused to the putative NLS of CA IX (right panel). While the isolated EGFP was distributed widely in the transfected cells, the putative NLS signal of CA IX led to some nuclear accumulation of the protein, despite a lower extent, compared

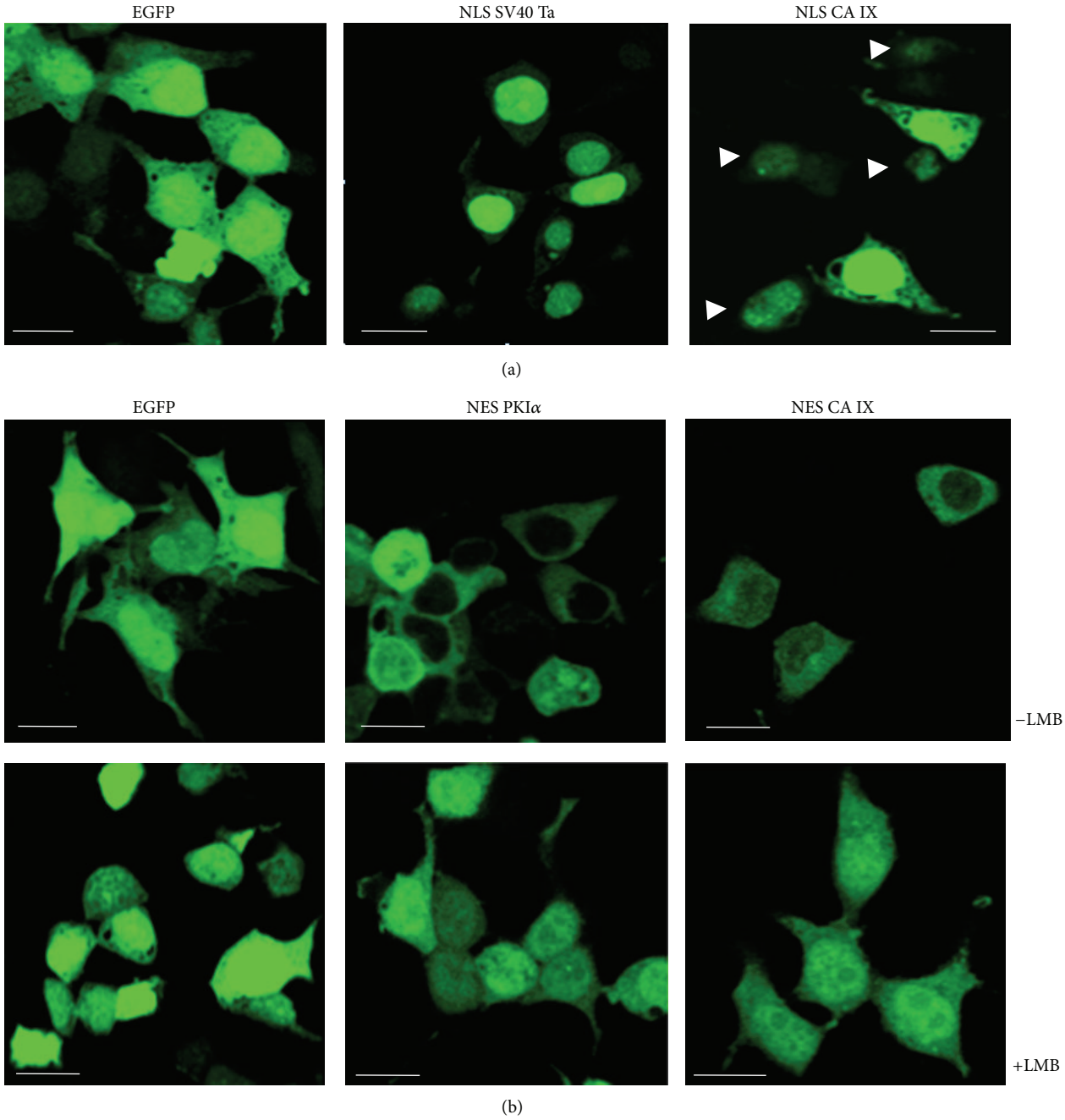

Figure 1: Analysis of the putative nuclear localization and nuclear export signals in CA IX. (a) EGFP protein or its fusions with a canonical NLS from SV40 Ta or with the region encompassing the putative NLS of the CA IX protein sequence (amino acid positions 434–459), as indicated, were expressed in HEK293 cells and visualized by confocal fluorescence microscopy. Arrowheads indicate cells, in which the EGFP protein fused to the putative CA IX NLS was almost exclusively nuclear. White bars: 10 μm. (b) In the upper panels, EGFP protein or its fusions with a canonical NES from PKIα or with the putative NES-containing region of the CA IX protein sequence (amino acid positions 412–429), as indicated, were expressed in HEK293 cells and visualized by confocal fluorescence microscopy. In the lower panels, transfected cells were treated with leptomycin B (LMB) to inhibit XPO1-mediated nuclear export. White bars: 10 μm.

to the NLS of SV40 Ta. In a complementary manner, as shown in the upper panels of Figure 1(b), the reference PKIα (middle) and the region containing the CA IX putative NES (right panel) sequences led to evident nuclear exclusion of the EGFP fluorescent proteins, compared to the isolated EGFP (left).

In order to confirm the actual function of the putative CA IX NES signal, the cells transfected with the various constructs were treated with leptomycin B, an inhibitor of nuclear export mediated by XPO1 [31]. Images (lower panels of Figure 1(b)) reveal that the isolated EGFP did not change its distribution (left) in the presence of leptomycin,

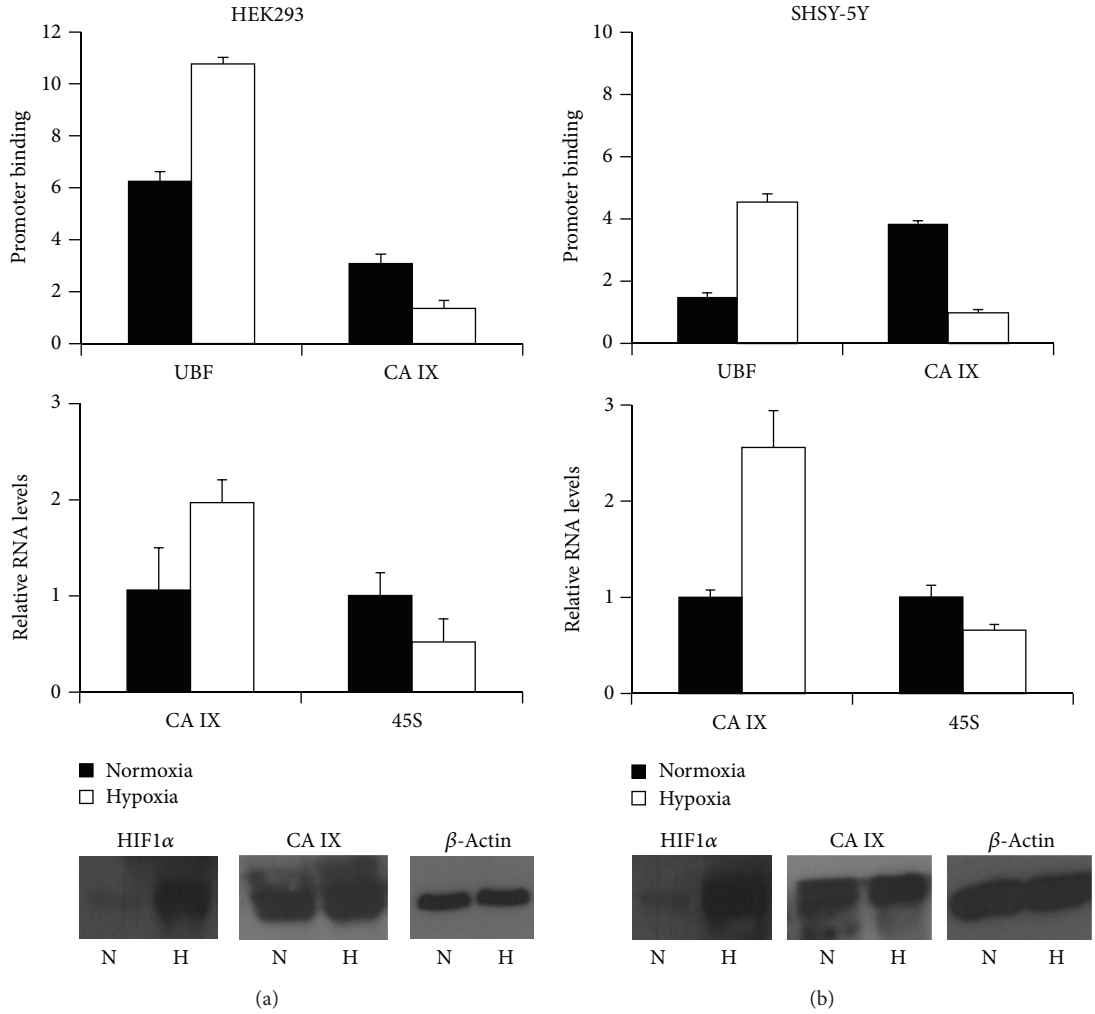

Figure 2: Chromatin immunoprecipitation analysis of CA IX and UBF1 binding to 45S rDNA precursor gene clusters. Normoxic or hypoxic HEK293 (a) and SHSY-5Y (b) cells were subjected to ChIP analysis with UBF1 or CA IX monoclonal antibodies, as indicated (upper charts). Binding of the proteins to 45S rDNA genes was evaluated via quantitative PCR analysis from triplicate samples. Calculated P values for pairwise comparisons of ChIP data were in the 0.0038 to 0.03 range (Student's t-test). The middle panels show the results of qRT-PCR analysis of CA IX or 45S rRNA transcripts from normoxic or hypoxic HEK293 (a) and SHSY-5Y (b) cells. Calculated P values for pairwise comparisons of qRT-PCR data were in the 0.0027 to 0.04 range. Lower panels show the hypoxia-induced increases in HIF1α and CA IX protein levels in normoxic (N) or hypoxic (H) HEK293 (a) and SHSY-5Y (b) cells. Filters were reprobed to β-actin, which was used as a loading control.

while a clear redistribution in nuclear compartments was appreciated for the fluorescent PKIα NES (middle) and for the region containing the CA IX putative NES (right panel), in comparison to the untreated cells (upper panels). Similar results were obtained in neuroblastoma SHSY-5Y cells (data not shown). Thus, the putative NLS and, to a major extent, the NES sequence in CA IX are actually functional. This indeed suggests that the nuclear trafficking of CA IX and its putative function are dependent on the binding to its interactors. Taken together, these results support a nuclear function for CA IX in human cells.

3.2. CA IX Is Bound to Nucleolar Chromatin in Human Cell Lines. One additional feature, emerging from our previous analysis of CA IX interactome, was the increased abundance of CA IX/XPO1 complexes and their peculiar enrichment in nucleoli in hypoxic cells. Thus, we hypothesized a nucleolar function for CA IX and for its complexes with XPO1. Nucleoli are the districts in which 45S rRNA synthesis and processing occur to allow ribosome biogenesis. 45S rRNA precursor is actively transcribed from arrays of 45S rDNA genes in nucleoli. We then evaluated, by chromatin immunoprecipitation (ChIP) analysis, the potential binding of CA IX to nucleolar chromatin in normoxic and hypoxic HEK293 and SHSY-5Y cells. ChIP analysis was also performed for UBF1, an architectural factor regulating RNA polymerase I transcription. The data shown in the panel A of Figure 2 demonstrated that both UBF1 and CA IX are actually bound to rDNA 45S genes in normoxic HEK293 cells. Even in the presence of increases in CA IX protein levels (lower panels of Figure 2(a)), the exposure of the cells to a hypoxic environment resulted in a decreased association of CA IX

to nucleolar chromatin, while UBF1 was stabilized on 45S rDNA genes. This was associated with decreased levels of 45S rRNA in hypoxic cells, as shown by the results of qRT-PCR in the middle panel of Figure 2(a). These data were consistently replicated in SHSY-5Y cells (Figure 2(b)). As previously demonstrated [17], CA IX levels and its nucleolar presence are increased in hypoxic cells, as for its participation in molecular complexes with XPO1. These novel results show that the increased formation of CA IX/XPO1 complex in the nucleoli of hypoxic cells is indeed associated with a decreased representation of CA IX on nucleolar chromatin and with a decreased transcription of 45S rDNA genes, both in HEK293 and in SHSY-5Y cells. These data support the hypothesis that in human cell lines CA IX might be associated with active transcription of 45S rDNA genes in normoxic condition.

3.3. Binding of CA IX to Nucleolar Chromatin Is Regulated by Its Interaction with XPO1 and by CA Activity. The data obtained so far support the hypothesis that CA IX acts as a positive modulator of transcription for rDNA 45S genes. In fact, decreased CA IX binding to nucleolar chromatin observed in hypoxic cells was associated with decreased 45S rRNA precursor transcript levels. What was also occurring in hypoxic cells was the increased representation of CA IX/XPO1 complexes in nucleoli [17]. Thus, XPO1 and its interaction with CA IX in the nucleoli of hypoxic cells may act as a decoy mechanism to prevent 45S rDNA genes' transcription during hypoxia. To validate this hypothesis, we evaluated 45S rDNA promoter binding by CA IX, 45S rRNA transcript levels, and CA IX/XPO1 colocalization in hypoxic HEK293 cells treated with the XPO1 inhibitor leptomycin B. As shown in Figure 3, CA IX binding to rDNA gene promoters (Figure 3(a)) was significantly decreased, and rRNA 45S transcript levels (Figure 3(b)) were underrepresented in hypoxic cells. As expected, the transcripts of the HIF1α targets, CA IX and LDHA, were upregulated in hypoxic cells (Figure 3(b)). Accordingly, some hypoxic cells showed increased representation of CA IX/XPO1 complexes, as demonstrated by the appearance of yellow nucleoli or nucleolar spots in the merged immunofluorescence experiment shown in Figure 3(c). Treatment of hypoxic cells with leptomycin B led to disappearance of these complexes (Figure 3(c)) and to increased representation of CA IX on rDNA 45S genes (Figure 3(a)). The levels of rRNA 45S transcripts were extremely low under this condition (Figure 3(b)), in agreement with the loss of UBF1 binding (Figure 3(a)).

Exposure of cells to stresses, including hypoxic condition, is characterized by altered cellular metabolism and attenuated protein synthesis [32]. In order to cope with this stressful condition and to support survival, glucose-deprived and hypoxic cells may decrease transcription of 45S rDNA genes by RNA polymerase I [33, 34], which is among the most energy-demanding processes in a cell, normally accounting for up to 60% of total cellular transcription [35]. While the increases in CA IX protein levels may represent a survival strategy for the hypoxic cells, concentration of a CA IX pool to complexes with exportins, and potentially with additional proteins of the nuclear trafficking, on one hand may represent a mechanism to decrease the energy-demanding 45S rDNA gene transcription. On the other hand, this can also represent a mechanism for CA IX storage in the nucleolar compartments, for putative adaptation of cells to the chronic hypoxia. XPO1 (also known as CRM1 homolog) function is commonly related to nuclear export of both proteins and RNAs [36, 37]; since XPO1 was also heavily redistributed to nucleoli in the hypoxic cells, this may represent a mechanism to decrease the nuclear export of mature ribosomal RNAs and of proteins exiting nuclear compartments during hypoxia, thus allowing the cells to react to nucleolar stress.

Thus, CA IX was able to interact with 45S rDNA gene promoters in normoxic cells, in which CA IX/XPO1 complexes were underrepresented or absent [17]. Acute hypoxia resulted in decreased binding of CA IX to the ribosomal gene clusters in nucleoli and in decreased expression of 45S rRNA precursor transcripts. Acetazolamide, a general inhibitor of CA enzymes, is known to induce metabolic acidosis in cultured cells and in mammals, including rats and humans [38–40]. Accordingly, acetazolamide induces normoxic induction of HIF1 alpha in cultured cells [38]. Thus, acetazolamide treatment should mimic what is actually observed during acute hypoxia, as shown in previous experiments. We then treated HEK293 cells with acetazolamide which, as expected, upregulated CA IX transcripts (Figure 4(a)). In a complementary manner, 45S rRNA transcript levels were downregulated. These results were associated with decreased binding of CA IX to 45S rDNA gene promoters (Figure 4(b)). Accordingly, as shown in Figure 4(c), treatment with acetazolamide induced, in HEK293 cells, the relocalization of CA IX and XPO1 in nucleoli. Thus, a drug-induced activation of cellular responses to hypoxic stress faithfully recapitulated the molecular events associated with regulated binding of CA IX to 45S rDNA promoters, adding support to the role of XPO1 in preventing this interaction during hypoxia. UBF1 binding to 45S rDNA genes was increased in hypoxic cells (Figure 3(a)), in accordance with a previous report [34], in which restriction of rRNA biosynthesis during hypoxia was associated with increased occupancy of UBF1 on 45S ribosomal gene clusters. Interestingly, UBF1 binding to 45S rDNA genes was decreased in acetazolamide-treated cells (Figure 4(b)), since cellular acidosis may not recapitulate in full the molecular effects, raised by acute hypoxia, on UBF1 interaction with rDNA genes.

4. Conclusions

The data reported in this paper for the first time describe a function for CA IX and for XPO1, one of its major interactors, in nucleoli. Firstly, we showed evidence for regulated binding of CA IX to nucleolar 45S rDNA genes in human cells. Additionally, we revealed, in hypoxic cells, a XPO1-based decoy mechanism, resulting in CA IX removal from nucleolar chromatin. The presence of the CA IX/XPO1 complexes, highly enriched in extrachromatinic nucleolar sites, was consistently associated with decreased transcription of 45S rDNA genes, both in hypoxic cells and in cells treated with acetazolamide, in which cellular acidosis was generated, as

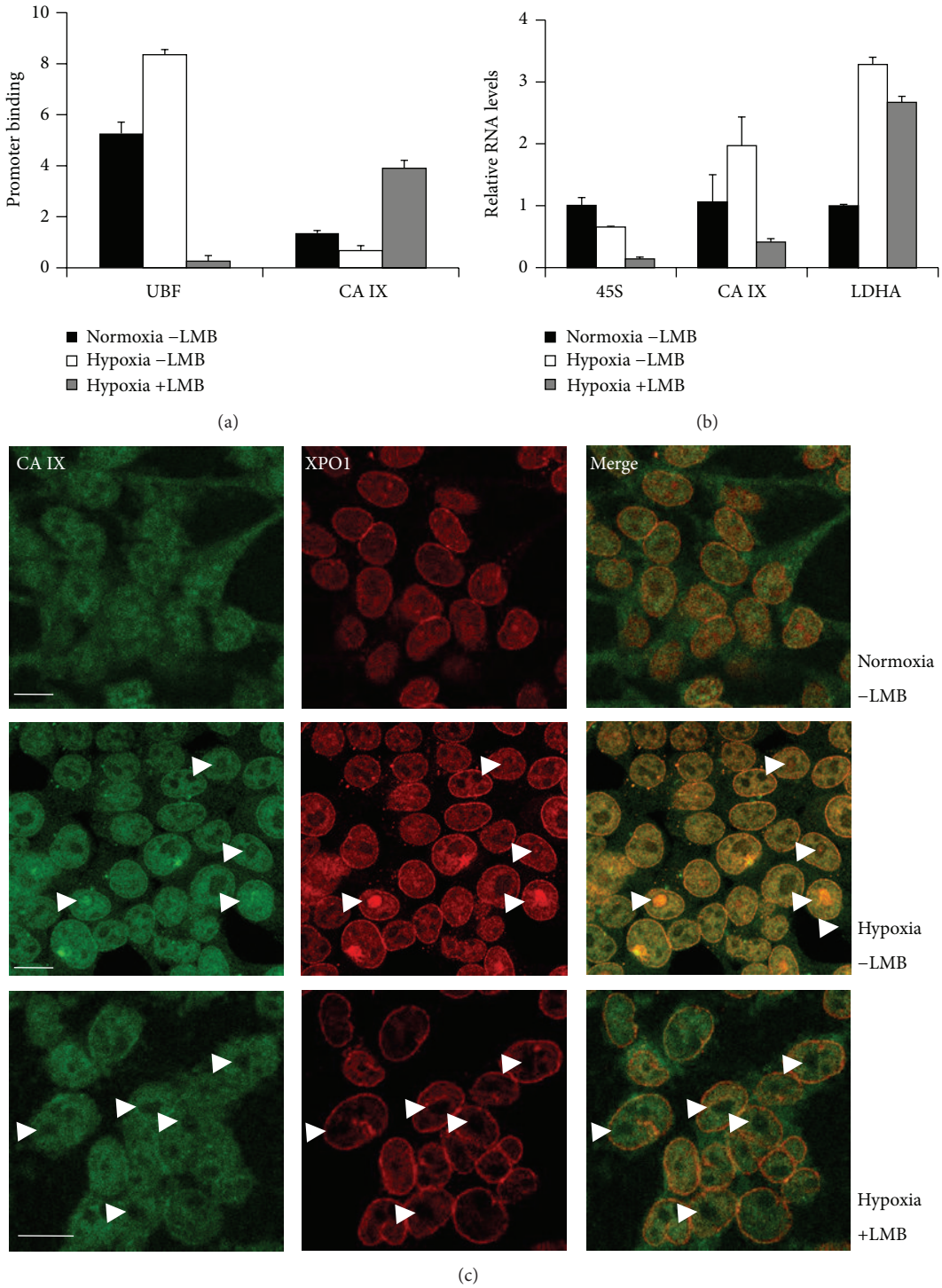

FIGURE 3: XPO1 controls binding of CA IX to 45S rDNA gene promoters. (a) Chromatin immunoprecipitation analysis of CA IX and UBF1 binding to 45S rDNA precursor gene clusters in a triplicate set of samples of normoxic and hypoxic HEK293 cells. Hypoxic cells were also exposed to leptomycin B (LMB) for 4 hours. Calculated P values for pairwise comparisons of ChIP data were in the 0.001 to 0.01 range (Student's t-test). (b) HEK293 cells from a triplicate set of samples exposed to normoxia, hypoxia, and hypoxia in the presence of leptomycin B were lysed for RNA extraction and qRT-PCR analysis of CA IX and LDHA mRNAs and 45S rRNA transcripts, as indicated. Calculated P values for pairwise comparisons of qRT-PCR data were in the 0.0005 to 0.01 range, with the exception of the CA IX transcript levels in normoxic and hypoxic/+LMB condition ($P = 0.4$, not significant) (Student's t-test). (c) Cells subjected to the same treatments, as in (a) and (b), were fixed, permeabilized, and exposed to antibodies for CA IX (green) and XPO1 (red) immunofluorescence analysis. Confocal images from representative fields were taken. White arrowheads in hypoxic cells (middle panels) indicate strong colocalization of CA IX and XPO1 in some nucleolar and subnucleolar areas. White arrowheads in hypoxic cells treated with leptomycin B (LMB) indicate the nucleoli, devoid of CA IX/XPO1 complexes. White bars: 10 μm.

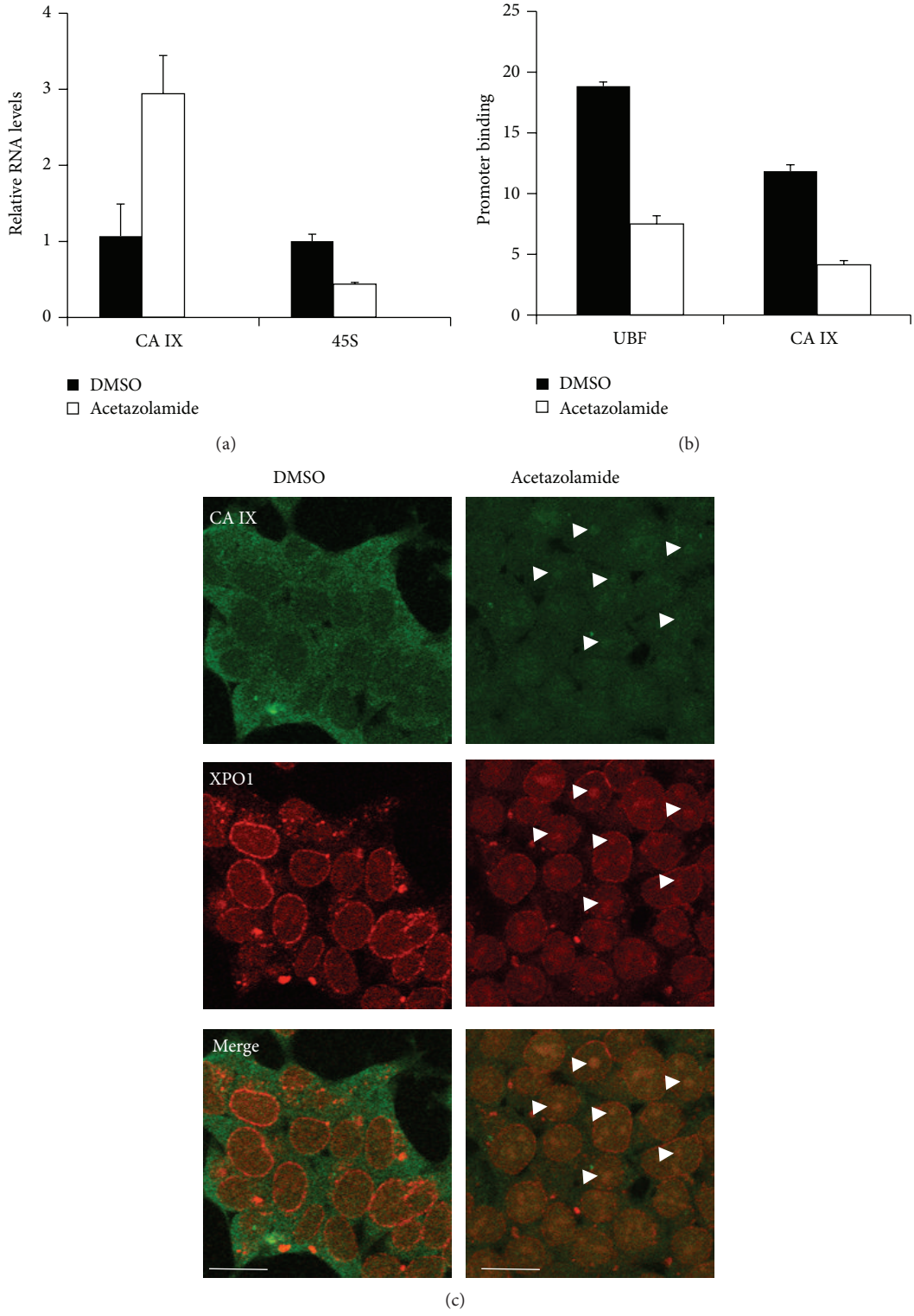

Figure 4: Cellular acidosis induced by acetazolamide mimics the hypoxia-induced relocalization of CA IX from 45S rDNA sites to nucleolar complexes with XPO1. (a) Analysis of CA IX mRNA and 45S rRNA transcripts in cells exposed to carrier DMSO and to acetazolamide. Transcript levels were evaluated via quantitative RT-PCR analysis from triplicate samples. Calculated P values for pairwise comparisons of qRT-PCR data were in the 0.003 to 0.03 range (Student's t-test). (b) Cells, treated as in (a), were subjected to chromatin immunoprecipitation analysis of CA IX and UBF1 binding to 45S rDNA precursor gene clusters in a triplicate set of samples. Calculated P values for pairwise comparisons of ChIP data were in the 0.03 to 0.01 range (Student's t-test). (c) Cells subjected to the same treatments, as in (a) and (b), were fixed, permeabilized, and exposed to antibodies for CA IX (green) and XPO1 (red) immunofluorescence analysis. Confocal images from representative fields were taken. White arrowheads show some representative enrichments of CA IX and XPO1 in nucleolar compartments. White bars: 10 μm.

a consequence of general CA inhibition. We believe that these events are related to cellular responses to both hypoxic and hypoxia-induced nucleolar stresses, in which survival mechanisms should be activated. These mechanisms, in first instance, should attenuate energy-demanding processes, such as ribosome biogenesis and translation, to allow cell survival in the progression towards the adaptation to the stressful conditions. The contribution of CA IX and its complexes with XPO1 to such responses may reveal novel mechanisms in cell and cancer biology.

Abbreviations

CA:	Carbonic anhydrase
ChIP:	Chromatin immunoprecipitation
EGFP:	Enhanced green fluorescent protein
LMB:	Leptomycin B
NES:	Nuclear export signal
NLS:	Nuclear localization sequence
qPCR:	Quantitative PCR
qRT-PCR:	Quantitative reverse-transcriptase PCR
rDNA:	Ribosomal DNA precursor gene
rRNA:	Ribosomal RNA.

Conflict of Interests

The authors declare that there is no conflict of interests regarding the publication of this paper.

Acknowledgments

The authors are indebted to Silvia Pastorekova for the kind gift of M75 and VII-20 anti-CA IX mouse monoclonal antibodies and Flora Cimmino for the kind gift of anti-HIF1α antibody; they also thank Claudiu Supuran and Giuseppina De Simone for critical discussions.

References

[1] D. Hanahan and R. A. Weinberg, "Hallmarks of cancer: the next generation," *Cell*, vol. 144, no. 5, pp. 646–674, 2011.

[2] C. T. Supuran, "Carbonic anhydrases: novel therapeutic applications for inhibitors and activators," *Nature Reviews Drug Discovery*, vol. 7, no. 2, pp. 168–181, 2008.

[3] M. Benej, S. Pastorekova, and J. Pastorek, "Carbonic anhydrase IX: regulation and role in cancer," *Sub-Cellular Biochemistry*, vol. 75, pp. 199–219, 2014.

[4] C. Cuvier, A. Jang, and R. P. Hill, "Exposure to hypoxia, glucose starvation and acidosis: effect on invasive capacity of murine tumor cells and correlation with cathepsin (L + B) secretion," *Clinical and Experimental Metastasis*, vol. 15, no. 1, pp. 19–25, 1997.

[5] V. Alterio, M. Hilvo, A. Di Fiore et al., "Crystal structure of the catalytic domain of the tumor-associated human carbonic anhydrase IX," *Proceedings of the National Academy of Sciences of the United States of America*, vol. 106, no. 38, pp. 16233–16238, 2009.

[6] A. Hulikova, M. Zatovicova, E. Svastova et al., "Intact intracellular tail is critical for proper functioning of the tumor-associated, hypoxia-regulated carbonic anhydrase IX," *FEBS Letters*, vol. 583, no. 22, pp. 3563–3568, 2009.

[7] O. Sedlakova, E. Svastova, M. Takacova, J. Kopacek, J. Pastorek, and S. Pastorekova, "Carbonic anhydrase IX, a hypoxia-induced catalytic component of the pH regulating machinery in tumors," *Frontiers in Physiology*, vol. 4, Article ID Article 400, 2014.

[8] G. Ilardi, N. Zambrano, F. Merolla et al., "Histopathological determinants of tumor resistance: a special look to the immunohistochemical expression of carbonic anhydrase ix in human cancers," *Current Medicinal Chemistry*, vol. 21, no. 14, pp. 1569–1582, 2014.

[9] S. M. Monti, C. T. Supuran, and G. de Simone, "Carbonic anhydrase IX as a target for designing novel anticancer drugs," *Current Medicinal Chemistry*, vol. 19, no. 6, pp. 821–830, 2012.

[10] G. De Simone, V. Alterio, and C. T. Supuran, "Exploiting the hydrophobic and hydrophilic binding sites for designing carbonic anhydrase inhibitors," *Expert Opinion on Drug Discovery*, vol. 8, no. 7, pp. 793–810, 2013.

[11] V. Alterio, A. Di Fiore, K. D'Ambrosio, C. T. Supuran, and G. De Simone, "Multiple binding modes of inhibitors to carbonic anhydrases: How to design specific drugs targeting 15 different isoforms?" *Chemical Reviews*, vol. 112, no. 8, pp. 4421–4468, 2012.

[12] M. Rami, L. Dubois, N.-K. Parvathaneni et al., "Hypoxia-targeting carbonic anhydrase IX inhibitors by a new series of nitroimidazole-sulfonamides/sulfamides/sulfamates," *Journal of Medicinal Chemistry*, vol. 56, no. 21, pp. 8512–8520, 2013.

[13] V. Alterio, P. Pan, S. Parkkila et al., "The structural comparison between membrane-associated human carbonic anhydrases provides insights into drug design of selective inhibitors," *Biopolymers*, vol. 101, no. 7, pp. 769–778, 2014.

[14] L. Dubois, S. G. J. A. Peeters, S. J. A. Van Kuijk et al., "Targeting carbonic anhydrase IX by nitroimidazole based sulfamides enhances the therapeutic effect of tumor irradiation: a new concept of dual targeting drugs," *Radiotherapy and Oncology*, vol. 108, no. 3, pp. 523–528, 2013.

[15] G. Caratù, D. Allegra, M. Bimonte et al., "Identification of the ligands of protein interaction domains through a functional approach," *Molecular and Cellular Proteomics*, vol. 6, no. 2, pp. 333–345, 2007.

[16] E. Sarafraz-Yazdi, M. R. Pincus, and J. Michl, "Tumor-targeting peptides and small molecules as anti-cancer agents to overcome drug resistance," *Current Medicinal Chemistry*, vol. 21, no. 14, pp. 1618–1630, 2014.

[17] P. Buanne, G. Renzone, F. Monteleone et al., "Characterization of carbonic anhydrase ix interactome reveals proteins assisting its nuclear localization in hypoxic cells," *Journal of Proteome Research*, vol. 12, no. 1, pp. 282–292, 2013.

[18] D. E. B. Swinson, J. L. Jones, D. Richardson et al., "Carbonic anhydrase IX expression, a novel surrogate marker of tumor hypoxia, is associated with a poor prognosis in non-small-cell lung cancer," *Journal of Clinical Oncology*, vol. 21, no. 3, pp. 473–482, 2003.

[19] J. V. Dungwa, L. P. Hunt, and P. Ramani, "Carbonic anhydrase IX up-regulation is associated with adverse clinicopathologic and biologic factors in neuroblastomas," *Human Pathology*, vol. 43, no. 10, pp. 1651–1660, 2012.

[20] M. Zaťovičová and S. Pastoreková, "Modulation of cell surface density of carbonic anhydrase IX by shedding of the ectodomain and endocytosis," *Acta Virologica*, vol. 57, no. 2, pp. 257–264, 2013.

[21] S. Hamperl, M. Wittner, V. Babl, J. Perez-Fernandez, H. Tschochner, and J. Griesenbeck, "Chromatin states at ribosomal DNA loci," *Biochimica et Biophysica Acta—Gene Regulatory Mechanisms*, vol. 1829, no. 3-4, pp. 405–417, 2013.

[22] N. Hein, K. M. Hannan, A. J. George, E. Sanij, and R. D. Hannan, "The nucleolus: an emerging target for cancer therapy," *Trends in Molecular Medicine*, vol. 19, no. 11, pp. 643–654, 2013.

[23] J. E. Quin, J. R. Devlin, D. Cameron, K. M. Hannan, R. B. Pearson, and R. D. Hannan, "Targeting the nucleolus for cancer intervention," *Biochimica et Biophysica Acta*, vol. 1842, no. 6, pp. 802–816, 2014.

[24] M. Kriegler, *Gene Transfer and Expression: A Laboratory Manual*, W.H. Freeman Publishers, New York, NY, USA, 1990.

[25] M. Zaťovičová, K. Tarábková, E. Švastová et al., "Monoclonal antibodies generated in carbonic anhydrase IX-deficient mice recognize different domains of tumour-associated hypoxia-induced carbonic anhydrase IX," *Journal of Immunological Methods*, vol. 282, no. 1-2, pp. 117–134, 2003.

[26] F. Monteleone, R. Rosa, M. Vitale et al., "Increased anaerobic metabolism is a distinctive signature in a colorectal cancer cellular model of resistance to antiepidermal growth factor receptor antibody," *Proteomics*, vol. 13, no. 5, pp. 866–877, 2013.

[27] L. Y. Li, H. Chen, Y. H. Hsieh et al., "Nuclear ErbB2 enhances translation and cell growth by activating transcription of ribosomal RNA genes," *Cancer Research*, vol. 71, no. 12, pp. 4269–4279, 2011.

[28] G. Amodio, O. Moltedo, F. Monteleone et al., "Proteomic signatures in thapsigargin-treated hepatoma cells," *Chemical Research in Toxicology*, vol. 24, no. 8, pp. 1215–1222, 2011.

[29] K. J. Livak and T. D. Schmittgen, "Analysis of relative gene expression data using real-time quantitative PCR and the 2-ΔΔCT method," *Methods*, vol. 25, no. 4, pp. 402–408, 2001.

[30] J. S. Yuan, A. Reed, F. Chen, and C. N. Stewart Jr., "Statistical analysis of real-time PCR data," *BMC Bioinformatics*, vol. 7, article 85, 2006.

[31] M. Fukuda, S. Asano, T. Nakamura et al., "CRM1 is responsible for intracellular transport mediated by the nuclear export signal," *Nature*, vol. 390, no. 6657, pp. 308–311, 1997.

[32] K. A. Spriggs, M. Bushell, and A. E. Willis, "Translational regulation of gene expression during conditions of cell stress," *Molecular Cell*, vol. 40, no. 2, pp. 228–237, 2010.

[33] X. Gao, S. Wei, K. Lai et al., "Nucleolar follistatin promotes cancer cell survival under glucose-deprived conditions through inhibiting cellular rRNA synthesis," *The Journal of Biological Chemistry*, vol. 285, no. 47, pp. 36857–36864, 2010.

[34] K. Mekhail, L. Rivero-Lopez, M. Khacho, and S. Lee, "Restriction of rRNA synthesis by VHL maintains energy equilibrium under hypoxia," *Cell Cycle*, vol. 5, no. 20, pp. 2401–2413, 2006.

[35] S. J. Goodfellow and J. C. B. M. Zomerdijk, "Basic mechanisms in RNA polymerase I transcription of the ribosomal RNA genes," *Sub-Cellular Biochemistry*, vol. 61, pp. 211–236, 2013.

[36] C. Verheggen and E. Bertrand, "CRM1 plays a nuclear role in transporting snoRNPs to nucleoli in higher eukaryotes," *Nucleus*, vol. 3, no. 2, pp. 132–137, 2012.

[37] J. G. Turner, J. Dawson, and D. M. Sullivan, "Nuclear export of proteins and drug resistance in cancer," *Biochemical Pharmacology*, vol. 83, no. 8, pp. 1021–1032, 2012.

[38] J. Xu, Z. Peng, R. Li et al., "Normoxic induction of cerebral HIF-1α by acetazolamide in rats: role of acidosis," *Neuroscience Letters*, vol. 451, no. 3, pp. 274–278, 2009.

[39] L. J. Teppema, E. L. A. van Dorp, and A. Dahan, "Arterial $[H^+]$ and the ventilatory response to hypoxia in humans: influence of acetazolamide-induced metabolic acidosis," *The American Journal of Physiology—Lung Cellular and Molecular Physiology*, vol. 298, no. 1, pp. L89–L95, 2010.

[40] T. Leniger, M. Wiemann, D. Bingmann, G. Widman, A. Hufnagel, and U. Bonnet, "Carbonic anhydrase inhibitor sulthiame reduces intracellular pH and epileptiform activity of hippocampal CA3 neurons," *Epilepsia*, vol. 43, no. 5, pp. 469–474, 2002.

Hindawi Publishing Corporation
BioMed Research International
Volume 2014, Article ID 389869, 9 pages
http://dx.doi.org/10.1155/2014/389869

Research Article

Carborane-Based Carbonic Anhydrase Inhibitors: Insight into CAII/CAIX Specificity from a High-Resolution Crystal Structure, Modeling, and Quantum Chemical Calculations

Pavel Mader,[1,2] Adam Pecina,[3] Petr Cígler,[3] Martin Lepšík,[3] Václav Šícha,[4] Pavel Hobza,[3,5] Bohumír Grüner,[4] Jindřich Fanfrlík,[3] Jiří Brynda,[1,3] and Pavlína Řezáčová[1,3]

[1] *Institute of Molecular Genetics, Academy of Sciences of the Czech Republic, Vídeňská 1083, 140 00 Prague 4, Czech Republic*
[2] *Structural Genomics Consortium, University of Toronto, Toronto, ON, Canada M5G 1L7*
[3] *Institute of Organic Chemistry and Biochemistry, Academy of Sciences of the Czech Republic, Gilead Sciences and IOCB Research Center, Flemingovo nam. 2, 166 10 Prague 6, Czech Republic*
[4] *Institute of Inorganic Chemistry, Academy of Sciences of the Czech Republic, v.v.i., Hlavní 1001, 250 68 Řež near Prague, Czech Republic*
[5] *Regional Center of Advanced Technologies and Materials, Department of Physical Chemistry, Palacký University, 77146 Olomouc, Czech Republic*

Correspondence should be addressed to Jindřich Fanfrlík; fanfrlik@uochb.cas.cz, Jiří Brynda; brynda@img.cas.cz, and Pavlína Řezáčová; rezacova@uochb.cas.cz

Received 24 April 2014; Accepted 8 June 2014; Published 18 September 2014

Academic Editor: Mariya Al-Rashida

Carborane-based compounds are promising lead structures for development of inhibitors of carbonic anhydrases (CAs). Here, we report structural and computational analysis applicable to structure-based design of carborane compounds with selectivity toward the cancer-specific CAIX isoenzyme. We determined the crystal structure of CAII in complex with 1-methylenesulfamide-1,2-dicarba-*closo*-dodecaborane at 1.0 Å resolution and used this structure to model the 1-methylenesulfamide-1,2-dicarba-*closo*-dodecaborane interactions with CAIX. A virtual glycine scan revealed the contributions of individual residues to the energy of binding of 1-methylenesulfamide-1,2-dicarba-*closo*-dodecaborane to CAII and CAIX, respectively.

1. Introduction

Carbonic anhydrases (CAs) play important roles in many physiological and pathophysiological processes. For example, extracellular CAs participate in tumor growth and progression [1]. CAIX, which is selectively expressed in a range of hypoxic tumors, is a validated diagnostic and therapeutic target (recently reviewed in [2–4]). There are 15 human CA isoenzymes, and due to the ubiquity of these enzymes in human tissues, selective inhibition is a very important aspect of drug design.

Three main classes of CA inhibitors have been described to date (reviewed in [5]): (i) metal ion binders (sulfonamides, sulfamides, sulfamates, dithiocarbamates, thiols, and hydroxamates); (ii) compounds that anchor the zinc-coordinated water molecule/hydroxide ion (phenols, carboxylates, polyamines, esters, and sulfocoumarins); and (iii) coumarins and related compounds that bind further away from the metal ion.

CA inhibitors from the first class (metal ion binders) contain specific functional groups that interact with the catalytic Zn^{2+} ion in the CA active site. These metal-binding functionalities are typically joined to a "ring" structure. This moiety is not necessarily aromatic; however, it is usually consisting of a 5- or 6-membered hydrocarbon ring or conjugated ring system containing nitrogen, oxygen, and/or sulfur. Numerous functional groups have been added to the ring structure scaffold to modify inhibitor properties such as specificity toward a particular CA isoenzyme, pK_a, or solubility (reviewed in [6]). Recently, we reported design of CA inhibitors containing

space-filling carborane clusters in place of the typical ring structure [7]. We showed that various carborane clusters act as CA inhibitors and that modifying these clusters with an appropriately attached sulfamide group and other substituents leads to compounds with selectivity toward the cancer-specific CAIX isoenzyme.

Boron is one of few chemical elements that can form binary hydrides composed of more than two atoms, which leads to formation of boron cluster compounds (boron hydrides or boranes). Their basic structural feature is formation of a polyhedron with triangular facets held together by 3-center 2-electron bonds with an extensive electron delocalization [8]. A typical structural archetype is represented by the divalent *closo*-$B_{12}H_{12}{}^{2-}$ anion, an extremely stable compound with a symmetrical 12-vertex icosahedron structure [9]. Replacement of one or more $\{BH^-\}$ in borane cage with $\{CH\}$ leads to series of carboranes and removal of BH vertices leads to various open-cage (*nido*-) species. Carboranes thus offer a large variety of structural archetypes that provide interesting counterparts to organic compounds [10].

Many features of icosahedral 12-vertex carboranes are useful in the design of biologically active compounds. Carboranes have high thermal and chemical stability; therefore, they generally do not undergo catabolism and are nontoxic to the host organism [11, 12]. The basic *closo*-$C_2B_{10}H_{12}$ carborane cluster is highly hydrophobic [13]; however, its controlled deboronation can generate water soluble 11-vertex *nido*-$C_2B_9H_{12}{}^-$. These anions represent important intermediates in the synthesis of a family of mainly anionic metal bis(dicarbollides) accessible via metal insertion. Incorporation of carborane cages into the structures of certain substances of medicinal interest can enhance hydrophobic interactions between the boron cluster-coupled pharmaceuticals and their protein targets, increase *in vivo* stability, and facilitate uptake through cellular membranes [14, 15]. The successful use of boron clusters as hydrophobic pharmacophores has recently been increasing [16, 17]. Examples of carborane pharmacophores include boron-containing antifolates [18], HIV protease inhibitors [19, 20], and estrogen receptor agonists and antagonists [21], among others [16, 22, 23].

Drug design efforts benefit greatly from knowledge of the 3D structures of protein-ligand complexes. X-ray crystallography has contributed considerably to the development of CA inhibitors; more than 500 structures of human CA isoenzymes (wild-type and mutant forms) in complex with various inhibitors have offered unprecedented insight into inhibitor binding modes (reviewed in [24]). Structural information coupled with experimental inhibition data can be used to validate various computational approaches to assess inhibitor binding strength. Once a particular theoretical approach reproduces the known data well, it can be used for prospective design. For studies involving metal ions and unusual compounds such as boranes, the use of quantum chemistry (QM) is warranted [25, 26]. Indeed, we recently used a quantum mechanics/molecular mechanics (QM/MM) methodology to quantitatively describe the binding of two carborane-based sulfamides to CAII [7] and to explain fundamental differences in the binding modes of *closo*- and *nido*-cages [27].

Here, we report the X-ray structure of CAII with bound 1-methylenesulfamide-1,2-dicarba-*closo*-dodecaborane (compound **1**, Figure 1(a)) determined at 1.0 Å resolution. This atomic-level resolution allowed us to assess in detail the positions of carbon and boron atoms in the carborane cage of **1**. Additionally, we modeled the complex of **1** with CAIX. We employed a virtual glycine scan to analyze the differences between the interactions of **1** with CAII and CAIX.

2. Materials and Methods

2.1. Protein Crystallization and Diffraction Data Collection. For crystallization of human CAII (Sigma, catalogue number C6165) in complex with 1-methylenesulfamide-1,2-dicarba-*closo*-dodecaborane (compound **1**), we adapted a previously described procedure [28]. CAII (at a concentration of 4 mg·mL^{-1}, dissolved in water) was incubated in aqueous solution containing a 2-fold molar excess of *p*-hydroxymercuribenzoate (Sigma, catalogue number 55540). The protein was concentrated to 10 mg·mL^{-1} and unbound *p*-hydroxymercuribenzoate was removed with Amicon Ultra-4 concentrators (Merck-Millipore MWCO 10 kDa).

The complex of CAII with **1** was prepared by adding a 1.1-fold molar excess of **1** (in DMSO) to the 10 mg·mL^{-1} solution of CAII in water without pH adjustment (the final DMSO concentration did not exceed 5% v/v).

The best diffracting crystals were obtained using the hanging-drop vapor diffusion method under the following conditions: 2 μL protein-inhibitor complex solution was mixed with 2 μL precipitant solution [2.5 M $(NH_4)_2SO_4$, 0.3 M NaCl, and 100 mM Tris-HCl, pH 8.2] and equilibrated over a reservoir containing 1 mL of precipitant solution at 18°C. Crystals with dimensions of 0.3 mm × 0.1 mm × 0.1 mm grew within 7 days.

For cryoprotection, the crystals were incubated in mother liquor supplemented with 25% glycerol for approximately 30 s, flash-frozen, and stored in liquid nitrogen. Diffraction data for the CAII complex were collected at 100 K at the X14.2 BESSY beamline in Berlin, Germany [29]. Data were collected in two passes: the high-resolution range (11.75–1.00 Å) and the low-resolution range (21.08–1.20 Å). The two datasets were integrated with iMOSFLM [30] and merged and scaled with SCALA [31]. Data collection and refinement statistics are summarized in Table 1.

2.2. Structure Determination, Refinement, and Analysis. Crystal structures were solved by difference Fourier method using the CAII structure (PDB code 3IGP [34]) as a starting model. The model was refined using REFMAC5 [35], part of the CCP4 program suite [36]. The model was initially refined with isotropic atomic displacement parameters (ADPs); hydrogen atoms in riding positions were added later. For the final rounds of refinement, we used a mixed isotropic-anisotropic model of ADPs: anisotropic ADPs were used for all atoms, and only atoms in alternative conformations were refined isotropically. Atomic coordinates for the structure of **1** were generated by quantum mechanics computation with DFT-D methodology [37] using the B-LYP functional and SVP basis set [38] in the Turbomole program [39].

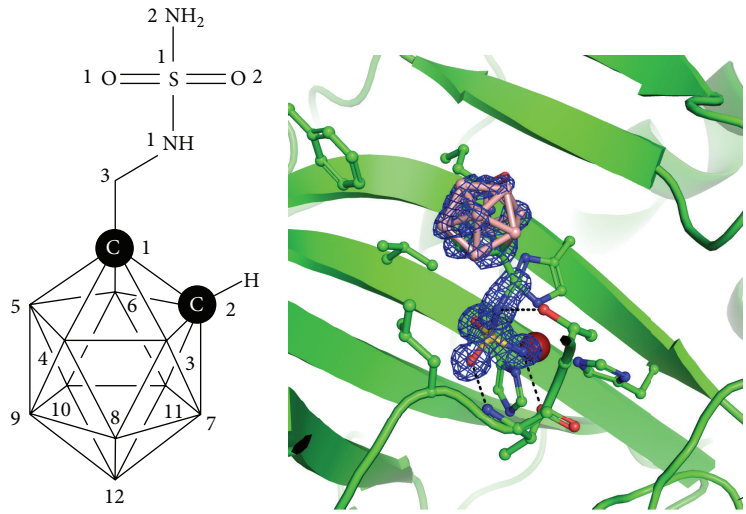

(a) (b)

Figure 1: (a) Structural formula of **1** with atom numbers used in the crystal structure coordinate file. The vertices in carborane cluster represent BH groups. (b) Crystal structure of CAII in complex with **1**. The CAII active site is shown in cartoon representation; residues involved in interactions with the Zn^{2+} ion (purple sphere) and **1** are shown in stick representation with carbon atoms colored green. Boron atoms are colored pink, and other heteroatoms are colored according to standard color coding: oxygen, red; nitrogen, blue; sulfur, yellow. The 2*Fo-Fc* electron density map for **1** is contoured at 1 σ.

A geometric library for **1** was generated using the Libcheck program from the CCP4 suite. Coot [40] was used for rebuilding. The quality of the refined model was assessed using MolProbity [33]. The coordinates and structure factors were deposited in the PDB under accession code 4Q78. Final refinement statistics are summarized in Table 1. All structural figures were prepared using PyMOL 1.4.1 [41].

2.3. Model of CAIX-1 Complex. The complex of CAIX and **1** was modeled by aligning the existing crystal structures of the CAIX catalytic domain (PDB code 3IAI [42]) with the CAII-**1** complex (PDB code 4MDG [7]) using PyMOL version 1.2 [43]. Preparation of structure coordinate files for further calculations was performed as described before for CAII [27].

The complex was fully optimized using a QM/MM procedure. We used ONIOM-like subtractive scheme [44] with link atoms and mechanical embedding to be consistent with our previous studies [27, 45–48]. The QM part is described at the DFT-D TPSS/TZVP//BLYP/SVP level of theory [39] and comprises 218 atoms including the atoms present in **1** and 8 amino acids (Trp5, Asn62, His64, Gln67, Gln92, Val131, Leu135, and Pro202). The MM part constituted the remainder of the protein, and the surrounding solvent was approximated by a generalized Born (GB) implicit model. Detailed description of the procedure was published in [27]. One crystal water molecule (Wat272) bridging the inhibitors and CAII residues Thr199, Glu106, and Tyr7 was retained to maintain the integrity of the active site. Other water molecules present in the crystal structures were omitted.

The positions of the added hydrogen atoms, **1**, and 15 amino acids surrounding the ligand (Trp5, Asn62, Gly63, His64, Gln67, Leu91, Gln92, Leu123, Val131, Leu135, Leu141, Thr200, Pro201, Pro202, and Ala204) were relaxed in a GB implicit solvent model using the FIRE algorithm followed by 10 ps annealing from 100 K or 150 K to 0 K using the Berendsen thermostat [49] in the SANDER module of the AMBER 10 package [50].

2.4. Virtual Glycine Scan. The contribution of the active site amino acids to inhibitor binding was examined by virtual glycine scanning. Individual amino acids in contact with **1** in the CAIX-**1** model and CAII-**1** crystal structure were substituted with glycine. The energy contributions ($\Delta\Delta G'_{int}$) were calculated as the difference between the original $\Delta G'_{int}$ at the QM/MM level with the wild-type amino acid and the new $\Delta G'_{int}$ with the mutated glycine residue [27].

3. Results and Discussion

*3.1. Crystal Structure of CAII in Complex with **1** at Atomic Resolution.* The overall structure of CAII in complex with **1** was refined to 1.0 Å resolution. This high resolution allowed us to observe details that could not be fully resolved in the complex structure determined previously at lower resolution. Atomic resolution was achieved by derivatization of CAII using the 4-(hydroxymercury)benzoic acid (abbreviated MBO in the cif library of small molecules) method described by [28]. The mercury atom of MBO covalently binds to Sγ of Cys206. This modification allows formation of a hydrogen bond between the OZ1 oxygen of the MBO carboxyl group and the main-chain amino group of Tyr40 in the neighboring protein molecule, reinforcing the crystal lattice and increasing the diffraction quality of the crystal. In our structure, MBO is modeled in two alternative conformations with occupancies of 0.6 and 0.2.

When our atomic resolution structure is compared with the structure of the CAII-**1** complex determined at 1.35 Å resolution (PDB code 4MDG [7]), the RMSD value for

Table 1: Data collection and refinement statistics.

Data collection statistics	
Space group	$P2_1$
Cell parameters (Å; °)	42.20, 41.73, 72.16; 90.0, 104.4, 90.0
Wavelength (Å)	0.9184
Resolution (Å)	21.08–1.00 (1.05–1.00)
Number of unique reflections	108,781 (15,490)
Multiplicity	3.5 (2.5)
Completeness (%)	83.1 (81.4)
R_{merge} [a]	0.056 (0.375)
Average $I/\sigma(I)$	10.8 (2.3)
Wilson B (Å^2)	6.5
Refinement statistics	
Resolution range (Å)	69.90–1.00 (1.03–1.00)
No. of reflections in working set	97,856 (7,831)
No. of reflections in test set	5,426 (412)
R value (%) [b]	17.5 (24.4)
R_{free} value (%) [c]	20.0 (26.2)
RMSD bond length (Å)	0.011
RMSD angle (°)	1.53
Number of atoms in AU	2297
Number of protein atoms in AU	2081
Number of water molecules in AU	176
Mean ADP value protein/inhibitor (Å^2)	12.0/17.6
Ramachandran plot statistics [d]	
Residues in favored regions (%)	96.56
Residues in allowed regions (%)	3.44

The data in parentheses refer to the highest-resolution shell.
[a] $R_{merge} = \sum_{hkl} \sum_i I_i(hkl) - \langle I(hkl)\rangle \mid / \sum_{hkl} \sum_i I_i(hkl)$, where $I_i(hkl)$ is the individual intensity of the ith observation of reflection hkl and $\langle I(hkl)\rangle$ is the average intensity of reflection hkl with summation over all data.
[b] R value $= ||F_o| - |F_c||/|F_o|$, where F_o and F_c are the observed and calculated structure factors, respectively.
[c] R_{free} is equivalent to R value but is calculated for 5% of reflections chosen at random and omitted from the refinement process [32].
[d] as determined by Molprobity [33].

superposition of the Cα atoms of residues 4–261 is 0.142 Å, a value typical for superposition of identical structures [51]. The N-terminal residue His3 is traced differently in the two structures; double conformations of numerous side chains (e.g., Glu14, His64, and Gln74) are resolved in the atomic resolution structure. We found an additional difference in the loop formed by amino acid residues 124–139, with a maximum difference of 0.738 Å for the position of Gln136 Cα. Gln136 forms van der Waals contacts with the MBO covalently attached to Cys206. The positions of Phe131 and Val135, which form a hydrophobic rim at the active site, are also influenced by MBO binding. This results in a subtle positional shift of the inhibitor, with an RMSD of 0.145 Å for superposition of 12 atoms in the carborane cage of **1** bound to CAII and CAII derivatized by MBO. This value is below the value observed for superposition of identical structures [51].

Atomic-level resolution allowed us to resolve the carbon and boron atom positions in the symmetrical carborane cage of **1**. When analyzing the values of the electron density map at positions of atoms bonded to the C1 atom, we can assume that positions with higher density levels are more likely to be carbon than boron atoms. Similar analysis was done by others for boron-containing inhibitor of human dihydrofolate reductase [18]. The C2 atom of the carborane cage (Figure 1(a)) was modeled into the position with an electron density value of 1.16 e/Å^3, which was approximately 0.15 e/Å^3 higher than those for the B3, B4, B5, and B6 atoms. To exclude the possibility that higher density is caused by model bias, we altered the composition of the cage by replacing the C2 atom with a boron atom. Electron density values did not change significantly after several rounds of refinement cycles.

Thus, we can conclude that the most probable position of the second carbon atom in the carborane cage of **1** is the position assigned to the C2 atom in our crystal structure. This is in good agreement with the recently published QM/MM modeling study [27].

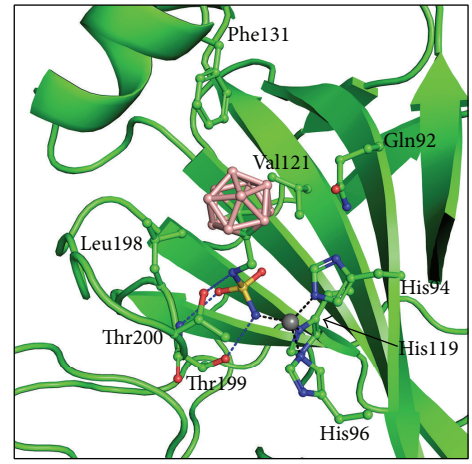

Figure 2: Interactions of **1** with CAII. The protein is shown in cartoon representation; residues involved in interactions with the Zn^{2+} ion (gray sphere) and **1** are shown in stick representation. Polar interactions are represented by blue dashed lines; Zn^{2+} ion coordination is shown as black dashed lines.

3.2. Detailed Analysis of Inhibitor Interactions with CAII. The crystal structure of human CAII in complex with **1** determined at 1.0 Å resolution confirmed the key interactions that our group observed previously [7]. The compound fits very well into the CAII active site cavity and makes numerous polar and nonpolar interactions with the residues in the enzyme active site. The sulfamide moiety, which forms key polar interactions with the active site Zn^{2+} ion, also makes polar interactions with Thr199 typical of other sulfamide inhibitors of CAII (Figure 2). The linker NH group forms an additional polar interaction with Oγ of Thr200. The compound makes several van der Waals interactions with residues Gln92, His94, His96, His119, Val121, Phe131, Leu198, and Thr200 (Figure 2). All interactions between the inhibitor and protein are summarized in Table 2.

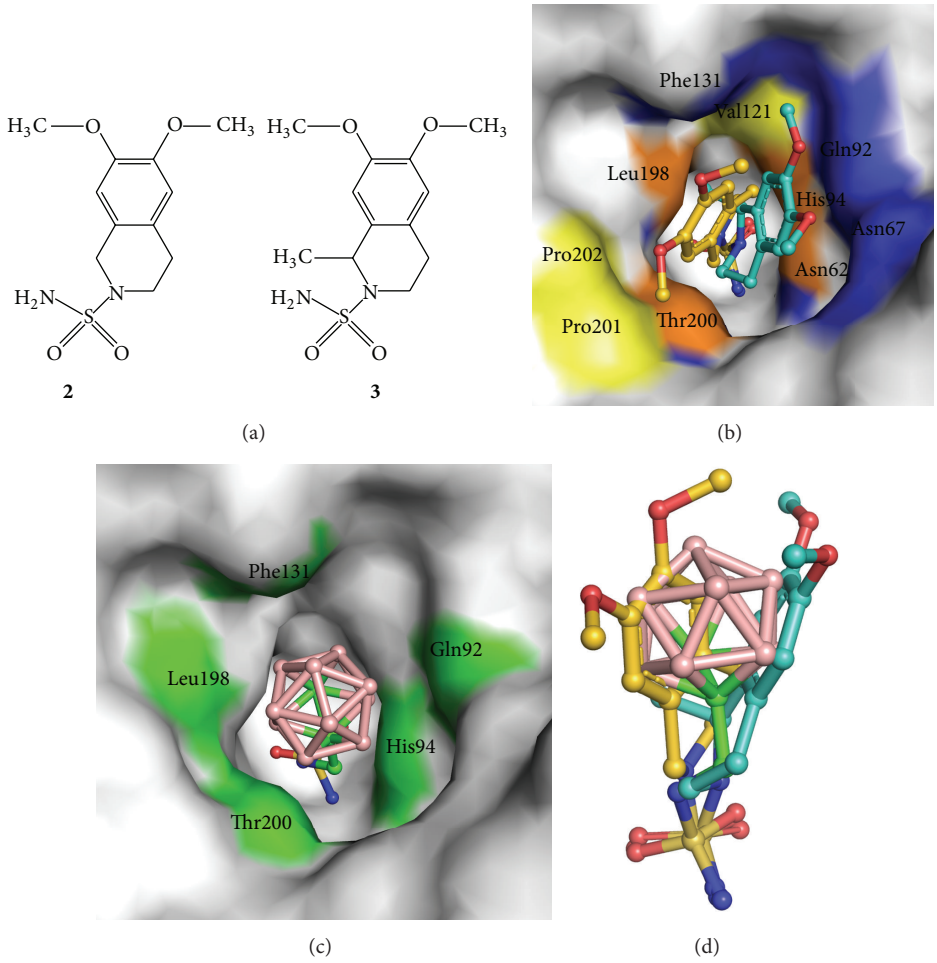

(a) (b) (c) (d)

FIGURE 3: (a) Structural formulas of **2** and **3**. (b) Interactions of **2** and **3** with the CAII active site. Compound **2** is represented with golden carbon atoms, while the carbon atoms of **3** are colored turquoise. Surface of residues making contacts with the isoquinoline moiety of **2** and **3** are highlighted in yellow and blue, respectively. Surface of residues colored orange make contacts with both compounds. Atoms involved in contacts with the sulfonamide groups are not highlighted. (c) Interactions of **1** with the CAII active site. Surface of residues making contacts with the carborane and linker moiety of **1** are highlighted in green. Atoms involved in contacts with the sulfonamide groups are not highlighted. (d) Superposition of binding poses of **1**, **2**, and **3** in the CAII active site. Superposition of the complex structures was based on the best fit for Cα atoms of CAII residues 6–261.

The idea of designing CA inhibitors containing a carborane cluster moiety originated from our previous structural studies of isoquinoline-containing sulfonamide inhibitors (Figure 3(a)). Structural analysis of CAII in complex with 6,7-dimethoxy-1,2,3,4-tetrahydroisoquinolin-2-ylsulfonamide (**2**, PDB code 3IGP, [34]) and 6,7-dimethoxy-1-methyl-1,2,3,4-tetrahydroisoquinolin-2-ylsulfonamide (**3**, PDB code 3PO6, [52]) revealed two distinct binding modes that engage two opposite sides of the enzyme active site cavity (Figure 3(b)). Following this analysis, we hypothesized that the binding space within the enzyme active site cavity could be effectively filled with a bulky hydrophobic molecule with a spherical structure. This led to design of **1** which exhibited inhibitory property to CAII and CAIX with Ki values in submicromolar range. Structural analysis of CAII-**1** indicates that our structure-based design was sound. We found that the carborane cluster interacts with both sides of the enzyme active site as predicted (Figure 3(c), Table 3) and that the position of **1** in the CAII active site superposes well with the two binding modes observed for 2 and 3 (Figure 3(d)).

3.3. Model of the CAIX-1 Complex. The CAII-**1** crystal structure was used to model binding of compound **1** into the CAIX active site using QM/MM methods (Figure 4).

The substrate binding sites of CAII and CAIX differ by only six amino acids: Asn67 of CAII is replaced by Gln in CAIX, Ile91 by Leu, Trp123 by Leu, Phe131 by Val, Val135 by Leu, and Leu204 by Ala. These variations result in a differently shaped active site cavity, which accommodated **1** in a slightly different pose (Figure 4). While the position of the sulfamide anchor remained unchanged, the carborane cluster shifted by 2.1 Å (expressed as a difference in the position of B12) away from the central β-sheet. In CAIX-**1**, the carborane interacts more with the opposite site of the active site, specifically with amino acid residues His94, His96, Glu106, Leu198, Thr199, Thr200, and Pro201 (Figure 4, Table 3). All polar and van der

Table 2: List of contacts between CAII and **1**.

CAII			**1**	
Residue		Atom	Atom[a]	Distance [Å][b]
	Zn	**ZN**	**N2**	**1.87**[c]
	Zn	ZN	S	3.04
	Zn	ZN	O2	3.05
92	Gln	OE1	B6	3.47
92	Gln	OE1	B11	3.52
92	Gln	CD	B6	3.84
94	His	CE1	O2	2.97
94	His	NE2	N2	3.23
94	His	NE2	O2	3.31
94	His	CE1	C3	3.67
94	His	NE2	S	3.81
94	His	CE1	N2	3.82
94	His	CE1	S	3.84
94	His	NE2	C3	3.94
96	His	NE2	N2	3.14
96	His	CE1	N2	3.56
119	His	ND1	N2	3.39
119	His	ND1	O2	3.88
119	His	CE1	N2	3.96
121	Val	CG2	O2	3.82
131	Phe	CZ	B8	3.83
131	Phe	CZ	B7	3.97
198	Leu	CA	O1	3.09
198	Leu	C	O1	3.36
198	Leu	CB	O1	3.60
198	Leu	CD2	O1	3.63
198	Leu	CD1	B3	3.86
199	**Thr**	**N**	**O1**	**2.70**
199	**Thr**	**OG1**	**N2**	**2.74**
199	Thr	OG1	O1	3.58
199	Thr	OG1	S	3.78
199	Thr	N	S	3.83
199	Thr	CA	O1	3.83
199	Thr	CB	N2	3.98
200	**Thr**	**OG1**	**N1**	**3.02**
200	Thr	OG1	C3	3.14
200	Thr	OG1	B4	3.36
200	Thr	OG1	B3	3.56
200	Thr	OG1	C1	3.66

[a]Atom labels correspond to those shown in Figure 1(a).
[b]All contacts with a distance between ligand and protein (or Zn) atoms less than or equal to 4 Å are listed.
[c]Polar interactions are highlighted in bold.

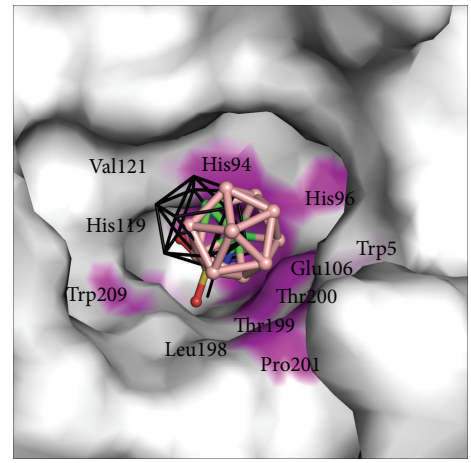

Figure 4: Interactions of **1** with the CAIX active site. Atoms making contacts with the carborane and linker moiety of **1** are highlighted in magenta. Atoms involved in contacts with the sulfonamide groups are not highlighted. Superposition of the binding pose of **1** in CAII is shown as black lines. Superposition is based on the best fit for Cα atoms of all residues of CAII onto CAIX.

Table 3: CAII or CAIX residues interacting with **1**, **2**, and **3**.

	CAII		CAIX
1[a]	**2**[b]	**3**[c]	**1**[d]
			Trp5
		Asn62	
		Asn67[e]	
Gln92	Gln92	Gln92	
His94	His94	His94	His94
His96	His96	His96	His96
			Glu106
His119	His119	His119	His119
Val121		Val121	Val121
Phe131	Phe131	Phe131	
	Val143	Val143	
Leu198	Leu198	Leu198	Leu198
Thr199	**Thr199**	**Thr199**	**Thr199**
Thr200	Thr200	Thr200	**Thr200**
	Pro201		Pro201
	Pro202		
	Trp209		Trp209

Interacting residues were identified from [a]crystal structure 4Q78 (this work); [b]crystal structure 3IGP [34]; [c]crystal structure 3PO6 [52]; [d]computational model (this work); [e]residues making polar interactions are highlighted in bold.

Waals interactions between CAIX and **1** are summarized in Table 4.

We used a virtual glycine scan to study the roles of individual amino acid side chains in the active sites of CAII and CAIX in binding of **1**. The changes in free energy of interaction ($\Delta\Delta G'_{int}$) upon mutation of a given amino acid residue to glycine are shown in Figure 5.

The largest energy change (2.6 kcal/mol) occurred for Trp5, which is positioned closer to **1** in CAIX-**1** than in CAII-**1**. The side chain of Trp5 forms several dihydrogen bonds with the carborane cage of **1**. The shortest one has a H⋯H distance of 2.3 Å. The other major contributor to strong

Table 4: Interactions between CAIX and **1**.

CAIX Residue		Atom	**1** Atom[a]	Distance [Å][b]
	Zn	**ZN**	**N2**	**2.1**[c]
	Zn	ZN	S	3.3
	Zn	ZN	O2	3.5
5	Trp	CZ2	B5	3.74
5	Trp	CZ2	B10	3.81
94	His	CE1	O2	3.15
94	His	CE1	C3	3.74
94	His	NE2	N2	3.36
94	His	NE2	S	3.88
94	His	NE2	O2	3.45
94	His	NE2	C3	3.76
96	His	CE1	N2	3.99
96	His	NE2	N2	3.49
106	Glu	OE2	N2	3.71
119	His	ND1	N2	3.37
119	His	CE1	N2	3.83
121	Val	CG2	O2	3.58
198	Leu	CA	O1	3.04
198	Leu	CB	O1	3.4
198	Leu	CD2	O1	3.43
198	Leu	C	O1	3.38
199	Thr	N	S	3.88
199	**Thr**	**N**	**O1**	**2.79**
199	Thr	CA	O1	3.96
199	Thr	CB	N2	3.85
199	**Thr**	**OG1**	**N2**	**2.63**
199	Thr	OG1	S	3.69
199	Thr	OG1	O1	3.65
200	Thr	OG1	C1	3.77
200	Thr	OG1	B5	3.56
200	**Thr**	**OG1**	**N1**	**3.13**
200	Thr	OG1	C3	3.31
200	Thr	OG1	B4	3.64
201	Pro	O	B4	3.6
201	Pro	O	B10	3.49
201	Pro	O	B8	3.96
209	Trp	CZ2	O1	3.74

[a]Atom labels correspond to those shown in Figure 1(a).
[b]All contacts with a distance less than or equal to 4 Å between ligand and protein (and Zn) atoms are listed.
[c]Polar interactions are highlighted in bold.

CAIX-**1** binding was Asn62; the energy of binding exceeded that in CAII-**1** by nearly 1 kcal/mol. These contributions were cancelled out by differences in binding energy contributions of amino acid residues 131 (Phe/Val) and 135 (Val/Leu), which were lower in CAIX by 0.7 and 0.9 kcal/mol, respectively. The energy changes of other residues were small.

When we compared binding of **1** to CAII and CAIX, we noted that the favorable energy changes in CAIX-**1** due to the binding of residues Trp5, Asn62, and His64 were slightly larger than the unfavorable changes in binding caused by the different amino acids at residues 131 and 135. This is in qualitative agreement with the experimental K_i values, which are 700 ± 141 nm for inhibition of CAII and 380 ± 111 nM for inhibition of CAIX [7].

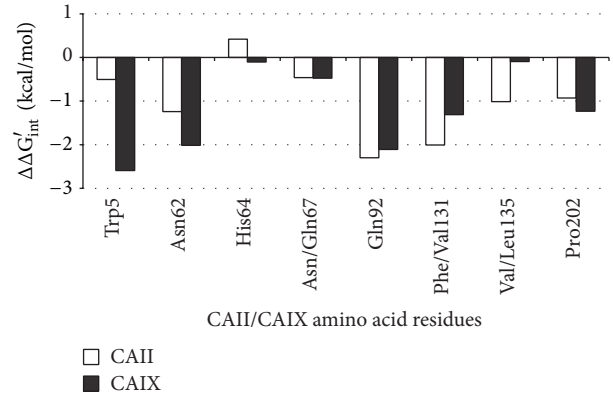

Figure 5: Results of virtual glycine scan showing contributions of individual residues to the energy of binding of **1** to CAII and CAIX, respectively.

4. Conclusions

We determined to atomic resolution the crystal structure of CAII in complex with 1-methylenesulfamide-1,2-dicarba-*closo*-dodecaborane (**1**), a parent compound of a recently reported series of CA inhibitors containing carborane cages [7]. Comparing this crystal structure with those of CAII complexes with conventional organic inhibitors showed that the three-dimensional cluster fills the enzyme active site cavity. Atomic-level resolution allowed us to distinguish the positions of carbon and boron atoms in the carborane cage. The crystal structure also served as a model for construction of the CAIX-**1** computational model. Virtual glycine scan enabled us to quantify the contributions of individual residues to the energy of binding of **1** to CAII and CAIX and uncover differences of the enzyme active site cavities. Structural and computational analysis will be used in future structure-based design of carborane compounds with selectivity toward the cancer-specific CAIX isoenzyme.

Conflict of Interests

The authors declare that there is no conflict of interests regarding the publication of this paper.

Authors' Contribution

Pavel Mader and Adam Pecina contributed equally to this work.

Acknowledgments

This work was supported by the Technology Agency of the Czech Republic (Project TE01020028) and in part by Research Projects RVO 68378050 and 61388963 awarded by

the Academy of Sciences of the Czech Republic. The authors acknowledge the financial support of the Czech Science Foundation (P208/12/G016) and the operational program Research and Development for Innovations of the European Social Fund (CZ 1.05/2.1.00/03/0058). They also thank Gilead Sciences and IOCB Research Centre for financial support. The use of MX14.2 operated by the Helmholtz-Zentrum Berlin at the BESSY II electron storage ring (Berlin-Adlershof, Germany) to collect diffraction data is acknowledged.

References

[1] P. Swietach, S. Patiar, C. T. Supuran, A. L. Harris, and R. D. Vaughan-Jones, "The role of carbonic anhydrase 9 in regulating extracellular and intracellular pH in three-dimensional tumor cell growths," *The Journal of Biological Chemistry*, vol. 284, no. 30, pp. 20299–20310, 2009.

[2] P. C. McDonald, J. Winum, C. T. Supuran, and S. Dedhar, "Recent developments in targeting carbonic anhydrase IX for cancer therapeutics," *Oncotarget*, vol. 3, no. 1, pp. 84–97, 2012.

[3] F. E. Lock, P. C. McDonald, Y. Lou et al., "Targeting carbonic anhydrase IX depletes breast cancer stem cells within the hypoxic niche," *Oncogene*, vol. 32, no. 44, pp. 5210–5219, 2013.

[4] N. K. Tafreshi, M. C. Lloyd, M. M. Bui, R. J. Gillies, and D. L. Morse, "Carbonic anhydrase IX as an imaging and therapeutic target for tumors and metastases," in *Carbonic Anhydrase: Mechanism, Regulation, Links to Disease, and Industrial Applications*, vol. 75 of *Subcellular Biochemistry*, pp. 221–254, 2014.

[5] S. M. Monti, C. T. Supuran, and G. de Simone, "Anticancer carbonic anhydrase inhibitors: a patent review (2008–2013)," *Expert Opinion on Therapeutic Patents*, vol. 23, no. 6, pp. 737–749, 2013.

[6] R. McKenna and C. T. Supuran, "Carbonic anhydrase inhibitors drug design," *Subcellular Biochemistry*, vol. 75, pp. 291–323, 2014.

[7] J. Brynda, P. Mader, V. Sicha et al., "Carborane-based carbonic anhydrase inhibitors," *Angewandte Chemie International Edition in English*, vol. 52, pp. 13760–13763, 2013.

[8] W. N. Lipscomb, *Boron Hydrides*, W.A. Benjamin, New York, NY, USA, 1963.

[9] P. R. Schleyer and K. Najafian, "Stability and three-dimensional aromaticity of closo-monocarbaborane anions, $Cb_{n-1}H_n^-$, and closo-dicarboranes, $C_2B_{n-2}H_n$," *Inorganic Chemistry*, vol. 37, pp. 3454–3470, 1998.

[10] R. E. Williams, in *The Borane , Carborane and Carbocation Continuum*, J. Casanova, Ed., pp. 3–57, John Wiley & Sons, New York, NY, USA, 1997.

[11] J. F. Valliant, K. J. Guenther, A. S. King et al., "The medicinal chemistry of carboranes," *Coordination Chemistry Reviews*, vol. 232, no. 1-2, pp. 173–230, 2002.

[12] Z. J. Lesnikowski, "Boron units as pharmacophores—new applications and opportunities of boron cluster chemistry," *Collection of Czechoslovak Chemical Communications*, vol. 72, no. 12, pp. 1646–1658, 2007.

[13] J. Plešek, "Potential applications of the boron cluster compounds," *Chemical Reviews*, vol. 92, no. 2, pp. 269–278, 1992.

[14] J. Seidler, S. L. McGovern, T. N. Doman, and B. K. Shoichet, "Identification and prediction of promiscuous aggregating inhibitors among known drugs," *Journal of Medicinal Chemistry*, vol. 46, no. 21, pp. 4477–4486, 2003.

[15] M. Sibrian-Vazquez, E. Hao, T. J. Jensen, and M. G. H. Vicente, "Enhanced cellular uptake with a cobaltacarborane-porphyrin-HIV-1 Tat 48-60 conjugate," *Bioconjugate Chemistry*, vol. 17, no. 4, pp. 928–934, 2006.

[16] M. Scholz, M. Steinhagen, J. T. Heiker, A. G. Beck-Sickinger, and E. Hey-Hawkins, "Asborin Inhibits Aldo/Keto Reductase 1A1," *ChemMedChem*, vol. 6, no. 1, pp. 89–93, 2011.

[17] F. Issa, M. Kassiou, and L. M. Rendina, "Boron in drug discovery: carboranes as unique pharmacophores in biologically active compounds," *Chemical Reviews*, vol. 111, no. 9, pp. 5701–5722, 2011.

[18] R. C. Reynolds, S. R. Campbell, R. G. Fairchild et al., "Novel boron-containing, nonclassical antifolates: synthesis and preliminary biological and structural evaluation," *Journal of Medicinal Chemistry*, vol. 50, no. 14, pp. 3283–3289, 2007.

[19] P. Cigler, M. Kozisek, P. Rezacova et al., "From nonpeptide toward noncarbon protease inhibitors: metallacarboranes as specific and potent inhibitors of HIV protease," *Proceedings of the National Academy of Sciences of the United States of America*, vol. 102, pp. 15394–15399, 2005.

[20] P. Řezáčová, J. Pokorná, J. Brynda et al., "Design of HIV protease inhibitors based on inorganic polyhedral metallacarboranes," *Journal of Medicinal Chemistry*, vol. 52, no. 22, pp. 7132–7141, 2009.

[21] Y. Endo, T. Iijima, Y. Yamakoshi et al., "Potent estrogen agonists based on carborane as a hydrophobic skeletal structure: a new medicinal application of boron clusters," *Chemistry & Biology*, vol. 8, no. 4, pp. 341–355, 2001.

[22] R. L. Julius, O. K. Farha, J. Chiang, L. J. Perry, and M. F. Hawthorne, "Synthesis and evaluation of transthyretin amyloidosis inhibitors containing carborane pharmacophores," *Proceedings of the National Academy of Sciences of the United States of America*, vol. 104, no. 12, pp. 4808–4813, 2007.

[23] S. Fujii, H. Masuno, Y. Taoda et al., "Boron cluster-based development of potent nonsecosteroidal vitamin D receptor ligands: direct observation of hydrophobic interaction between protein surface and carborane," *Journal of the American Chemical Society*, vol. 133, no. 51, pp. 20933–20941, 2011.

[24] V. M. Krishnamurthy, G. K. Kaufman, A. R. Urbach et al., "Carbonic anhydrase as a model for biophysical and physical-organic studies of proteins and protein-ligand binding," *Chemical Reviews*, vol. 108, no. 3, pp. 946–1051, 2008.

[25] K. Raha, M. B. Peters, B. Wang et al., "The role of quantum mechanics in structure-based drug design," *Drug Discovery Today*, vol. 12, no. 17-18, pp. 725–731, 2007.

[26] M. Lepšík, J. Řezáč, M. Kolář, A. Pecina, P. Hobza, and J. Fanfrlík, "The semiempirical quantum mechanical scoring function for in silico drug design," *ChemPlusChem*, vol. 78, pp. 921–931, 2013.

[27] A. Pecina, M. Lepsik, J. Rezac et al., "QM/MM calculations reveal the different nature of the interaction of two carborane-based sulfamide inhibitors of human carbonic anhydrase II," *The Journal of Physical Chemistry B*, vol. 117, pp. 16096–16104, 2013.

[28] C. A. Behnke, I. Le Trong, J. W. Godden et al., "Atomic resolution studies of carbonic anhydrase II," *Acta Crystallographica D: Biological Crystallography*, vol. 66, no. 5, pp. 616–627, 2010.

[29] U. Mueller, N. Darowski, M. R. Fuchs et al., "Facilities for macromolecular crystallography at the Helmholtz-Zentrum Berlin," *Journal of Synchrotron Radiation*, vol. 19, no. 3, pp. 442–449, 2012.

[30] T. G. G. Battye, L. Kontogiannis, O. Johnson, H. R. Powell, and A. G. Leslie, "iMOSFLM: a new graphical interface for diffraction-image processing with MOSFLM," *Acta Crystallographica D*, vol. 67, no. 4, pp. 271–281, 2011.

[31] P. Evans, "Scaling and assessment of data quality," *Acta Crystallographica Section D: Biological Crystallography*, vol. 62, no. 1, pp. 72–82, 2006.

[32] A. T. Brunger, "Free *R* value: a novel statistical quantity for assessing the accuracy of crystal strucutres," *Nature*, vol. 355, no. 6359, pp. 472–475, 1992.

[33] S. C. Lovell, I. W. Davis, W. B. Arendall III et al., "Structure validation by Cα geometry: φ,ψ and Cβ deviation," *Proteins*, vol. 50, no. 3, pp. 437–450, 2003.

[34] R. Gitto, S. Agnello, S. Ferro et al., "Identification of 3,4-dihydroisoquinoline-2(1H)-sulfonamides as potent carbonic anhydrase inhibitors: synthesis, biological evaluation, and enzyme-ligand X-ray studies," *Journal of Medicinal Chemistry*, vol. 53, no. 6, pp. 2401–2408, 2010.

[35] G. N. Murshudov, A. A. Vagin, and E. J. Dodson, "Refinement of macromolecular structures by the maximum-likelihood method," *Acta Crystallographica D*, vol. 53, no. 3, pp. 240–255, 1997.

[36] "The CCP4 suite: programs for protein crystallography," *Acta Crystallographica D*, vol. 50, pp. 760–763, 1994.

[37] P. Jurečka, J. Černý, P. Hobza, and D. R. Salahub, "Density functional theory augmented with an empirical dispersion term. Interaction energies and geometries of 80 noncovalent complexes compared with ab initio quantum mechanics calculations," *Journal of Computational Chemistry*, vol. 28, no. 2, pp. 555–569, 2007.

[38] F. Weigend and R. Ahlrichs, "Balanced basis sets of split valence, triple zeta valence and quadruple zeta valence quality for H to Rn: design and assessment of accuracy," *Physical Chemistry Chemical Physics*, vol. 7, no. 18, pp. 3297–3305, 2005.

[39] R. Ahlrichs, M. Bär, M. Häser, H. Horn, and C. Kölmel, "Electronic structure calculations on workstation computers: the program system turbomole," *Chemical Physics Letters*, vol. 162, no. 3, pp. 165–169, 1989.

[40] P. Emsley and K. Cowtan, "Coot: model-building tools for molecular graphics," *Acta Crystallographica D: Biological Crystallography*, vol. 60, no. 12, pp. 2126–2132, 2004.

[41] W. L. DeLano, *The PyMOL Molecular Graphics System*, DeLano Scientific LLC, San Carlos, Calif, USA, 2002, http://www.pymol.org.

[42] V. Alterio, M. Hilvo, A. Di Fiore et al., "Crystal structure of the catalytic domain of the tumor-associated human carbonic anhydrase IX," *Proceedings of the National Academy of Sciences of the United States of America*, vol. 106, no. 38, pp. 16233–16238, 2009.

[43] W. L. DeLano, *The PymoL Molecular Graphics System*, DeLano Scientific, Palo Alto, Calif, USA, 2002.

[44] M. Svensson, S. Humbel, R. D. J. Froese, T. Matsubara, S. Sieber, and K. Morokuma, "ONIOM: a multilayered integrated MO + MM method for geometry optimizations and single point energy predictions. A test for Diels-Alder reactions and Pt(P(t-Bu)$_3$)$_2$ + H$_2$ oxidative addition," *The Journal of Physical Chemistry*, vol. 100, no. 50, pp. 19357–19363, 1996.

[45] A. Pecina, O. Přenosil, J. Fanfrlík et al., "On the reliability of the corrected semiempirical quantum chemical method (PM6-DH2) for assigning the protonation states in HIV-1 protease/inhibitor complexes," *Collection of Czechoslovak Chemical Communications*, vol. 76, no. 5, pp. 457–479, 2011.

[46] P. S. Brahmkshatriya, P. Dobeš, J. Fanfrlík et al., "Quantum mechanical scoring: structural and energetic insights into cyclin-dependent kinase 2 inhibition by pyrazolo[1,5-a]pyrimidines," *Current Computer—Aided Drug Design*, vol. 9, no. 1, pp. 118–129, 2013.

[47] J. Fanfrlík, M. Kolář, M. Kamlar et al., "Modulation of aldose reductase inhibition by halogen bond tuning," *ACS Chemical Biology*, vol. 8, pp. 2484–2492, 2013.

[48] J. Fanfrlík, P. S. Brahmkshatriya, J. Řezáč et al., "Quantum mechanics-based scoring rationalizes the irreversible inactivation of parasitic *Schistosoma mansoni* cysteine peptidase by vinyl sulfone inhibitors," *Journal of Physical Chemistry B*, vol. 117, pp. 14973–14982, 2013.

[49] H. J. C. Berendsen, J. P. M. Postma, W. F. Van Gunsteren, A. Dinola, and J. R. Haak, "Molecular dynamics with coupling to an external bath," *The Journal of Chemical Physics*, vol. 81, no. 8, pp. 3684–3690, 1984.

[50] D. A. Case, T. E. Cheatham III, T. Darden et al., "The Amber biomolecular simulation programs," *Journal of Computational Chemistry*, vol. 26, no. 16, pp. 1668–1688, 2005.

[51] M. J. Betts and M. J. E. Sternberg, "An analysis of conformational changes on protein-protein association: implications for predictive docking," *Protein Engineering*, vol. 12, no. 4, pp. 271–283, 1999.

[52] P. Mader, J. Brynda, R. Gitto et al., "Structural Basis for the Interaction between Carbonic Anhydrase and 1,2,3,4-tetrahydroisoquinolin-2-ylsulfonamides," *Journal of Medicinal Chemistry*, vol. 54, no. 7, pp. 2522–2526, 2011.

Hindawi Publishing Corporation
BioMed Research International
Volume 2014, Article ID 162928, 10 pages
http://dx.doi.org/10.1155/2014/162928

Research Article

Sulfa Drugs as Inhibitors of Carbonic Anhydrase: New Targets for the Old Drugs

Mariya al-Rashida,[1] Sajad Hussain,[1] Mehwish Hamayoun,[2] Aisha Altaf,[2] and Jamshed Iqbal[2]

[1] *Department of Chemistry, Forman Christian College (A Chartered University), Ferozepur Road, Lahore 54600, Pakistan*
[2] *Centre for Advanced Drug Research, COMSATS Institute of Information Technology, Abbottabad 22060, Pakistan*

Correspondence should be addressed to Mariya al-Rashida; maria_al_rashida@hotmail.com and Jamshed Iqbal; drjamshed@ciit.net.pk

Received 28 February 2014; Revised 19 June 2014; Accepted 15 July 2014; Published 8 September 2014

Academic Editor: Anna Di Fiore

Sulfa drugs are well-known antibacterial agents containing N-substituted sulfonamide group on para position of aniline ring (NH_2RSO_2NHR'). In this study 2,4-dichloro-1,3,5-triazine derivatives of sulfa drugs, sulfamerazine (**1b**), sulfaquinoxaline (**2b**), sulfadiazine (**3b**), sulfadimidine (**4b**), and sulfachloropyrazine (**5b**) (**1a**–**5a**) were synthesized and characterized. Their carbonic anhydrase inhibition activity was evaluated against bovine cytosolic carbonic anhydrase isozyme II (bCA II). For the sake of comparison the CA inhibition activity of the parent sulfa drugs (**1b**–**5b**) was also evaluated. A significant increase in CA inhibition activity of sulfa drugs was observed upon substitution with 2,4-dichloro-1,3,5-triazine moiety. Molecular docking studies were carried out to highlight binding site interactions. ADME properties were calculated to evaluate drug likeness of the compounds.

1. Introduction

Carbonic anhydrase (CA, EC 4.2.1.1) is a well-known ubiquitous zinc containing metalloenzyme that is found in animals including man, plants, bacteria, and archaea. The active site zinc ion (Zn^{2+}) has been conserved in all classes of carbonic anhydrases [1]. This enzyme catalyzes an apparently simple yet physiologically important reaction of interconversion of water and carbon dioxide into bicarbonate and protons. Therefore CA has an important role to play in the transport of CO_2 from metabolizing tissues to lungs. It is also responsible for maintaining acid/base and electrolyte balance in blood [2, 3]. Certain biosynthetic reactions are also assisted by CA such as lipogenesis, at the level of pyruvate carboxylation [4, 5], ureagenesis [6], and gluconeogenesis [6, 7]. In mammals carbonic anhydrase has sixteen different isozymes based on their distribution in tissues and subcellular localization. The cytosolic isozymes are CA I, CA II, CA III, CA VII, and CA XIII, whereas CA IV, CA IX, CA XII, CA XIV, and CA XV are membrane bound isozymes, and CA VA and CA VB are mitochondrial isozymes; CA VI is secreted isozyme mainly present in the saliva [8]. There are certain physiological disorders that are characterized by overexpression of CA [9–11], hence CAs have emerged as valuable drug targets. Many clinically established drugs are CA inhibitors and are used to treat disorders such as glaucoma, acidic ulcers, mountain/sea sickness, and epilepsy [12]. Carbonic anhydrase is also an important drug target for treating obesity and many sulfonamide inhibitors have proved to be efficient antiobesity agents [13–16]. The transmembrane isozymes CA IX and CA XII have been found to be overexpressed in hypoxic tumors (having acidic environment) whereas their distribution in normal cells remains low [17–22].

Sulfonamides and their derivatives are well-known inhibitors of carbonic anhydrase [18, 23]. Sulfa drugs are derived from sulfonamides; however all sulfonamides are not sulfa drugs, and the term sulfa drug is only used for clinically used antibacterial agents that are structurally derived from 4-aminobenzenesulfonamide, where the sulfonamide nitrogen is substituted (NH_2RSO_2NHR') [24, 25]. The carbonic

anhydrase inhibition activity of sulfa drugs has not been explored. Previously 1,3,5-triazine [26, 27] and 1,2,4-triazine [28] derivatives of different sulfonamides have been reported as efficient inhibitors of CA. Herein we report the synthesis of new 2,4,6-trichloro-1,3,5-triazine (TCT) derivatives of sulfa drugs (**1a**–**5a**) and their carbonic anhydrase inhibition activity against bovine cytosolic carbonic anhydrase II (bCA II). For the purpose of comparison, the carbonic anhydrase inhibition activity of parent sulfa drugs (**1b**–**5b**) is also reported.

2. Material and Methods

All chemicals used were purchased from either Sigma or Aldrich and used as such without further purification. Commercially available solvents were used. Ethanol was distilled and dried using standard methods and stored over molecular sieves. Reaction progress and product purity were checked via precoated TLC plates (silica gel, 0.2 mm, 60 HF_{254}, Merck). TLC spots were visualized under short and long wavelength UV light. Bovine cytosolic carbonic anhydrase II (bCA II) was used. Melting points were taken on a Gallenkamp melting point apparatus and were uncorrected. FTIR spectra were taken on Perkin Elmer Spectrum BX-II. LECO CHNS 630 series elemental analyzer (model 630-200-200) was used for elemental analysis. For ^{1}H and ^{13}C-NMR analysis Bruker Avance DRX500 spectrometer was used with TMS as an internal standard and DMSO-d_6 as solvent.

2.1. General Method of Synthesis. For the synthesis of TCT derived sulfa drugs, 2,4,6-trichloro-1,3,5-triazine (TCT, 0.01 mol), respective sulfa drug (0.01 mol), and sodium carbonate (0.1–0.2 g) were taken in a round bottom flask, 20 mL of ethanol and 5–7 mL acetone were added to it, and stirring was continued until a clear solution resulted. The reaction mixture was refluxed with constant stirring. After 2 hours solid precipitate began to appear in the reaction mixture; the reaction was allowed to continue for another hour after which the solid product was filtered, washed, and dried. Compounds were recrystallized with a mixture of acetone and acetonitrile.

*2.1.1. Synthesis of 4-[(4,6-Dichloro-1,3,5-triazin-2-yl)amino]-N-(4-methylpyrimidin-2-yl)benzenesulfonamide (**1a**).* Yield 80%; m.p. 235–237°C; IR (ν, cm^{-1}): 3438 (NH_2), 1145 (SO_2^{sym}), 1341 (SO_2^{asym}), 779 (C–Cl); Anal. calcd for $C_{14}H_{11}Cl_2N_7O_2S$: C(40.79%), H(2.69%), N(23.78%), S(7.78%); found C(39.89%), H(3.4%), N(23.18%), S(7.54%). ^{1}H-NMR (500 MHz, DMSO-d_6), δ (ppm): 2.29 (s, 3H, $-CH_3$), 8.31 (1H, m, H4″), 7.99 (2H, d, ^3J = 10 Hz, H3′, H5′), 7.65 (2H, d, ^3J = 10 Hz, H2′, H6′), 7.78 (1H, d, ^3J = 5 Hz, H5″), 11.13 (s, 1H, SO_2NH), 8.34 (s, 1H, NH). ^{13}C-NMR (125 MHz, DMSO-d_6), δ (ppm): 157.70 (C1, C2), 156.99 (C3), 156.65 (C1″), 150.02 (C1′), 130.08 (C3″, C5″), 129.11 (C3′, C5′), 120.74 (C4′), 119.59 (C2′, C6′), 114.85 (C4″), 23.45 (CH_3).

*2.1.2. Synthesis of 4-[(4,6-dichloro-1,3,5-triazin-2-yl)amino]-N-(quinoxalin-2-yl)benzenesulfonamide (**2a**).* Yield 87%; m.p. 268–270°C; IR (ν, cm^{-1}): 3248 (NH_2), 1151 (SO_2^{sym}), 1314 (SO_2^{asym}), 727 (C–Cl); Anal. calcd for $C_{17}H_{11}Cl_2N_7O_2S$: C (45.55%) H(2.47%), N (21.87%), S(7.15%); found C(44.87%), H(2.71%), N(20.90%), S(7.54%). ^{1}H-NMR (500 MHz, DMSO-d_6), δ (ppm): 8.08 (2H, d, ^3J = 10 Hz, H3′, H5′), 7.93 (2H, d, ^3J = 10 Hz, H2′, H6′), 7.79 (1H, s, H9″), 7.78 (2H, m, H4″, H7″), 7.72 (2H, m, H5″, H6″), 10.82 (s, 1H, SO_2NH), 8.63 (s, 1H, NH). ^{13}C-NMR (125 MHz, DMSO-d_6), δ (ppm): 164.08 (C3), 154.14 (C1, C2), 150.02 (C1″), 146.19 (C1′), 142.16 (C3″), 131.09 (C8″), 129.12 (C3′, C5′), 128.87 (C4″, C7″), 127.41 (C5″, C6″), 120.91 (C4′), 120.06 (C2′, C6′).

*2.1.3. Synthesis of 4-[(4,6-Dichloro-1,3,5-triazin-2-yl)amino]-N-(pyrimidin-2-yl)benzenesulfonamide (**3a**).* Yield 88%; m.p. 221–223°C; IR (ν, cm^{-1}): 3286 (NH_2), 1143 (SO_2^{sym}), 1335 (SO_2^{asym}), 688 (C–Cl); Anal. calcd for $C_{13}H_9Cl_2N_7O_2S$: C(39.21%), H(2.28%), N(24.62%), S(8.05%); found C(39.19%), H(2.46%), N(24.17%), S(8.51%). ^{1}H-NMR (500 MHz, DMSO-d_6), δ (ppm): 8.50 (2H, d, ^3J = 10 Hz, H3′, H5′), 7.96 (2H, d, ^3J = 10 Hz, H2′, H6′), 7.77 (2H, d, ^3J = 5 Hz, H3″, H5″), 7.04 (1H, t, ^3J = 5 Hz, H4″), 8.0 (1H, s, NH), 10.82 (1H, s, SO_2NH). ^{13}C-NMR (125 MHz, DMSO-d_6), δ (ppm): 158.48 (C1, C2), 157.03 (C3), 154.21 (C1″), 141.81 (C1′), 134.89 (C3″, C5″), 128.92 (C3′, C5′), 120.81 (C4′), 120.07 (C2′, C6′), 115.91 (C4″).

*2.1.4. Synthesis of 4-[(4,6-Dichloro-1,3,5-triazin-2-yl)amino]-N-(4,6-dimethylpyrimidin-2-yl)benzenesulfonamide (**4a**).* Yield 84%; m.p. 327–329°C; IR (ν, cm^{-1}): 3211 (NH_2), 1161 (SO_2^{sym}), 1334 (SO_2^{asym}), 697 (C–Cl); Anal. calcd for $C_{15}H_{13}Cl_2N_7O_2S$: C(42.26%), H(3.07%), N(23.00%), S(7.52%); found C(42.87%), H(2.91%), N(23.20%), S(7.56). ^{1}H-NMR (500 MHz, DMSO-d_6), δ (ppm): 2.24 (6H, s, CH_3), 6.74 (1H, s, H4″), 7.95 (2H, d, ^3J = 10 Hz, H3′, H5′), 7.85 (2H, d, ^3J = 10 Hz, H2′, H6′), 7.83 (1H, s, NH), 10.61 (1H, s, SO_2NH). ^{13}C-NMR (125 MHz, DMSO-d_6), δ (ppm): 23.02 (CH_3), 164.0 (C1, C2), 156.33 (C3), 142.20 (C1′), 129.21 (C3″, C5″), 129.09 (C3′, C5′), 120.02 (C4′), 119.71 (C4″).

*2.1.5. Synthesis of N-(6-Chloropyrazin-2-yl)-4-[(4,6-dichloro-1,3,5-triazin-2-yl)amino]benzenesulfonamide (**5a**).* Yield 85%; m.p. 236–238°C; IR (ν, cm^{-1}): 3255 (NH_2), 1158 (SO_2^{sym}), 1336 (SO_2^{asym}), 692 (C–Cl); Anal. calcd for $C_{13}H_8Cl_3N_7O_2S$: C(36.09%), H(1.86%), N(22.66%), S(7.41%); found C(36.15%), H(1.94%), N(22.03%), S(7.44%). ^{1}H-NMR (500 MHz, DMSO-d_6), δ (ppm): 8.01 (2H, d, ^3J = 10 Hz, H3′, H5′), 7.62 (2H, d, ^3J = 10 Hz, H2′, H6′), 7.58 (1H, s, H4″), 7.32 (1H, s, H6″), 10.71 (s, 1H, SO_2NH), 8.54 (s, 1H, NH). ^{13}C-NMR (125 MHz, DMSO-d_6), δ (ppm): 164.08 (C3), 154.14 (C1, C2), 150.02 (C1″), 146.19 (C1′), 152.10 (C3″), 129.12 (C3′, C5′), 132.87 (C4″), 128.41 (C6″), 121.21 (C4′), 120.13 (C2′, C6′).

2.2. In Vitro Carbonic Anhydrase Inhibition Assay. Carbonic anhydrase inhibition was measured by the reported method

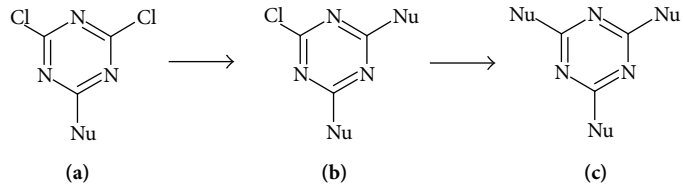

Figure 1: Decreasing order of ease of nucleophilic substitution on 2,4,6-trichloro-1,3,5-trizine ring, where Nu is a nucleophile [37].

[29] after standardization of reaction conditions such as concentration of enzyme and substrate, buffer pH, and duration of reaction. The method is based on spectrophotometric determination *p*-nitrophenol, the CA catalyzed hydrolysis product of *p*-nitrophenyl acetate. The reaction mixture consisted of 60 μL of 50 mM Tris-sulfate buffer (pH 7.6, containing 0.1 mM $ZnCl_2$), 10 μL (0.5 mM) test compound in 1% DMSO, and 10 μL (50 U) bovine enzyme per well. Contents were mixed together and preincubated at 25°C for 10 minutes. Plates were preread at 348 nm using a 96-well plate reader. Substrate, *p*-nitrophenyl acetate (6 mM stock using <5% acetonitrile in buffer), 20 μL was freshly prepared and added per well to achieve 0.6 mM concentration per well. Total reaction volume was made to 100 μL. After incubating for 30 minute at 25°C, the contents were mixed and read at 348 nm. Suitable controls with DMSO and standard inhibitor acetazolamide (AZM) were included in the assay. Results reported are mean of three independent experiments (±SEM) and expressed as percent inhibitions calculated by the following formula: Inhibition (%) = [100 − (abs of test comp/abs of control) × 100)]. IC_{50} values of compounds (0.5 mM concentration) exhibiting >50% inhibition activity were calculated after suitable dilutions.

2.3. Molecular Docking Studies

2.3.1. Receptor and Ligand Preparation. High resolution crystal structures of hCA II (0.90 Å) [30] and bCA II (1.95 Å) [31] were downloaded from the Protein Data Bank (PDB-IDs: 3K34 and 1V9E, resp.). Structural comparison and percent similarity (87.3%) and percent identity (80%) between bovine and human CA II have already been reported by our research group [32]. The RMSD with respect to the active site residues of the two proteins is 0.22 Å [32]. Method validation was done by redocking the bound ligand extracted from the active site of hCA-II (3K34). The docking method was able to reproduce the experimentally bound conformation of ligand in the active site with an RMSD of <2 Å. Method validation via self-docking could not be carried out for bCA II, since this enzyme did not contain any cocrystallized ligand. On this basis hCA-II was selected to carry out further molecular docking studies. For docking the receptor (hCA II) was prepared using DockPrep utility of Chimera software [33], which includes standard preparation steps such as adding hydrogen atoms and adding gasteiger charges using ANTECHAMBER [34] and repairing incomplete side chains (if any) using Dunbrack rotamer library. A charge of +2 was added on the zinc atom. Before docking the structures of all molecules were drawn using ACD/ChemSketch [35]. Gasteiger charges were added on each ligand using ANTECHAMBER [34] and the energy of each molecule was minimized through 100 steepest descents and 100 conjugate gradient steps using a step size of 0.02 each using Chimera [33]. Before docking, compounds were protonated (as in aqueous environment) using LeadIT 2.1.7 [36].

2.3.2. Docking Methodology. For docking studies the binding site was defined, using LeadIT [36] with the aid of reference ligand which had cocrystallized with the enzyme. The binding site included amino acid residues within 8.0 Å of the active site. Docking studies were carried out using LeadIT [36] program that incorporates FlexX for docking calculations. The default docking and scoring parameters were kept for the docking calculations; first top 10 docked conformations of lowest energy were retained for detailed analysis of binding site interactions and binding modes. In order to validate the docking protocol, method validation was carried out by redocking the ligand extracted from 3K34; the docking was successfully able to reproduce the correct binding mode for the native ligand with an RMSD of <2.

3. Results and Discussion

3.1. Chemistry. 2,4,6-Trichloro-1,3,5-triazine is an important and versatile molecule that provides the possibility of nucleophilic replacement at all three chlorine atoms. The synthetic utility and biological activities of this molecule are well known [37]. The ease of nucleophilic chloride replacement decreases as the number of chlorine atoms to be replaced decreases; thus nucleophilic replacement that results in synthesis of (**a**) proceeds far more swiftly than subsequent reactions that result in synthesis of molecules of types (**b**) and (**c**) (Figure 1).

Thus by reacting equimolar amounts of 2,4,6-trichloro-1,3,5-triazine and sulfa drugs, sulfamerazine (**1b**), sulfaquinoxaline (**2b**), sulfadiazine (**3b**), sulfadimidine (**4b**), and sulfachloropyrazine (**5b**), products of type (**a**) (see Scheme 1) were easily obtained without interference from di- or tri-substituted products. The structures of sulfa drugs used **1b**–**5b** are given in Figure 2.

3.2. bCA II Inhibition Studies and SAR. The synthesized compounds (**1a**–**5a**) and their parent sulfa drugs (**1b**–**5b**) were screened against bovine cytosolic carbonic anhydrase II (bCA II). The CA active site residues involved in direct zinc binding are His94, His96, and His119. In addition

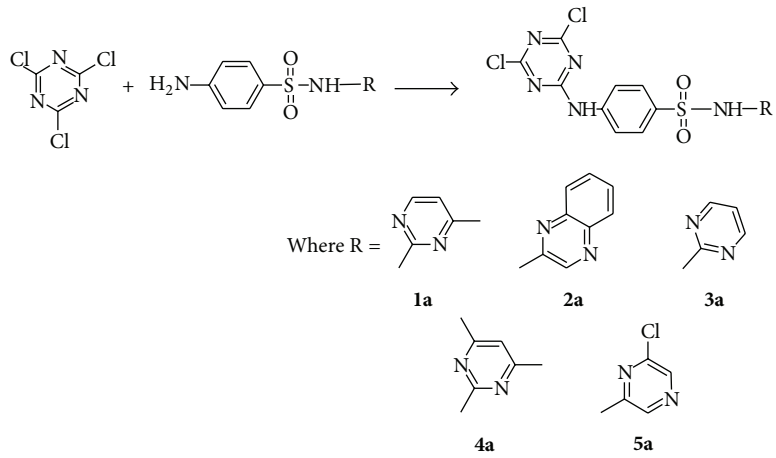

Scheme 1: Synthesis of 2,4,6-trichloro-1,3,5-triazine (TCT) derivatives (**1a**–**5a**) of sulfa drugs sulfamerazine (**1b**), sulfaquinoxaline (**2b**), sulfadiazine (**3b**), sulfadimidine (**4b**), and sulfachloropyrazine (**5b**), respectively.

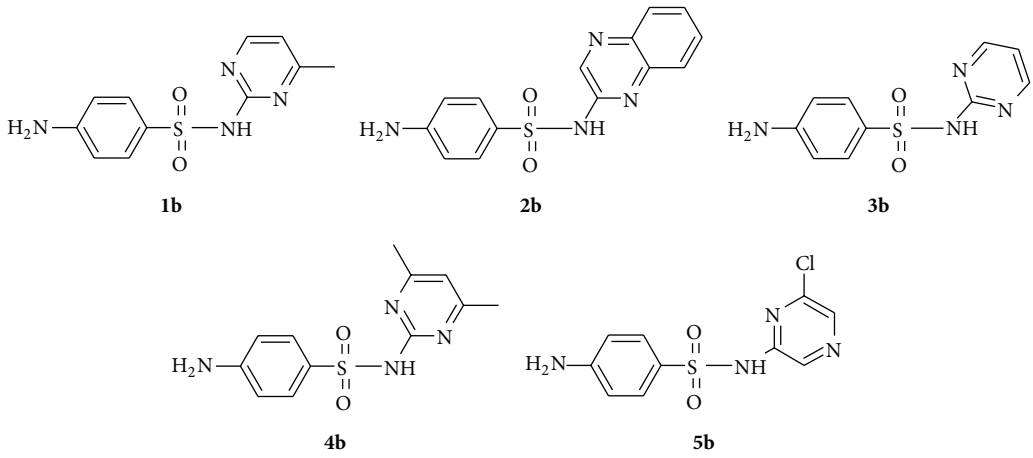

Figure 2: Structures of sulfa drugs, sulfamerazine (**1b**), sulfaquinoxaline (**2b**), sulfadiazine (**3b**), sulfadimidine (**4b**), and sulfachloropyrazine (**5b**).

the substrate (CO_2) association pocket, Thr199 loop, and the histidine proton shuttle mechanism (for regeneration of active site Zn bound hydroxide ion) are essential for CA catalytic activity and are highly conserved in all alpha class CAs. For this reason initial screening against bCA-II was carried out. For comparison the bCA II inhibition activity of clinically used standard CA inhibitor acetazolamide (AZM) was also carried out (Table 1). The CA inhibition activity for all compounds is given in Table 1. All chloro triazine derived compounds were active inhibitors of bCA II. A significant increase in CA inhibition activity was observed for sulfa drugs containing chloro triazine moieties. Sulfa drugs (**1b**–**5b**) also exhibited the potential to inhibit bCA II; however their inhibitor potency is not significant. The most active sulfa drug was **2b** showing CA inhibition up to 51.8% followed by **5b** (42.4%). The corresponding chloro triazine derivative of **5b**, that is, compound **5a**, was the most active inhibitor of bCA II having IC_{50} value of 1.49 μM. For compounds **1a**–**5a**, the bCA II inhibition activity decreases in the order **5a** > **1a** > **4a** > **3a** > **2a**, whereas for the parent sulfa drugs **1b**–**5b**, the inhibition activity decreases as **2b** > **5b** > **4b** > **3b** > **1b**.

Molecular docking studies were carried out to investigate the mode of binding as well as important binding site interactions that could possibly explain the increased CA inhibition observed for chloro triazine derived compounds. Molecular docking studies were performed using LeadIT software. Before starting the molecular docking studies, the docking methodology was validated by redocking the ligand (that had cocrystallized with the hCA II enzyme 3K34). The docking method successfully reproduced the binding mode of native ligand with an RMSD of <2 Å. Although none of the compounds tested here contained a free sulfonamide group (SO_2NH_2), which is the typical zinc binding function that binds directly to the Zn^{2+} metal center of CA, still all compounds were able to inhibit this enzyme. Molecular docking studies reveal that, in addition to forming stable hydrogen bond interactions with surrounding amino acid residues as well as certain favorable hydrophobic interactions, these

Table 1: bCA II inhibition data for compounds **1a**–**5a** and their parent compounds **1b**–**5b**.

Compounds	IC_{50} ± SEM (μM) (or % inhibition)[a]
1a	4.14 ± 0.02
2a	105.3 ± 0.16
3a	24.9 ± 0.03
4a	14.9 ± 0.02
5a	1.49 ± 0.006
1b	(19.6 ± 0.2)
2b	(51.8 ± 0.6)
3b	(31.2 ± 0.5)
4b	(41.7 ± 1.2)
5b	(42.4 ± 0.7)
AZM	1.16 ± 0.02

[a]% inhibition at 0.5 mM concentration of tested compounds; AZM: acetazolamide.

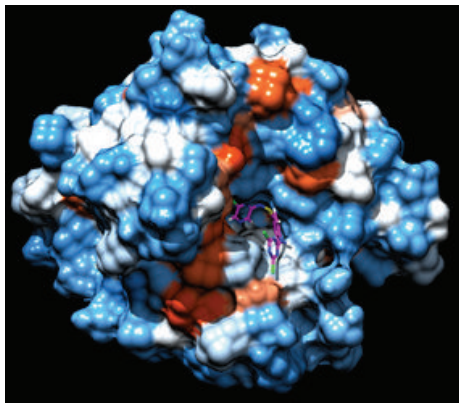

Figure 3: Compound **5a** inside binding pocket of hCA II. **5a** is shown in magenta color with sticks representation. The hydrophobic surfaces are drawn using Chimera and the color scheme is according to *Kyte-Doolittle coloring scheme;* blue color indicates most hydrophilic surface (hence polar residues), white for neutral, and orange for hydrophobic surface (nonpolar residues).

molecules were able to inhibit the enzyme by fitting inside the entrance of the active site such that the aryl group substituted on the sulfonamide nitrogen fits inside the hydrophobic pocket (the typical arylsulfonamide binding pocket) and the dichloro-triazine moiety fills the adjacent hydrophilic pocket (Figures 3 and 4). In all compounds studied, the sulfonamide group did not form a direct bond with the Zn^{2+} metallic centre, as expected, since the sulfonamide nitrogen atom is not free and is substituted. The binding modes of compounds were similar to one another. In general, for compounds **1a**–**5a**, the sulfonamide nitrogen makes hydrogen bond interaction with Gln92 and sulfonamide oxygen makes hydrogen bond interactions with Asn62 and Asn67 (Figure 5). Similar interactions were observed for sulfonamide group of sulfa drugs **1b**–**5b** (Figure 6). In most binding conformations for **1a**–**5b**, the nitrogen atom of the triazine ring was found to be involved in hydrogen bond contact with Trp5. Common

Table 2: Docking scores and their corresponding ranks as judged by Hyde affinity assessment.

Compound	Docking score	Rank	ΔG (KJ/mol)
1a	−15.96	7	−6
2a	−19.87	1	−2
3a	−15.04	9	−5
4a	−16.64	9	−1
5a	−17.06	6	−15
1b	−20.37	7	−8
2b	−20.37	7	−8
3b	−20.66	6	−7
4b	−18.18	7	−11
5b	−15.55	8	−5

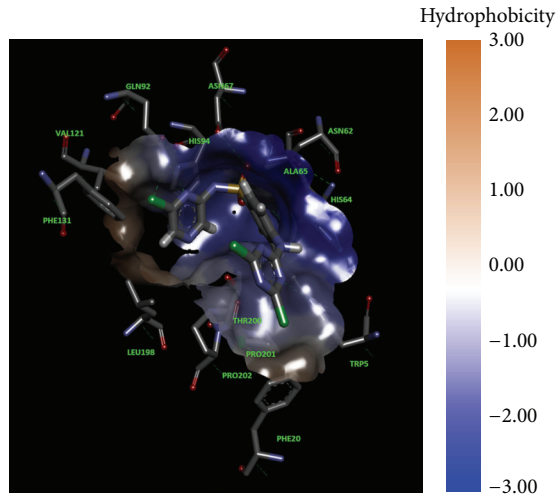

Figure 4: Interactions of compound **5a** with active site residues.

residues involved in hydrophobic and van der Waals interactions are Leu198, Val121, His94, Thr200, and Phe131. As indicated by molecular docking studies compounds **1a**–**5a** are better able to inhibit CA II as compared to compounds **1b**–**5b**, due to the presence of additional 2,4-dichloro-1,3,5-triazine moiety that fits in the adjacent hydrophilic pocket as seen in Figures 3 and 4.

Docking scores and their corresponding ranks are given in Table 2. The ranks of docked ligand conformations with most favorable binding mode were decided after running Hyde affinity assessment of first 10 lowest energy docked conformations. Hyde Affinity Assessment is a utility included in the LeadIT software; it allows selection of best docked conformation on the basis of calculated binding free energy. The docked conformation which has the least binding free energy (ΔG, KJ/mol) is most favorable. Thus, out of 10 lowest energy conformations, the conformation that had the lowest binding free energy ΔG, after Hyde assessment, was chosen and its corresponding rank and docking score are given in Table 2. The 2D interaction diagrams of binding site interactions are given in Figures 5 and 6.

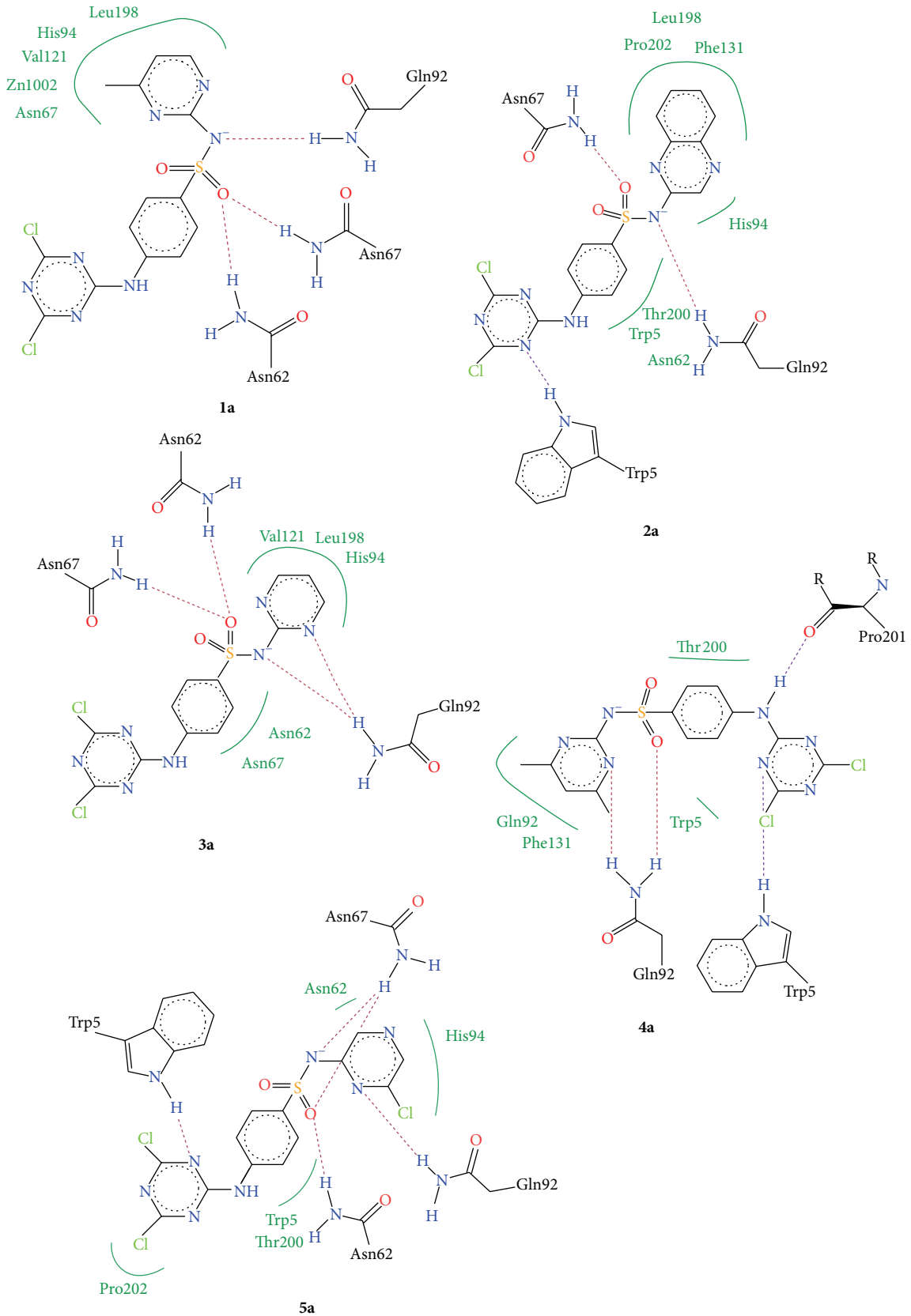

Figure 5: Interaction diagrams of the selected docked conformations for compounds **1a**–**5a**. Hydrogen bond interactions are indicated with dotted lines and hydrophobic interactions are shown with green lines.

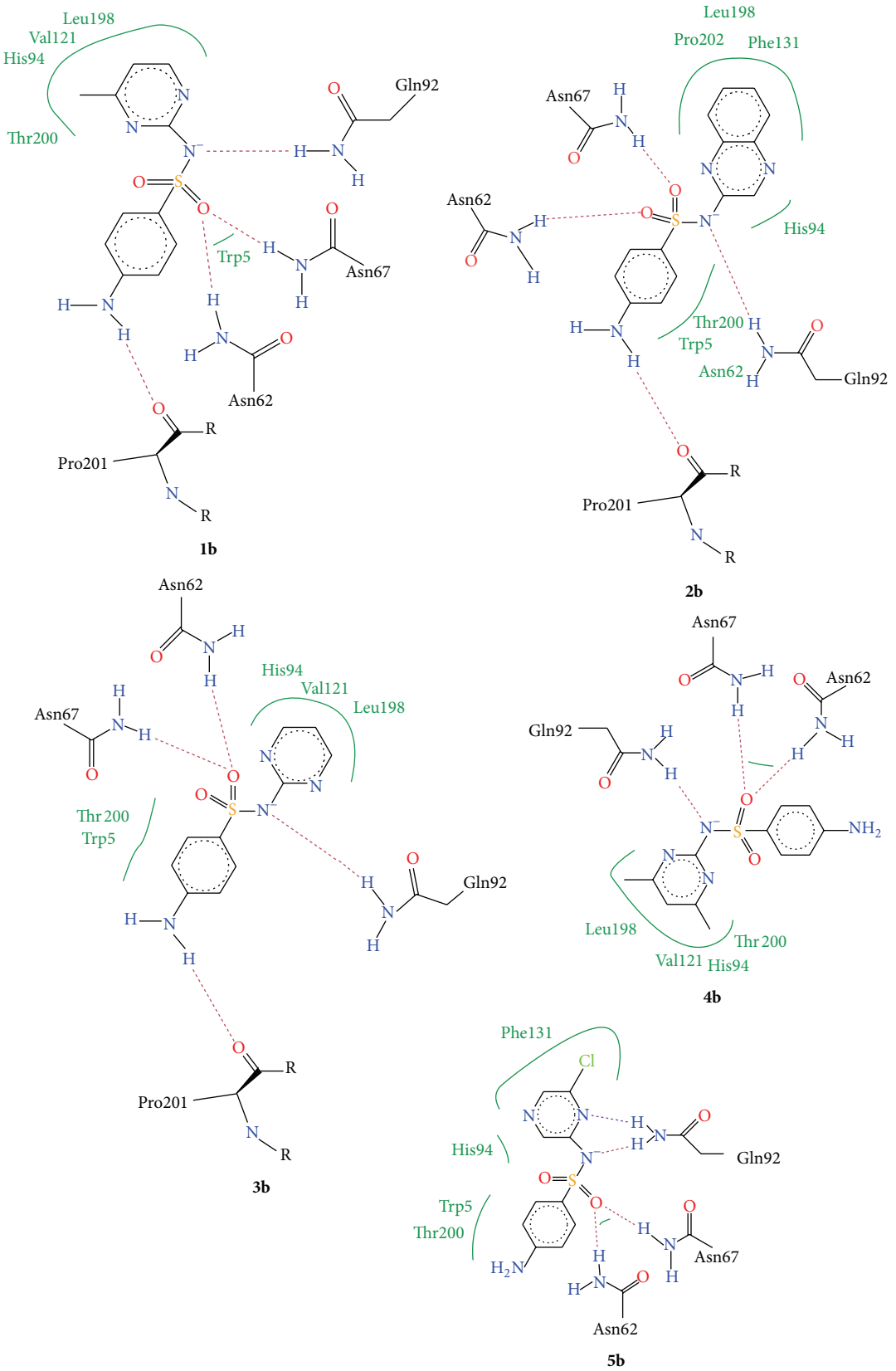

FIGURE 6: Interaction diagrams of the selected docked conformations for compounds **1b**–**5b**. Hydrogen bond interactions are indicated with dotted lines and hydrophobic interactions are shown with green lines.

Table 3: Calculated ADME properties of compounds **1a**–**5a** and **1b**–**5b**.

Compound	$S + \log P$	$S + \log D$	$M \log P$	MWt	HBDH	MNO	TPSA
1a	2.712	1.523	1.93	412.259	2	9	122.65
2a	3.346	2.077	1.69	448.292	2	9	122.65
3a	2.397	0.965	1.681	398.232	2	9	122.65
4a	2.997	2.08	2.173	426.286	2	9	122.65
5a	2.766	0.588	1.118	432.677	2	9	122.65
1b	0.542	−0.112	0.779	264.307	3	6	97.97
2b	1.168	0.676	0.633	300.341	3	6	97.97
3b	0.169	−0.681	0.487	250.28	3	6	97.97
4b	0.926	0.484	1.06	278.334	3	6	97.97
5b	0.811	−0.468	0.235	284.725	3	6	97.97

In drug discovery process, the evaluation of ADME properties (Absorption, Distribution, Metabolism, and Excretion) is of considerable importance, since the likelihood of success of a molecule as a drug greatly depends on its favorable ADME. Accordingly the parameters selected for this study include octanol-water distribution coefficients ($S + \log P$ and $M \log P$), the pH dependent octanol-water distribution coefficient ($S + \log D$), number of hydrogen bond donors (HBDH), hydrogen bond acceptor (sum of nitrogen and oxygen atoms MNO), and topological polar surface area (TPSA). The evaluation of TPSA is used as a model to assess the ability of compounds to cross the blood brain barrier (BBB). Molecules with TPSA < 60 Å^2 are usually expected to be completely absorbed whereas molecules with TPSA > 140 Å^2 are generally unwanted and cannot be expected to exhibit sufficient bioavailability [38]. Typically, compounds having molecular weight less than 500, number of hydrogen bond acceptor (HBDH) less than 10, number of hydrogen bond donor (MNO) less than 5, and a $\log P$ value of less than 5 are considered to be orally bioavailable with favorable ADME profile [39, 40]. The calculated ADME properties of compounds **1a**–**5a** and **1b**–**5b** are given in Table 3. All synthesized compounds showed favorable ADME properties. No violation of Lipinski's rule of 5 was observed.

4. Conclusions

Sulfa drugs are well known antibacterial agents containing N-substituted sulfonamide group on para position of aniline ring (NH_2RSO_2NHR'). In this study 2,4-dichloro-1,3,5-triazine derivatives of sulfa drugs (sulfamerazine, sulfaquinoxaline, sulfadiazine, sulfadimidine, and sulfachloropyrazine) (**1a**–**5a**) were synthesized and characterized. Their carbonic anhydrase inhibition activity was evaluated against bCA II isozyme. For the sake of comparison the CA inhibition activity of parent sulfa drugs (**1b**–**5b**) was also evaluated. It is interesting to note here that although all compounds including sulfa drugs contained an N-substituted sulfonamide group, they were still able to inhibit CA activity. Sulfa drugs exhibited weak CA inhibition (19.6–51.8%). However 2,4-dichloro-1,3,5-triazine derivatives of sulfa drugs (**1a**–**5a**) had significantly improved CAI activity (IC_{50} = 1.49–24.9 μM) and only compound **2a** had IC_{50} value of 105.3 μM. For compounds **1a**-**5a**, the bCA II inhibition activity decreases in the order **5a** > **1a** > **4a** > **3a** > **2a**, whereas for the parent sulfa drugs **1b**–**5b**, the inhibition activity decreases as **2b** > **5b** > **4b** > **3b** > **1b**. Molecular docking studies were carried out to give insights into the binding site interactions. ADME properties were calculated to evaluate the drug likeness of synthesized compounds. All compounds indicated a favorable ADME profile.

Conflict of Interests

The authors declare that there is no conflict of interests regarding the publication of this paper.

Acknowledgments

This work was financially supported by the German-Pakistani Research Collaboration Programme. The authors are grateful to Dr. Mohammad Shahid for help with docking studies.

References

[1] B. C. Tripp, K. Smith, and J. G. Ferry, "Carbonic anhydrase: new insights for an ancient enzyme," *The Journal of Biological Chemistry*, vol. 276, no. 52, pp. 48615–48618, 2001.

[2] S. Breton, "The cellular physiology of carbonic anhydrases," *Journal of the Pancreas*, vol. 2, no. 4, pp. 159–164, 2001.

[3] R. P. Henry, "Multiple roles of carbonic anhydrase in cellular transport and metabolism," *Annual Review of Physiology*, vol. 58, pp. 523–538, 1996.

[4] C. J. Lynch, H. Fox, S. A. Hazen, B. A. Stanley, S. Dodgson, and K. F. Lanoue, "Role of hepatic carbonic anhydrase in de novo lipogenesis," *Biochemical Journal*, vol. 310, no. 1, pp. 197–202, 1995.

[5] S. A. Hazen, A. Waheed, W. S. Sly, K. F. LaNoue, and C. J. Lynch, "Differentiation-dependent expression of CA V and the role of carbonic anhydrase isozymes in pyruvate carboxylation in adipocytes," *The FASEB Journal*, vol. 10, no. 4, pp. 481–490, 1996.

[6] G. N. Shah, T. S. Rubbelke, J. Hendin et al., "Targeted mutagenesis of mitochondrial carbonic anhydrases VA and VB implicates both enzymes in ammonia detoxification and glucose metabolism," *Proceedings of the National Academy of*

Sciences of the United States of America, vol. 110, no. 18, pp. 7423–7428, 2013.

[7] S. J. Dodgson and K. Cherian, "Mitochondrial carbonic anhydrase is involved in rat renal glucose synthesis," *American Journal of Physiology—Endocrinology and Metabolism*, vol. 257, pp. E791–E796, 1989.

[8] V. Alterio, A. di Fiore, K. D'Ambrosio, C. T. Supuran, and G. de Simone, "Multiple binding modes of inhibitors to carbonic anhydrases: how to design specific drugs targeting 15 different isoforms?" *Chemical Reviews*, vol. 112, no. 8, pp. 4421–4468, 2012.

[9] J. P. Kirkpatrick, Z. N. Rabbani, R. C. Bentley et al., "Elevated CAIX expression is associated with an increased risk of distant failure in early-stage cervical cancer," *Biomarker Insights*, vol. 2008, no. 3, pp. 45–55, 2008.

[10] T. Dorai, I. S. Sawczuk, J. Pastorek, P. H. Wiernik, and J. P. Dutcher, "The role of carbonic anhydrase IX overexpression in kidney cancer," *European Journal of Cancer*, vol. 41, no. 18, pp. 2935–2947, 2005.

[11] A. Scozzafava and C. T. Supuran, "Glaucoma and the applications of carbonic anhydrase inhibitors," *Subcellular Biochemistry*, vol. 75, pp. 349–359, 2014.

[12] C. T. Supuran and A. Scozzafava, "Carbonic anhydrases as targets for medicinal chemistry," *Bioorganic & Medicinal Chemistry*, vol. 15, no. 13, pp. 4336–4350, 2007.

[13] C. T. Supuran, A. di Fiore, and G. de Simone, "Carbonic anhydrase inhibitors as emerging drugs for the treatment of obesity," *Expert Opinion on Emerging Drugs*, vol. 13, no. 2, pp. 383–392, 2008.

[14] A. Scozzafava, C. T. Supuran, and F. Carta, "Antiobesity carbonic anhydrase inhibitors: a literature and patent review," *Expert Opinion on Therapeutic Patents*, vol. 23, no. 6, pp. 725–735, 2013.

[15] G. de Simone and C. T. Supuran, "Antiobesity carbonic anhydrase inhibitors," *Current Topics in Medicinal Chemistry*, vol. 7, no. 9, pp. 879–884, 2007.

[16] G. de Simone, A. Dio Fiore, and C. T. Supuran, "Are carbonic anhydrase inhibitors suitable for obtaining antiobesity drugs?" *Current Pharmaceutical Design*, vol. 14, no. 7, pp. 655–660, 2008.

[17] C. T. Supuran, "Inhibition of bacterial carbonic anhydrases and zinc proteases: from orphan targets to innovative new antibiotic drugs," *Current Medicinal Chemistry*, vol. 19, no. 6, pp. 831–844, 2012.

[18] C. T. Supuran and A. Scozzafava, "Carbonic anhydrase inhibitors: aromatic sulfonamides and disulfonamides act as efficient tumor growth inhibitors," *Journal of Enzyme Inhibition*, vol. 15, no. 6, pp. 597–610, 2000.

[19] S. Pastorekova, M. Zatovicova, and J. Pastorek, "Cancer-associated carbonic anhydrases and their inhibition," *Current Pharmaceutical Design*, vol. 14, no. 7, pp. 685–698, 2008.

[20] A. Thiry, J.-M. Dogné, B. Masereel, and C. T. Supuran, "Targeting tumor-associated carbonic anhydrase IX in cancer therapy," *Trends in Pharmacological Sciences*, vol. 27, no. 11, pp. 566–573, 2006.

[21] O. O. Guler, G. de Simone, and C. T. Supuran, "Drug design studies of the novel antitumor targets carbonic anhydrase IX and XII," *Current Medicinal Chemistry*, vol. 17, no. 15, pp. 1516–1526, 2010.

[22] J.-Y. Winum, M. Rami, A. Scozzafava, J.-L. Montero, and C. Supuran, "Carbonic anhydrase IX: a new druggable target for the design of antitumor agents," *Medicinal Research Reviews*, vol. 28, no. 3, pp. 445–463, 2008.

[23] C. T. Supuran, F. Briganti, S. Tilli, W. R. Chegwidden, and A. Scozzafava, "Carbonic anhydrase inhibitors: sulfonamides as antitumor agents?" *Bioorganic and Medicinal Chemistry*, vol. 9, no. 3, pp. 703–714, 2001.

[24] C. C. Brackett, H. Singh, and J. H. Block, "Likelihood and mechanisms of cross-allergenicity between sulfonamide antibiotics and other drugs containing a sulfonamide functional group," *Pharmacotherapy*, vol. 24, no. 7, pp. 856–870, 2004.

[25] S. Knowles, L. Shapiro, and N. H. Shear, "Should celecoxib be contraindicated in patients who are allergic to sulfonamides? Revisiting the meaning of "sulfa– allergy," *Drug Safety*, vol. 24, no. 4, pp. 239–247, 2001.

[26] V. Garaj, L. Puccetti, G. Fasolis et al., "Carbonic anhydrase inhibitors: novel sulfonamides incorporating 1,3,5-triazine moieties as inhibitors of the cytosolic and tumour-associated carbonic anhydrase isozymes I, II and IX," *Bioorganic and Medicinal Chemistry Letters*, vol. 15, no. 12, pp. 3102–3108, 2005.

[27] F. Carta, V. Garaj, A. Maresca et al., "Sulfonamides incorporating 1,3,5-triazine moieties selectively and potently inhibit carbonic anhydrase transmembrane isoforms IX, XII and XIV over cytosolic isoforms i and II: solution and X-ray crystallographic studies," *Bioorganic and Medicinal Chemistry*, vol. 19, no. 10, pp. 3105–3119, 2011.

[28] V. Garaj, L. Puccetti, G. Fasolis et al., "Carbonic anhydrase inhibitors: synthesis and inhibition of cytosolic/tumor-associated carbonic anhydrase isozymes I, II, and IX with sulfonamides incorporating 1,2,4-triazine moieties," *Bioorganic & Medicinal Chemistry Letters*, vol. 14, no. 21, pp. 5427–5433, 2004.

[29] Y. Pocker and J. T. Stone, "The catalytic versatility of erythrocyte carbonic anhydrase. III. Kinetic studies of the enzyme-catalyzed hydrolysis of p-nitrophenyl acetate," *Biochemistry*, vol. 6, no. 3, pp. 668–678, 1967.

[30] C. A. Behnke, I. Le Trong, J. W. Godden et al., "Atomic resolution studies of carbonic anhydrase II," *Acta Crystallographica Section D: Biological Crystallography*, vol. 66, no. 5, pp. 616–627, 2010.

[31] R. Saito, T. Sato, A. Ikai, and N. Tanaka, "Structure of bovine carbonic anhydrase II at 1.95 Å resolution," *Acta Crystallographica Section D*, vol. 60, no. 4, pp. 792–795, 2004.

[32] Z. Ul-Haq, S. Usmani, U. Mahmood, M. Al-Rashida, and G. Abbas, "In-silico analysis of chromone containing sulfonamide derivatives as human carbonic anhydrase inhibitors," *Medicinal Chemistry*, vol. 9, no. 4, pp. 608–616, 2013.

[33] E. F. Pettersen, T. D. Goddard, C. C. Huang et al., "UCSF Chimera—a visualization system for exploratory research and analysis," *Journal of Computational Chemistry*, vol. 25, no. 13, pp. 1605–1612, 2004.

[34] J. Wang, W. Wang, P. A. Kollman, and D. A. Case, "Automatic atom type and bond type perception in molecular mechanical calculations," *Journal of Molecular Graphics and Modelling*, vol. 25, no. 2, pp. 247–260, 2006.

[35] ACD/ChemSketch, version 12.01, Advanced Chemistry Development, Inc., Toronto, ON, Canada, 2013, http://www.acdlabs.com/.

[36] http://www.biosolveit.de/LeadIT/.

[37] C. A. M. Afonso, N. M. T. Lourenço, and A. A. de Rosatella, "Synthesis of 2,4,6-tri-substituted-1,3,5-triazines," *Molecules*, vol. 11, no. 1, pp. 81–102, 2006.

[38] P. Zakeri-Milani, H. Tajerzadeh, Z. Islambolchilar, S. Barzegar, and H. Valizadeh, "The relation between molecular properties

of drugs and their transport across the intestinal membrane," *Daru*, vol. 14, no. 4, pp. 164–171, 2006.

[39] K. Asokkumar, L. T. Prathyusha, M. Umamaheshwari et al., "Design, ADMET and docking studies on some novel chalcone derivatives as soluble epoxide hydrolase enzyme inhibitors," *Journal of the Chilean Chemical Society*, vol. 57, no. 4, pp. 1442–1446, 2012.

[40] D. E. Clark and S. D. Pickett, "Computational methods for the prediction of "drug-likeness"," *Drug Discovery Today*, vol. 5, no. 2, pp. 49–58, 2000.

Hindawi Publishing Corporation
BioMed Research International
Volume 2014, Article ID 638902, 9 pages
http://dx.doi.org/10.1155/2014/638902

Research Article

Saccharin Sulfonamides as Inhibitors of Carbonic Anhydrases I, II, VII, XII, and XIII

Vaida Morkūnaitė,[1] Lina Baranauskienė,[1] Asta Zubrienė,[1] Visvaldas Kairys,[2] Jekaterina Ivanova,[3] Pēteris Trapencieris,[3] and Daumantas Matulis[1]

[1] *Department of Biothermodynamics and Drug Design, Institute of Biotechnology, Vilnius University, Graičiūno 8, LT-02241 Vilnius, Lithuania*
[2] *Department of Bioinformatics, Institute of Biotechnology, Vilnius University, Graičiūno 8, LT-02241 Vilnius, Lithuania*
[3] *Department of Organic Chemistry, Latvian Institute of Organic Synthesis, Aizkraukles 21, Riga LV-1006, Latvia*

Correspondence should be addressed to Daumantas Matulis; daumantas.matulis@bti.vu.lt

Received 28 February 2014; Revised 28 April 2014; Accepted 28 May 2014; Published 3 September 2014

Academic Editor: Vincenzo Alterio

A series of modified saccharin sulfonamides have been designed as carbonic anhydrase (CA) inhibitors and synthesized. Their binding to CA isoforms I, II, VII, XII, and XIII was measured by the fluorescent thermal shift assay (FTSA) and isothermal titration calorimetry (ITC). Saccharin bound the CAs weakly, exhibiting the affinities of 1–10 mM for four CAs except CA I where binding could not be detected. Several sulfonamide-bearing saccharines exhibited strong affinities of 1–10 nM towards particular CA isoforms. The functional group binding Gibbs free energy additivity maps are presented which may provide insights into the design of compounds with increased affinity towards selected CAs.

1. Introduction

Carbonic anhydrases (CAs) belong to the lyase family of enzymes and catalyze the reversible reaction of carbon dioxide hydration to bicarbonate ion and proton. There are 15 CA isoforms in human body: twelve of them are catalytically active [1–3], while three are inactive (CAs VIII, X, and XI). The CA is linked to many diseases such as edema, glaucoma, epilepsy, and cancer. Therefore, CA is an important target for pharmaceutical research [4].

Heterocyclic sulfonamides are the most investigated CA inhibitors. Among them, saccharines play a special role, because they already contain the sulfonamide functionality in the heterocyclic system. Therefore, saccharin itself has shown some binding capacity to several CA isoforms. Saccharin has been previously described as a selective inhibitor of CA IX and CA XII at submicromolar level [5, 6]. The bovine CA II and human erythrocyte CAs I and II have been shown to be inhibited by saccharin [7, 8]. Furthermore, 20 newly prepared N-substituted saccharines have been shown to exhibit higher selective binding to CA IX and CA XII isoforms than saccharin itself [9]. Here, we describe the binding properties of saccharin sulfonamides [10] as CA inhibitors. They exhibited good inhibition properties.

The dissociation constants of synthesized compounds to five CA isoforms (I, II, VII, XII, and XIII) were determined by the fluorescent thermal shift assay (FTSA) and isothermal titration calorimetry (ITC) methods. FTSA (also called ThermoFluor, differential scanning fluorimetry, DSF) [11–17] is a rapid screening method that requires low amounts of protein and is based on the shift of protein melting temperature (T_m) that occurs upon ligand binding. The T_m is determined by the change of the fluorescence signal observed upon heat-induced protein unfolding. Isothermal titration calorimetry directly determines the dissociation constant and also the enthalpy and entropy of binding. The enthalpy and entropy are not the subject of this paper. Furthermore, ITC requires larger amounts of protein compared to FTSA and cannot determine very weak or too tight binding. However, these

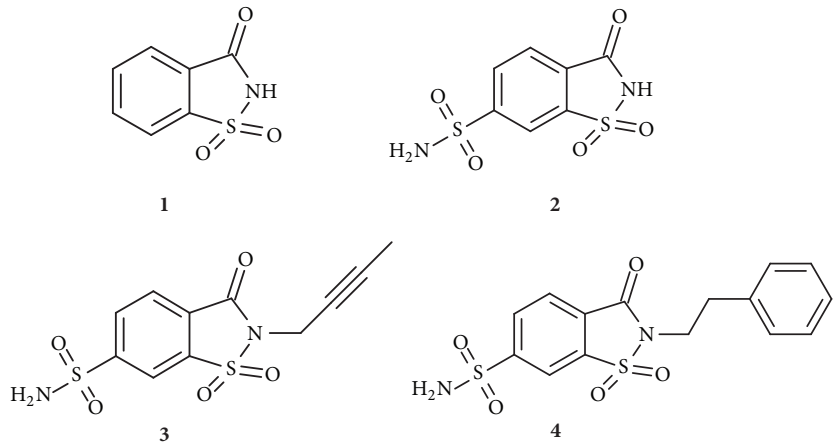

Figure 1: The chemical structures of compounds used in this study. Compound **1** is saccharin, a secondary sulfonamide. Compound **2** is sulfonamide-modified saccharin containing both the primary and secondary sulfonamide groups, while compounds **3** and **4** contain only the primary sulfonamide groups and are modified on the secondary sulfonamide nitrogen.

two independent methods complement each other for better accuracy of interaction measurements.

2. Results

2.1. Binding Results. The binding of four saccharin sulfonamides (including saccharin itself, chemical structures shown in Figure 1) to five isoforms of human recombinant catalytic domains of carbonic anhydrases (CAs) was determined by the fluorescent thermal shift assay (FTSA) and isothermal titration calorimetry (ITC). Figure 2 shows an example of the FTSA data compounds **1**, **3**, and **4** binding to CA XIII. Figures 2(a), 2(b), and 2(c) show the thermal denaturation curves of CA XIII in the presence of various saccharin **1** and saccharin sulfonamides **3** and **4** concentrations. There was no shift of the melting temperature when saccharin was added to 200 μM concentration (Figures 2(a) and 2(d)). The shift became visible only at higher saccharin concentrations (see Figure 3(a)). However, the shift was significant for the saccharin sulfonamides **3** and **4** (Figures 2(b) and 2(c)). Figure 2(d) shows the dosing curves and the melting temperatures as a function of added compound concentrations. Lines were simulated as described in Materials and Methods.

Figure 3 shows the dosing curves of the least potent compound **1** (saccharin) and the most potent compound **4** binding to all five tested CA isoforms. There is weak shift exhibited by saccharin (**1**) only at highest concentrations around 1–10 mM, while a significant shift of the melting temperature with compound **4** was observed. However, visual comparison of the affinities is complicated because the melting temperatures of all five CA isoforms are different, varying from about 49°C (CA VII) through 58°C (CAs I and XIII).

The observed dissociation constants K_ds for all four compounds binding to the five CA isoforms as determined by the FTSA are listed in Table 1. Saccharin sulfonamide derivatives bound CAs with nanomolar affinities. The affinity of compound **4** reached 330 pM for CA I and 25 nM for CA XII (Table 1). Compound **2**, however, exhibited weakest binding of the three saccharin sulfonamides. Its affinity for CA I was only about 3.0 μM but reached about 200 nM for CA XIII.

Saccharin has been previously demonstrated to inhibit numerous CAs, especially CA VII. Our results confirm that CA VII bound saccharin most strongly of the five tested isoforms. However, our determined dissociation constants are in the range of about 1–10 mM and thus are significantly weaker than some previously determined affinities. The FTSA determined that CA VII bound saccharin with the K_d of 1.0 mM; CA XIII, 2.0 mM; CA II, 2.9 mM; CA XII, 5.9 mM; and CA I did not exhibit any detectable shift up to 7.5 mM added saccharin; thus, its K_d is weaker than 10 mM.

In order to confirm the FTSA measurements, all four compounds binding to five CA isoforms were also measured by the isothermal titration calorimetry (ITC). Figure 4 shows representative ITC data of compound **2** binding to CA II and CA XIII and saccharin binding to CA II. The ITC data for all compounds and CAs are listed in Table 2. Dissociation constants obtained by ITC were essentially confirming the FTSA results. However, the most potent compounds that exhibited affinity stronger than 20 nM by FTSA bound too tight to CA for accurate K_d determination by ITC. As described in [13], the Wiseman c factor must be between 10 and 100 for precise K_d determination by ITC (could be still determined in the range of 5–1000 with lower accuracy). In titrations of compound **4** with CAs I, II, and VII, the c value surpassed 1000. Therefore, such determinations could not be confirmed by ITC. Saccharin itself did not exhibit any binding by ITC as seen in Figure 4(c).

Dissociation constants were recalculated to the Gibbs free energies of binding in order to make easy comparison between different compound structures in the order of increasing affinities. Figure 5 shows such Gibbs free energy additivity scheme for all five CA isoforms. The addition of the alkyne group (compound **3** versus **2**) significantly strengthened the binding to CAs I, II, VII, and XIII but not

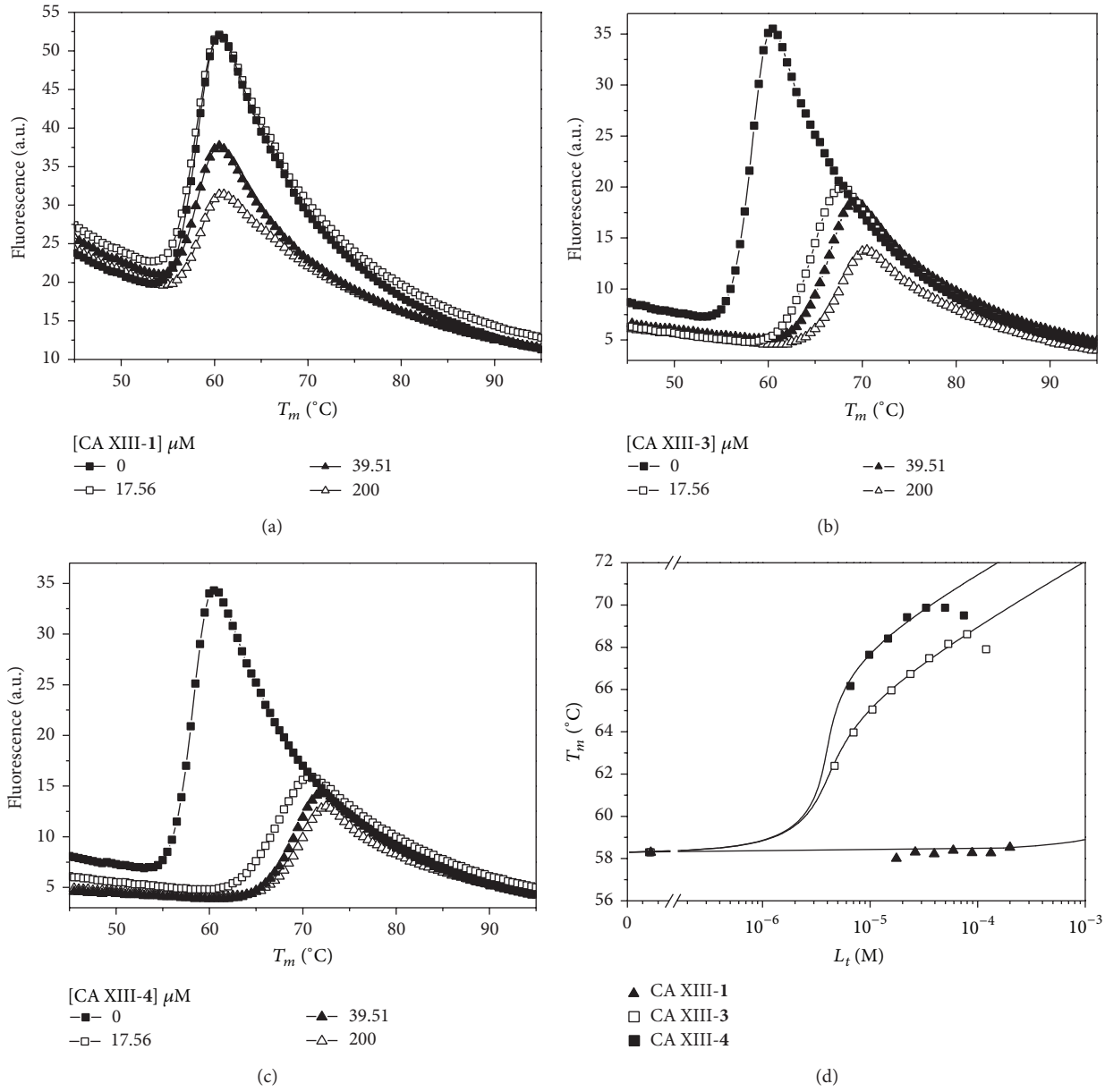

Figure 2: The binding of compounds **1**, **3**, and **4** to CA XIII, determined by the fluorescent thermal shift assay (FTSA). Panels (a)–(c) show the protein melting fluorescence curves as a function of temperature at several added compound concentrations. Saccharin did not exhibit a T_m shift (a) while compounds **3** (b) and **4** (c) exhibited a significant shift. Panel (d) shows the resultant three compound dosing curves, the dependencies of the protein melting temperature T_m on the added three compound concentrations. Datapoints are the experimental values obtained from panels (a)–(c) and the solid lines are simulated according to the model as described in Materials and Methods. Experiments were performed at pH 7.0 in sodium phosphate buffer.

towards CA XII. However, consecutive replacement of the alkyne group with the phenyl group (compound **4**) increased the binding affinity towards all five CAs. The energetic contribution was greatest for CA I (−14.5 and −24.8 kJ/mol, resp.). Compound **4** exhibited the largest affinities towards all five CA isoforms. However, affinity itself does not automatically increase selectivity towards a particular CA isoform. Selectivity towards a particular CA isoform is often a goal for a drug that would not have side effects by inhibiting a nondesired isoform. These Gibbs free energy diagrams helped design a very potent compound **4** that is also quite selective towards CA I isoform.

2.2. Docking Results. To explore the ligand-protein interactions for the complexes which did not have available X-ray structures, compounds **3** and **4** were docked in the active site of CA II using Vdock docking program [18, 19]. Here, we assumed that sulfonamide group is bound to the active site zinc as is indicated from the binding results. Furthermore,

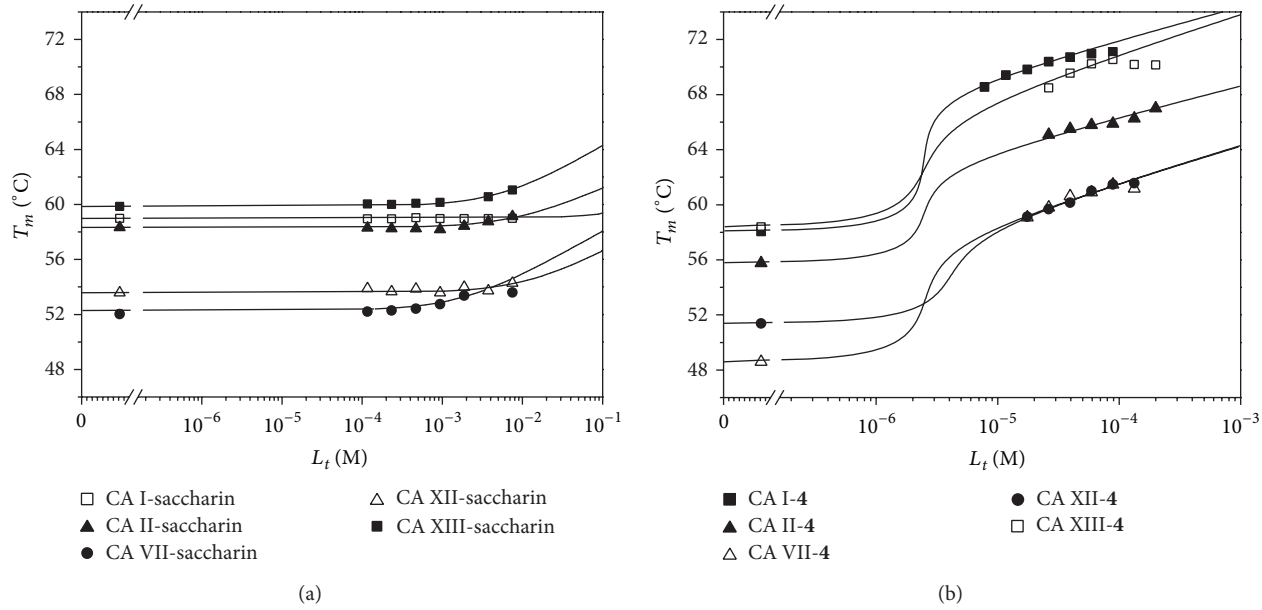

Figure 3: The FTSA dosing curves of compounds **1** (saccharin, panel (a)) and **4** (b) binding to CAs I, II, VII, XII, and XIII. Saccharin was dosed up to 7.5 mM and a small T_m shift was observed for all CAs except CA I. Compound **4** was dosed up to 200 μM with a significant shift. The determined dissociation constants for all compounds are listed in Table 1. There was no added DMSO while dosing saccharin and there was 2% (v/v) final DMSO concentration while dosing **4**. This explains the reduced T_m of the protein in the absence of compound with DMSO (b) compared to (a) that in the absence of DMSO.

Table 1: Compound dissociation constants of human recombinant carbonic anhydrase isoforms I, II, VII, XII, and XIII, as determined by the fluorescent thermal shift assay (FTSA, 37°C, pH 7.0). Acetazolamide (**AZM**) was used as a control. Saccharin bound with the K_d of 1 to over 10 mM while compound **4** reached the affinity of 0.3 to 25 nM.

Compound	Dissociation constants K_d (nM) and CA isoforms				
	CA I	CA II	CA VII	CA XII	CA XIII
1 (saccharin)	>10,000,000	2,900,000	1,000,000	5,900,000	2,000,000
2	3000	400	770	220	200
3	18	20	110	290	45
4	0.33	2.5	4.3	25	6.7
AZM	1400	38	17	130	50

Uncertainties of the FTSA measurements are approximately 1.6-fold in K_d.

similar to our previous study [20], we used constrained docking to achieve reasonable results. A spatial constraint was imposed on the zinc-bound nitrogen to mimic a strong coordination between the zinc and sulfonamide nitrogen. An additional constraint was imposed on the sulfur-benzene ring bond torsional angle to maintain the correct rotamer. The main reason for the torsional constraints was an apparent lack of correct torsional potentials for the bond connecting the bulk of ligand with the sulfonamide group [21, 22].

The preliminary docking showed that the benzene ring had a strong tendency towards aligning with the sulfonamide S–N bond, while a visual inspection of the structures available in the PDB showed that many structures are staggered or nearly aligned with one of the S=O bonds. To verify this, we performed a survey of the available PDB [23] structures. A search revealed 115 CA structures with 124 ligand conformations in which the active center zinc-bound sulfanilamide group is attached to a benzene ring with both hydrogen substituents at the orthoposition. We explored the statistics of the torsional angles that the benzene ring plane makes with respect to the sulfonamide oxygens. The vast majority of the angles were in a narrow range characterized by an approximately staggered conformation on one end and an eclipsed rotamer in which the benzene ring was aligned with one of the S=O bonds on the other end of the range. Out of the 124 ligand conformations, there were only five outliers (PDB ID: 3ca2, 3b4f, 3nj9, 3p3h, and 3p3j) in which the benzene ring was aligned with the sulfonamide nitrogen. These five ligands are characterized by bulky substituents at the meta- or paraposition of the benzene ring. Because of the small number of the outliers and because of a small size of compounds **3** and **4,** we felt these outliers can be rather safely not taken into statistics for our purposes. Among the rest of the 119 ligand conformations, the average torsion angle between the S=O and the plane of the benzene ring was 14.7° (σ = 7.8°).

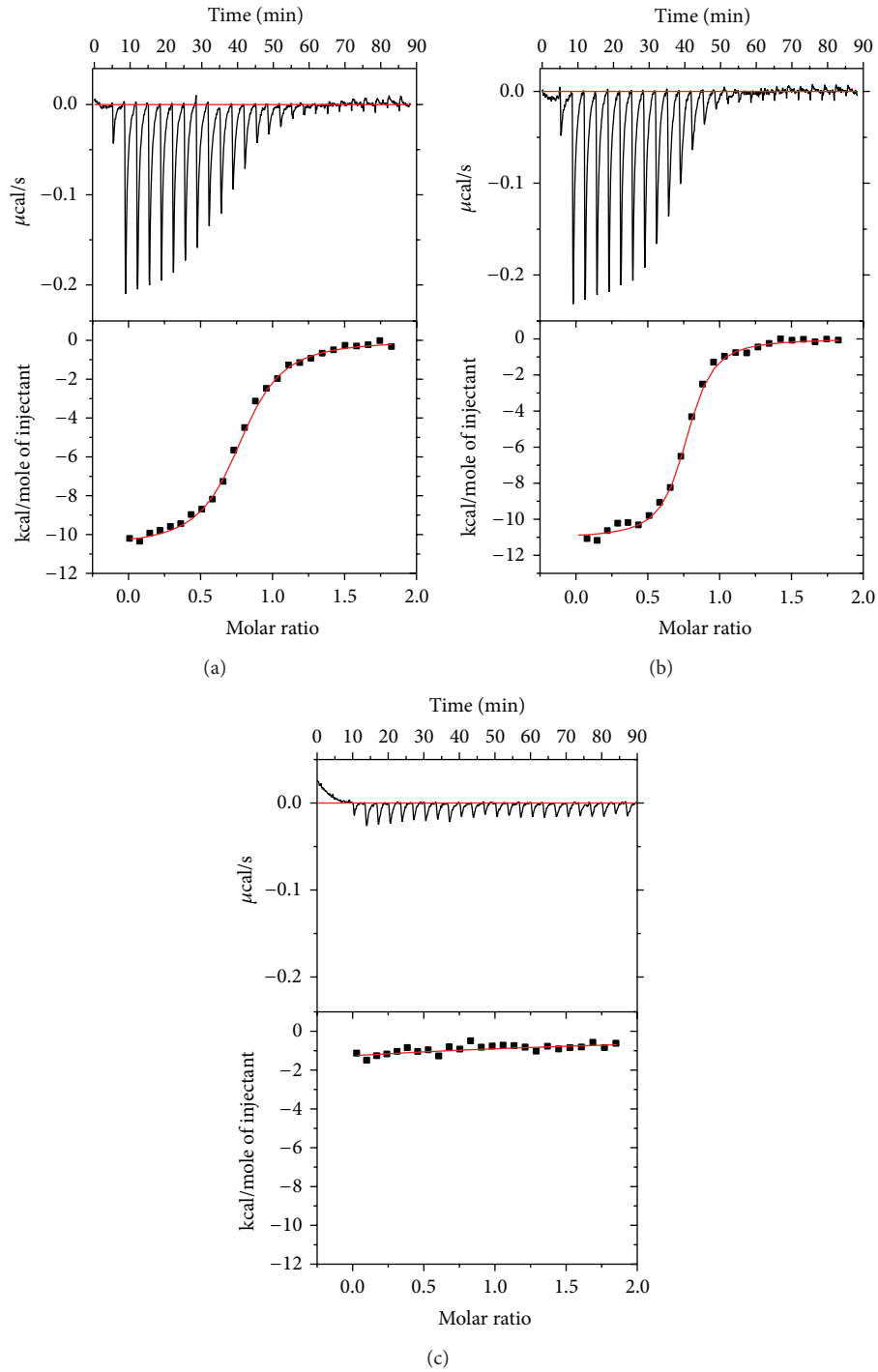

Figure 4: Isothermal titration calorimetry (ITC, 37°C) binding curves for compound **2** to CA II (panel (a), K_d = 290 nM) and CA XIII (panel (b), K_d = 120 nM) and saccharin (**1**) to CA II (panel (c), $K_d > 10^{-4}$ M, could not be accurately determined). Table 2 lists the dissociation constants obtained by ITC for the tested compounds binding to all five CAs.

Based on the findings, we chose as a reference a compound having a similar ring structure to **3**-**4,** indane-5-sulfonamide ligand (PDB ID: 2qoa) [24] with O=S–C–C torsion angle 18.0°, which is close to the average described above. A ±15° constraint around the indane-5-sulfonamide value was imposed on the corresponding dihedral angles of **3**-**4** during the docking. The docking results are shown in Figure 6. The hydrophobic tails of the ligands **3**-**4** lie in the hydrophobic groove framed by residues Phe131, Val135, Pro202, and Leu204. The side chain of Thr200 forms the hydrogen bonds with the sulfonyl oxygens in the thiazole ring of **3** and **4**.

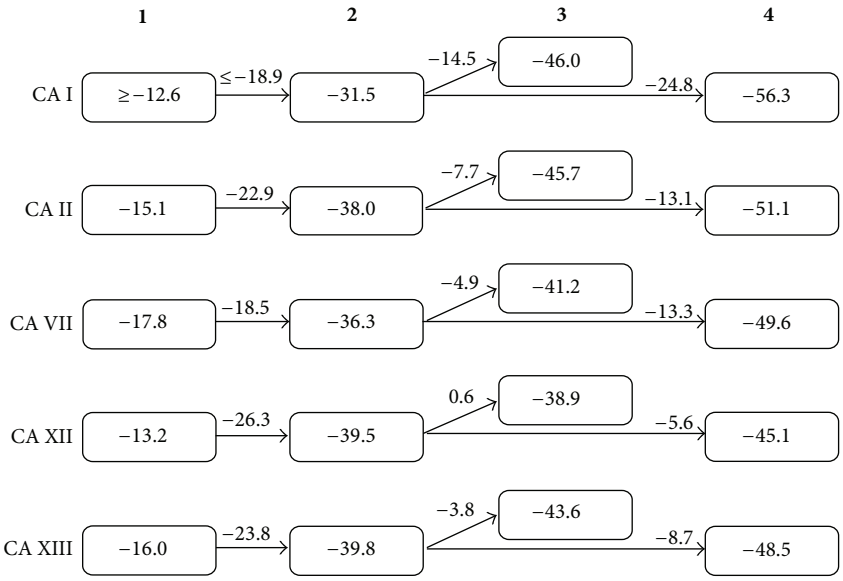

Figure 5: The thermodynamics of saccharin (**1**) and saccharin derivatives (**2**–**4**) binding to five CA isoforms, determined by FTSA at pH 7.0 and 37°C. The numbers within the shapes represent the Gibbs free energies of binding to a particular CA while the numbers on arrows show the differences in ΔG between two compounds that are most similar in chemical structure (kJ/mol). These differences represent the functional group contributions to the overall binding thermodynamics.

Table 2: Compound dissociation constants of human recombinant CA isoforms I, II, VII, XII, and XIII, as determined by ITC (37°C, pH 7.0). Acetazolamide (**AZM**) was used as a control. The affinity range of ITC determinations is quite narrow. At our experimental conditions, 5–10 μM CA in the calorimeter cell, the range may cover 1000–50 nM affinities (for the Wiseman factor of 100 to 10). With some approximation, the range could be expanded to cover affinities of 100 μM to 20 nM. These ITC measurements essentially confirm the FTSA results.

Compound	Dissociation constants K_d (nM) and CA isoforms				
	CA I	CA II	CA VII	CA XII	CA XIII
1	>100,000	>100,000	>100,000	>100,000	>100,000
2	1400	290	560	99	120
3	28	56	160	250	47
4	<20	<20	<20	40	<20
AZM	810	46	63	130	60

Uncertainties of the ITC measurements are approximately 2.0-fold in K_d.

Compounds **3**-**4** were also docked into CA XII (PDB ID: 1jd0 [25]) to possibly rationalize a relatively poor binding of **3** and **4** compared to CA II. Somewhat unexpectedly, these two compounds docked in a reverse binding mode compared to CA II: in CA XII the benzothiazole ring of these ligands is flipped (Figure 6(b)). In the reverse binding mode, one of the oxygen atoms of the sulfonyl group in the thiazole ring forms a hydrogen bond with Gln92 side chain. However, this hydrogen bond is likely to be much weaker compared to the complex with CA II because the hydrogen bond length is larger by more than 0.4 Å in the complex with CA XII as compared to CA II.

3. Discussion

Sulfonamides are the most investigated inhibitors of carbonic anhydrases. Primary SO_2NH_2 group binds to zinc atom in the active site and inhibits the protein catalytic activity. However, it is desirable to make compounds that would be good inhibitors of selected CA isoforms and would not bear the sulfonamide group. One such compound is saccharin that was previously shown to be a potent and quite selective inhibitor towards selected CA isoforms [5]. Furthermore, the crystal structure of saccharin bound to CA II has been determined.

This study confirmed that saccharin bound four of the tested five CA isoforms by direct biophysical techniques such as the fluorescent thermal shift assay. Interestingly, the binding of saccharin modified with sulfonamide group exhibited strong binding to all tested CA isoforms. Saccharin binding was carefully measured several times and could be detected for any of the tested CA isoforms only at concentrations of 1–10 mM. The K_ds for saccharin binding to four CA isoforms ranged from 1.0 to 5.9 mM (except CA I where there was no shift detected). This result significantly contradicts earlier finding by Köhler et al. and D'Ascenzio et al., where all tested 14 isoforms of CA bound saccharin with nanomolar to micromolar affinity [5, 9]. The CA VII has been shown to bind

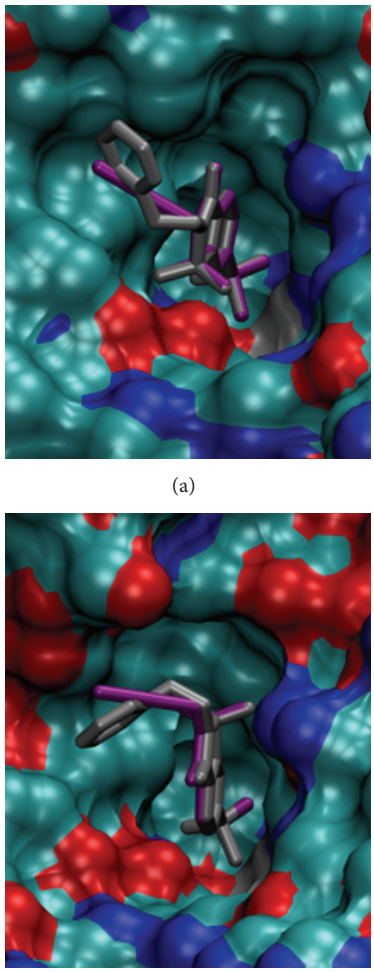

(a)

(b)

Figure 6: The dockingof compounds **3** (purple) and **4** (gray) into the active site of CA II (a) and CA XII (b). The solvent accessible surface of the protein is displayed to demonstrate how well the ligand fits the active site of CA II. Compound tails are arranged quite differently in CAs II and XII. The protein surface is colored to show oxygen atoms (red), nitrogen atoms (blue), and zinc atom (gray), and the rest is in cyan-blue.

saccharin with 10 nM affinity [5]. Our results indicate that the affinity is 100,000-fold weaker. However, our results confirm that saccharin bound CA VII, the strongest of the five tested isoforms. Therefore, selectivity towards CA VII is shown by both FTSA and inhibition methods. Isothermal titration calorimetry confirmed that saccharin bound all tested CAs with the K_d weaker than 100 μM.

There is no clear explanation for such significant discrepancy between the binding measurements by FTSA-ITC and inhibition of activity measurements by stopped-flow CO_2 hydration assay. However, different approaches sometimes yield different results and it may be necessary to further investigate this reaction by other techniques.

The thermodynamics-structure correlation diagrams, as shown in Figure 5, could help design compounds with desired properties such as increased affinities or increased selectivity toward a desired CA isoform. However, it should be kept in mind that the diagrams in Figure 5 and the values in Tables 1 and 2 represent only the observed K_ds that are valid exclusively for pH 7.0 and 37°C. These values depend on pH because there are linked protonation reactions observed upon compound binding to CA [26, 27]. In order to better understand the structure-thermodynamics correlations, it would be important to obtain the intrinsic values of binding by subtracting the contributing protonation reactions. However, such subtraction is not the subject of this paper because the actual affinities occurring at pH 7.0 are the observed values and it is important to compare them with the ones obtained by other methods such as stopped-flow CO_2 hydration assay [5, 9].

Saccharine contains only a secondary sulfonamide group that apparently binds CAs significantly weaker than modified compounds bearing primary sulfonamide groups. Their binding is expected to be quite different and thus exhibits significantly different affinities for CAs. Compound **2** bears both the primary and secondary sulfonamide groups, but it is expected to bind through its primary sulfonamide to the zinc of CA as confirmed by docking. Furthermore, it bound significantly stronger than saccharin itself.

Compounds **3** and **4** are the strongest binders of the four tested compounds towards all CAs. It was interesting to see if some of their structural moieties could be used for the design of compounds with even greater affinity or increased selectivity towards a desired CA isoform. Docking showed that the compounds bound in a quite different structural arrangement when comparing CA II and CA XII docked structures. This indicates that these and similar functional groups could be used to further increase the selectivity towards, for example, cancer related CA XII.

The affinity of several millimolar is sufficient to detect binding by X-ray crystallography if the added compound concentration is of the order of 1 mM. Therefore, there is no contradiction between our results that show weak saccharin binding and crystallographic structures that demonstrate saccharin bound in the active site of a CA.

4. Materials and Methods

4.1. Organic Synthesis of the Compounds. Saccharin (**1**) was purchased while compounds **2**–**4** were synthesized as previously described in [10]. Figure 1 shows the chemical structures of saccharin (**1**) and the three saccharin sulfonamide derivatives (**2**, **3**, and **4**) that are the subject of this paper.

4.2. Protein Preparation. Carbonic anhydrase isoforms I, II, VII, XII, and XIII were expressed and purified as previously described: CA I in [28], CA II in [29], CAs VII and XIII in [30], and CA XII in [26].

4.3. Determination of Compound Binding to CA Isoforms

4.3.1. Fluorescent Thermal Shift Assay. The fluorescent thermal shift assay (FTSA) measurements were performed in a Corbett Rotor-Gene 6000 (QIAGEN Rotor-Gene Q) instrument using the blue channel (excitation 365 ± 20, detection

460 ± 15 nm). The samples (20 μL volume) contained 5–10 μM protein, 0–200 μM compound, and 50 μM ANS (8-anilino-1-naphthalene sulfonate) in 50 mM sodium phosphate buffer (pH 7.0), 50 mM NaCl, and 0 or 2% DMSO (concentration in the final assay, v/v). The applied heating rate was 1°C/min. Data analysis was performed as previously described [28].

4.3.2. Isothermal Titration Calorimetry. Isothermal titration calorimetry (ITC) experiments were performed using VP-ITC instrument (Microcal, Inc., Northampton, USA) with 4–10 μM protein solution in the cell and 40–100 μM of the ligand solution in the syringe. A typical experiment consisted of 25 injections (10 μL each) within 3 min intervals. Experiments were performed at 37°C in 50 mM sodium phosphate buffer containing 50 mM NaCl at pH 7.0, with a final DMSO concentration of 2%, equal in the syringe and the cell.

4.3.3. Docking. Docking was performed using Vdock program [18, 19]. Structures 1jd0 [25] and 4g0c [31] were used to build CA II and CA XII receptors, respectively. The ligands were built using Avogadro v. 1.1.0 [32]. Force fields CHARMM22 [33] and CHARMm with Momany-Rone charges [34] were used to model the protein and ligand, respectively. The ligand parameters were generated using Discovery Studio Visualizer v. 3.5 (Accelrys Software Inc., San Diego, CA). Sulfonamide nitrogen was fixed at an X-ray position by setting it as a translational center and placing it into the translational box whose dimension was reduced to zero. The solvent effect during docking was modeled with the distance-dependent dielectric approximation, $\varepsilon_{ij} = 4r_{ij}$ [35]. One hundred minima were generated (instead of the default 20) and the genetic algorithm was switched off during docking to ensure a more thorough search of the conformational space. The docked structures were graphically represented using VMD [36].

5. Conclusions

The saccharin sulfonamides exhibited nanomolar and subnanomolar affinities toward selected CA isoforms. However, unmodified saccharin bound the tested CAs with only 1–10 mM affinity. Saccharin is a secondary sulfonamide and bound CAs significantly weaker than saccharin sulfonamide derivatives that are primary sulfonamides. The Gibbs free energies of binding show the functional group influence on the binding constants of saccharin and its sulfonamide derivatives.

Conflict of Interests

The authors declare that there is no conflict of interests regarding the publication of this paper.

Acknowledgments

This research was funded by a Grant (no. LIG-09/2012) from the Research Council of Lithuania (DM). This study was supported by the Latvian National Research Programme 2010–2013 "BIOMEDICINE" (PT). The authors acknowledge FP7-REGPOT-2009-1 Grant "MoBiLi" agreement no. 245721 and the COST Projects TD0905 and CM0804.

References

[1] C. T. Supuran, "Carbonic anhydrases: novel therapeutic applications for inhibitors and activators," *Nature Reviews Drug Discovery*, vol. 7, no. 2, pp. 168–181, 2008.

[2] V. M. Krishnamurthy, G. K. Kaufman, A. R. Urbach et al., "Carbonic anhydrase as a model for biophysical and physical-organic studies of proteins and protein-ligand binding," *Chemical Reviews*, vol. 108, no. 3, pp. 946–1051, 2008.

[3] W. S. Sly and P. Y. Hu, "Human carbonic anhydrases and carbonic anhydrase deficiencies," *Annual Review of Biochemistry*, vol. 64, pp. 375–401, 1995.

[4] V. Alterio, A. Di Fiore, K. D'Ambrosio, C. T. Supuran, and G. De Simone, "Multiple binding modes of inhibitors to carbonic anhydrases: how to design specific drugs targeting 15 different isoforms?" *Chemical Reviews*, vol. 112, no. 8, pp. 4421–4468, 2012.

[5] K. Köhler, A. Hillebrecht, J. Schulze Wischeler et al., "Saccharin inhibits carbonic anhydrases: possible explanation for its unpleasant metallic aftertaste," *Angewandte Chemie—International Edition*, vol. 46, no. 40, pp. 7697–7699, 2007.

[6] M. Rami, J.-Y. Winum, A. Innocenti, J.-L. Montero, A. Scozzafava, and C. T. Supuran, "Carbonic anhydrase inhibitors: copper(II) complexes of polyamino-polycarboxylamido aromatic/heterocyclic sulfonamides are very potent inhibitors of the tumor-associated isoforms IX and XII," *Bioorganic and Medicinal Chemistry Letters*, vol. 18, no. 2, pp. 836–841, 2008.

[7] F. Sonmez, C. Bilen, S. Sumersan et al., "In vitro inhibition effect and structure-activity relationships of some saccharin derivatives on erythrocyte carbonic anhydrase I and II," *Journal of Enzyme Inhibition and Medicinal Chemistry*, vol. 29, pp. 118–123, 2014.

[8] J. M. Wilson, Q. Tanko, M. M. Wendland, J. E. Meany, J. F. Nedved, and Y. Pocker, "The inhibition of bovine carbonic anhydrase by saccharin and 2- and 4-carbobenzoxybenzene sulfonamide," *Physiological Chemistry and Physics and Medical NMR*, vol. 30, no. 2, pp. 149–162, 1998.

[9] M. D'Ascenzio, S. Carradori, C. De Monte, D. Secci, M. Ceruso, and C. T. Supuran, "Design, synthesis and evaluation of n-substituted saccharin derivatives as selective inhibitors of tumor-associated carbonic anhydrase XII," *Bioorganic & Medicinal Chemistry*, vol. 22, pp. 1821–1831, 2014.

[10] E. M. Ivanova, E. Y. Simin, I. V. Vozny, P. Trapencieris, and R. Žalubovskis, "Synthesis of 6-sulfamoylsaccharin and study of its reactivity in alkylation reactions," *Chemistry of Heterocyclic Compounds*, vol. 47, no. 12, pp. 1561–1564, 2012.

[11] D. Matulis, J. K. Kranz, F. R. Salemme, and M. J. Todd, "Thermodynamic stability of carbonic anhydrase: measurements of binding affinity and stoichiometry using thermofluor," *Biochemistry*, vol. 44, no. 13, pp. 5258–5266, 2005.

[12] T. M. Mezzasalma, J. K. Kranz, W. Chan et al., "Enhancing recombinant protein quality and yield by protein stability profiling," *Journal of Biomolecular Screening*, vol. 12, no. 3, pp. 418–428, 2007.

[13] A. Zubriene, J. Matuliene, L. Baranauskiene et al., "Measurement of nanomolar dissociation constants by titration calorimetry and thermal shift assay—radicicol binding to Hsp90 and

ethoxzolamide binding to CAII," *International Journal of Molecular Sciences*, vol. 10, no. 6, pp. 2662–2680, 2009.

[14] P. Cimmperman and D. Matulis, "Protein thermal denaturation measurements via a fluorescent dye," *RSC Biomolecular Sciences*, pp. 247–274, 2011.

[15] F. H. Niesen, H. Berglund, and M. Vedadi, "The use of differential scanning fluorimetry to detect ligand interactions that promote protein stability," *Nature Protocols*, vol. 2, no. 9, pp. 2212–2221, 2007.

[16] J. F. Brandts and L.-N. Lin, "Study of strong to ultratight protein interactions using differential scanning calorimetry," *Biochemistry*, vol. 29, no. 29, pp. 6927–6940, 1990.

[17] M. W. Pantoliano, E. C. Petrella, J. D. Kwasnoski et al., "High-density miniaturized thermal shift assays as a general strategy for drug discovery," *Journal of Biomolecular Screening*, vol. 6, no. 6, pp. 429–440, 2001.

[18] V. Kairys and M. K. Gilson, "Enhanced docking with the mining minima optimizer: acceleration and side-chain flexibility," *Journal of Computational Chemistry*, vol. 23, no. 16, pp. 1656–1670, 2002.

[19] L. David, R. Luo, and M. K. Gilson, "Ligand-receptor docking with the Mining Minima optimizer," *Journal of Computer-Aided Molecular Design*, vol. 15, no. 2, pp. 157–171, 2001.

[20] E. Čapkauskaite, A. Zubriene, L. Baranauskiene et al., "Design of [(2-pyrimidinylthio)acetyl]benzenesulfonamides as inhibitors of human carbonic anhydrases," *European Journal of Medicinal Chemistry*, vol. 51, pp. 259–270, 2012.

[21] S. Senger, M. A. Convery, C. Chan, and N. S. Watson, "Arylsulfonamides: a study of the relationship between activity and conformational preferences for a series of factor Xa inhibitors," *Bioorganic and Medicinal Chemistry Letters*, vol. 16, no. 22, pp. 5731–5735, 2006.

[22] S. Senger, C. Chan, M. A. Convery et al., "Sulfonamide-related conformational effects and their importance in structure-based design," *Bioorganic and Medicinal Chemistry Letters*, vol. 17, no. 10, pp. 2931–2934, 2007.

[23] H. M. Berman, J. Westbrook, Z. Feng et al., "The protein data bank," *Nucleic Acids Research*, vol. 28, no. 1, pp. 235–242, 2000.

[24] K. D'Ambrosio, B. Masereel, A. Thiry, A. Scozzafava, C. T. Supuran, and G. De Simone, "Carbonic anhydrase inhibitors: binding of indanesulfonamides to the human isoform II," *ChemMedChem*, vol. 3, no. 3, pp. 473–477, 2008.

[25] D. A. Whittington, A. Waheed, B. Ulmasov et al., "Crystal structure of the dimeric extracellular domain of human carbonic anhydrase XII, a bitopic membrane protein overexpressed in certain cancer tumor cells," *Proceedings of the National Academy of Sciences of the United States of America*, vol. 98, no. 17, pp. 9545–9550, 2001.

[26] V. Jogaite, A. Zubriene, V. Michailoviene, J. Gylyte, V. Morkunaite, and D. Matulis, "Characterization of human carbonic anhydrase XII stability and inhibitor binding," *Bioorganic and Medicinal Chemistry*, vol. 21, no. 6, pp. 1431–1436, 2013.

[27] L. Baranauskienė and D. Matulis, "Intrinsic thermodynamics of ethoxzolamide inhibitor binding to human carbonic anhydrase XIII," *BMC Biophysics*, vol. 5, article 12, 2012.

[28] L. Baranauskiene, M. Hilvo, J. Matuliene et al., "Inhibition and binding studies of carbonic anhydrase isozymes I, II and IX with benzimidazo[1,2-c][1,2,3]thiadiazole-7-sulphonamides," *Journal of Enzyme Inhibition and Medicinal Chemistry*, vol. 25, no. 6, pp. 863–870, 2010.

[29] P. Cimmperman, L. Baranauskiene, S. Jachimovičiute et al., "A quantitative model of thermal stabilization and destabilization of proteins by ligands," *Biophysical Journal*, vol. 95, no. 7, pp. 3222–3231, 2008.

[30] J. Sdžius, L. Baranauskien, D. Golovenko et al., "4-[N-(Substituted 4-pyrimidinyl)amino]benzenesulfonamides as inhibitors of carbonic anhydrase isozymes I, II, VII, and XIII," *Bioorganic and Medicinal Chemistry*, vol. 18, no. 21, pp. 7413–7421, 2010.

[31] S. Z. Fisher, M. Aggarwal, A. Y. Kovalevsky, D. N. Silverman, and R. McKenna, "Neutron diffraction of acetazolamide-bound human carbonic anhydrase II reveals atomic details of drug binding," *Journal of the American Chemical Society*, vol. 134, no. 36, pp. 14726–14729, 2012.

[32] M. D. Hanwell, D. E. Curtis, D. C. Lonie, T. Vandermeerschd, E. Zurek, and G. R. Hutchison, "Avogadro: an advanced semantic chemical editor, visualization, and analysis platform," *Journal of Cheminformatics*, vol. 4, no. 8, article 17, 2012.

[33] A. D. MacKerell Jr., D. Bashford, M. Bellott et al., "All-atom empirical potential for molecular modeling and dynamics studies of proteins," *Journal of Physical Chemistry B*, vol. 102, no. 18, pp. 3586–3616, 1998.

[34] F. A. Momany and R. Rone, "Validation of the general purpose quanta 3. 2/charmm force field," *Journal of Computational Chemistry*, vol. 13, pp. 888–900, 1992.

[35] B. R. Gelin and M. Karplus, "Side-chain torsional potentials: effect of dipeptide, protein, and solvent environment," *Biochemistry*, vol. 18, no. 7, pp. 1256–1268, 1979.

[36] W. Humphrey, A. Dalke, and K. Schulten, "VMD: visual molecular dynamics," *Journal of Molecular Graphics*, vol. 14, no. 1, pp. 33–38, 1996.

Hindawi Publishing Corporation
BioMed Research International
Volume 2014, Article ID 523210, 11 pages
http://dx.doi.org/10.1155/2014/523210

Research Article

Hydrophobic Substituents of the Phenylmethylsulfamide Moiety Can Be Used for the Development of New Selective Carbonic Anhydrase Inhibitors

Giuseppina De Simone,[1] Ginta Pizika,[2] Simona Maria Monti,[1] Anna Di Fiore,[1] Jekaterina Ivanova,[2] Igor Vozny,[2] Peteris Trapencieris,[2] Raivis Zalubovskis,[2] Claudiu T. Supuran,[3,4] and Vincenzo Alterio[1]

[1] *Istituto di Biostrutture e Bioimmagini, CNR, Via Mezzocannone 16, 80134 Naples, Italy*
[2] *Latvian Institute of Organic Synthesis, Aizkraukles 21, Riga LV-1006, Latvia*
[3] *Laboratorio di Chimica Bioinorganica, Università degli Studi di Firenze, Room 188, Via della Lastruccia 3, 50019 Sesto Fiorentino, Florence, Italy*
[4] *Dipartimento di Scienze Farmaceutiche, Università degli Studi di Firenze, Polo Scientifico, Via Ugo Schiff 6, 50019 Sesto Fiorentino, Florence, Italy*

Correspondence should be addressed to Raivis Zalubovskis; raivis@osi.lv and Vincenzo Alterio; vincenzo.alterio@cnr.it

Received 28 February 2014; Accepted 13 April 2014; Published 2 September 2014

Academic Editor: Mariya Al-Rashida

A new series of compounds containing a sulfamide moiety as zinc-binding group (ZBG) has been synthesized and tested for determining inhibitory properties against four human carbonic anhydrase (hCA) isoforms, namely, CAs I, II, IX, and XII. The X-ray structure of the cytosolic dominant isoform hCA II in complex with the best inhibitor of the series has also been determined providing further insights into sulfamide binding mechanism and confirming that such zinc-binding group, if opportunely derivatized, can be usefully exploited for obtaining new potent and selective CAIs. The analysis of the structure also suggests that for drug design purposes the but-2-yn-1-yloxy moiety tail emerges as a very interesting substituent of the phenylmethylsulfamide moiety due to its capability to establish strong van der Waals interactions with a hydrophobic cleft on the hCA II surface, delimited by residues Phe131, Val135, Pro202, and Leu204. Indeed, the complementarity of this tail with the cleft suggests that different substituents could be used to discriminate between isoforms having clefts with different sizes.

1. Introduction

Carbonic anhydrases (CAs, EC 4.2.1.1) are ubiquitous metalloenzymes found in prokaryotes and eukaryotes, which catalyze the reversible hydration of carbon dioxide to bicarbonate ion and proton ($CO_2 + H_2O \leftrightarrows HCO_3^- + H^+$) [1, 2]. In humans 15 different isoforms have been identified so far, among which 12 are catalytically active (CAs I-IV, VA-VB, VI-VII, IX, and XII-XIV), whereas the remaining three (CAs VIII, X, and XI), named as CA-related proteins (CARPs), are devoid of any catalytic activity [2]. All the catalytically active isoforms contain in their active site a zinc ion tetrahedrally coordinated by three conserved histidine residues and a water molecule/hydroxide ion [1, 2].

Over the past few years, the discovery of the involvement of several CA isoforms in human diseases has greatly increased the attention on these enzymes in regard to their consideration as interesting targets for drug design [3]. Indeed, a wealth of derivatives, mainly containing a primary sulfonamide (RSO_2NH_2) [1, 2, 4–6] and its bioisosteres, such as the sulfamate ($ROSO_2NH_2$) [1, 7, 8] and sulfamide ($RNHSO_2NH_2$) [1, 2, 9–18] as zinc anchoring groups, have been investigated as CA inhibitors (CAIs) with some of them (principally sulfonamides and sulfamates) being explored for

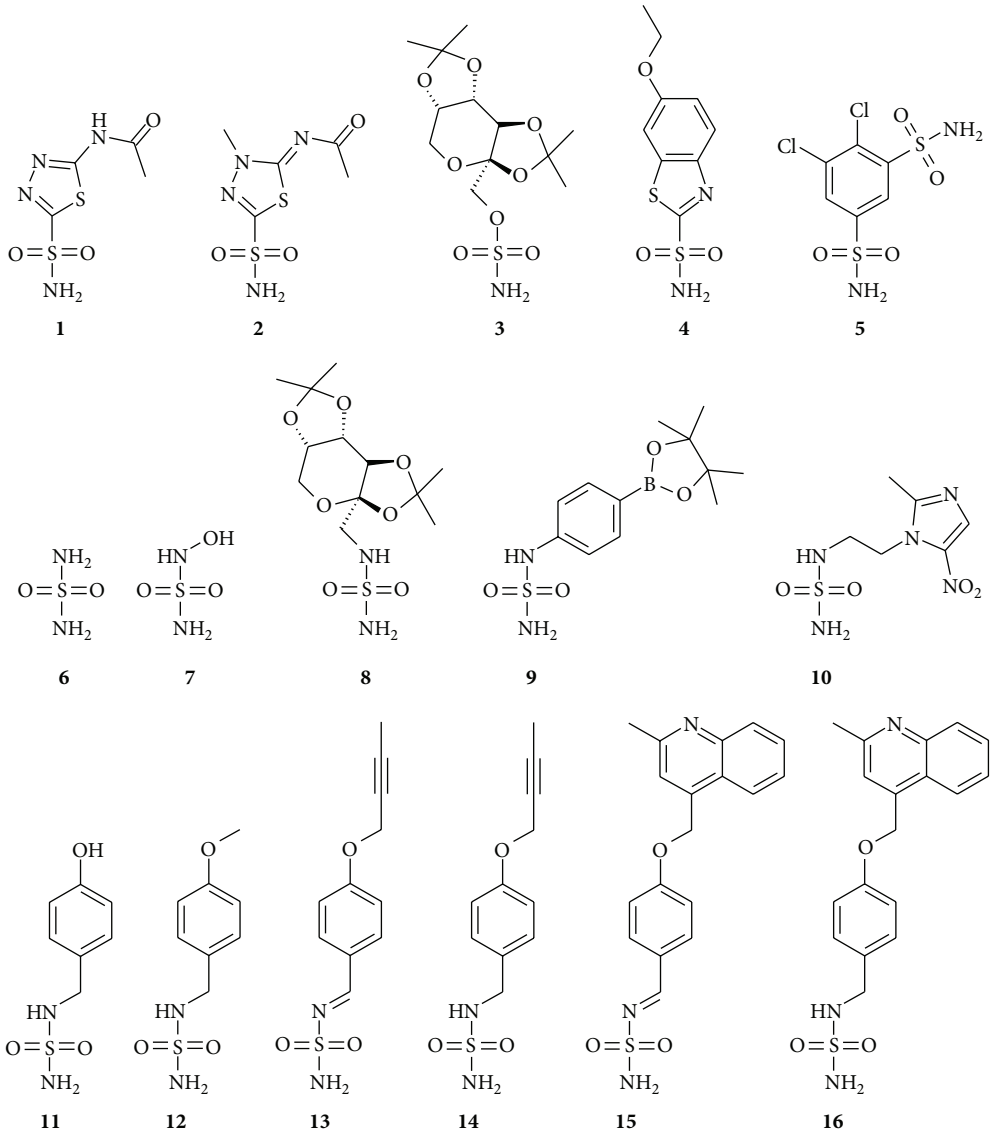

Figure 1: Chemical formulas of inhibitors **1–16**.

the treatment of a variety of disorders such as glaucoma [19–22], acid-base disequilibria [23], epilepsy [24, 25] neuromuscular diseases [26], edema [27], and obesity [28, 29] and for the management of hypoxic tumors [30]. Acetazolamide (AAZ) **1** [31], methazolamide (MZA) **2** [31], topiramate (TPM) **3** [32], ethoxzolamide (EZA) **4** [33], and dichlorphenamide (DCP) **5** [31] represent some examples of such pharmacologically relevant CAIs (Figure 1). However, it is important to highlight that none of the currently clinically used CAIs shows selectivity for a specific isozyme [1].

The knowledge of the inhibition profile of CAIs against all human isoforms and of their detailed binding to the enzyme (which can be obtained from crystallographic data) can allow for a better understanding of their mechanism of action and can provide an efficient molecular basis for the rational drug design of isozyme-selective compounds [1, 34]. In the last decade a huge number of X-ray structural studies of CA adducts principally with sulfonamides and sulfamates have been reported. On the contrary, sulfamide-containing derivatives have been only poorly investigated as CAIs, because they were initially supposed not to be particularly suitable for obtaining potent CA inhibitors, exhibiting just a moderate-to-weak inhibition potency [35, 36]. However, many recent studies, predominantly by Supuran's group, have supported the idea that sulfamide derivatives can be considered interesting candidates for obtaining CAIs, showing such several compounds with relatively high CA affinity [12–15]. At present, only 5 sulfamide-containing derivatives have been characterized by means of X-ray crystallography for their interaction with CAs: the simple sulfamide **6** [9, 16], the N-hydroxy-sulfamide **7** [10, 18], the sulfamide derivative of the antiepileptic drug topiramate **8** [11–15, 17], the boron containing derivative **9** [37], and the nitroimidazole-sulfamide **10** [38] (Figure 1). Thus we decided to investigate

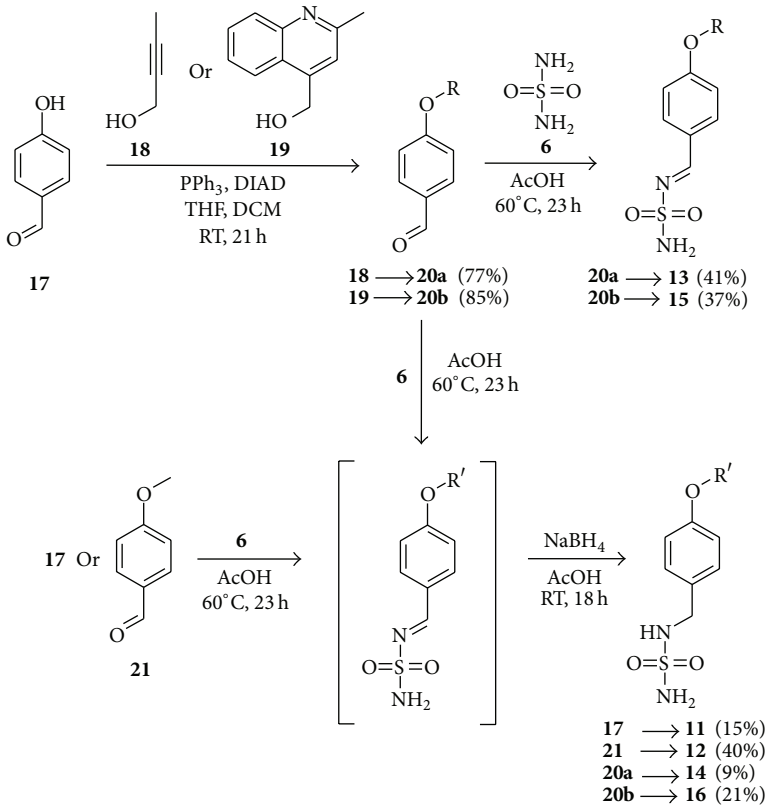

Scheme 1: Synthesis of compounds **11**–**16**.

in more detail this class of inhibitors by means of kinetic and crystallographic studies. In particular, in this paper we describe the synthesis and the inhibition analysis of a series of new sulfamides (compounds **11**–**16**) with CA isoforms I, II, IX, and XII. Furthermore, to better understand at structural level the molecular features determining the inhibition profiles of such compounds, we also report the high-resolution crystallographic structure of the cytosolic dominant isoform hCA II in complex with the highest affinity inhibitor (compound **14**) in the newly synthesized series.

2. Results and Discussion

2.1. Chemistry. Synthesis of aza-benzylidene derivatives of sulfamide, like compound **13**, from aryl aldehydes and sulfamide, is reported in the patent literature [39]. Our first efforts to reproduce a published procedure where ethanol was used as a solvent resulted in formation of trace amounts of desired product. After screening of several solvents we found that the use of glacial acetic acid gave reproducible results. With the improved procedure, where equimolar amounts of aryl aldehydes (compounds **20a**-**b**) and sulfamide (compound **6**) were used, monosubstituted aza-benzylidene derivatives **13** and **15** were isolated in acceptable yields (Scheme 1). Substituted aryl aldehydes **20a**-**b** were prepared from 4-hydroxybenzaldehyde **17** and corresponding alcohols **18** or **19** under Mitsunobu reaction conditions [40].

For the synthesis of monobenzyl derivatives of sulfamide, we chose one-pot two-step procedure [39], where the first step is the condensation reaction of sulfamide (compound **6**) and aryl aldehydes and the second step is the treatment of reaction mixture with $NaBH_4$, where the reduction of C=N double bond takes place. Under these conditions utilizing aldehydes **20a**-**b**, **17,** and **21,** monosubstituted sulfamides **11**, **12**, **14**, and **16** were obtained (Scheme 1).

2.2. CA Inhibition and Structure-Activity Relationship (SAR). Sulfamides **11**–**16** were investigated as inhibitors of four physiologically relevant CA isoforms, the cytosolic hCAs I and II, and the transmembrane, tumor-associated hCAs IX and XII (Table 1). The following SAR can be observed from the data of Table 1.

(i) hCA I was poorly inhibited by sulfamides **11**–**16**, which showed a compact behavior of medium-potency, weak inhibitors, with K_Is ranging from 1440 to 4050 nM. Interestingly, the compounds with the bulkier tails, **15** and **16,** were more effective as hCA I inhibitors compared to the derivatives with the OH, OMe, or alkynyl-ether moieties **11**–**14**. It may be observed that the standard drug acetazolamide (AAZ, a clinically used drug) was a more effective hCA I inhibitor compared to the sulfamides reported here.

(ii) The new sulfamides inhibited the physiologically dominant cytosolic isoform hCA II with K_Is ranging from 9.5 to 188 nM. It is interesting to note that derivatives **13** and **14** were effective hCA II inhibitors (comparable to AAZ),

Table 1: hCAs I, II, IX, and XII inhibition data with sulfamides **11–16**. Acetazolamide (AAZ) has been used as standard drug. Analyses were performed with a CO_2 hydrase, stopped-flow assay [41].

Compounds	K_I (nM)*			
	hCA I	hCA II	hCA IX	hCA XII
11	2180	74.1	40.7	5.8
12	4050	134	60.0	6.6
13	1940	9.8	59.1	8.4
14	1810	9.5	61.7	8.1
15	1650	188	56.3	6.5
16	1440	43.3	62.1	6.6
AAZ	250	12	25	5.7

*Mean from 3 different assays, errors in the range of ±10% of the reported values.

with inhibition constants of 9.5–9.8 nM (Table 1). The two compounds incorporate the same but-2-yn-1-yloxy-tail and only differ by the presence of Schiff's base (imine) moiety in compound **13**, which is reduced to the secondary amine in compound **14**. It is obvious that this structural modification has a minimal effect on the hCA II inhibitory properties, whereas the nature of the tail present in position 4 of the benzene ring (with respect to the zinc-binding group) has a crucial role in their binding affinity to the enzyme. Indeed, the compounds with such smaller moieties (than the but-2-yn-1-yloxy-one), like **11** and **12**, but also those with larger and bulkier such tails (compounds **15** and **16**), were less effective CAIs compared to compounds **13** and **14** against hCA II. Indeed, compounds **11** and **16** were medium-potency hCA II inhibitors (K_Is ranging from 43.3 to 74.1 nM) whereas compounds **12** and **15** were even weaker, with inhibition constants in the range of 134–188 nM (Table 1). The net difference of activity between compounds **11** and **12** which only differ by a CH_3 moiety should be noted. In the case of the imine-amine pair **15**, **16**, the imine **15** was 4.3 times a weaker hCA II inhibitor compared to the amine **16**.

(iii) Both transmembrane isoforms, hCA IX and XII, were effectively inhibited by sulfamides **11–16**, with little SAR evident from data of Table 1. Thus, for hCA IX the inhibition constants only ranged between 40.7 and 62.1 nM, whereas against hCA XII they were in the range of 5.8–8.4 nM. Thus all these sulfamides were medium-potency hCA IX inhibitors and were highly effective as hCA XII inhibitors (Table 1).

2.3. Crystallography. To better understand at structural level the molecular features determining the inhibition profiles of this new series of compounds against hCAs, we have solved the crystal structure of the cytosolic dominant isoform hCA II in complex with its highest affinity inhibitor (compound **14**) in the series.

Crystals of hCA II/**14** adduct were isomorphous with those of the native protein [42], allowing for the analysis of the structure by difference Fourier techniques. Data collection and refinement statistics are shown in Table 2. Inhibitor binding did not generate major changes in the structure of hCA II as proved by the low value of the RMSD calculated by superposing the Cα atoms in the adduct and the noninhibited enzyme (0.3 Å). The overall quality of the model was high, with 88.6% of the non-glycine residues located in the allowed regions of the Ramachandran plot (Table 2).

The inspection of the electron density maps at various stages of the crystallographic refinement revealed the binding of two inhibitor molecules: the first one on the protein surface

Table 2: Crystal parameters, data collection, and refinement statistics.

Crystal parameters	
Space group	$P2_1$
a (Å)	42.4
b (Å)	41.3
c (Å)	71.8
γ (°)	104.3
Number of independent molecules	1
Data collection statistics	
Resolution (Å)	50–1.85
Wavelength (Å)	1.54178
Temperature (K)	100
R_{merge} (%)[a]	3.4 (7.1)
Mean $I/\sigma(I)$	35.8 (13.6)
Total reflections	80810
Unique reflections	20026
Redundancy (%)	4.0 (2.5)
Completeness (%)	96.1 (84.8)
Refinement statistics	
R_{factor} (%)[b]	15.6
R_{free} (%)[b]	19.6
RMSD from ideal geometry	
Bond lengths (Å)	0.012
Bond angles (°)	1.7
Number of protein atoms	2091
Number of water molecules	215
Number of inhibitor atoms (2 molecules)	34
Average B factor (Å^2)	
All atoms	12.6
Protein atoms	11.6
Inhibitor 1 atoms	19.9
Inhibitor 2 atoms	27.1
Water molecules	20.6
Ramachandran plot	
Residues in the most favored regions (%)	88.6
Residues in additional allowed regions (%)	11.0
Residues in generously allowed regions (%)	0.5

[a] $R_{merge} = \sum_{hkl} \sum_i |I_i(hkl) - \langle I(hkl)\rangle| / \sum_{hkl} \sum_i I_i(hkl)$, where $I_i(hkl)$ is the intensity of an observation and $\langle I(hkl)\rangle$ is the mean value for its unique reflection; summations are over all reflections.

[b] $R_{factor} = \sum_h ||\mathrm{Fo}(h)| - |\mathrm{Fc}(h)|| / \sum_h |\mathrm{Fo}(h)|$, where Fo and Fc are the observed and calculated structure-factor amplitudes, respectively. R_{free} is calculated in same manner as R_{factor}, except that it uses 5% of the data omitted from refinement.

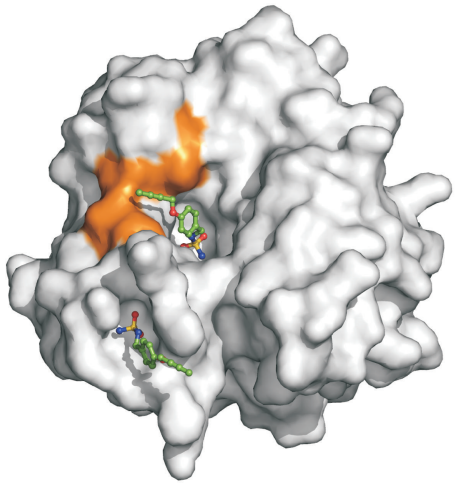

Figure 2: Solvent accessible surface of hCA II in its complex with **14**. The two molecules of the inhibitor bound within the active site cavity and on the protein surface are shown in stick representation. The hydrophobic cleft defined by residues Phe131, Val135, Pro202, and Leu204 is highlighted in orange.

and the second in the active site cavity (Figure 2). The binding of the inhibitor on the protein surface will not be discussed here, since it occurs far from the active site; thus it is not correlated with the inhibition properties of the molecule. On the contrary the binding of the molecule in the active site will be analyzed in detail since it is clearly associated with the high inhibitory potency of the investigated sulfamide.

As clearly evidenced in Figure 3(a) the electron density for the molecule bound in the active-site is very well defined for the phenylmethyl sulfamide moiety and slightly less defined for the but-2-yn-1-yloxy tail indicating some flexibility of this region. The compound is anchored to the active site coordinating the catalytic Zn^{2+} ion by means of one nitrogen atom of the sulfamide group (N1) and displacing the zinc bound water molecule/hydroxide ion (Figure 3(a)), similarly to what is observed for other sulfamides (compounds **6**–**10**) and sulfonamides/sulfamates whose crystal structures in adduct with CAs have been reported [16–18, 34, 37]. The same nitrogen atom N1 also interacts with Thr199 forming a hydrogen bond with its side chain, whereas one of sulfamide oxygen atoms forms a second hydrogen bond with the backbone nitrogen atom of the same residue (Figure 3(a)). It is interesting to note that the single bond N2-C1 adopts a trans-conformation (dihedral angle S1-N2-C1-C2 of about 175°), close to the trans-conformation expected for compound **13**, which contains in the same position a double bond. Thus it is tempting to speculate that this behavior should be at the basis of the almost identical affinity that the two molecules show for hCA II (see Table 1).

The phenyl ring of the inhibitor resides in the middle of the active site channel, making various van der Waals interactions with the side chains of Phe131, Leu198, Pro201, and Thr200 while the but-2-yn-1-yloxy tail lies in a small hydrophobic cleft on the protein surface, defined by residues Phe131, Val135, Pro202, and Leu204 (Figure 3(b)). This cleft has already been identified as an important region in the recognition of CAIs [1, 43]. In agreement with these data, this interaction seems to have important consequences on the inhibitory properties of this series of compounds against hCA II (see Table 1); indeed, inhibitors containing the but-2-yn-1-yloxy tail (compounds **13** and **14**) are those with the best inhibitory properties against the enzyme, while compounds with shorter (compounds **11** and **12**) or bulkier (compounds **15** and **16**) tails have less inhibitory potency. Indeed, compounds with shorter tails probably establish less extensive interactions with this cleft, while those with bulkier tails are unable to interact with it.

A so clear correlation between the tail and the inhibition constants is not observed for the other studied isoforms. Indeed in the case of hCA IX [44] and hCA XII [45] all studied compounds, although showing good affinity for the enzymes, present a much flat inhibition profile, not correlated to the size of the tail (see Table 1). Interestingly, in both cases the aforementioned hydrophobic cleft is larger (Figures 3(c) and 3(d)) and probably does not interact opportunely with the tail and does not allow a good discrimination.

A different situation is observed in the case of hCA I for which much higher inhibition constants are observed. The structural superposition of hCA II/**14** complex with hCA I [46] (Figure 3(f)) can give a reasonable explanation of these data. Indeed, most of the residues involved in the interaction of the inhibitor with hCA II are conserved also in the isoform I. However, the substitution of Thr200 with His200 in hCA I plays an important role in destabilizing the enzyme-inhibitor interaction since this residue is much more bulky and makes the active site narrower (Figures 3(e) and 3(f)). Therefore only an important structural rearrangement of the enzyme active site could allow the binding of the inhibitor, determining the very low affinity toward hCA I, as previously observed for other hCA I/inhibitor complexes [47].

As mentioned above very few papers describing sulfamide-containing derivatives crystallized with hCA II have been reported [16–18, 37, 38]. In these adducts a very weak additional H-bond interaction is observed between the Thr200OG atom and the second nitrogen atom of the sulfamide moiety. This weak interaction is absent in our case. The finding that compound **14** still remains a very good CA inhibitor despite this absence further confirms that such interaction does not have a great effect on the stabilization of the binding.

In conclusion, in this paper we report the X-ray structure of a new sulfamide inhibitor of CAs in complex with hCA II, together with an inhibition study of a family of structurally related compounds for the CA isoforms I, II, IX, and XII. The data reported here provide further insights into sulfamide binding mechanism confirming that this zinc-binding group could be usefully exploited for obtaining new potent and selective CAIs. In particular, the but-2-yn-1-yloxy tail emerges as a very interesting group for this purpose due to its capability to establish strong van der Waals interactions with a hydrophobic cleft on the hCA II surface delimited by residues Phe131, Val135, Pro202, and Leu204. Indeed, the complementarity of the tail with the cleft suggests that

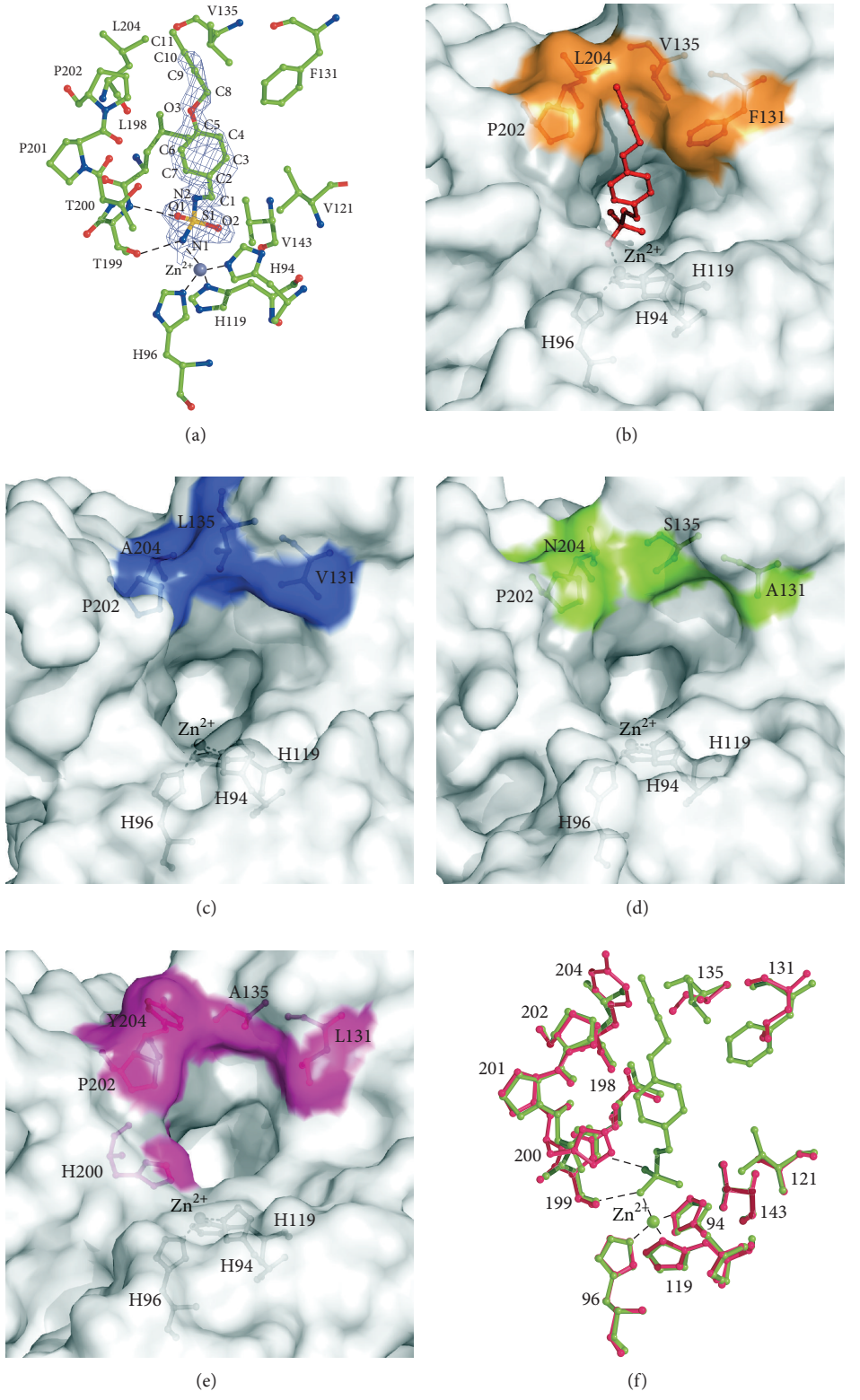

FIGURE 3: (a) Active site region of the hCA II/**14** complex. The inhibitor is shown in association with a σA-weighted |2Fo – Fc| map (at 1.0 σ). Hydrogen bonds, van der Waals interactions (distance of <4.0 Å), and the active site Zn^{2+}-ion coordination are also shown. (b, c, d, and e) Solvent accessible surface of hCAs II, IX, XII, and I: the hydrophobic cleft defined by residues 131, 135, 202, and 204 is highlighted in orange (hCA II), blue (hCA IX), green (hCA XII), and magenta (hCA I). For hCA I His200 is also showed in magenta. (f) Structural superposition of the hCA I (magenta) and hCA II (green) active sites. The inhibitor **14** is shown as bound in its complex with hCA II.

different substituents could be used to discriminate between isoforms having cleft with different sizes.

3. Materials and Methods

3.1. Chemistry. Reagents and starting materials were obtained from commercial sources and used as received. Compound **19** was synthesized according to literature procedure [48]. The solvents were purified and dried by standard procedures prior to use; petroleum ether (PE) of boiling range 40–60°C was used. Flash chromatography was carried out using Merck silica gel (230–400 mesh). Thin-layer chromatography was performed on silica gel; spots were visualized with UV light (254 and 365 nm). Melting points were determined on an OptiMelt automated melting point system. NMR spectra were recorded on Varian Mercury (400 MHz) spectrometer with chemical shifts values (δ) in ppm relative to TMS using the residual DMSO-d_6 signal as an internal standard. Elemental analyses were performed on a Carlo Erba CHNS-O EA-1108 apparatus.

3.1.1. General Procedure for the Synthesis of 4-Alkoxy Substituted Benzaldehydes. To a mixture of 4-hydroxybenzaldehyde (**17**) (15.58 mmol), PPh_3 (16.22 mmol), and corresponding alcohol under argon atmosphere dry DCM (100 mL) and dry THF (100 mL) were added. To this mixture at 0°C diisopropyl azodicarboxylate (DIAD) (15.76 mmol) was slowly added and reaction mixture was stirred at room temperature for 21 h. H_2O (75 mL) and brine (15 mL) were added and the mixture was extracted with DCM (3 × 100 mL). Organic layers were combined, dried over Na_2SO_4, and solvent was evaporated. The crude product was purified by column chromatography on silica gel.

*3.1.2. 4-(But-2-yn-1-yloxy)benzaldehyde (**20a**).* Compound **20a** was obtained from 4-hydroxybenzaldehyde (**17**) (1.90 g, 15.58 mmol), PPh_3 (4.27 g, 16.27 mmol), but-2-yn-1-ol (**18**) (0.87 mL, 11.54 mmol), and DIAD (3.13 mL, 15.82 mmol). The crude product was purified by column chromatography (toluene) and crystallized from EtOH to yield **20a** (1.55 g, 77%) as white solid. Mp 66–68°C.

^{1}H NMR (400 MHz, DMSO-d_6) δ: 1.84 (t, 3H, J = 2.3 Hz), 4.88 (q, 2H, J = 2.3 Hz), 7.13–7.17 (m, 2H), 7.86–7.90 (m, 2H), 9.88 (s, 1H).

^{13}C NMR (100 MHz, DMSO-d_6) δ: 3.1, 56.3, 74.1, 84.2, 115.2, 130.0, 131.7, 162.3, 191.3.

Anal. Calcd. for $C_{11}H_{10}O_2$ (174.20): C, 75.84; H, 5.79. Found: C, 75.60; H, 5.81.

*3.1.3. 4-[(2-Methylquinolin-4-yl)methoxy]benzaldehyde (**20b**).* Compound **20b** was obtained from 4-hydroxybenzal-dehyde (**17**) (1.90 g, 15.58 mmol), PPh_3 (4.27 g, 16.27 mmol), (2-methylquinolin-4-yl)methanol(**19**) [48] (2.00 g, 11.54 mmol), and DIAD (3.13 mL, 15.82 mmol). The crude product was purified by column chromatography (PE/EtOAC 3:1 then 1:1) to yield **20b** (2.70 g, 85%) as yellow solid. Mp 98–100°C.

^{1}H NMR (400 MHz, DMSO-d_6) δ: 2.66 (s, 3H), 5.72 (s, 2H), 7.31–7.36 (m, 2H), 7.55 (s, 1H), 7.58 (t, 1H, J = 7.7 Hz), 7.75 (t, 1H, J = 7.7 Hz), 7.88–7.93 (m, 2H), 7.98 (d, 1H, J = 8.4 Hz), 8.10 (d, 1H, J = 8.4 Hz), 9.90 (s, 1H).

^{13}C NMR (100 MHz, DMSO-d_6) δ: 25.0, 66.6, 115.4, 120.2, 123.7, 123.8, 125.9, 128.9, 129.4, 130.1, 131.9, 141.5, 147.4, 158.6, 163.0, 191.3.

Anal. Calcd. for $C_{18}H_{15}NO_2$ (277.32): C, 77.96; H, 5.45; N, 5.05. Found: C, 77.66; H, 5.47; N, 5.03.

3.1.4. General Procedure for the Synthesis Benzylidene Sulfamides. To sulfamide (**6**) (3.12 mmol) glacial acetic acid (5 mL) followed by the corresponding benzaldehyde (3.12 mmol) was added. Reaction mixture was stirred at 60°C for 23 h. EtOH was added and solvent was evaporated in vacuum. The crude product was purified by column chromatography on silica gel.

*3.1.5. N-([4-(But-2-yn-1-yloxy)phenyl]methylidene)sulfuric Diamide (**13**).* Compound **13** was obtained from sulfamide (**6**) (0.30 g, 3.12 mmol) and 4-(but-2-yn-1-yloxy)benzaldehyde (**20a**) (0.54 g, 3.12 mmol). The crude product was purified by column chromatography (PE/EtOAc 2 : 1) and crystallized from MeCN/H_2O to yield **13** (0.32 g, 41%) as white solid. Mp 192–194°C.

^{1}H NMR (400 MHz, DMSO-d_6) δ: 1.84 (t, 3H, J = 2.4 Hz), 4.88 (q, 2H, J = 2.4 Hz), 7.12–7.17 (m, 2H), 7.29 (s, 2H), 7.93–7.98 (m, 2H), 8.83 (s, 1H).

^{13}C NMR (100 MHz, DMSO-d_6) δ: 3.2, 56.4, 74.1, 84.3, 115.6, 125.6, 132.5, 162.1, 165.7.

Anal. Calcd. for $C_{11}H_{12}N_2O_3S$ (252.29): C, 52.37; H, 4.79; N, 11.10. Found: C, 52.03; H, 4.72; N, 11.07.

*3.1.6. N-({4-[(2-Methylquinolin-4-yl) methoxy]phenyl}methylidene)sulfuric Diamide (**15**).* Compound **15** was obtained from sulfamide (**6**) (0.30 g, 3.12 mmol) and 4-[(2-methylquinolin-4-yl) methoxy]benzaldehyde (**20b**) (0.87 g, 3.12 mmol). The crude product was purified by column chromatography (PE/EtOAc 2 : 1 then neat EtOAc) and crystallized from EtOH/H_2O to yield **15** (0.41 g, 37%) as white solid. Mp 99–101°C.

^{1}H NMR (400 MHz, DMSO-d_6) δ: 2.67 (s, 3H), 5.75 (s, 2H), 7.31 (s, 2H), 7.33–7.38 (m, 2H), 7.57 (s, 1H), 7.57–7.63 (m, 1H), 7.73–7.78 (m, 1H), 7.96–8.03 (m, 3H), 8.12 (d, 1H, J = 8.4 Hz), 8.86 (s, 1H).

^{13}C NMR (100 MHz, DMSO-d_6) δ: 25.0, 66.6, 115.8, 120.2, 123.7, 123.8, 125.7, 126.0, 128.9, 129.5, 132.7, 141.6, 147.4, 158.6, 162.8, 165.8.

Anal. Calcd. for $C_{18}H_{17}N_3O_3S$ (355.41): C, 60.83; H, 4.82; N, 11.82. Found: C, 60.39; H, 4.87; N, 11.71.

3.1.7. General One-Pot Procedure for the Synthesis of Monosubstituted Sulfamide. To sulfamide (**6**) (1 eq) glacial acetic acid followed by the corresponding benzaldehyde (1 eq) was added. Reaction mixture was stirred at 60°C for 23 h. $NaBH_4$ (10 eq) portionwise was added followed by extra glacial acetic acid. Reaction mixture was stirred at room temperature for 18 h before it was quenched with sat. aq. NH_4Cl. EtOH was added and solvent was evaporated in vacuum. H_2O was added and mixture was extracted with

EtOAc. Combined organic layers were dried over Na_2SO_4 and purified by column chromatography on silica gel.

*3.1.8. N-(4-Hydroxybenzyl)sulfuric Diamide (**11**).* Compound **11** was obtained from sulfamide (**6**) (0.30 g, 3.12 mmol), 4-hydroxybenzaldehyde (**17**) (0.38 g, 3.12 mmol) in AcOH (5 mL), and $NaBH_4$ (1.18 g, 31.2 mmol) with extra AcOH (15 mL). Reaction mixture was quenched with sat. aq. NH_4Cl (15 mL), diluted with H_2O (40 mL), and extracted with EtOAc (3 × 30 mL). The crude product was purified by column chromatography (PE/EtOAc 1 : 1) to yield **11** (0.10 g, 15%) as white solid. Mp 140–142°C.

^{1}H NMR (400 MHz, DMSO-d_6) δ: 3.94 (d, 2H, J = 6.5 Hz), 6.55 (s, 2H), 6.67–6.72 (m, 2H), 6.84 (t, 1H, J = 6.5 Hz), 7.10–7.15 (m, 2H), 9.28 (s, 1H).

^{13}C NMR (100 MHz, DMSO-d_6) δ: 45.8, 114.9, 128.7, 129.0, 156.4.

Anal. Calcd. for $C_7H_{10}N_2O_3S$ (202.23): C, 41.57; H, 4.98; N, 13.85. Found: C, 41.02; H, 5.07; N, 13.67.

*3.1.9. N-(4-Methoxybenzyl)sulfuric Diamide (**12**).* Compound **12** was obtained from sulfamide (**6**) (0.30 g, 3.12 mmol), 4-methoxybenzaldehyde (**21**) (0.38 mL, 3.12 mmol) in AcOH (5 mL), and $NaBH_4$ (1.18 g, 31.2 mmol) with extra AcOH (15 mL). Reaction mixture was quenched with sat. aq. NH_4Cl (3 mL), diluted with H_2O (50 mL), and extracted with EtOAc (3 × 30 mL). The crude product was purified by column chromatography (PE/EtOAc 2 : 1) and crystallized from EtOH/H_2O to yield **12** (0.27 g, 40%) as white solid. Mp 118–120°C.

^{1}H NMR (400 MHz, DMSO-d_6) δ: 3.73 (s, 3H), 4.00 (d, 2H, J = 6.5 Hz), 6.88 (s, 2H), 6.85–6.90 (m, 2H), 6.93 (t, 1H, J = 6.5 Hz), 7.23–7.28 (m, 2H).

^{13}C NMR (100 MHz, DMSO-d_6) δ: 45.6, 55.1, 113.6, 129.0, 130.5, 158.3.

Anal. Calcd. for $C_8H_{12}N_2O_3S$ (216.26): C, 44.43; H, 5.59; N, 12.95. Found: C, 44.54; H, 5.52; N, 12.81.

*3.1.10. N-[4-(But-2-yn-1-yloxy)benzyl]sulfuric Diamide (**14**).* Compound **14** was obtained from sulfamide (**6**) (0.26 g, 2.67 mmol), 4-(but-2-yn-1-yloxy)benzaldehyde (**20a**) (0.47 g, 2.67 mmol) in AcOH (5 mL), and $NaBH_4$ (1.01 g, 26.7 mmol) with extra AcOH (15 mL). Reaction mixture was quenched with sat. aq. NH_4Cl (15 mL), diluted with H_2O (40 mL), and extracted with EtOAc (3 × 30 mL). The crude product was purified by column chromatography (PE/EtOAc 2 : 1 then 1 : 1) and crystallized from DCM to yield **14** (0.04 g, 9%) as white solid. Mp 93–95°C.

^{1}H NMR (400 MHz, DMSO-d_6) δ: 1.82 (t, 3H, J = 2.3 Hz), 4.00 (d, 2H, J = 6.3 Hz), 4.71 (q, 2H, J = 2.3 Hz), 6.59 (s, 2H), 6.88–6.97 (m, 3H), 7.23–7.28 (m, 2H).

^{13}C NMR (100 MHz, DMSO-d_6) δ: 3.1, 45.6, 55.8, 74.8, 83.4, 114.4, 128.9, 131.1, 156.4.

Anal. Calcd. for $C_{11}H_{14}N_2O_3S$ (254.31): C, 51.95; H, 5.55; N, 11.02. Found: C, 51.82; H, 5.56; N, 10.97.

*3.1.11. N-{4-[(2-Methylquinolin-4-yl)methoxy]benzyl}sulfuric Diamide (**16**).* Compound **16** was obtained from sulfamide (**6**) (0.17 g, 1.80 mmol), 4-[(2-methylquinolin-4-yl) methoxy] benzaldehyde (**20b**) (0.50 g, 1.80 mmol) in AcOH (5 mL), and $NaBH_4$ (0.68 g, 18.0 mmol) with extra AcOH (15 mL). Reaction mixture was quenched with sat. aq. NH_4Cl (10 mL), diluted with H_2O (40 mL), and extracted with EtOAc (3 × 30 mL). The crude product was purified by column chromatography (PE/EtOAc 1 : 2) to yield **16** (0.14 g, 21%) as yellow solid. Mp 180-181°C.

^{1}H NMR (400 MHz, DMSO-d_6) δ: 2.66 (s, 3H), 4.02 (d, 2H, J = 6.4 Hz), 5.60 (s, 2H), 6.60 (s, 2H), 6.97 (t, 1H, J = 6.4 Hz), 7.07–7.12 (m, 2H), 7.28–7.33 (m, 2H), 7.55 (s, 1H), 7.56–7.61 (m, 1H), 7.72–7.77 (m, 1H), 7.97 (d, 1H, J = 8.4 Hz), 8.10 (d, 1H, J = 8.4 Hz).

^{13}C NMR (100 MHz, DMSO-d_6) δ: 25.0, 45.6, 66.2, 114.6, 120.1, 123.7, 123.9, 125.9, 128.9, 129.1, 129.4, 131.3, 142.4, 147.4, 157.1, 158.6.

Anal. Calcd. for $C_{18}H_{19}N_3O_3S$ (357.43): C, 60.49; H, 5.36; N, 11.76. Found: C, 60.37; H, 5.38; N, 11.81.

3.2. CA Inhibition Assays. A stopped-flow CO_2 hydration assay with an Applied Photophysics instrument was used for measuring the inhibition of hCAs I, II, IX, and XII by the new compounds reported here. Phenol red (at a concentration of 0.2 mM) has been used as indicator, working at the absorbance maximum of 557 nm, with 20 mM Hepes (pH 7.4) or 20 mM Tris (pH 8.3) as buffers, and 20 mM Na_2SO_4 or $NaClO_4$ (for maintaining the ionic strength constant). The initial rates of the CA-catalyzed CO_2 hydration reaction were followed for a period of 10–100 s [41]. The concentrations of substrate (CO_2) ranged from 1.7 to 17 mM for the determination of the inhibition constants, with at least six traces of the initial 5–10% of the reaction being used for determining the initial velocity, for each inhibitor. The uncatalyzed rates were determined and subtracted from the total observed rates. Stock solutions of inhibitors (10 mM) were prepared in distilled-deionized water and dilutions up to 0.01 nM were done with the assay buffer. Enzyme and inhibitor solutions were preincubated prior to assay for 15 min (at room temperature), in order to allow for the formation of the E-I complex. The inhibition constants were obtained by nonlinear least-squares methods using PRISM 3 and the Cheng-Prusoff equation as reported earlier by our groups. The kinetic parameters for the uninhibited enzymes were derived from Lineweaver-Burk plots, as reported earlier [49–51], and represent the mean from at least three different determinations.

3.3. X-Ray Studies. hCA II/**14** complex was obtained by adding a 5-molar excess of inhibitor to a 10 mg/mL protein solution in 20 mM Tris-HCl pH 8, 0.1% DMSO. Crystals of the complex were obtained using the hanging drop vapor diffusion technique. In particular 2 μL of complex solution and 2 μL of precipitant solution (1.4 M Na-Citrate, 100 mM Tris-HCl pH 8.0) were mixed and suspended over a reservoir containing 1 mL of precipitant solution at 20°C. X-ray diffraction data were collected at 100 K, using a copper rotating anode generator developed by Rigaku and equipped with a Rigaku Saturn CCD detector. Prior to cryogenic freezing, the crystals

were transferred to the precipitant solution with the addition of 15% (v/v) glycerol. Data were processed using the HKL2000 package [52]. Diffraction data were indexed in the $P2_1$ space group with one molecule in the asymmetric unit. Unit cell parameters and data reduction statistics are reported in Table 2. The atomic coordinates of hCA II (PDB entry 1CA2) [42] were used as a starting model for crystallographic refinement after deletion of non-protein atoms. Structure refinement (in the 20.0–1.85 Å resolution range) was carried out using CNS [53] and model building was performed with O [54]. Inhibitor molecules were identified from peaks in |Fo| – |Fc| maps and gradually built into the model over several rounds of refinement. Restraints on inhibitor bond angles and distances were taken from similar structures in the Cambridge Structural Database [55] whereas standard restraints were used on protein bond angles and distances throughout refinement. The correctness of stereochemistry was finally checked using PROCHECK [56]. Final refinement statistics are presented in Table 2. The atomic coordinates of hCA II/**14** complex were deposited in the Protein Data Bank, accession code 4PQ7.

Conflict of Interests

The authors declare that there is no conflict of interests regarding the publication of this paper.

Acknowledgments

The authors thank Maurizio Amendola and Giosuè Sorrentino for their skillful technical assistance with X-ray measurements.

References

[1] V. Alterio, A. di Fiore, K. D'Ambrosio, C. T. Supuran, and G. de Simone, "Multiple binding modes of inhibitors to carbonic anhydrases: how to design specific drugs targeting 15 different isoforms?" *Chemical Reviews*, vol. 112, no. 8, pp. 4421–4468, 2012.

[2] C. T. Supuran, "Carbonic anhydrases: novel therapeutic applications for inhibitors and activators," *Nature Reviews Drug Discovery*, vol. 7, no. 2, pp. 168–181, 2008.

[3] C. T. Supuran and A. Scozzafava, "Carbonic anhydrases as targets for medicinal chemistry," *Bioorganic and Medicinal Chemistry*, vol. 15, no. 13, pp. 4336–4350, 2007.

[4] C. T. Supuran, "Carbonic anhydrases as drug targets—general presentation," in *Drug Design of Zinc-Enzyme Inhibitors: Functional, Structural, and Disease Applications*, J.-Y. Winum, Ed., pp. 15–38, John Wiley & Sons, Hoboken, NJ, USA, 2009.

[5] J.-Y. Winum, M. Rami, A. Scozzafava, J.-L. Montero, and C. T. Supuran, "Carbonic anhydrase IX: a new druggable target for the design of antitumor agents," *Medicinal Research Reviews*, vol. 28, no. 3, pp. 445–463, 2008.

[6] C. T. Supuran, A. Scozzafava, and A. Casini, "Carbonic anhydrase inhibitors," *Medicinal Research Reviews*, vol. 23, no. 2, pp. 146–189, 2003.

[7] J. Winum, D. Vullo, A. Casini, J. Montero, A. Scozzafava, and C. T. Supuran, "Carbonic anhydrase inhibitors. Inhibition of cytosolic isozymes I and II and transmembrane, tumor-associated isozyme IX with sulfamates including EMATE also acting as steroid sulfatase inhibitors," *Journal of Medicinal Chemistry*, vol. 46, no. 11, pp. 2197–2204, 2003.

[8] J. Winum, D. Vullo, A. Casini, J. Montero, A. Scozzafava, and C. T. Supuran, "Carbonic anhydrase inhibitors: inhibition of transmembrane, tumor-associated isozyme IX, and cytosolic isozymes I and II with aliphatic sulfamates," *Journal of Medicinal Chemistry*, vol. 46, no. 25, pp. 5471–5477, 2003.

[9] J.-Y. Winum, A. Scozzafava, J.-L. Montero, and C. T. Supuran, "Therapeutic potential of sulfamides as enzymes inhibitors," *Medicinal Research Reviews*, vol. 26, no. 6, pp. 767–792, 2006.

[10] J.-Y. Winum, A. Scozzafava, J.-L. Montero, and C. T. Supuran, "The sulfamide motif in the design of enzyme inhibitors," *Expert Opinion on Therapeutic Patents*, vol. 16, no. 1, pp. 27–47, 2006.

[11] A. Scozzafava, M. D. Banciu, A. Popescu, and C. T. Supuran, "Carbonic anhydrase inhibitors: inhibition of isozymes I, II and IV by sulfamide and sulfamic acid derivatives," *Journal of Enzyme Inhibition and Medicinal Chemistry*, vol. 15, no. 5, pp. 443–453, 2000.

[12] A. Casini, J. Winum, J. Montero, A. Scozzafava, and C. T. Supuran, "Carbonic anhydrase inhibitors: inhibition of cytosolic isozymes I and II with sulfamide derivatives," *Bioorganic and Medicinal Chemistry Letters*, vol. 13, no. 5, pp. 837–840, 2003.

[13] A. Casini, J. Antel, F. Abbate et al., "Carbonic anhydrase inhibitors: SAR and X-ray crystallographic study for the interaction of sugar sulfamates/sulfamides with isozymes I, II and IV," *Bioorganic and Medicinal Chemistry Letters*, vol. 13, no. 5, pp. 841–845, 2003.

[14] J. Winum, A. Innocenti, J. Nasr et al., "Carbonic anhydrase inhibitors: Synthesis and inhibition of cytosolic/tumor-associated carbonic anhydrase isozymes I, II, IX, and XII with *N*-hydroxysulfamides—a new zinc-binding function in the design of inhibitors," *Bioorganic and Medicinal Chemistry Letters*, vol. 15, no. 9, pp. 2353–2358, 2005.

[15] J.-Y. Winum, A. Cecchi, J.-L. Montero, A. Innocenti, A. Scozzafava, and C. T. Supuran, "Carbonic anhydrase inhibitors. Synthesis and inhibition of cytosolic/tumor-associated carbonic anhydrase isozymes I, II, and IX with boron-containing sulfonamides, sulfamides, and sulfamates: toward agents for boron neutron capture therapy of hypoxic tumors," *Bioorganic and Medicinal Chemistry Letters*, vol. 15, no. 13, pp. 3302–3306, 2005.

[16] F. Abbate, C. T. Supuran, A. Scozzafava, P. Orioli, M. T. Stubbs, and G. Klebe, "Nonaromatic sulfonamide group as an ideal anchor for potent human carbonic anhydrase inhibitors: role of hydrogen-bonding networks in ligand binding and drug design," *Journal of Medicinal Chemistry*, vol. 45, no. 17, pp. 3583–3587, 2002.

[17] J. Winum, C. Temperini, K. El Cheikh et al., "Carbonic anhydrase inhibitors: clash with Ala65 as a means for designing inhibitors with low affinity for the ubiquitous isozyme II, exemplified by the crystal structure of the topiramate sulfamide analogue," *Journal of Medicinal Chemistry*, vol. 49, no. 24, pp. 7024–7031, 2006.

[18] C. Temperini, J. Winum, J. Montero, A. Scozzafava, and C. T. Supuran, "Carbonic anhydrase inhibitors: The X-ray crystal structure of the adduct of N-hydroxysulfamide with isozyme II explains why this new zinc binding function is effective in the design of potent inhibitors," *Bioorganic and Medicinal Chemistry Letters*, vol. 17, no. 10, pp. 2795–2801, 2007.

[19] R. E. Marquis and J. T. Whitson, "Management of glaucoma: Focus on pharmacological therapy," *Drugs and Aging*, vol. 22, no. 1, pp. 1–21, 2005.

[20] D. Vullo, A. Innocenti, I. Nishimori et al., "Carbonic anhydrase inhibitors. Inhibition of the transmembrane isozyme XII with sulfonamides—a new target for the design of antitumor and antiglaucoma drugs?" *Bioorganic and Medicinal Chemistry Letters*, vol. 15, no. 4, pp. 963–969, 2005.

[21] C. T. Supuran, A. Casini, and A. Scozzafava, "Development of sulfonamide carbonic anhydrase inhibitors (CAIs)," in *Carbonic Anhydrase—Its Inhibitors and Activators*, C. T. Supuran, A. Scozzafava, and J. Conway, Eds., pp. 67–148, CRC Press, Boca Raton, Fla, USA, 2004.

[22] F. Fabrizi, F. Mincione, T. Somma et al., "A new approach to antiglaucoma drugs: carbonic anhydrase inhibitors with or without NO donating moieties. Mechanism of action and preliminary pharmacology," *Journal of Enzyme Inhibition and Medicinal Chemistry*, vol. 27, no. 1, pp. 138–147, 2012.

[23] F. B. Loiselle, P. E. Morgan, B. V. Alvarez, and J. R. Casey, "Regulation of the human NBC_3 Na^+/HCO_3^- cotransporter by carbonic anhydrase II and PKA," *The American Journal of Physiology—Cell Physiology*, vol. 286, no. 6, pp. C1423–C1433, 2004.

[24] C. Rivera, J. Voipio, and K. Kaila, "Two developmental switches in GABAergic signalling: the K^+-Cl^- cotransporter KCC2 and carbonic anhydrase CAVII," *Journal of Physiology*, vol. 562, no. 1, pp. 27–36, 2005.

[25] D. Vullo, J. Voipio, A. Innocenti et al., "Carbonic anhydrase inhibitors. Inhibition of the human cytosolic isozyme VII with aromatic and heterocyclic sulfonamides," *Bioorganic and Medicinal Chemistry Letters*, vol. 15, no. 4, pp. 971–976, 2005.

[26] K. E. Lyons, R. Pahwa, C. L. Comella et al., "Benefits and risks of pharmacological treatments for essential tremor," *Drug Safety*, vol. 26, no. 7, pp. 461–481, 2003.

[27] K. Hori, S. Ishida, M. Inoue et al., "Treatment of cystoid macular edema with oral acetazolamide in a patient with best vitelliform macular dystrophy," *Retina*, vol. 24, no. 3, pp. 481–482, 2004.

[28] C. T. Supuran, "Carbonic anhydrase inhibitors in the treatment and prophylaxis of obesity," *Expert Opinion on Therapeutic Patents*, vol. 13, no. 10, pp. 1545–1550, 2003.

[29] J. Y. Winum, A. Scozzafava, J. L. Montero, and C. T. Supuran, "Sulfamates and their therapeutic potential," *Medicinal Research Reviews*, vol. 25, no. 2, pp. 186–228, 2005.

[30] E. Švastová, A. Hulíková, M. Rafajová et al., "Hypoxia activates the capacity of tumor-associated carbonic anhydrase IX to acidify extracellular pH," *FEBS Letters*, vol. 577, no. 3, pp. 439–445, 2004.

[31] G. Splendiani and S. Condò, "Diuretic therapy in heart failure," *Giornale Italiano di Nefrologia*, vol. 23, pp. S74–S76, 2006.

[32] K. M. Gadde, D. B. Allison, D. H. Ryan et al., "Effects of low-dose, controlled-release, phentermine plus topiramate combination on weight and associated comorbidities in overweight and obese adults (CONQUER): a randomised, placebo-controlled, phase 3 trial," *The Lancet*, vol. 377, no. 9774, pp. 1341–1352, 2011.

[33] W. F. Brechue and T. H. Maren, "A comparison between the effect of topical and systemic carbonic anhydrase inhibitors on aqueous humor secretion," *Experimental Eye Research*, vol. 57, no. 1, pp. 67–78, 1993.

[34] V. Alterio, A. di Fiore, K. D'Ambrosio, C. T. Supuran, and G. de Simone, "X-ray crystallography of CA inhibitors and its importance in drug design," in *Drug Design of Zinc-Enzyme Inhibitors: Functional, Structural, and Disease Applications*, C. T. Supuran and J. Y. Winum, Eds., pp. 73–138, John Wiley & Sons, Hoboken, NJ, USA, 2009.

[35] B. E. Maryanoff, D. F. McComsey, M. J. Costanzo, C. Hochman, V. Smith-Swintosky, and R. P. Shank, "Comparison of sulfamate and sulfamide groups for the inhibition of carbonic anhydrase-II by using topiramate as a structural platform," *Journal of Medicinal Chemistry*, vol. 48, no. 6, pp. 1941–1947, 2005.

[36] A. L. Klinger, D. F. McComsey, V. Smith-Swintosky, R. P. Shank, and B. E. Maryanoff, "Inhibition of carbonic anhydrase-II by sulfamate and sulfamide groups: An investigation involving direct thermodynamic binding measurements," *Journal of Medicinal Chemistry*, vol. 49, no. 12, pp. 3496–3500, 2006.

[37] A. Di Fiore, S. M. Monti, A. Innocenti, J. Winum, G. de Simone, and C. T. Supuran, "Carbonic anhydrase inhibitors: crystallographic and solution binding studies for the interaction of a boron-containing aromatic sulfamide with mammalian isoforms I-XV," *Bioorganic and Medicinal Chemistry Letters*, vol. 20, no. 12, pp. 3601–3605, 2010.

[38] M. Rami, L. Dubois, N.-K. Parvathaneni et al., "Hypoxia-targeting carbonic anhydrase IX inhibitors by a new series of nitroimidazole-sulfonamides/sulfamides/sulfamates," *Journal of Medicinal Chemistry*, vol. 56, no. 21, pp. 8512–8520, 2013.

[39] A. F. Abdel-Magid and S. J. Mehrman, "Process for preparation of sulfamide derivatives," Patent Cooperation Treaty International Application WO 2006/127184 A1, 2006.

[40] O. Mitsunobu, "The use of diethyl azodicarboxylate and triphenylphosphine in synthesis and transformation of natural products," *Synthesis*, vol. 1, no. 1, pp. 1–28, 1981.

[41] R. G. Khalifah, "The carbon dioxide hydration activity of carbonic anhydrase. I. Stop-flow kinetic studies on the native human isoenzymes B and C.," *The Journal of Biological Chemistry*, vol. 246, no. 8, pp. 2561–2573, 1971.

[42] A. E. Eriksson, T. A. Jones, and A. Liljas, "Refined structure of human carbonic anhydrase II at 2.0 Å resolution," *Proteins: Structure, Function and Genetics*, vol. 4, no. 4, pp. 274–282, 1988.

[43] F. Pacchiano, M. Aggarwal, B. S. Avvaru et al., "Selective hydrophobic pocket binding observed within the carbonic anhydrase II active site accommodate different 4-substituted-ureidobenzenesulfonamides and correlate to inhibitor potency," *Chemical Communications*, vol. 46, no. 44, pp. 8371–8373, 2010.

[44] V. Alterio, M. Hilvo, A. Di Fiore et al., "Crystal structure of the catalytic domain of the tumor-associated human carbonic anhydrase IX," *Proceedings of the National Academy of Sciences of the United States of America*, vol. 106, no. 38, pp. 16233–16238, 2009.

[45] D. A. Whittington, A. Waheed, B. Ulmasov et al., "Crystal structure of the dimeric extracellular domain of human carbonic anhydrase XII, a bitopic membrane protein overexpressed in certain cancer tumor cells," *Proceedings of the National Academy of Sciences of the United States of America*, vol. 98, no. 17, pp. 9545–9550, 2001.

[46] K. K. Kannan, M. Ramanadham, and T. A. Jones, "Structure, refinement, and function of carbonic anhydrase isozymes: Refinement of human carbonic anhydrase I," *Annals of the New York Academy of Sciences*, vol. 429, pp. 49–60, 1984.

[47] V. Alterio, S. M. Monti, E. Truppo, C. Pedone, C. T. Supuran, and G. de Simone, "The first example of a significant active site conformational rearrangement in a carbonic anhydrase-inhibitor adduct: the carbonic anhydrase I-topiramate complex," *Organic and Biomolecular Chemistry*, vol. 8, no. 15, pp. 3528–3533, 2010.

[48] Y. Wang, M. Papamichelakis, W. Chew et al., "Development of a suitable process for the preparation of a TNF-α converting enzyme inhibitor, WAY-281418," *Organic Process Research and Development*, vol. 12, no. 6, pp. 1253–1260, 2008.

[49] P. Joseph, F. Turtaut, S. Ouahrani-Bettache et al., "Cloning, characterization, and inhibition studies of a β-carbonic anhydrase from brucella suis," *Journal of Medicinal Chemistry*, vol. 53, no. 5, pp. 2277–2285, 2010.

[50] P. Pan, G. C. Rodrigues, A. Scozzafava et al., "Cloning, characterization, and sulfonamide and thiol inhibition studies of an α-carbonic anhydrase from *Trypanosoma cruzi*, the causative agent of Chagas disease," *Journal of Medicinal Chemistry*, vol. 56, no. 4, pp. 1761–1771, 2013.

[51] M. Minakuchi, I. Nishimori, D. Vullo, A. Scozzafava, and C. T. Supuran, "Molecular cloning, characterization, and inhibition studies of the Rv1284 beta-carbonic anhydrase from Mycobacterium tuberculosis with sulfonamides and a sulfamate," *Journal of Medicinal Chemistry*, vol. 52, no. 8, pp. 2226–2232, 2009.

[52] Z. Otwinowski and W. Minor, "Processing of X-ray diffraction data collected in oscillation mode," *Methods in Enzymology*, vol. 276, pp. 307–326, 1997.

[53] A. T. Brünger, P. D. Adams, G. M. Clore et al., "Crystallography & NMR system: a new software suite for macromolecular structure determination," *Acta Crystallographica Section D*, vol. 54, no. 5, pp. 905–921, 1998.

[54] T. A. Jones, J. Y. Zou, and S. W. Cowan, "Improved methods for building protein models in electron density maps and the location of errors in these models," *Acta Crystallographica A: Foundations of Crystallography*, vol. 47, no. 2, pp. 110–119, 1991.

[55] F. H. Allen, "The Cambridge Structural Database: a quarter of a million crystal structures and rising," *Acta Crystallographica Section B: Structural Science*, vol. 58, no. 3, pp. 380–388, 2002.

[56] R. A. Laskowski, M. W. MacArthur, D. S. Moss, and J. M. Thornton, "PROCHECK: a program to check the stereochemical quality of protein structures," *Journal of Applied Crystallography*, vol. 26, no. 2, pp. 283–291, 1993.

Hindawi Publishing Corporation
BioMed Research International
Volume 2014, Article ID 374079, 6 pages
http://dx.doi.org/10.1155/2014/374079

Research Article

Natural Product Polyamines That Inhibit Human Carbonic Anhydrases

Rohan A. Davis,[1] Daniela Vullo,[2] Claudiu T. Supuran,[2] and Sally-Ann Poulsen[1]

[1] *Eskitis Institute for Drug Discovery, Griffith University, Nathan, QLD 4111, Australia*
[2] *Polo Scientifico, Laboratorio di Chimica Bioinorganica, Rm. 188, Università degli Studi di Firenze, Via della Lastruccia 3, Sesto Fiorentino, 50019 Florence, Italy*

Correspondence should be addressed to Claudiu T. Supuran; claudiu.supuran@unifi.it and Sally-Ann Poulsen; s.poulsen@griffith.edu.au

Received 24 February 2014; Accepted 14 July 2014; Published 5 August 2014

Academic Editor: Vincenzo Alterio

Natural product compound collections have proven an effective way to access chemical diversity and recent findings have identified phenolic, coumarin, and polyamine natural products as atypical chemotypes that inhibit carbonic anhydrases (CAs). CA enzymes are implicated as targets of variable drug therapeutic classes and the discovery of selective, drug-like CA inhibitors is essential. Just two natural product polyamines, spermine and spermidine, have until now been investigated as CA inhibitors. In this study, five more complex natural product polyamines **1–5**, derived from either marine sponge or fungi, were considered for inhibition of six different human CA isozymes of interest in therapeutic drug development. All compounds share a simple polyamine core fragment, either spermine or spermidine, yet display substantially different structure activity relationships for CA inhibition. Notably, polyamines **1–5** were submicromolar inhibitors of the cancer drug target CA IX, this is more potent than either spermine or spermidine.

1. Introduction

Carbonic anhydrases (CAs) catalyze the reversible hydration of carbon dioxide to bicarbonate anion and a proton: $CO_2 + H_2O \leftrightarrows HCO_3^- + H^+$ [1]. This equilibrium underpins a range of physiological processes including pH regulation, carbon metabolism, and ion transport. The therapeutic potential for modulating this reaction is well recognized across a number of diseases affecting humans, with the discovery that interfering with pH plays a major role in survival, growth, and metastasis of hypoxic tumours driving a need for small molecule CA inhibitors [2]. The active site of CA enzymes comprises a zinc cation that is coordinated to three conserved histidine residues and a hydroxide anion (OH^-). The zinc-bound OH^- reacts with CO_2 to generate HCO_3^- and H^+; these ions are then rapidly released to the microenvironment and the active enzyme is regenerated. The structural similarities in active site architecture across human CA isozymes are substantial and for drug discovery that is dependent on selectively targeting specific CA isozymes this presents a considerable hurdle [3]. Primary sulfonamide compounds ($R–SO_2NH_2$) coordinate as an anion ($R–SO_2NH^-$) to the CA active site zinc in place of the usual OH^- anion and are highly effective inhibitors of CAs. Many primary sulfonamide compounds are however nonselective, resulting in broad acting CA inhibitors that are a major drawback to drug discovery. The identification of new CA inhibitor chemotypes with better CA isozyme selectivity profiles is needed to address this drawback. Natural product (NP) compound collections have proven an effective way to access new chemotypes, and notably NPs have provided a significant portion of FDA approved drugs, particularly in the cancer therapeutics drug class [4]. Recent findings have identified phenol, [5–7] coumarin [8, 9], and polyamine [10] NPs that inhibit CAs. Using protein X-ray crystallography researchers have shown that each of these chemotypes interacts differently with the CA active site, and unlike primary sulfonamides none directly interact with the active site zinc [11]. The number of NPs that have so far been investigated for inhibition of CAs is however small and just a single innovative study that describes the

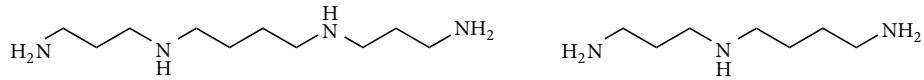

Spermine Spermidine

Figure 1: Natural product polyamine CA inhibitors, spermine and spermidine [10].

inhibition of CAs with simple NP polyamines, spermine and spermidine, is reported (Figure 1) [10]. The inspiration for the present study is to further examine NP polyamines, particularly those with greater structural complexity than spermine and spermidine. With so few polyamines investigated for CA inhibitory activity, we hoped to broaden our understanding of the potential of polyamine alkaloids as an alternate nonclassical chemotype for CA inhibition.

Polyamines have been isolated from terrestrial and marine animals, plants, fungi, and bacteria [12]. These polycationic alkaloids are able to strongly interact with anionic biomolecules such as DNA and RNA and to a lesser extent proteins. This interaction may modulate a selection of cellular activities including gene expression, cell proliferation, translation, cell signaling, membrane stabilization, and ion channels [13–18]. The CA activity for two of the simplest NP polyamines, spermine and spermidine, and 16 semisynthetic polyamine analogues has been reported [10]. In this study, the inhibition of all 12 catalytically active human CA isozymes was assessed and the variation in K_i values ranged from low nanomolar to millimolar. The standout CA isozyme was CA IV, a transmembrane anchored enzyme with an extracellular orientated active site [19]. Both NP polyamines achieved lower K_i values, 0.010 μM and 0.112 μM for spermine and spermidine, respectively, at CA IV compared to all other tested CAs. An X-ray crystal structure of spermine in complex with CA II showed that it binds differently compared to primary sulfonamides. Spermine is a polycation at the experimental pH (pH = 7.4) and was found indirectly anchored to the zinc cation via the zinc-bound water ligand. Furthermore, a complex network of hydrogen bonds between spermine and CA active site residues was observed, including the terminal amine moiety which forms hydrogen bonds with residues Thr200 and Pro201. This CA binding mode suggests that NP polyamines may have potential to provide additional CA inhibitors with this altered mechanism of binding and inhibition of CAs. As polycations, compounds spermine and spermidine are not expected to enter cells by passive membrane diffusion, and this may give them some selectivity for extracellular facing CAs (CAs IV, IX, XII, and XIV) in cell models, and these isozymes are the focus of the present study.

2. Materials and Methods

2.1. Chemistry. Compounds were isolated from two marine sponge samples and one mushroom specimen, archived in the Nature Bank biota repository, [20] located at the Eskitis Institute for Drug Discovery, Griffith University. Nature Bank is a unique drug discovery resource that consists of >50,000 biota samples collected from Australia, China, and Papua New Guinea along with >200,000 fractionated natural product samples [21]. The five NP polyamines (**1**–**5**) investigated in this study were identified as previously reported NPs ianthelliformisamine A (**1**), ianthelliformisamine B (**2**), ianthelliformisamine C (**3**), spermatinamine (**4**), and pistillarin (**5**) following NMR and MS data analysis and comparison with literature values [17, 22–25]. Prior to biological evaluation all compounds were subjected to purity analysis by ^{1}H NMR spectroscopy and shown to be >95%.

2.2. CA Inhibition Assay. An Applied Photophysics stopped-flow instrument was used for assaying the CA-catalyzed CO_2 hydration activity [26]. IC_{50} values were obtained from dose response curves working at seven different concentrations of test compound; by fitting the curves using PRISM (http://www.graphpad.com/) and nonlinear least squares methods, values represent the mean of at least three different determinations as described by us previously [27]. The inhibition constants (K_i) were then derived by using the Cheng-Prusoff equation [28] as follows: $K_i = IC_{50}/(1 + [S]/K_m)$, where [S] represents the CO_2 concentration at which the measurement was carried out and K_m is the concentration of substrate at which the enzyme activity is at half maximal. All enzymes used were recombinant, produced in *E. coli* as reported earlier [29, 30]. The concentrations of enzymes used in the assay were as follows: hCA I, 10.2 nM; hCA II, 9.5 nM; hCA IV, 8.9 nM; hCA IX, 8.7 nM; hCA XII, 10.9 nM; and hCA XIV, 12.6 nM.

3. Results and Discussion

The Davis Group at Eskitis has built up a unique in-house compound library over the past 10 years that currently consists of 352 distinct structures, the majority of which have been obtained from natural sources. Briefly, the NPs in this collection have been isolated from endophytic fungi, [31] macrofungi, [32] plants, [33], and marine invertebrates (e.g., sponges [34] and ascidians [35]) with quantities ranging from 0.4 mg to >1 g. Approximately 15% of this library contains semisynthetic NP analogues, [32, 36] while a small percentage (~5%) of the library is known commercial drugs or synthetic compounds inspired by NPs. A substructure search on this NP-based library against the spermidine fragment identified five secondary metabolites as hits. These included NP polyamines, ianthelliformisamines A–C (**1**–**3**), [17] spermatinamine (**4**) [22], and pistillarin (**5**) [23–25] (Figure 2), all of which have had various biological activities reported, but no CA bioactivity. Ianthelliformisamines A–C (**1**–**3**) were initially isolated from the marine sponge *Suberea*

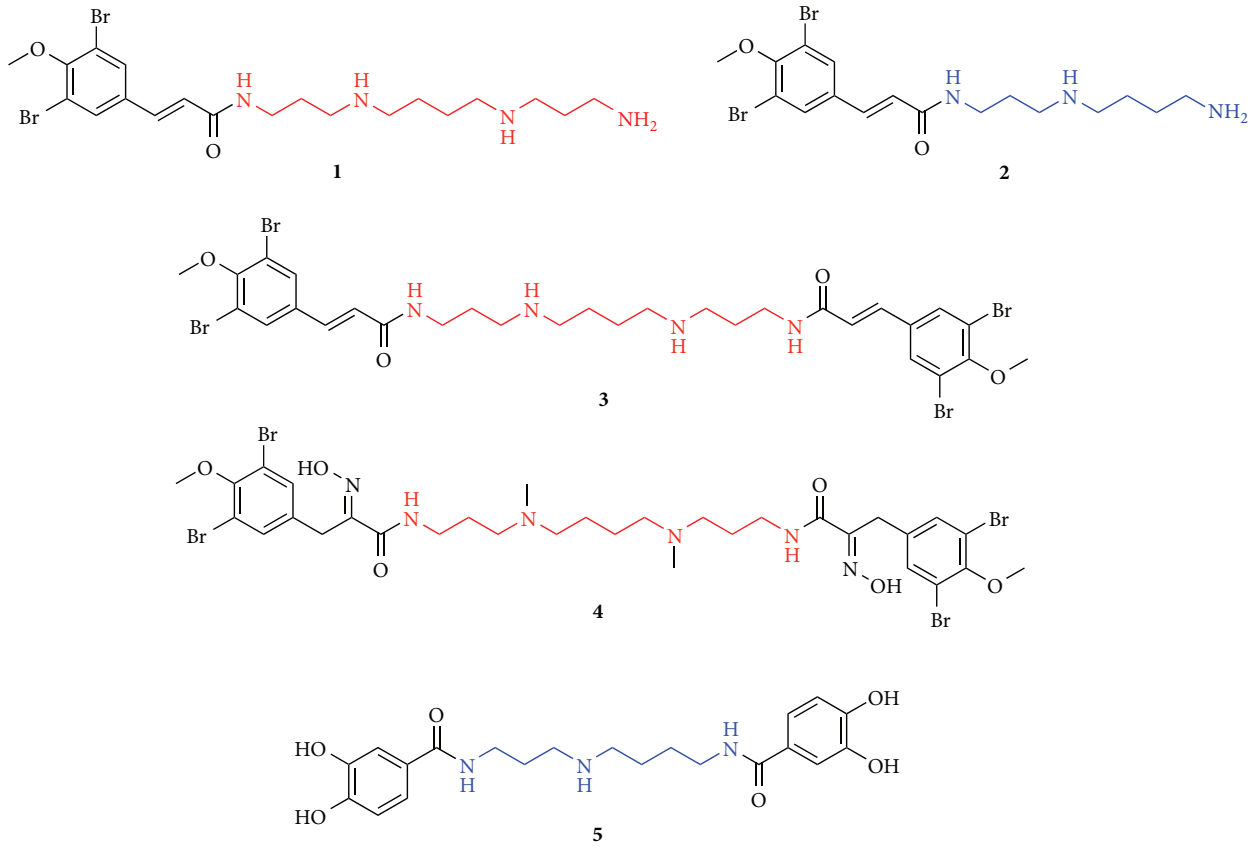

FIGURE 2: Natural product polyamines **1**–**5** sourced from the Davis compound library. Red: spermine core fragment and blue: spermidine core fragment.

ianthelliformis and display varying levels of inhibitory activity against the Gram-negative bacteria *Pseudomonas aeruginosa* [17]. Specifically, ianthelliformisamine A (**1**) was the most potent antibacterial agent from this particular series with an IC_{50} value of 6.8 μM (MIC 35 μM) [17]. Spermatinamine (**4**) was originally isolated from the sponge *Pseudoceratina* sp. and was the first NP inhibitor of isoprenylcysteine carboxyl methyltransferase (ICMT), which catalyzes the carboxyl methylation of oncogenic proteins in the final step of a series of post-translational modifications [22]. ICMT has been proposed as an attractive and novel anticancer target [22]. More recently spermatinamine (**4**) and a series of related NPs have been shown to inhibit Gram-negative bacteria [18]. Pistillarin (**5**) has been isolated from a variety of fungal species including *Penicillium bilaii* [23], *Gomphus floccosus* [24], *Clavariadelphus pistillaris* [25], and several *Ramaria* species [25, 32] and is a known siderophore [37]. In addition, compound **5** has recently been shown to exhibit significant protective effects against DNA damage caused by hydroxyl radicals generated from the Fenton reaction *via* iron chelation and to exhibit free radical-scavenging activity [24]. Pistillarin (**5**) and NP polyamines **1**–**4** have all recently been evaluated for their antimalarial activity, [32] with **4** and **5** identified as the most potent polyamines towards a drug sensitive *Plasmodium falciparum* parasite line (3D7) with IC_{50} values of 0.23 and 1.9 μM, respectively. These complex NP polyamines **1**–**5** (Figure 2) form the basis of the present paper wherein we describe the CA inhibition against six human CA isozymes.

The inhibition activity data for the simple NP polyamines spermine and spermidine reported earlier and the more complex NP polyamines **1**–**5** against six human CA isozymes of interest in therapeutic drug development is presented in Table 1. CA I and CA II are the predominant off-target isozymes (there are exceptions, e.g., CA inhibitors as antiglaucoma agents), while CAs IV, IX, XII, and XIV all have an extracellular oriented active site. CA IX and CA XII are overexpressed in many tumors [38, 39], CA IV plays a role in eye and kidney pathology [40, 41], while CA XIV is less well studied but has a role in a number of organs [42]. Polyamines **1**, **3**, and **4** comprise the polyamine fragment [–NH–$(CH_2)_3$–NR–$(CH_2)_4$–NR–$(CH_2)_3$–NH–] that is present in spermine (R = H), while polyamines **2** and **5** comprise the shorter polyamine chain [–NH–$(CH_2)_3$–NH–$(CH_2)_4$–NH–] of spermidine. Compounds **1** and **2** are derivatized at one terminal amine group of the base polyamine fragment with the other terminal amine unmodified, while compounds **3**–**5** are derivatized at both terminal amine groups and so lack a primary amine end group. Polyamines **1**–**4** are metabolites derived from bromotyrosine, with compound **4** comprising even further structural complexity including two oxime groups and methylation of the two central amines resulting in tertiary amines in place of secondary amines

Table 1: Inhibition data of human CA isozymes with simple natural product polyamines: spermine and spermidine [10] and complex natural product polyamines **1**–**5** and the clinically used CA inhibitor, acetazolamide.

Polyamine	K_i (μM)[a]					
	CA I	CA II	CA IV	CA IX	CA XII	CA XIV
Spermine	231	84	0.010	13.3	27.6	0.86
Spermidine	1.40	1.11	0.112	1.37	44.1	1.00
1	1.76	0.41	6.72	0.20	2.81	2.12
2	0.77	0.37	9.10	0.35	3.48	2.28
3	0.86	0.35	9.08	0.27	3.50	6.96
4	0.85	0.48	>20	0.34	>20	2.72
5	0.79	0.34	7.03	0.36	4.21	1.52
Acetazolamide	0.25	0.012	0.074	0.025	0.006	0.041

[a]Errors in the range of ±5% of the reported value, from three determinations using a stopped-flow CO_2 anhydrase assay.

within the central polyamine fragment. Polyamine **5** differs to compounds **1**–**4** as it comprises two catechol end groups. As both catechol and oxime moieties feature in the structure of known metal ion chelators [43, 44] polyamines **4** and **5** have the potential for a companion action to any bioactivity based on CA enzyme inhibition.

The polyamines spermine and spermidine have two primary amine end groups and a flexible, linear polyamine backbone. In contrast, as described above, compounds **1**–**5** are more complex in structure and these structural differences result in considerably altered SAR for **1**–**5** compared to the simpler NP fragments (Table 1). There are a number of general SAR trends of **1**–**5** that differ; these include (i) ~200-fold greater inhibition of off-target CA I and CA II than spermine, yet similar CA I and CA II inhibition to the shorter chain spermidine, (ii) inhibition of both the cancer associated CA isozymes CA IX and CA XII in the submicromolar range, which is better than both spermine and spermidine, and (iii) generally inhibit the other two extracellular CAs, CA IV and CA XIV, more weakly than both spermine and spermidine. Polyamine **4** has greater structural complexity than all other polyamines of this study and has much weaker inhibition of CA IV and CA XII (>20 μM), and this indicates that the greater complexity lessens the binding interaction with CA IV and CA XII. It is interesting that this lessened activity is not observed for the other four CAs, suggesting that the structural features of **4** may be interacting at CA active site hot spots [45]. Compounds **1** and **2** are modified at only one terminal amine of the base polyamine fragment yet have very similar SAR to compounds **3** and **5** that are modified at each end and lack a primary amine group. This SAR suggests that it may be the combination of both primary amine end groups of spermine and spermidine that underpin their differing CA enzyme inhibition profile. Future efforts from our groups will employ protein X-ray crystallography and molecular modelling to investigate if altered binding orientations of these NP polyamines do contribute to the differing SAR observed.

4. Conclusions

The discovery of new CA inhibitors with an alternate mechanism of inhibition to classical zinc binding functional groups can benefit from the unique chemical diversity provided in NP compound collections and so far is relatively underexplored. The structural features of polyamines **1**–**5** in this study, compared to the much simpler polyamine fragments of spermine and spermidine, further contribute to our understanding of the potential of both NPs and alternate chemotypes to contribute useful ligands to better enable the direction of the CA drug discovery field.

Conflict of Interests

The authors declare that there is no conflict of interests regarding the publication of this paper.

Acknowledgments

This research was financed by the Australian Research Council (Grant nos. DP110100071 and FT10100185 to S-AP) and two EU Grants of the 7th framework program (Metoxia and Dynano projects to CTS). The authors thank Ron Quinn for access to the sponge and fungal specimens associated with these studies. These specimens form part of the Eskitis Institute's Nature Bank biota repository. Nature Bank extracts and fractions are housed at Compounds Australia, formerly the Queensland Compound Library [21].

References

[1] C. T. Supuran, "Carbonic anhydrases: novel therapeutic applications for inhibitors and activators," *Nature Reviews Drug Discovery*, vol. 7, no. 2, pp. 168–181, 2008.

[2] D. Neri and C. T. Supuran, "Interfering with pH regulation in tumours as a therapeutic strategy," *Nature Reviews Drug Discovery*, vol. 10, no. 10, pp. 767–777, 2011.

[3] V. Alterio, A. di Fiore, K. D'Ambrosio, C. T. Supuran, and G. De Simone, "Multiple binding modes of inhibitors to carbonic anhydrases: how to design specific drugs targeting 15 different isoforms?" *Chemical Reviews*, vol. 112, no. 8, pp. 4421–4468, 2012.

[4] D. J. Newman and G. M. Cragg, "Natural products as sources of new drugs over the 30 years from 1981 to 2010," *Journal of Natural Products*, vol. 75, no. 3, pp. 311–335, 2012.

[5] A. Innocenti, S. Beyza Öztürk Sarikaya, I. Gülçin, and C. T. Supuran, "Carbonic anhydrase inhibitors: inhibition of mammalian isoforms I-XIV with a series of natural product polyphenols and phenolic acids," *Bioorganic and Medicinal Chemistry*, vol. 18, no. 6, pp. 2159–2164, 2010.

[6] R. A. Davis, A. Innocenti, S. Poulsen, and C. T. Supuran, "Carbonic anhydrase inhibitors. Identification of selective inhibitors of the human mitochondrial isozymes VA and VB over the cytosolic isozymes I and II from a natural product-based phenolic library," *Bioorganic and Medicinal Chemistry*, vol. 18, no. 1, pp. 14–18, 2010.

[7] R. A. Davis, A. Hofmann, A. Osman et al., "Natural product-based phenols as novel probes for mycobacterial and fungal carbonic anhydrases," *Journal of Medicinal Chemistry*, vol. 54, no. 6, pp. 1682–1692, 2011.

[8] A. Maresca, C. Temperini, H. Vu et al., "Non-zinc mediated inhibition of carbonic anhydrases: coumarins are a new class of suicide inhibitors," *Journal of the American Chemical Society*, vol. 131, no. 8, pp. 3057–3062, 2009.

[9] R. A. Davis, D. Vullo, A. Maresca, C. T. Supuran, and S.-A. Poulsen, "Natural product coumarins that inhibit human carbonic anhydrases," *Bioorganic and Medicinal Chemistry*, vol. 21, no. 6, pp. 1539–1543, 2013.

[10] F. Carta, C. Temperini, A. Innocenti, A. Scozzafava, K. Kaila, and C. T. Supuran, "Polyamines inhibit carbonic anhydrases by anchoring to the zinc-coordinated water molecule," *Journal of Medicinal Chemistry*, vol. 53, no. 15, pp. 5511–5522, 2010.

[11] C. T. Supuran, "Carbonic anhydrase inhibition with natural products: novel chemotypes and inhibition mechanisms," *Molecular Diversity*, vol. 15, no. 2, pp. 305–316, 2011.

[12] "Dictionary of Natural Products (DVD)," version 21.1, 2012.

[13] R. A. Casero and L. J. Marton, "Targeting polyamine metabolism and function in cancer and other hyperproliferative diseases," *Nature Reviews Drug Discovery*, vol. 6, no. 5, pp. 373–390, 2007.

[14] I. A. Fleidervish, L. Libman, E. Katz, and M. J. Gutnick, "Endogenous polyamines regulate cortical neuronal excitability by blocking voltage-gated Na+ channels," *Proceedings of the National Academy of Sciences of the United States of America*, vol. 105, no. 48, pp. 18994–18999, 2008.

[15] H. M. Wallace and K. Niiranen, "Polyamine analogues: an update," *Amino Acids*, vol. 33, no. 2, pp. 261–265, 2007.

[16] K. Soda, Y. Dobashi, Y. Kano, S. Tsujinaka, and F. Konishi, "Polyamine-rich food decreases age-associated pathology and mortality in aged mice," *Experimental Gerontology*, vol. 44, no. 11, pp. 727–732, 2009.

[17] M. Xu, R. A. Davis, Y. Feng et al., "Ianthelliformisamines A-C, antibacterial bromotyrosine-derived metabolites from the marine sponge *Suberea ianthelliformis*," *Journal of Natural Products*, vol. 75, no. 5, pp. 1001–1005, 2012.

[18] S. Yin, R. A. Davis, T. Shelper et al., "Pseudoceramines A-D, new antibacterial bromotyrosine alkaloids from the marine sponge *Pseudoceratina* sp.," *Organic and Biomolecular Chemistry*, vol. 9, no. 19, pp. 6755–6760, 2011.

[19] T. Stams, S. K. Nair, T. Okuyama, A. Waheed, W. S. Sly, and D. W. Christianson, "Crystal structure of the secretory form of membrane-associated human carbonic anhydrase IV at 2.8-Å resolution," *Proceedings of the National Academy of Sciences of the United States of America*, vol. 93, no. 24, pp. 13589–13594, 1996.

[20] D. Camp, S. Newman, N. B. Pham, and R. J. Quinn, "Nature bank and the Queensland Compound Library: unique international resources at the Eskitis Institute for drug discovery," *Combinatorial Chemistry and High Throughput Screening*, vol. 17, no. 3, pp. 201–209, 2014.

[21] M. Simpson and S.-A. Poulsen, "An overview of Australia's compound management facility: the Queensland Compound Library," *ACS Chemical Biology*, vol. 9, pp. 28–33, 2014.

[22] M. S. Buchanan, A. R. Carroll, G. A. Fechner et al., "Spermatinamine, the first natural product inhibitor of isoprenylcysteine carboxyl methyltransferase, a new cancer target," *Bioorganic and Medicinal Chemistry Letters*, vol. 17, no. 24, pp. 6860–6863, 2007.

[23] R. J. Capon, M. Stewart, R. Ratnayake, E. Lacey, and J. H. Gill, "Citromycetins and bilains A-C: new aromatic polyketides and diketopiperazines from Australian marine-derived and terrestrial *Penicillium* spp.," *Journal of Natural Products*, vol. 70, no. 11, pp. 1746–1752, 2007.

[24] I. Lee, D. Ki, S. Kim, J. Yeom, Y. Kim, and B. Yun, "Pistillarin salt, a dicatecholspermidine family member from *Gomphus floccosus*, inhibits DNA single strand breakage by the fenton reaction," *Journal of Applied Biological Chemistry*, vol. 54, no. 2, pp. 312–315, 2011.

[25] W. S. Steglich, B. Stroech, K. Wolf, and M. Pistillarin, "A characteristic metabolite of *Clavariadelphus pistillaris* and several *Ramaria* species (Basidiomycetes)," *Zeitschrift für Naturforschung C*, vol. 39, pp. 10–12, 1984.

[26] R. G. Khalifah, "The carbon dioxide hydration activity of carbonic anhydrase. I. Stop-flow kinetic studies on the native human isoenzymes B and C.," *Journal of Biological Chemistry*, vol. 246, no. 8, pp. 2561–2573, 1971.

[27] M. Lopez, N. Drillaud, L. F. Bornaghi, and S. Poulsen, "Synthesis of S-glycosyl primary sulfonamides," *Journal of Organic Chemistry*, vol. 74, no. 7, pp. 2811–2816, 2009.

[28] C. Yung-Chi and W. H. Prusoff, "Relationship between the inhibition constant (KI) and the concentration of inhibitor which causes 50 per cent inhibition (I50) of an enzymatic reaction," *Biochemical Pharmacology*, vol. 22, no. 23, pp. 3099–3108, 1973.

[29] J.-Y. Winum, D. Vullo, A. Casini, J.-L. Montero, A. Scozzafava, and C. T. Supuran, "Carbonic anhydrase inhibitors: inhibition of cytosolic isozymes I and II and transmembrane, tumor-associated isozyme IX with sulfamates including EMATE also acting as steroid sulfatase inhibitors," *Journal of Medicinal Chemistry*, vol. 46, no. 11, pp. 2197–2204, 2003.

[30] D. Vullo, A. Innocenti, I. Nishimori et al., "Carbonic anhydrase inhibitors. Inhibition of the transmembrane isozyme XII with sulfonamides—a new target for the design of antitumor and antiglaucoma drugs?" *Bioorganic and Medicinal Chemistry Letters*, vol. 15, no. 4, pp. 963–969, 2005.

[31] R. A. Davis, A. R. Carroll, K. T. Andrews et al., "Pestalactams A-C: novel caprolactams from the endophytic fungus *Pestalotiopsis* sp.," *Organic and Biomolecular Chemistry*, vol. 8, no. 8, pp. 1785–1790, 2010.

[32] V. Choomuenwai, B. D. Schwartz, K. D. Beattie, K. T. Andrews, S. Khokhar, and R. A. Davis, "The discovery, synthesis and antimalarial evaluation of natural product-based polyamine alkaloids," *Tetrahedron Letters*, vol. 54, no. 38, pp. 5188–5191, 2013.

[33] C. Levrier, M. Balastrier, K. D. Beattie et al., "Pyridocoumarin, aristolactam and aporphine alkaloids from the Australian rainforest plant *Goniothalamus australis*," *Phytochemistry*, vol. 86, pp. 121–126, 2013.

[34] E. C. Barnes, N. A. B. M. Said, E. D. Williams, J. N. A. Hooper, and R. A. Davis, "Ecionines A and B, two new cytotoxic pyridoacridine alkaloids from the Australian marine sponge, *Ecionemia geodides*," *Tetrahedron*, vol. 66, no. 1, pp. 283–287, 2010.

[35] M. S. Liberio, D. Sooraj, E. D. Williams, Y. Feng, and R. A. Davis, "Kingamide A, a new indole alkaloid from the ascidian *Leptoclinides kingi*," *Tetrahedron Letters*, vol. 52, no. 50, pp. 6729–6731, 2011.

[36] E. C. Barnes, V. Choomuenwai, K. T. Andrews, R. J. Quinn, and R. A. Davis, "Design and synthesis of screening libraries based on the muurolane natural product scaffold," *Organic and Biomolecular Chemistry*, vol. 10, no. 20, pp. 4015–4023, 2012.

[37] B. Holinsworth and J. D. Martin, "Siderophore production by marine-derived fungi," *BioMetals*, vol. 22, no. 4, pp. 625–632, 2009.

[38] E. Švastová, A. Hulíková, M. Rafajová et al., "Hypoxia activates the capacity of tumor-associated carbonic anhydrase IX to acidify extracellular pH," *FEBS Letters*, vol. 577, no. 3, pp. 439–445, 2004.

[39] S. Pastorekova, M. Zatovicova, and J. Pastorek, "Cancer-associated carbonic anhydrases and their inhibition," *Current Pharmaceutical Design*, vol. 14, no. 7, pp. 685–698, 2008.

[40] R. Datta, G. N. Shah, T. S. Rubbelke et al., "Progressive renal injury from transgenic expression of human carbonic anhydrase IV folding mutants is enhanced by deficiency of p58IPK," *Proceedings of the National Academy of Sciences of the United States of America*, vol. 107, no. 14, pp. 6448–6452, 2010.

[41] R. Datta, A. Waheed, G. Bonapace, G. N. Shah, and W. S. Sly, "Pathogenesis of retinitis pigmentosa associated with apoptosis-inducing mutations in carbonic anhydrase IV," *Proceedings of the National Academy of Sciences of the United States of America*, vol. 106, no. 9, pp. 3437–3442, 2009.

[42] M. Hilvo, C. T. Supuran, and S. Parkkila, "Characterization and inhibition of the recently discovered carbonic anhydrase isoforms CA XIII, XIV, and XV," *Current Topics in Medicinal Chemistry*, vol. 7, no. 9, pp. 893–899, 2007.

[43] J. B. Neilands, "Siderophores of bacteria and fungi," *Microbiological Sciences*, vol. 1, no. 1, pp. 9–14, 1984.

[44] E. L. Rue and K. W. Bruland, "Complexation of iron(III) by natural organic ligands in the Central North Pacific as determined by a new competitive ligand equilibration/adsorptive cathodic stripping voltammetric method," *Marine Chemistry*, vol. 50, no. 1–4, pp. 117–138, 1995.

[45] M. Aggarwal, B. Kondeti, and R. McKenna, "Insights towards sulfonamide drug specificity in α-carbonic anhydrases," *Bioorganic and Medicinal Chemistry*, vol. 21, no. 6, pp. 1526–1533, 2013.

Hindawi Publishing Corporation
BioMed Research International
Volume 2014, Article ID 594879, 8 pages
http://dx.doi.org/10.1155/2014/594879

Research Article

Synthesis and In Vitro Inhibition Effect of New Pyrido[2,3-d]pyrimidine Derivatives on Erythrocyte Carbonic Anhydrase I and II

Hilal Kuday,[1] Fatih Sonmez,[2] Cigdem Bilen,[3] Emre Yavuz,[3] Nahit Gençer,[3] and Mustafa Kucukislamoglu[1]

[1] *Department of Chemistry, Faculty of Art and Sciences, Sakarya University, 54140 Sakarya, Turkey*
[2] *Pamukova Vocational High School, Sakarya University, 54900 Sakarya, Turkey*
[3] *Department of Chemistry, Faculty of Art and Sciences, Balikesir University, 10145 Balikesir, Turkey*

Correspondence should be addressed to Nahit Gençer; ngencer@balikesir.edu.tr

Received 21 February 2014; Revised 13 June 2014; Accepted 8 July 2014; Published 4 August 2014

Academic Editor: Anna Di Fiore

In vitro inhibition effects of indolylchalcones and new pyrido[2,3-d]pyrimidine derivatives on purified human carbonic anhydrase I and II (hCA I and II) were investigated by using CO_2 as a substrate. The results showed that all compounds inhibited the hCA I and hCA II enzyme activities. Among all the synthesized compounds, **7e** (IC_{50} = 6.79 μM) was found to be the most active compound for hCA I inhibitory activity and **5g** (IC_{50} = 7.22 μM) showed the highest hCA II inhibitory activity. Structure-activity relationships study showed that indolylchalcone derivatives have higher inhibitory activities than pyrido[2,3-d]pyrimidine derivatives on hCA I and hCA II. Additionally, methyl group bonded to uracil ring increases inhibitory activities on both hCA I and hCA II.

1. Introduction

Carbonic anhydrase (CA, EC 4.2.1.1) is a ubiquitous zinc enzyme. Basically, there are several mammalian cytosolic forms (CA-I, CA-II, CA-III, CA-VII, and CA-XIII), four membrane-bound forms (CA-IV, CA-IX, CA-XII, and CA-XIV), one mitochondrial form (CA-V), and a secreted CA form (CA-VI) [1, 2]. They all catalyze a very simple physiological reaction, the interconversion between carbon dioxide and the bicarbonate ion, and are thus involved in crucial physiological processes connected with respiration and transport of CO_2/bicarbonate between metabolizing tissues and the lungs, pH and CO_2 homeostasis, electrolyte secretion in a variety of tissues/organs, biosynthetic reactions (such as the gluconeogenesis, lipogenesis, and ureagenesis), bone resorption, calcification, tumorigenicity, and many other physiologic or pathologic processes [1–3]. CA inhibitors have now been a mainstay of human clinical intervention for several decades, with at least 25 clinically used drugs that are CA inhibitors [4]. Although there are many studies on this enzyme, the CA enzyme family continues to capture the attention of drug discovery scientists and clinicians as the knowledge regarding the therapeutic implications associated with this enzyme class continues to grow [4, 5].

Indoles are one of the most important nitrogen containing heterocyclic molecules, found extensively in biological system which play vital role in biochemical processes. Indole ring constitutes an important template for drug design such as the classical nonsteroidal anti-inflammatory drugs (NSAIDs) indomethacin and indoxole [6]. Further indole derivatives have been reported to possess promising biological activities including analgesic [7], antipyretic [8], antifungal [9], anti-inflammatory [10, 11], antitumor [12], anticonvulsant [13], and selective COX-2 inhibitory activities [14]. Thus the efficient synthesis of novel substituted indole derivative compounds still represents highly pursued target.

Pyrido[2,3-d]pyrimidines have received considerable attention over the past years because of their wide range of biological activities, which include antitumor [15], antibacterial [16], anti-inflammatory [17], and antifungal activities

[18], and also act as cyclin-dependent kinase 4 inhibitors [19]. Also these compounds are considered to be important for synthetic drugs (e.g., barbituric acid derivatives), chemotherapeutic agents (e.g., sulfadiazine), and agricultural chemicals [20].

In this study, a series of 7 indolylchalcone and 11 new pyrido[2,3-d]pyrimidine derivatives containing indole ring were synthesized and their effects on human carbonic anhydrase (hCA) I and II were evaluated. Additionally, structure-activity relationship was examined.

2. Materials and Methods

2.1. General Chemistry. Melting points were taken on a Barnstead Electrothermal 9200. IR spectra were measured on a Shimadzu Prestige-21 (200 VCE) spectrometer. ^{1}H and ^{13}C NMR spectra were measured on a Varian Infinity Plus spectrometer at 300 and 75 Hz, respectively. ^{1}H and ^{13}C chemical shifts are referenced to the internal deuterated solvent. Mass spectra were obtained using MICROMASS Quattro LC-MS-MS spectrometer. Solvents were dried following standard methods. Sepharose 4B, L-tyrosine, sulfonamide, synthetic starting material, reagents, and solvents were purchased from Merck, Alfa Easer, Sigma-Aldrich, and Fluka.

2.2. Synthetic Procedures and Spectral Data

*1H-Indole-3-carbaldehyde (**2**).* Phosphorous oxychloride (1 mL) was added dropwise to cold anhydrous DMF (3 mL) and the mixture was stirred at 0°C for 1 h. The indole (1.17 g), dissolved in anhydrous DMF, was added dropwise to above formylation complex solution at below 10°C. The mixture was warmed to 35–40°C and stirred for 1 hour. Then $NaOH_{(aq)}$ (5.5 g NaOH, 14.6 mL water) was added. The mixture was warmed to 100°C and stirred for 1 h; then it was cooled, filtrated, and dried in vacuum oven for overnight. Pink powder was obtained in 94% yield. ^{1}H NMR ($CDCl_3$, 300 MHz) δ: 10.07 (1H, s), 8.82 (1H, s, NH), 8.32–8.34 (1H, dd, J_1 = 2.0 Hz, J_2 = 7.3 Hz), 7.85 (1H, d, J = 2.9 Hz), 7.44–7.46 (1H, m), 7.30–7.36 (2H, m) ppm; ^{13}C NMR ($CDCl_3$, 75 MHz) δ: 185.7, 139.2, 137.7, 124.8, 124.2, 122.8, 121.5, 118.8, 113.1 ppm.

*N-Methyl Indole-3-carboxaldehyde (**3**).* K_2CO_3 (0.95 g) and CH_3I (2 mL) were added to solution of indole-3-carboxaldehyde (1 g) in 10 mL DMF. The mixture was stirred at 100°C for 4 hours and then cooled and poured onto ice-water. The precipitate was filtrated and dried in vacuum oven. White solid was obtained in 95% yield. ^{1}H NMR ($CDCl_3$, 300 MHz) δ: 9.97 (1H, s), 8.29–8.31 (1H, dd, J_1 = 1.8 Hz, J_2 = 7.3 Hz), 7.66 (1H, s), 7.29–7.37 (3H, m), 3.86 (3H, s) ppm; ^{13}C NMR ($CDCl_3$, 75 MHz) δ: 184.7, 139.9, 138.0, 125.3, 124.2, 123.1, 122.0, 118.0, 110.2, 33.8 ppm.

*Synthesis of Indolylchalcone Derivatives (**5a**–**g**).* A solution of $NaOH_{(aq)}$ (40%, 5 mL) was added to mixture of 1-methyl-1H-indole-3-carbaldehyde (1 mmol) **3** and acetophenone derivatives (1 mmol) **4a**–**g** in absolute ethanol. The mixture was stirred at room temperature for 2 hours. Then it was poured into ice-cold water, neutralized with acid, filtrated, and washed with water. The filtrate was dried in vacuum oven.

*(E)-1-(3,4-Dimethoxyphenyl)-3-(1-methyl-1H-indol-3-yl) prop-2-en-1-one (**5a**).* Yield: 75%, yellow powder, mp: 271°C, IR (KBr): 3089.9, 3008.9, 2910.5, 2839.2, 1645.2, 1597.0, 1556.5, 1373.3, 1255.6, 1166.9, 1022.7, 804.3 ν (cm^{-1}); ^{1}H NMR ($CDCl_3$, 300 MHz) δ: 8.08 (1H, d, J = 15.5 Hz), 8.01–8.03 (1H, dd, J_1 = 2.0 Hz, J_2 = 6.1 Hz), 7.71–7.74 (1H, dd, J_1 = 1.8 Hz, J_2 = 8.5 Hz), 7.66 (1H, d, J = 1.8 Hz), 7.57 (1H, d, J = 15.5 Hz), 7.47 (1H, s), 7.30–7.39 (3H, m), 6.95 (1H, d, J = 8.5 Hz), 3.99 (3H, s), 3.97 (3H, s), 3.84 (3H, s) ppm; ^{13}C NMR ($CDCl_3$, 75 MHz) δ: 189.1, 152.8, 149.2, 138.4, 138.1, 134.7, 132.3, 126.3, 123.3, 122.7, 121.7, 121.0, 116.6, 113.1, 110.8, 110.4, 110.1, 56.3, 56.2, 33.5 ppm; LC-MS (m/z): 322.57 [MH^+].

*(E)-1-(4-Methoxyphenyl)-3-(1-methyl-1H-indol-3-yl) prop-2-en-1-one (**5b**).* Yield: 65%, yellow powder, mp: 254°C, IR (KBr): 3128.5, 3045.6, 2935.6, 2841.1, 1649.1, 1598.9, 1373.3, 1253.7, 1166.9, 1026.1 ν (cm^{-1}); ^{1}H NMR ($CDCl_3$, 300 MHz) δ: 8.00–8.10 (4H, m), 7.57 (1H, d, J = 15.5 Hz), 7.46 (1H, s), 7.30–7.37 (3H, m), 7.00 (2H, d, J = 8.8 Hz), 3.89 (3H, s), 3.83 (3H, s) ppm; ^{13}C NMR ($CDCl_3$, 75 MHz) δ: 187.2, 161.2, 136.4, 136.1, 132.7, 130.1, 128.7, 124.3, 121.5, 119.7, 119.0, 114.9, 111.9, 111.2, 108.4, 53.7, 31.5 ppm; LC-MS (m/z): 293.00 [MH^+].

*(E)-3-(1-Methyl-1H-indol-3-yl)-1-p-tolylprop-2-en-1-One (**5c**).* Yield: 85%, dark yellow powder, mp: 240°C, IR (KBr): 3101.5, 3022.4, 2914.4, 1647.2, 1579.7, 1556.5, 1371.3, 1280.7, 1174.6, 1029.9 804.3 ν (cm^{-1}); ^{1}H NMR ($CDCl_3$, 300 MHz) δ: 8.08 (1H, d, J = 15.5 Hz), 8.00–8.03 (1H, dd, J_1 = 2.0 Hz, J_2 = 6.5 Hz), 7.97 (2H, d, J = 8.0 Hz), 7.55 (1H, d, J = 15.5 Hz), 7.46 (1H, s), 7.31–7.39 (3H, m), 7.29 (2H, d, J = 8.0 Hz), 3.84 (3H, s), 2.44 (3H, s) ppm; ^{13}C NMR ($CDCl_3$, 75 MHz) δ: 190.4, 143.1, 138.5, 138.4, 136.7, 134.7, 129.4, 128.6, 126.3, 123.3, 121.7, 121.0, 117.1, 113.2, 110.4, 33.5, 21.9 ppm, LC-MS (m/z): 276.25 [MH^+].

*(E)-1-(4-Chlorophenyl)-3-(1-methyl-1H-indol-3-yl)prop-2-en-1-one (**5d**).* Yield: 96%, yellow powder, mp: 248°C, IR (KBr): 3103.4, 3085.2, 2908.8, 2807.7, 1645.2, 1580.7, 1371.9, 1282.6, 1029.9, 1008.7, ν (cm^{-1}); ^{1}H NMR ($CDCl_3$, 300 MHz) δ: 8.09 (1H, d, J = 15.5 Hz), 7.98–8.02 (3H, m), 7.46–7.52 (4H, m), 7.32–7.40 (3H, m), 3.85 (3H, s) ppm; ^{13}C NMR ($CDCl_3$, 75 MHz) δ: 189.6, 139.5, 138.7, 138.5, 137.6, 135.3, 129.9, 129.0, 126.3, 123.5, 121.9, 121.1, 116.4, 113.1, 110.5, 33.6 ppm; LC-MS (m/z): 296.61 [MH^+].

*(E)-3-(1-Methyl-1H-indol-3-yl)-1-phenylprop-2-en-1-one (**5e**).* Yield: 86%, light yellow powder, mp: 227°C, IR (KBr): 3095.7, 3055.2, 2933.7, 1643.3, 1581.6, 1554.6, 1462.0, 1371.3, 1278.8, 1213.2, 1076.2 ν (cm^{-1}); ^{1}H NMR ($CDCl_3$, 300 MHz) δ: 8.09 (1H, d, J = 15.2 Hz), 8.00–8.06 (3H, m), 7.47–7.57 (5H, m), 7.29–7.39 (3H, m), 3.84 (3H, s) ppm; ^{13}C NMR ($CDCl_3$, 75 MHz) δ: 190.9, 139.3, 138.9, 138.4, 135.0, 132.4, 128.7, 128.5, 126.3, 123.4, 121.8, 121.0, 117.0, 113.1, 110.4, 33.5 ppm; LC-MS (m/z): 262.26 [MH^+].

*(E)-3-(1-Methyl-1H-indol-3-yl)-1-(4-nitrophenyl)prop-2-en-1-one (**5f**).* Yield: 88%, orange powder, mp: 278°C, IR (KBr):

ν (cm^{-1}); 3097.68, 3035.96, 1903.74, 1737.86, 1649.14, 1604.77, 1558.48, 1517.98, 1340.53, 1209.37, 813.96. ^{1}H NMR ($CDCl_3$, 300 MHz) δ: 8.32–8.39 (3H, m), 8.18 (1H, s), 8.13–8.16 (1H, m), 8.07 (1H, d, J = 15.5 Hz), 7.63 (1H, d, J = 15.5 Hz), 7.58 (1H, s), 7.29–7.35 (3H, m), 3.88 (3H, s) ppm; ^{13}C NMR ($CDCl_3$, 75 MHz) δ: 183.4, 140.0, 136.0, 134.4, 131.0, 125.1, 121.5, 120.6, 119.5, 118.5, 117.3, 116.2, 110.6, 108.3, 105.8, 29.0 ppm; LC-MS (m/z): 307.52 [MH^+].

*(E)-3-(1-Methyl-1H-indol-3-yl)-1-(3-nitrophenyl)prop-2-en-1-one (**5g**)*. Yield: 87%, light orange powder, mp: 267°C, IR (KBr): 3099.6, 2605.8, 1649.1, 1583.5, 1519.9, 1467.8, 1369.4, 1342.4, 1282.6, 1070.4, 819.7 ν (cm^{-1}); ^{1}H NMR ($CDCl_3$, 300 MHz) δ: 8.86 (1H, s), 8.39 (2H, t, J = 8.2 Hz), 8.17 (1H, d, J = 15.5 Hz), 7.99–8.02 (1H, m), 7.70 (1H, t, J = 7.9 Hz), 7.55 (1H, s), 7.50 (1H, d, J = 15.5 Hz), 7.33–7.43 (3H, m), 3.87 (3H, s) ppm; ^{13}C NMR ($CDCl_3$, 75 MHz) δ: 183.3, 143.7, 136.0, 133.8, 131.0, 129.4, 125.1, 121.9, 121.5, 118.9, 118.5, 117.5, 116.2, 110.6, 108.3, 105.8, 28.9 ppm; LC-MS (m/z): 307.29 [MH^+].

*Synthesis of Pyrido[2,3-d]pyrimidines Derivatives (**7a**–**k**)*. A mixture of 6-aminouracil derivatives (1 mmol) **6a** or **6b**, chalcone derivatives **5a**–**g** (1 mmol), and NaOH (1 mmol) in 30 mL absolute ethanol was refluxed for 18 hours. The mixture was cooled and poured into ice-cold water. The precipitate was filtrated, washed with water, and dried in vacuum oven for overnight. The crude products were recrystallized from ethanol.

*7-(3,4-Dimethoxyphenyl)-1-methyl-5-(1-methyl-1H-indol-3-yl)pyrido[2,3-d]pyrimidine-2,4(1H,3H)-dione (**7a**)*. Yield: 90%, dark yellow powder, mp: 333-334°C, IR (KBr): 3169.3, 3044.5, 2940.1, 2835.6, 1685.9, 1583.8, 1518.4, 1387.6, 1256.7, 1023.8 ν (cm^{-1}); ^{1}H NMR ($CDCl_3$, 300 MHz): 10.88 (1H, s, NH), 7.81–7.85 (2H, m), 7.75 (1H, s), 7.70 (1H, s), 7.51 (1H, d, J = 8.2 Hz), 7.40 (1H, d, J = 7.6 Hz), 7.20 (1H, t, J = 7.5 Hz), 7.03–7.12 (2H, m), 3.89 (3H, s), 3.87 (3H, s), 3.84 (3H, s), 3.66 (3H, s) ppm; ^{13}C NMR ($CDCl_3$, 75 MHz): δ 160.6, 158.3, 152.4, 151.5, 151.4, 149.4, 148.3, 136.9, 130.8, 130.5, 127.4, 122.3, 120.8, 120.7, 119.8, 118.4, 112.8, 111.2, 110.3, 110.1, 106.1, 56.2, 56.1, 33.4, 30.0 ppm; LC-MS (m/z): 443.41 [MH^+].

*1-Methyl-5-(1-methyl-1H-indol-3-yl)-7-p-tolylpyrido[2,3-d]pyrimidine-2,4(1H,3H)-dione (**7b**)*. Yield: 55%, light yellow powder, mp: 399-400°C, IR (KBr): 3165.1, 3047.1, 2848.8, 1685.7, 1589.3, 1519.9, 1394.5, 1257.5, 1093.6 ν (cm^{-1}); ^{1}H NMR ($CDCl_3$, 300 MHz) δ: 11.39 (1H, s, NH), 8.14 (2H, d, J = 8.2 Hz), 7.79 (1H, s), 7.71 (1H, s), 7.52 (1H, d, J = 7.6 Hz), 7.42 (1H, d, J = 7.6 Hz), 7.36 (2H, d, J = 8.2 Hz), 7.21 (1H, t, J = 7.3 Hz), 7.07 (1H, t, J = 7.3 Hz), 3.86 (3H, s), 3.66 (3H, s), 2.39 (3H, s) ppm; ^{13}C NMR ($CDCl_3$, 75 MHz): δ 161.0, 156.6, 154.1, 151.3, 150.7, 149.5, 139.6, 139.2, 133.5, 131.9, 129.9, 129.6, 125.7, 122.1, 120.5, 118.3, 113.2, 110.9, 107.8, 33.4, 29.4, 24.1 ppm; LC-MS (m/z): 396.98 [MH^+].

*7-(4-Chlorophenyl)-1-methyl-5-(1-methyl-1H-indol-3-yl)pyrido[2,3-d]pyrimidine-2,4(1H,3H)-dione (**7c**)*. Yield: 60%, light yellow powder, mp: 385–389°C, IR (KBr): 3172.9, 3043.6, 2927.9, 2848.8, 1685.9, 1521.0, 1392.6, 1257.9, 1091.7, 1012.8, 729.0 ν (cm^{-1}); ^{1}H NMR (DMSO, 300 MHz) δ: 11.40 (1H, s, NH), 8.26 (2H, d, J = 8.5 Hz), 7.78 (1H, s), 7.74 (1H, s), 7.59 (2H, d, J = 8.5 Hz), 7.49 (1H, d, J = 8.2 Hz), 7.40 (1H, d, J = 7.3 Hz), 7.18 (1H, t, J = 7.6 Hz), 7.04 (1H, t, J = 7.6 Hz), 3.86 (3H, s), 3.62 (3H, s) ppm; ^{13}C NMR ($CDCl_3$, 75 MHz) δ: 161.0, 156.6, 154.1, 151.3, 148.2, 137.1, 136.6, 135.9, 131.9, 129.7, 129.6, 127.2, 122.1, 120.6, 120.5, 118.3, 113.2, 110.9, 107.8, 33.4, 29.5 ppm; LC-MS (m/z): 418.36 [MH^+].

*1-Methyl-5-(1-methyl-1H-indol-3-yl)-7-(3-nitrophenyl)pyrido[2,3-d]pyrimidine-2,4(1H,3H)-dione (**7d**)*. Yield: 41%, mustard powder, mp: 397°C, IR (KBr): 3176.7, 3049.4, 1681.9, 1591.2, 1523.7, 1454.3, 1346.3, 1253.7, 1085.9, 732.9 ν (cm^{-1}); ^{1}H NMR ($CDCl_3$, 300 MHz) δ: 12.01 (1H, s, NH), 8.98 (1H, t, J = 1.7 Hz), 8.66 (1H, d, J = 8.2 Hz), 8.32–8.35 (1H, dd, J_1 = 1.5 Hz, J_2 = 8.2 Hz), 7.82 (1H, d, J = 8.2 Hz), 7.79 (2H, s), 7.50 (1H, d, J = 8.2 Hz), 7.42 (1H, d, J = 7.6 Hz), 7.20 (1H, t, J = 7.0 Hz), 7.05 (1H, t, J = 7.0 Hz), 3.88 (3H, s), 3.65 (3H, s) ppm; ^{13}C NMR ($CDCl_3$, 75 MHz) δ: 161.2, 157.3, 152.8, 152.6, 150.0, 149.8, 138.8, 138.4, 137.5, 134.0, 131.9, 130.9, 127.2, 125.5, 120.8, 120.7, 119.6, 118.3, 113.3, 110.9, 108.9, 33.5, 28.9 ppm; LC-MS (m/z): 428.66 [MH^+].

*7-(3,4-Dimethoxyphenyl)-1,3-dimethyl-5-(1-methyl-1H-indol-3-yl)pyrido[2,3-d]pyrimidine-2,4(1H,3H)-dione (**7e**)*. Yield: 50%, yellow powder, mp: 340-341°C, IR (KBr): 3078.3, 2937.9, 2839.2, 1693.5, 1647.1, 1419.6, 1329.4, 1220.9, 1134.1, 1022.2 ν (cm^{-1}); ^{1}H NMR ($CDCl_3$, 300 MHz): 7.70–7.75 (3H, m), 7.54 (1H, d, J = 8.2 Hz), 7.51 (1H, s), 7.41 (1H, d, J = 8.2 Hz), 7.31 (1H, d, J = 7.0 Hz), 7.18 (1H, t, J = 7.0 Hz), 6.98 (1H, d, J = 8.2 Hz), 3.99 (3H, s), 3.96 (3H, s), 3.91 (3H, s), 3.90 (3H, s), 3.42 (3H, s) ppm; ^{13}C NMR ($CDCl_3$, 75 MHz): 161.0, 158.3, 152.5, 151.8, 151.4, 149.4, 148.3, 136.9, 130.8, 130.5, 127.4, 122.3, 120.8, 120.7, 119.8, 118.4, 112.8, 111.2, 110.3, 110.1, 106.1, 56.2, 56.1, 33.4, 30.3, 28.7 ppm; LC-MS (m/z): 458.18 [MH^+].

*7-(4-Methoxyphenyl)-1,3-dimethyl-5-(1-methyl-1H-indol-3-yl)pyrido[2,3-d]pyrimidine-2,4(1H,3H)-dione (**7f**)*. Yield: 20%, yellow powder, mp: 335.7–336°C, IR (KBr): 3057.1, 2960.7, 2839.2, 1699.2, 1651.0, 1516.0, 1473.6, 1356.6, 1024.2 ν (cm^{-1}); ^{1}H NMR ($CDCl_3$, 300 MHz): 8.11 (2H, d, J = 8.8 Hz), 7.69 (1H, s), 7.54 (1H, d, J = 7.8 Hz), 7.50 (1H, s), 7.40 (1H, d, J = 8.2 Hz), 7.27(1H, d, J = 7.0 Hz), 7.17 (1H, t, J = 7.8 Hz), 7.01 (2H, d, J = 8.8 Hz), 3.90 (3H, s), 3.88 (6H, s), 3.42 (3H, s) ppm; ^{13}C NMR ($CDCl_3$, 75 MHz): 161.6, 160.8, 158.1, 152.3, 151.6, 148.0, 136.7, 130.6, 130.0, 128.9, 127.2, 122.0, 120.4, 119.6, 118.0, 114.2, 112.6, 109.8, 105.8, 55.4, 33.2, 30.1, 28.4 ppm; LC-MS (m/z): 428.04 [MH^+].

*1,3-Dimethyl-5-(1-methyl-1H-indol-3-yl)-7-p-tolylpyrido[2,3-d]pyrimidine-2,4(1H,3H)-dione (**7g**)*. Yield: 40%, yellow powder, mp: 340-341°C, IR (KBr): 3021.3, 2960.7, 2908.6, 1707.0, 1660.7, 1523.7, 1473.6, 1394.5, 1365.6, 1257.5, 1016.4 ν (cm^{-1}); ^{1}H NMR ($CDCl_3$, 300 MHz) δ: 8.04 (2H, d, J = 8.2 Hz), 7.73 (1H, s), 7.54 (1H, d, J = 8.2 Hz), 7.51 (1H, s), 7.39 (1H, d, J = 8.2 Hz), 7.25–7.32 (3H, m), 7.17 (1H, t, J = 7.3 Hz), 3.90 (3H, s), 3.89 (3H, s), 3.42 (3H, s), 2.43 (3H, s) ppm; ^{13}C NMR ($CDCl_3$, 75 MHz) δ: 160.9, 158.6, 152.4, 151.6, 148.2, 140.8, 136.7, 134.8, 130.6, 129.6, 127.3, 127.2, 122.1, 120.5, 119.6,

118.5, 112.6, 109.9, 106.2, 33.2, 30.2, 28.4, 21.4 ppm; LC-MS (m/z): 411.33 [MH^+].

*7-(4-Chlorophenyl)-1,3-dimethyl-5-(1-methyl-1H-indol-3-yl)pyrido[2,3-d]pyrimidine 2,4(1H,3H)-dione (**7h**)*. Yield: 76%, yellow powder, mp: 358-359°C, IR (KBr): 3064, 3045, 2943, 1701, 1654 ν (cm^{-1}); ^{1}H NMR ($CDCl_3$, 300 MHz) δ: 8.07 (2H, d, J = 8.5 Hz), 7.73 (1H, s), 7.52–7.55 (2H, m), 7.47 (2H, d, J = 8.5 Hz), 7.41 (1H, d, J = 8.2 Hz), 7.29 (1H, t, J = 7.5 Hz), 7.18 (1H, t, J = 7.0 Hz), 3.90 (3H, s), 3.88 (3H, s), 3.42 (3H, s) ppm; ^{13}C NMR ($CDCl_3$, 75 MHz): δ 161.0, 157.5, 152.7, 151.8, 148.8, 136.9, 136.8, 136.2, 131.0, 129.3, 128.9, 127.3, 122.4, 120.8, 119.8, 118.8, 112.6, 110.2, 106.8, 33.5, 30.5, 28.7 ppm; LC-MS (m/z): 432.37 [MH^+].

*1,3-Dimethyl-5-(1-methyl-1H-indol-3-yl)-7-phenylpyrido[2,3-d]pyrimidine-2,4(1H,3H)-dione (**7i**)*. Yield: 32%, yellow powder, mp: 320°C, IR (KBr): 3070.6, 3037.8, 2933.7, 1697.3, 1651.0, 1591.2, 1533.4, 1419.6, 1390.6, 1259.5, 1053.1 ν (cm^{-1}); ^{1}H NMR ($CDCl_3$, 300 MHz) δ: 8.13–8.15 (2H, dd, J_1 = 2.0 Hz, J_2 = 7.5 Hz), 7.77 (1H, s), 7.49–7.56 (5H, m), 7.41 (1H, d, J = 8.2 Hz), 7.29 (1H, t, J = 7.0 Hz), 7.18 (1H, t, J = 7.0 Hz), 3.91 (3H, s), 3.90 (3H, s), 3.42 (3H, s) ppm; ^{13}C NMR ($CDCl_3$, 75 MHz) δ: 161.1, 158.7, 152.6, 151.8, 148.6, 137.8, 136.9, 131.0, 130.6, 129.1, 127.6, 127.4, 122.4, 120.7, 119.9, 119.1, 112.7, 110.1, 106.6, 33.5, 30.5, 28.7 ppm; LC-MS (m/z): 397.51 [MH^+].

*1,3-Dimethyl-5-(1-methyl-1H-indol-3-yl)-7-(4-nitrophenyl)pyrido[2,3-d]pyrimidine-2,4(1H,3H)-dione (**7j**)*. Yield: 60%, light orange powder, mp: 347–349°C, IR (KBr): 3157.4, 3049.4, 2945.3, 1703.1, 1658.7, 1585.4, 1519.9, 1342.4, 852.5 ν (cm^{-1}); ^{1}H NMR ($CDCl_3$, 300 MHz) δ: 8.52 (2H, d, J = 7.9 Hz), 8.37 (2H, d, J = 7.9 Hz), 7.92 (1H, s), 7.82 (1H, s), 7.53 (1H, d, J = 8.2 Hz), 7.42 (1H, d, J = 7.9 Hz), 7.23 (1H, t, J = 7.1 Hz), 7.08 (1H, t, J = 7.0 Hz), 3.90 (3H, s), 3.75 (3H, s), 3.24 (3H, s) ppm; ^{13}C NMR ($CDCl_3$, 75 MHz) δ: 160.8, 155.3, 152.8, 151.6, 148.9, 148.7, 137.2, 134.4, 132.0, 129.2, 127.2, 124.6, 121.7, 120.7, 119.8, 118.6, 113.3, 110.9, 108.1, 33.4, 30.5, 28.8 ppm; LC-MS (m/z): 442.19 [MH^+].

*1,3-Dimethyl-5-(1-methyl-1H-indol-3-yl)-7-(3-nitrophenyl)pyrido[2,3-d]pyrimidine-2,4(1H,3H)-dione (**7k**)*. Yield: 70%, mustard powder, mp: 349-350°C, IR (KBr): 3344.5, 3170.9, 3074.5, 2929.8, 1703.1, 1656.8, 1591.2, 1477.4, 1352.1, 1031.9 ν (cm^{-1}); ^{1}H NMR ($CDCl_3$, 300 MHz) δ: 8.99 (1H, s), 8.69 (1H, d, J = 8.0 Hz), 8.34 (1H, d, J = 8.0 Hz), 7.92 (1H, s), 7.80–7.86 (2H, m), 7.52 (1H, d, J = 8.2 Hz), 7.39 (1H, d, J = 6.9 Hz), 7.20 (1H, t, J = 7.0 Hz), 7.07 (1H, t, J = 7.0 Hz), 3.89 (3H, s), 3.74 (3H, s), 3.21 (3H, s) ppm; ^{13}C NMR ($CDCl_3$, 75 MHz) δ: 160.3, 157.4, 153.3, 152.8, 150.0, 149.9, 138.4, 138.2, 137.2, 134.0, 132.0, 130.9, 127.2, 125.8, 120.7, 120.5, 119.8, 118.6, 113.2, 110.9, 108.7, 33.5, 30.6, 28.9 ppm; LC-MS (m/z): 442.17 [MH^+].

2.3. Preparation and Purification of Hemolysate from Blood Red Cells. Blood samples (25 mL) were taken from healthy human volunteers. They were anticoagulated with acid-citrate-dextrose and centrifuged at 2000 g for 20 min at 4°C and the supernatant was removed. The packed erythrocytes were washed three times with 0.9% NaCl and then haemolysed in cold water. The ghosts and any intact cells were removed by centrifugation at 2000 g for 25 min at 4°C, and the pH of the haemolysate was adjusted to pH 8.5 with solid Tris-base. The 25 mL haemolysate was applied to an affinity column containing L-tyrosine-sulfonamide-sepharose-4B [21] equilibrated with 25 mM Tris-HCl/0.1 M Na_2SO_4 (pH 8.5). The affinity gel was washed with 50 mL of 25 mM Tris-HCl/22 mM Na_2SO_4 (pH 8.5). The hCA isozymes were then eluted with 0.1 M NaCl/25 mM Na_2HPO_4 (pH 6.3) and 0.1 M CH_3COONa/0.5 M $NaClO_4$ (pH 5.6), which recovered hCA I and hCA II, respectively. Fractions of 3 mL were collected and their absorbance was measured at 280 nm.

2.4. CA Enzyme Assay. CA activity was measured by the Maren method which is based on determination of the time required for the pH to decrease from 10.0 to 7.4 due to CO_2 hydration [22]. The assay solution was 0.5 M Na_2CO_3/0.1 M $NaHCO_3$ (pH 10.0) and Phenol Red was added as the pH indicator. CO_2-hydratase activity (enzyme units (EU)) was calculated by using the equation $t_0 - t_c/t_c$, where t_0 and t_c are the times for pH change of the nonenzymatic and the enzymatic reactions, respectively.

2.5. In Vitro Inhibition Studies. For the inhibition studies of indolylchalcone and pyrido[2,3-d]pyrimidine derivatives, different concentrations of these compounds were added to the enzyme. Activity percentage values of CA for different concentrations of each pyrimidine derivatives were determined by regression analysis using Microsoft Office 2000 Excel. CA enzyme activity without these compounds was accepted as 100% activity.

3. Results and Discussion

3.1. Chemistry. The synthetic procedures are depicted in Scheme 1. The indolylchalcone derivatives **5a**–**g**, prepared by the condensing various acetophenones and indolylaldehyde **3** with NaOH as a base, were reacted with 3-methyl-6-aminouracil **6a** and 6-aminouracil **6b** to get pyrido[2,3-d]pyrimidine derivatives (**7a**–**k**) at high yields. The large J value (15.5 Hz) clearly reveals the E-geometry for the chalcones.

3.2. Biological Evaluation of Indolylchalcone and Pyrido[2,3-d]pyrimidine Derivatives for hCA I and hCA II Inhibitory Activities. For evaluating the hCA I and II inhibitory effect, all compounds were subjected to hCA I and II inhibition assay with CO_2 as a substrate. The result showed that all synthesized compounds (**5a**–**g** and **7a**–**k**) inhibited the hCA I and hCA II enzyme activities.

The IC_{50} values and inhibition constants of **5a**–**g** and **7a**–**k** analogues against hCA I and hCA II were summarized in Table 1 and the IC_{50} graphs were given in Figure 1.

We have determined the IC_{50} values of 6.79–26.21 μM for the inhibition of hCA I and 7.22–31.10 μM for the inhibition of hCA II. Among all compounds, **7e** (IC_{50} = 6.79 μM) was found to be the most active one for hCA I inhibitory

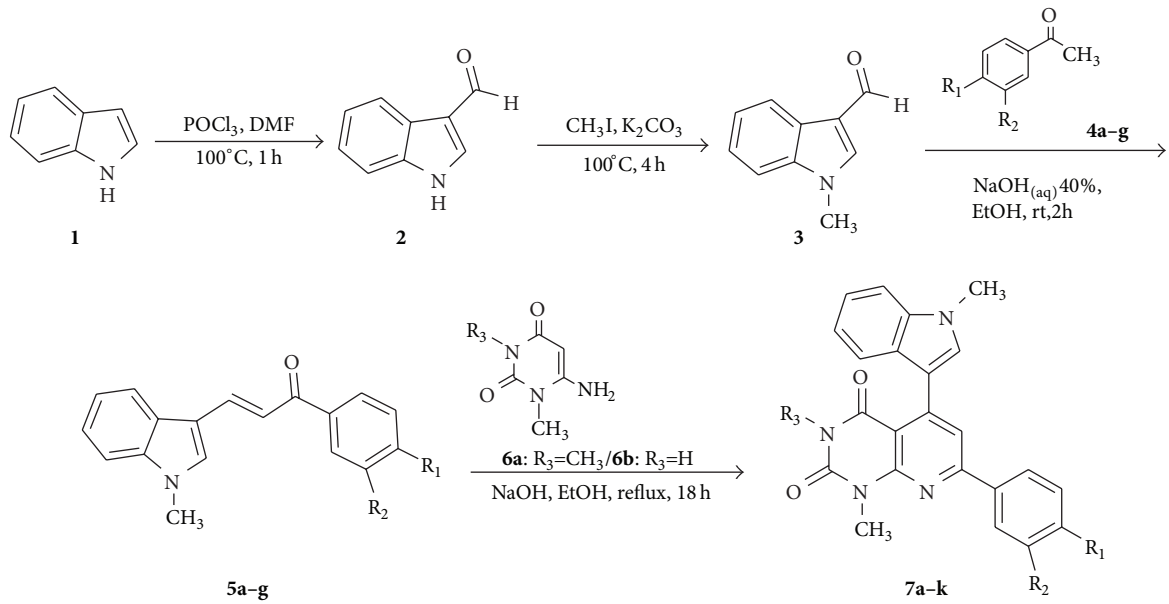

	5a	5b	5c	5d	5e	5f	5g	7a	7b	7c	7d	7e	7f	7g	7h	7i	7j	7k
R_1	OCH_3	OCH_3	CH_3	Cl	H	NO_2	H	OCH_3	CH_3	Cl	H	OCH_3	OCH_3	CH_3	Cl	H	NO_2	H
R_2	OCH_3	H	H	H	H	H	NO_2	OCH_3	H	H	NO_2	OCH_3	H	H	H	H	H	NO_2
R_3	—	—	—	—	—	—	—	H	H	H	H	CH_3	CH_3	CH_3	CH_3	CH_3	CH_3	CH_3

Scheme 1: Synthesis of pyrido[2,3-d]pyrimidine derivatives (**7a**–**k**).

Table 1: Inhibitory effect of indolylchalcone (**5a–g**) and pyrido[2,3-d]pyrimidine derivatives (**7a–k**) on hCA I and hCA II.

Compound	hCA I IC_{50} (μM)	hCA II IC_{50} (μM)
5a	8.34	8.88
5b	7.42	10.35
5c	13.07	12.28
5d	8.20	8.26
5e	12.84	9.15
5f	10.87	9.31
5g	8.38	7.22
7a	16.29	19.42
7b	11.56	12.06
7c	21.09	31.10
7d	12.14	13.66
7e	6.79	8.06
7f	26.21	25.40
7g	7.61	7.57
7h	12.36	24.67
7i	8.72	8.14
7j	10.19	9.56
7k	22.30	26.68

activity and **5g** (IC_{50} = 7.22 μM) showed the highest hCA II inhibitory activity. **5b** (IC_{50} = 7.42 μM) was found to be the most active one for hCA I inhibitory activity and **5g** (IC_{50} = 7.22 μM) showed the highest hCA II inhibitory activity for the indolylchalcone derivatives. Among the pyrido[2,3-d]pyrimidine derivatives, **7e** (IC_{50} = 6.79 μM) showed the highest hCA I inhibitory activity and **7g** (IC_{50} = 7.57 μM) showed the highest hCA II inhibitory activity.

It was reported that 1,4-dihydropyrimidinone substituted diarylurea compounds were synthesized and their effects on the hCA I and II enzyme activities were examined. Their minimum concentrations to achieve 50% inhibition were between 66.23 and 197.70 μM for hCA I, 63.09 and 169.71 μM for hCA II [23]. It is evident that the indolylchalcone and pyrido[2,3-d]pyrimidine derivatives, synthesized in this work, showed better hCA I and II inhibitory activities than 1,4-dihydropyrimidinone substituted diarylurea compounds.

3.3. Structure-Activity Relationships (SAR). Generally, we have seen that indolylchalcone derivatives have higher inhibitory activities than pyrido[2,3-d]pyrimidine derivatives on hCA I and hCA II. The following structure-activity relationship (SAR) observations can be drawn from the data.

(a) For the indolylchalcone derivatives, the presence of one electron-donating group (methoxy) bonded to paraposition of phenyl ring (**5b**) increased inhibitory activity on hCA I. Electron-withdrawing group (nitro) bonded to metaposition of phenyl ring (**5g**) has the highest hCA II inhibitory activity (IC_{50} = 7.22 μM).

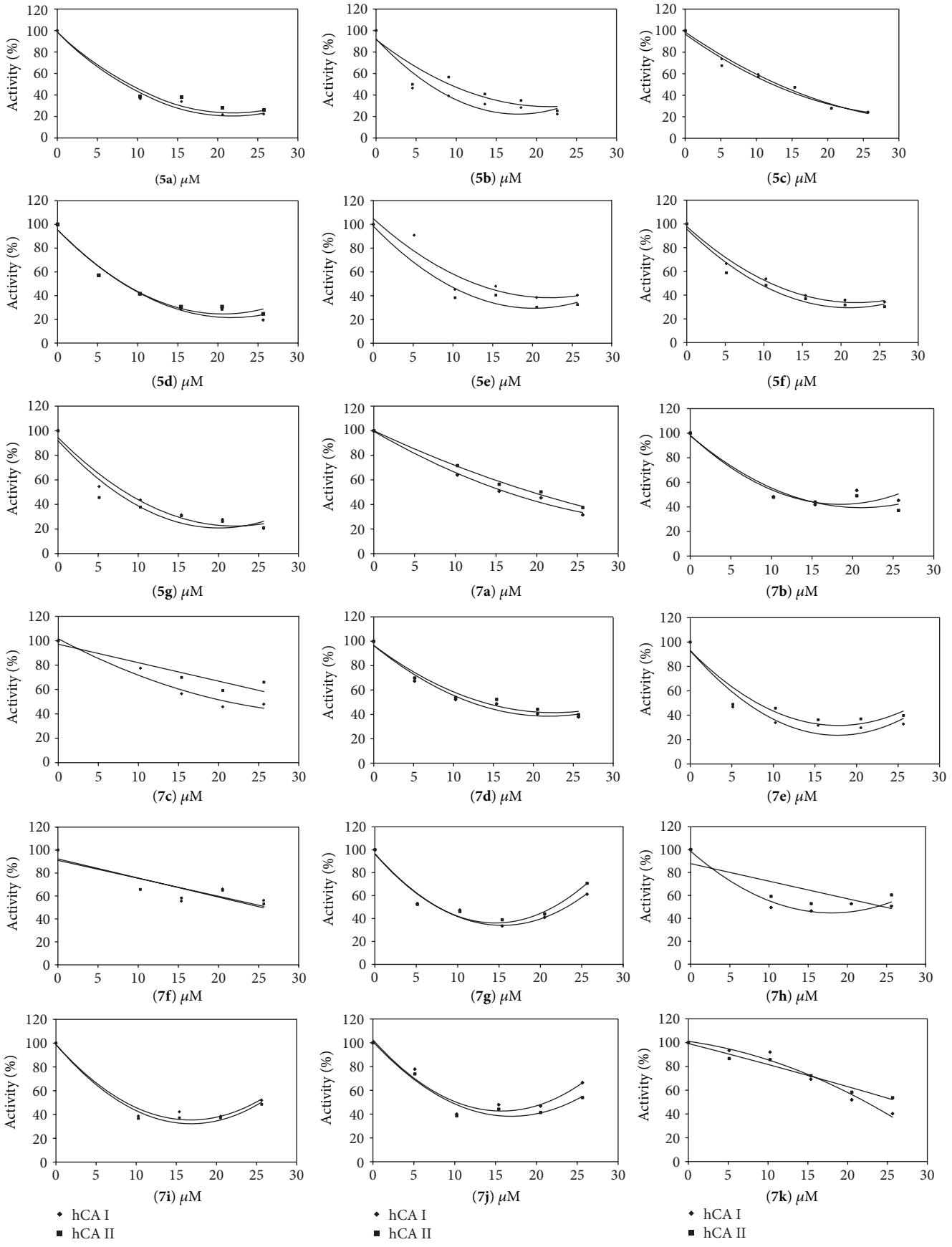

Figure 1: IC_{50} graphics of indolylchalcone (**5a**–**g**) and pyrido[2,3-d]pyrimidine (**7a**–**k**) derivatives on hCA I and hCA II.

(b) For the pyrido[2,3-d]pyrimidine derivatives, (i) the compounds (**7e**, **7g**, and **7h**) which have methyl group at the 3-position of uracil ring showed a higher inhibitory effect than the compounds (**7a**–**c**) which have hydrogen atom at the 3-position of uracil ring and have the same groups at the phenyl ring against both hCA I and hCA II (compare **7e** with **7a**, **7g** with **7b**, and **7h** with **7c**). (ii) Electron-withdrawing group (nitro) bonded to metaposition of phenyl ring (**7k**) has a very low hCA I inhibitory activity (IC_{50} = 22.30 μM). (iii) Mostly, the pyrido[2,3-d]pyrimidine derivatives have higher inhibitory activities on hCA I than hCA II.

Sulfonamides are coordinated to the zinc (II) ion within the hCA active site, whereas their organic scaffold fills the entire active site cavity, making an extensive series of van der Waals and polar interactions with amino acid residues delimiting this cavity [24, 25]. As the synthesized compounds are very bulky and do not contain a classical zinc-binding group [4], it can be hypothesized that they are not able to bind near the zinc ion showing a different mechanism of action. Structural studies of the complexes that these compounds form with the human isoform II could clarify this important issue.

4. Conclusions

In conclusion, series of 7 indolylchalcone and 11 new pyrido[2,3-d]pyrimidine derivatives containing indole ring were synthesized. Their activities as hCA I and hCA II inhibitors and structure-activity relationships were examined. All compounds inhibited both hCA I and hCA II enzyme activities. Most of compounds containing electron-donating groups at phenyl ring were generally stronger inhibitors of hCA I and hCA II. Additionally, methyl group bonded to 3-position of uracil ring generally increased inhibitory activities on both hCA I and hCA II. Thus, the present study revealed that the type and position of substituent of the phenyl and uracil rings could be exploited to modulate the CA inhibitors efficacy.

In summary, enzyme inhibition is an important issue for drug design [26–28]. Our results showed that new pyrido[2,3-d]pyrimidine derivatives inhibited the hCA I and II enzyme activity. Therefore, the compounds here investigated are likely to be adopted as good candidates as drugs and may be taken for further evaluation in in vivo studies.

Conflict of Interests

The authors declare that there is no conflict of interests regarding the publication of this paper.

References

[1] C. T. Supuran, D. Vullo, G. Manole, A. Casini, and A. Scozzafava, "Designing of novel carbonic anhydrase inhibitors and activators," *Current Medicinal Chemistry: Cardiovascular and Hematological Agents*, vol. 2, no. 1, pp. 49–68, 2004.

[2] C. T. Supuran and A. Scozzafava, "Carbonic-anhydrase inhibitors and their therapeutic potential," *Expert Opinion on Therapeutic Patents*, vol. 10, no. 5, pp. 575–600, 2000.

[3] D. Hewett-Emmet, "Evolution and distribution of the carbonic anhydrase gene families," in *The Carbonic Anhydrase—New Horizons*, W. R. Chegwidden, Y. Edwrds, and N. Carter, Eds., pp. 29–78, Birkhäuser, Basel, Switzerland, 2000.

[4] C. T. Supuran, "Carbonic anhydrases: novel therapeutic applications for inhibitors and activators," *Nature Reviews Drug Discovery*, vol. 7, no. 2, pp. 168–181, 2008.

[5] S. Poulsen, "Carbonic anhydrase inhibition as a cancer therapy: a review of patent literature, 2007–2009," *Expert Opinion on Therapeutic Patents*, vol. 20, no. 6, pp. 795–806, 2010.

[6] R. J. Sundberg, *Indoles*, Academic Press, London, UK, 1996.

[7] M. A. H. Zahran and A. M. Ibrahim, "Synthesis and cellular cytotoxicities of new N-substituted indole-3-carbaldehyde and their indolylchalcones," *Journal of Chemical Sciences*, vol. 121, no. 4, pp. 455–462, 2009.

[8] R. S. Chavan, H. N. More, and A. V. Bhosale, "Synthesis, characterization and evaluation of analgesic and anti-inflammatory activities of some novel indoles," *Tropical Journal of Pharmaceutical Research*, vol. 10, no. 4, pp. 463–473, 2011.

[9] D. Tian, G. Luo, H. Chen, X. Tang, and Y. Liu, "N-Cyclohexyl-2-(5-fluoro-1H-indol-3-yl)-2-oxoacetamide," *Acta Crystallographica Section E*, vol. 67, no. 7, p. o1851, 2011.

[10] V. E. Dilli, M. Mastan, and R. T. Sobha, "Synthesis and biological evaluation of 2-aryl-3-isoxazolinyl-indole derivatives as anti-inflammatory agents," *IOSR Journal of Applied Chemistry*, vol. 2, no. 3, pp. 44–49, 2012.

[11] R. S. Chavan, H. N. More, and A. V. Bhosale, "Synthesis and evaluation of analgesic and anti-inflammatory activities of a novel series of 3-(4 ,5 -dihydropyrazolyl)-indoles," *International Journal of Pharmaceutical and Biomedical Research*, vol. 1, no. 4, pp. 135–143, 2010.

[12] D. Kumar, N. M. Kumar, K. Akamatsu, E. Kusaka, H. Harada, and T. Ito, "Synthesis and biological evaluation of indolyl chalcones as antitumor agents," *Bioorganic and Medicinal Chemistry Letters*, vol. 20, no. 13, pp. 3916–3919, 2010.

[13] H. Wang and J. Zeng, "Iodine-catalyzed efficient synthesis of chalcones by grinding under solvent-free conditions," *Canadian Journal of Chemistry*, vol. 87, no. 9, pp. 1209–1212, 2009.

[14] S. Attar, Z. O'Brien, H. Alhaddad, M. L. Golden, and A. Calderón-Urrea, "Ferrocenyl chalcones versus organic chalcones: a comparative study of their nematocidal activity," *Bioorganic and Medicinal Chemistry*, vol. 19, no. 6, pp. 2055–2073, 2011.

[15] Z. Huang, Y. Hu, Y. Zhou, and D. Shi, "Efficient one-pot three-component synthesis of fused pyridine derivatives in ionic liquid," *ACS Combinatorial Science*, vol. 13, no. 1, pp. 45–49, 2011.

[16] D. Q. Shi, Y. Zhou, and H. Liu, "An efficient synthesis of pyrido[2,3-d]pyrimidine derivatives in ionic liquid," *Journal of Heterocyclic Chemistry*, vol. 47, no. 1, pp. 131–135, 2010.

[17] D. G. Powers, D. S. Casebier, D. Fokas, W. J. Ryan, J. R. Troth, and D. L. Coffen, "Automated parallel synthesis of chalcone-based screening libraries," *Tetrahedron*, vol. 54, no. 16, pp. 4085–4096, 1998.

[18] M. G. Bursavich, N. Brooijmans, L. Feldberg et al., "Novel benzofuran-3-one indole inhibitors of PI3 kinase-α and the mammalian target of rapamycin: hit to lead studies," *Bioorganic & Medicinal Chemistry Letters*, vol. 20, no. 8, pp. 2586–2590, 2010.

[19] A. S. El-Ahl, "Reaction of 2-oxoindolin-3-ylidene derivatives with heterocyclic enamines. A convenient one-pot synthesis of pyrimido [5,4:5',6']pyrido[2,3-b]-indole-2, 4-dione and spiro indolin-2-one-3, 5'-pyrido[2,3-d] pyrimidines," *Synthetic Communications*, vol. 30, no. 12, pp. 2223–2231, 2000.

[20] C. Shilpa, S. Dipak, S. Vimukta, and D. Arti, "Comparative study of microwave and conventional synthesis and pharmacological activity of pyrimidines: a review," *International Journal of Pharmaceutical Sciences Review and Research*, vol. 15, no. 1, pp. 15–22, 2012.

[21] O. Arslan, B. Nalbantoglu, N. Demir, H. Ozdemir, and O. I. Kufrevioglu, "A new method for the purification of carbonic anhydrase isozymes by affinity chromatography," *Turkish Journal of Medical Sciences*, vol. 26, no. 2, pp. 163–166, 1996.

[22] T. H. Maren, "A simplified micromethod for the determination of carbonic anhydrase and its inhibitors," *The Journal of Pharmacology and Experimental Therapeutics*, vol. 130, no. 1, pp. 26–29, 1960.

[23] F. Celik, M. Arslan, E. Yavuz, D. Demir, and N. Gencer, "Synthesis and carbonic anhydrase inhibitory properties of novel 1,4-dihydropyrimidinone substituted diarylureas," *Journal of Enzyme Inhibition and Medicinal Chemistry*, vol. 29, no. 1, pp. 18–22, 2014.

[24] F. Pacchiano, M. Aggarwal, B. S. Avvaru et al., "Selective hydrophobic pocket binding observed within the carbonic anhydrase II active site accommodate different 4-substituted-ureido-benzenesulfonamides and correlate to inhibitor potency," *Chemical Communications*, vol. 46, no. 44, pp. 8371–8373, 2010.

[25] F. Pacchiano, F. Carta, P. C. McDonald et al., "Ureido-substituted benzenesulfonamides potently inhibit carbonic anhydrase IX and show antimetastatic activity in a model of breast cancer metastasis," *Journal of Medicinal Chemistry*, vol. 54, no. 6, pp. 1896–1902, 2011.

[26] N. Gençer, A. Ergün, and D. Demir, "In vitro effects of some herbicides and fungicides on human erythrocyte carbonic anhydrase activity," *Fresenius Environmental Bulletin*, vol. 21, no. 3, pp. 549–552, 2012.

[27] D. Demir, N. Gençer, and A. Er, "Purification and characterization of prophenoloxidase from *Galleria mellonella* L.," *Artificial Cells, Blood Substitutes, and Biotechnology*, vol. 40, no. 6, pp. 391–395, 2012.

[28] N. Gençer and O. Arslan, "In vitro effects of some pesticides on PON1Q192 and PON1R192 isoenzymes from human serum," *Fresenius Environmental Bulletin*, vol. 20, no. 3, pp. 590–596, 2011.